Flow and wakes in large wind farms: Final report for UpWind WP8

Barthelmie, Rebecca Jane; Frandsen, Sten Tronæs; Rathmann, Ole; Hansen, Kurt Schaldemose; Politis, E.; Prospathopoulos, J.; Schepers, J.G.; Rados, K.; Cabezon, D.; Schlez, W.

Total number of authors:
12

Publication date:
2011

Document Version
Publisher's PDF, also known as Version of record

Flow and wakes in large wind farms: Final report for UpWind WP8

Risø-R-Report

R.J. Barthelmie, S.T. Frandsen, O. Rathmann, K. Hansen, E.S. Politis, J. Prospathopoulos, J.G. Schepers, K. Rados, D. Cabezón, W. Schlez, Neubert, A. and Heath, M.

Report number Risø-R-1765(EN)

February 2011

Risø DTU
National Laboratory for Sustainable Energy

Author: R.J. Barthelmie[1,2], S.T. Frandsen[1], O. Rathmann[1], K. Hansen[3], E. Politis[4], J. Prospathopoulos[4], J.G. Schepers[5], K. Rados[6], D. Cabezón[7], W. Schlez[8], Neubert, A. and Heath, M.[8]

[1]Risø DTU (DK), [2]Indiana University (USA), [3]DTU (DK), [4]CRES (GR), [5]ECN (NL), [6]NTUA (GR), [7]CENER (ES), [8]Garrad Hassan and Partners (DE, UK)

Title: Flow and wakes in large wind farms: Final report for UpWind WP8

Division: Wind Energy

Abstract (max. 2000 char.):

This report summarises the research undertaken through the European Commission funded project UpWind Wp8:Flow. The objective of the work was to develop understanding of flow in large wind farms and to evaluate models of power losses due to wind turbine wakes focusing on complex terrain and offshore. A cross-cutting activity was to improve and compare the performance of computational fluid dynamics models with wind farm models.

Report number Risø-R-1765(EN)

Publication date February 2011

ISSN 0106-2840

ISBN 978-87-550-3878-3

Contract no.:
019945 (SES6)

Group's own reg. no.:
(Føniks PSP-element)

Sponsorship:

Cover :

Pages:

Tables:

References:

Information Service Department
Risø National Laboratory for Sustainable Energy
Technical University of Denmark
P.O.Box 49
DK-4000 Roskilde
Denmark
Telephone +45 46774005
bibl@risoe.dtu.dk

Preface: Sten Frandsen

STEN T. FRANDSEN had a classical education in Structural/ Hydraulic Engineering at the Technical University of Denmark. He developed his career in the Wind Energy Department at RisøNational Laboratory and was a formative influence in a wide range of issues relating to wind energy. He participated in numerous international projects in e.g. Egypt and China. As coordinator of the RECOFF and many other European and Danish projects he focussed on addressing uncertainty in models, measurements and standards. His manifold contributions influence many areas of wind energy research but in particular he is known for his ground breaking and enduring research results used as the basis for evaluating turbulence intensity in offshore wind farms – affectionately known as the Sten Frandsen model and used in the IEC standards. His persistent efforts, particularly on design criteria for offshore wind turbines, and his development of new approaches to standards are especially noteworthy. He was a major player in the first offshore wind farm research project at Vindeby and used this work to help develop recommendations for offshore wind turbine design. Later he was a key player in new research projects at both Horns Rev and Nysted leading to the development of a new model for wakes in large offshore wind farms. In 2007, he was awarded the Danish doctoral degree for his thesis 'Turbulence and turbulence generated structural loading in wind turbine clusters'. This is the highest Danish doctoral degree, awarded to mature researchers upon their public defence of a thesis, usually based on a minimum of five to eight years of individual and original research.

Beyond his technical achievements Sten was an enlightened scholar pushing the boundaries of our understanding of how wind turbines and wind farms interact with the atmosphere and opening new fields of research to assist in the further development of wind energy. He is universally respected for his progressive ideas and honesty and a highly appreciated member of many committees for his good-humoured and valuable contributions.

Sten was instrumental in the development of the technical and organization sides of the European Commission project UpWind. Many of his ideas were expanded during the project including the use of metrology in wind energy and work on wind farm clusters that was undertaken within the Workpackage represented here; WP8 Flow. Sten was well-known to all of us in a work context and a good friend to many of us on a personnel level. It was a sad day for all of us when Sten passed away in October 2010 as the project was coming to its successful completion. Therefore we agreed to include this memorial to our friend and colleague Sten Frandsen in recognition of his enduring legacy in wind energy research and implementation.

Contents

Summary

1.1 The challenge

Wind farms or arrays containing large numbers of wind turbines are particularly challenging to model. The impact of multiple wind turbine wakes (interactions between the flow downwind of turbines and the atmosphere) are of critical importance to the wind energy industry because they directly impact both the power output and the turbulence level that determines the turbine lifetime. Because wake effects are influenced by both the environment (wind speed distribution, shear, veer, turbulence etc) and the wind farm characteristics (turbine type, spacing etc) they are complex systems. Since power losses due to wakes can be between 5 and 20% of total power output there is considerable benefit to improving wake and wind farm modelling that can assist in developing optimised wind farm layouts.

The main areas requiring improved modelling capabilities are in complex terrain and for large wind farms offshore. Our WP has also focused on improved data analysis and quality control for wake model evaluation, wake model evaluation benchmarks, including computational fluid dynamics (CFD) models in wake model comparisons, data analysis to elucidate controlling factors on wind turbine wakes, evaluating multiple wakes, impacts of complex terrain and exploration of new techniques for reducing wake losses. Finally we recognise the need to integrate both power losses and loads in wake models to provide lifetime estimates of wind farm performance.

1.2 Model verification data

Clustering wind turbines in wind farms results in wake losses. An important task in WP8 has been to categorize these losses and identify the most important parameters. The verification has been based on SCADA data, which was recorded on three types of wind farms ranging from a small onshore wind farm (5 wt) with a spacing of 4D located in flat terrain, a complex terrain wind farm (43 wt) with a spacing of 13D and 3 large offshore wind farms (80wt, 72wt & 36wt) with a primary spacing between 7D – 11D.

The flow model verification in complex terrain has been rather difficult due to interpretation of the terrain effects, irregular wt locations, short data periods and poor data quality. The flow model verification for offshore wind farms has been possible due to a large number of observations, regular wt arrangement and high data quality.

The power deficit along rows of wind turbines depends of the flow angle as shown in Figure 1 and the directional power deficit has a Gaussian shape, as shown in Figure 2. The maximum power deficit for three different spacing shows a consistent relationship with decreasing with increasing turbulence intensity in Figure 3. The offshore climate analysis shows a clear correlation between atmospheric stability, the ambient turbulence and the power deficit. Figure 4 demonstrates how the wake size increases in very stable conditions, caused by decreased turbulent mixing of the wake.

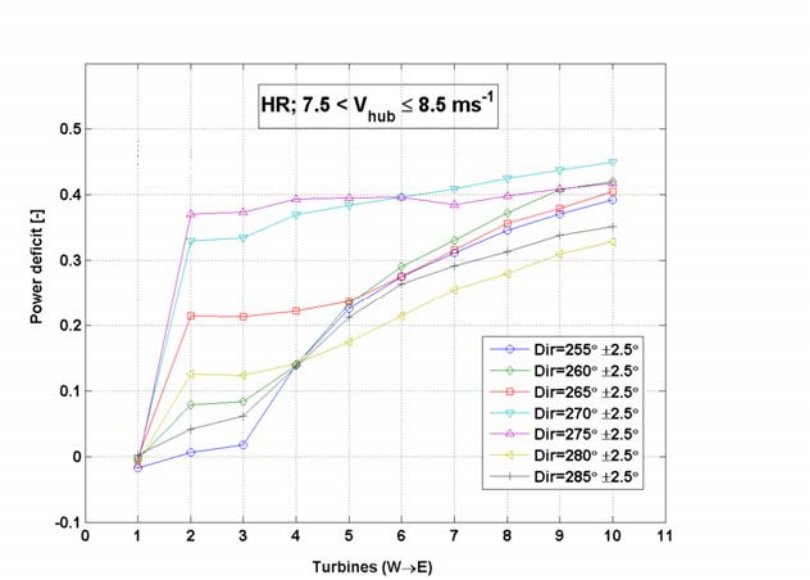

Figure 1: Power deficit along rows consisting of 10 wind turbines and 7D spacing at 8 m/s.

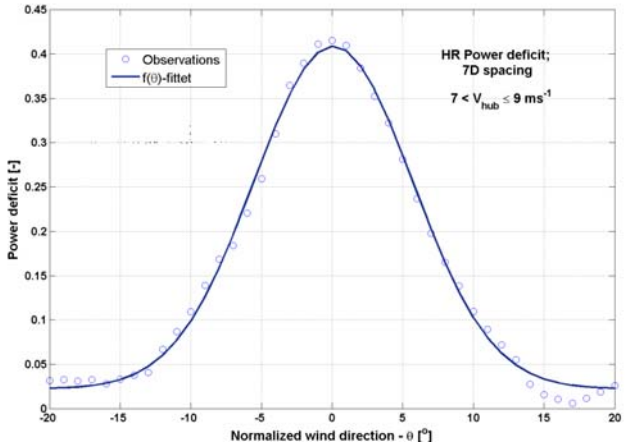

Figure 2: Power deficit distribution as function of normalized wind direction for 7D spacing.

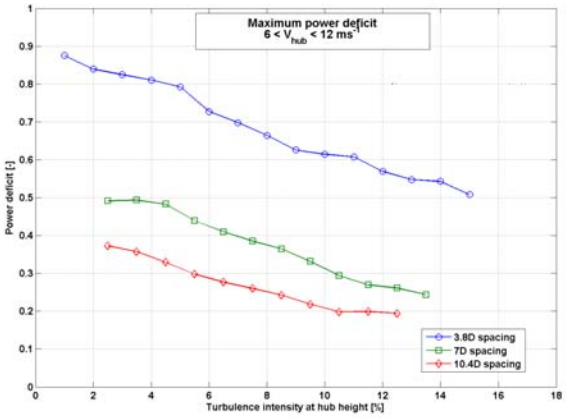

Figure 3: Maximum power deficit for 3.8D, 7D and 10.4D spacing as function of turbulence intensity.

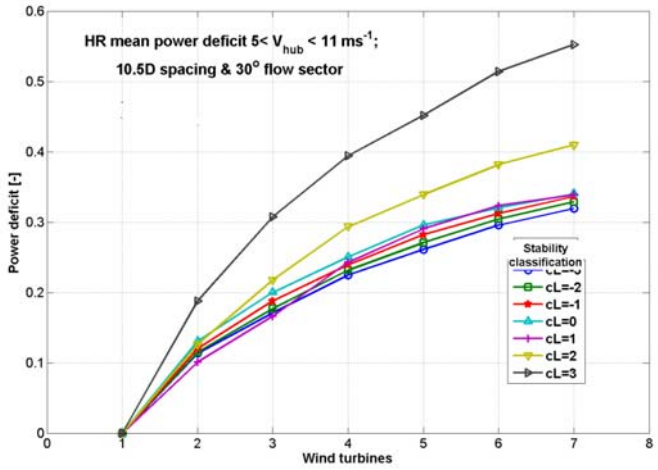

Figure 4: Power deficit along rows with 7 wind turbines and 10.4D spacing, grouped on stability classes.

1.3 Offshore

Our WP performed a comprehensive model evaluation of wakes in large offshore wind farms using data from the large offshore wind farms at Horns Rev and Nysted. The range of models included is shown in Table 1. During the course of the project, many of the models were improved showing a considerable degree of agreement between the models and the measurements. Figures 5 and 6 show the model simulations for one case study at the Nysted and Horns Rev wind farms (respectively). The wind speed bin is 8.0±0.5 m/s which, according to the thrust curves for the wind turbines, is close to the maximum wake loss. The narrow direction sectors directly down the turbine rows are also selected to provide the maximum wake signal (270±2.5° for Horns Rev and 278±2.5° for Nysted, except for the WasP model that uses a bin width of ±5°).

Table 1. Wake and wind farm models evaluated in WP8

Name	Company	Type
WAsP	Risø DTU	Engineering
WindFarmer	GH	Ainslie -CFD
“Canopy”	Risø DTU	Under
Wakefarm	ECN	Parabolised
CFDWake	CENER	CFD
FlowNS	CRES	CFD
NTUA	NTUA	CFD

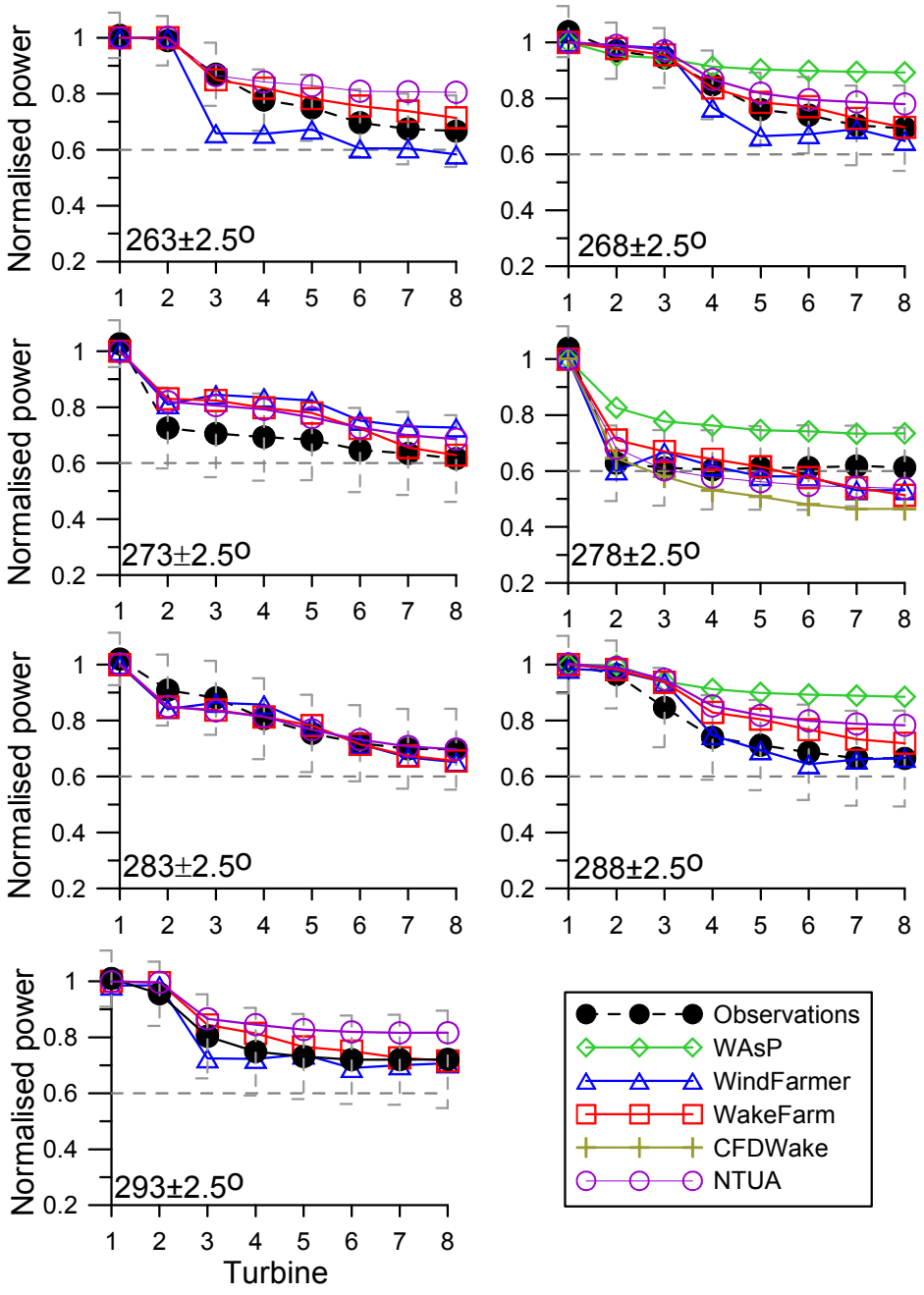

Figure 5. Model simulations in comparison with observations for one case study at the Nysted wind farm. The wind speed bin is 8.0±0.5 m/s which, according to the thrust curves for the wind turbines, is close to the maximum wake loss. The narrow direction sectors directly down the turbine rows are also selected to provide the maximum wake signal (278±2.5° for Nysted, except for the WasP model that uses a bin width of ±5°).

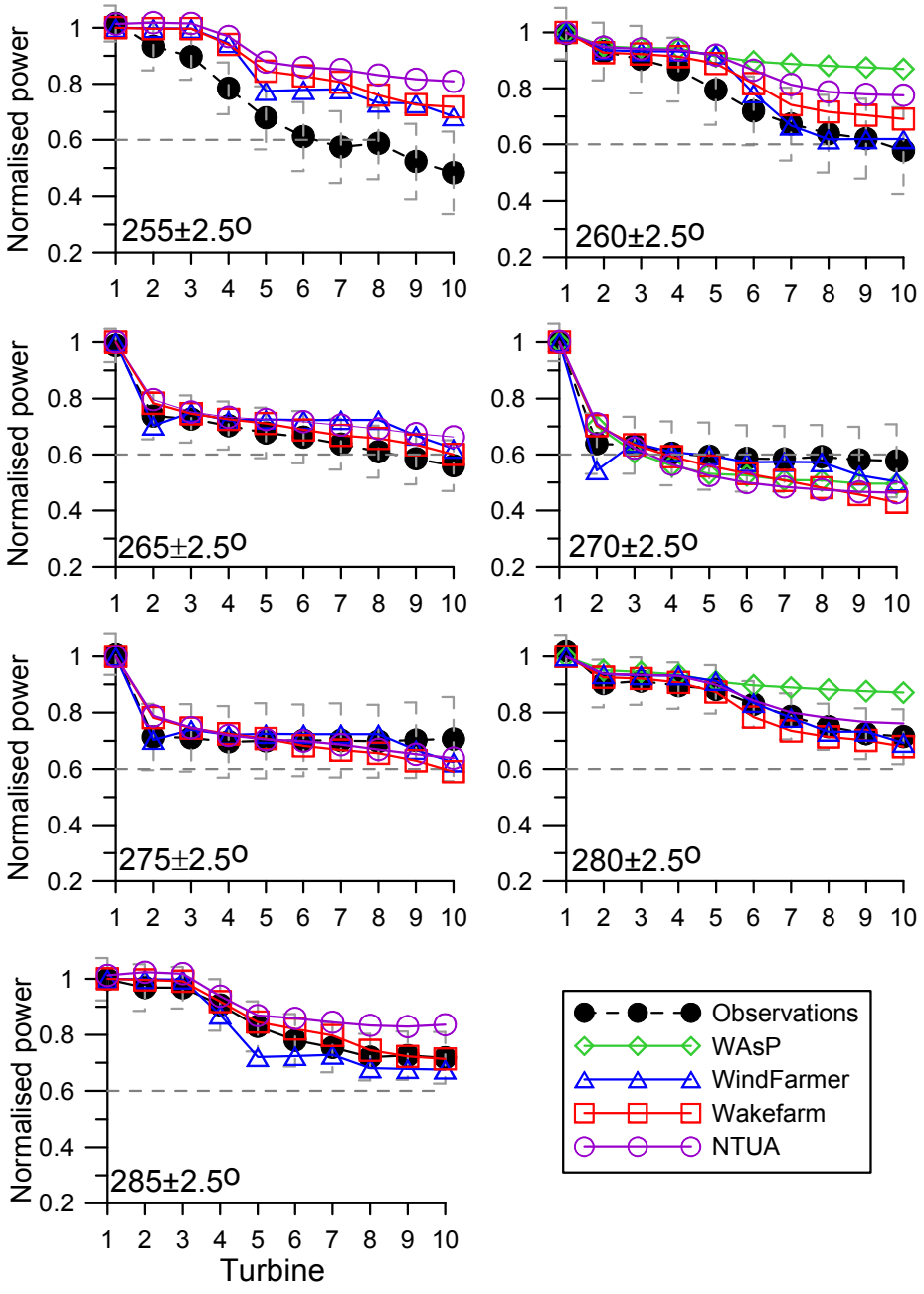

Figure 6. Model simulations in comparison with observations for one case study at the Horns Rev wind farm. The wind speed bin is 8.0±0.5 m/s which, according to the thrust curves for the wind turbines, is close to the maximum wake loss. The narrow direction sectors directly down the turbine rows are also selected to provide the maximum wake signal (278±2.5° for Nysted, except for the WasP model that uses a bin width of ±5°).

The main findings for both wind farms are summarized in Figure 7. can be summarized as acknowledging that wake losses in the centre of large wind farms offshore are larger than modeled using standard wind farm model parameterizations but, once corrected, model results were improved in comparison with data from existing data sets. Analyses of the wind farm data also show the primary importance of wind speed on wake development but also that turbulence and atmospheric stability play an important role in determining the magnitude of wake losses in wind farm offshore (Barthelmie and Jensen, 2010; Hansen et al., 2010).

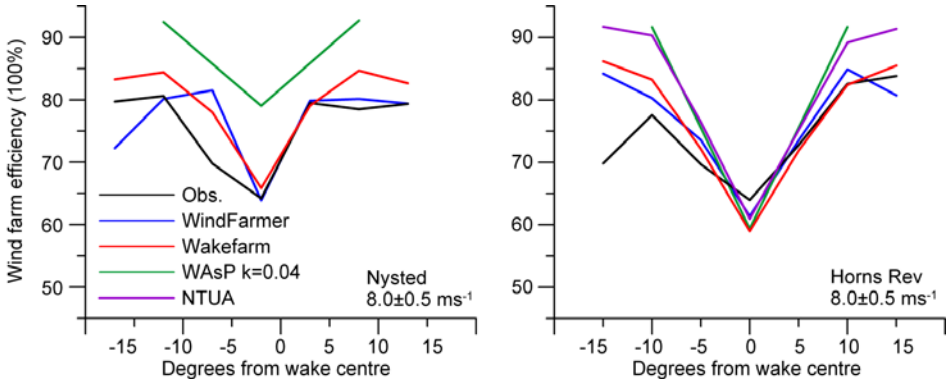

Figure 7. Summary wake model evaluation for specific wind speed of 8.0±0.5 ms-1 and directions at Horns Rev and Nysted. The wake centre refers to 270^{o} at Horns Rev and 278^{o} at Nysted (after Barthelmie et al. 2010).

1.4 Complex Terrain

Our WP also performed a comprehensive model evaluation of wakes in complex terrain using three different cases: (i) Gaussian-type topographies where CFD models and wind farm models were compared for the case of one hill-top wind turbine to identify differences in the wake development between flat and complex terrain (see Prospathopoulos et al 2008), (ii) CFD models comparisons for the case of five turbines in flat terrain to evaluate the modeling of wind turbines in wake simulations, and (iii) CFD models and wind farm models simulations of a large wind farm comprising 43 turbines in complex terrain. The obvious breakthrough in this kind of application stems from the fact that is the first time that CFD tools are employed for power predictions in large wind farms in complex terrain. CFD predictions have been considerably improved in flat terrain (see Figure 8) and Prospathopoulos et al 2010a. In complex terrain (see Figure 9), there is still room for improvement especially in the application of the actuator disk technique (Prospathopoulos et al 2010b).

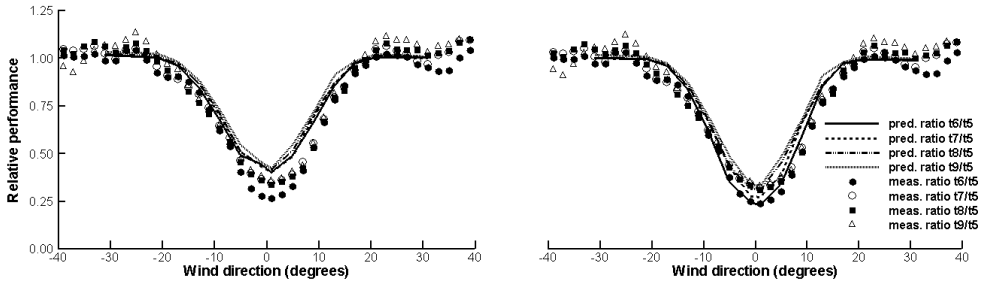

(a) (b)

Figure 8. Predicted relative performances for the ECN test farm with 5 W/Ts in a row. (a) Baseline calculations (b) Calculations including Masson's correction with C=3. 0^o correspond to the direction of the W/T's row. Measurements are taken from Machielse et al (2007)

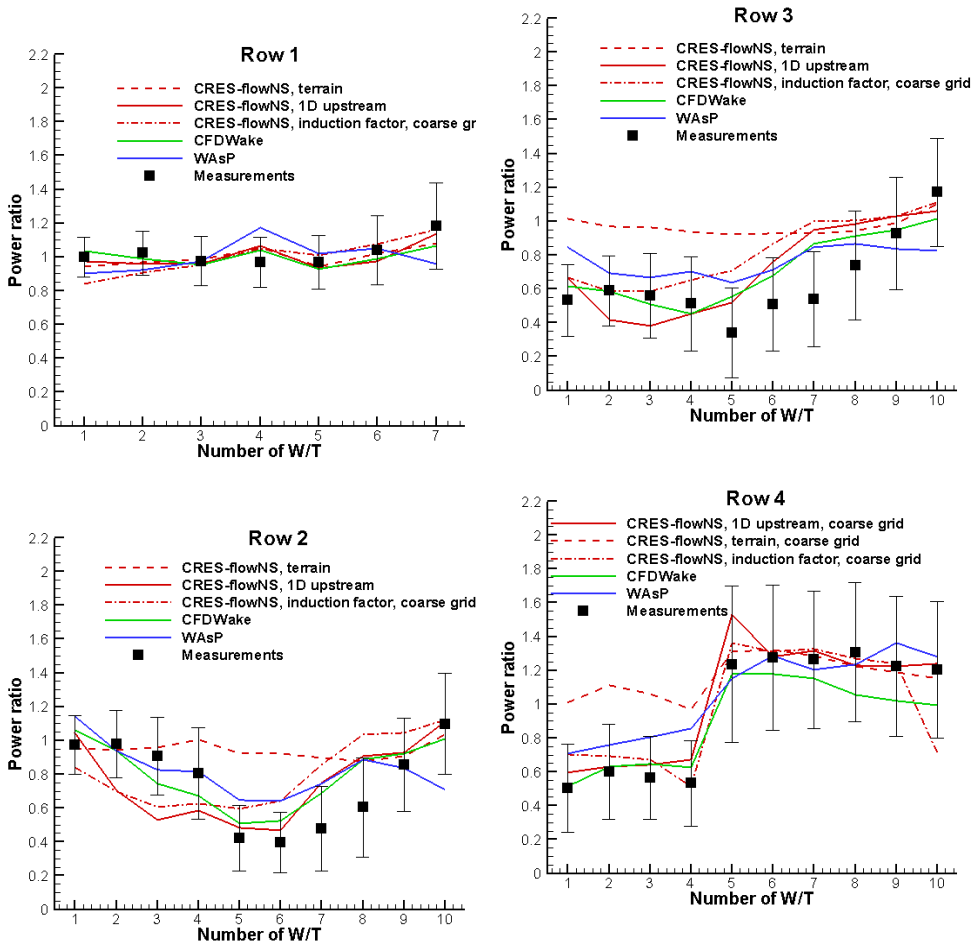

Figure 9. Power ratios of the W/Ts in the four rows of a large complex terrain wind farm, with reference to the average power of the seven W/Ts of the first row, for the complex terrain wind farm for wind direction 327^o. CRES–flowNS, CFDWake and WAsP predictions are compared with operational data.

1.5 Wake reducing concepts

Within WP8 several wake reducing approaches have been investigated. These approaches aim to optimize the performance of the **entire wind farm** with the underlying idea that it may be beneficial to reduce wake effects by sacrificing some performance of the upstream turbines. Thereto the upstream turbine operates at sub-optimal conditions (sub-optimal in terms of individual wind turbine performance) where one can think of a non-optimal pitch angle/rotor speed, or a yaw misalignment. These sub-optimal settings will however lead to lower wake effects and hence an increased performance of the downstream turbines which can (over)compensate the loss in performance of the upstream turbines.

An intermediate approach lies in upscaling, since the rated power of a wind turbine increases with D^2 and the wake losses increase with size but to a smaller extent. Hence upscaling allows to reach the same rated wind farm power on a given land area at lower wake losses.

Also non-conventional wind farms, eg wind farms which consist of turbines with unequal size may lead to an overall gain in energy production, since different sized wind turbines yield a different (and possibly a positive) wake impact. Furthermore the diameter can be used to design a 'wake specific' wind turbine (like it can be used to design a 'site specific' turbine, ie a turbine for a low wind speed climate will generally have a larger diameter).

The result of this study is reported in (Schepers et al., 2010). It was found that all of the above mentioned approaches have potential. These conclusions are however largely based on calculations where it is realized that the calculational methods generally suffer from large uncertainties. Some ideas on how to assess scaling effects on wake models (an important question when considering upscaling) have also been formulated.

Figure 10 shows the experimental validation from the ECN Wind Turbine Test Site Wieringermeer of the Heat and Flux concept, ie the concept where the pitch angle of the first turbine is set to a non-optimal value. The figure left shows the power of the upstream turbine for the optimal (red) and suboptimal (Heat and Flux) pitch angle (green). The power production is almost similar where the power production of the downstream turbine shows a slight increase for the Heat and Flux operation

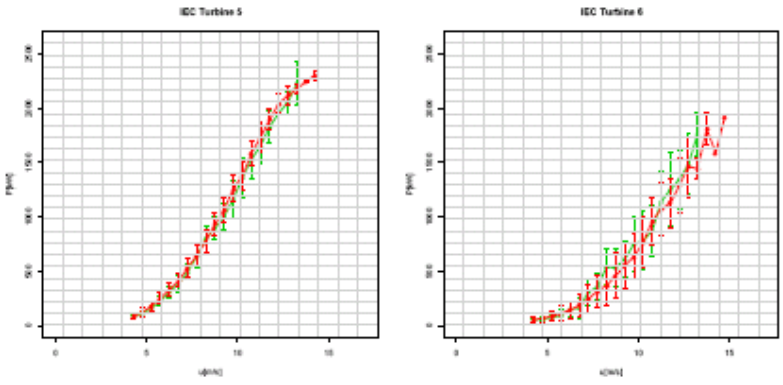

Figure 10: Power performance of turbine 5(left) and 6(right) for scenario 20000 (green triangles) and scenario 00000(red bullets)

.

Indiana University/RISOE-DTU, CRES and ECN performed studies in which it was investigated how the size of wind turbines and the scale of wind farms impacts the amount of energy that can be extracted from a given land area. Several options have been considered. Table 2 and Figure 11 show the results from Indiana University/RISOE-DTU. In this study several options were investigated on a 500 MW farm on which simulations were conducted with WAsP for different turbine size and spacing as shown in Figure 11. The results are summarized in Table 2. This research indicates that increasing turbine size from 5 MW to 20 MW could increase energy capture from about 28.3 to at least 34.7 GWh km^{-2} where the wake losses can be decreased from 14.5% to 6.5%. Similar conclusions have been drawn from the studies of the other institutes. However, it must be noted that these results are based on linear scaling on wake losses.

Table 2. Prediction of power output using WAsP

	Option 1	**Option 2 "Equal area"**	**Option 3 "Equal spacing"**
Turbine	5 MW	20 MW	20 MW
Hub height/rotor diameter (m)	90/126	153/252	153/252
Installed capacity (MW)	500	500	500
Area of installation (km^2)	8.8 × 8.8 = 77.4	8.8 × 8.8 = 77.4	8.8 × 7.1 = 62.1
Area capacity ($W\ m^{-2}$)	6.5	6.5	8.1
Turbine wake losses (%) (WAsP k=0.04, U=8.6 ms^{-1})	14.5	6.5	9.0
Annual production ($GWh\ a^{-1}$) (WAsP k=0.04, U=8.6 ms^{-1})	2197	2211	2152
Production density ($GWh\ km^{-2}$)	28.3	28.6	34.7

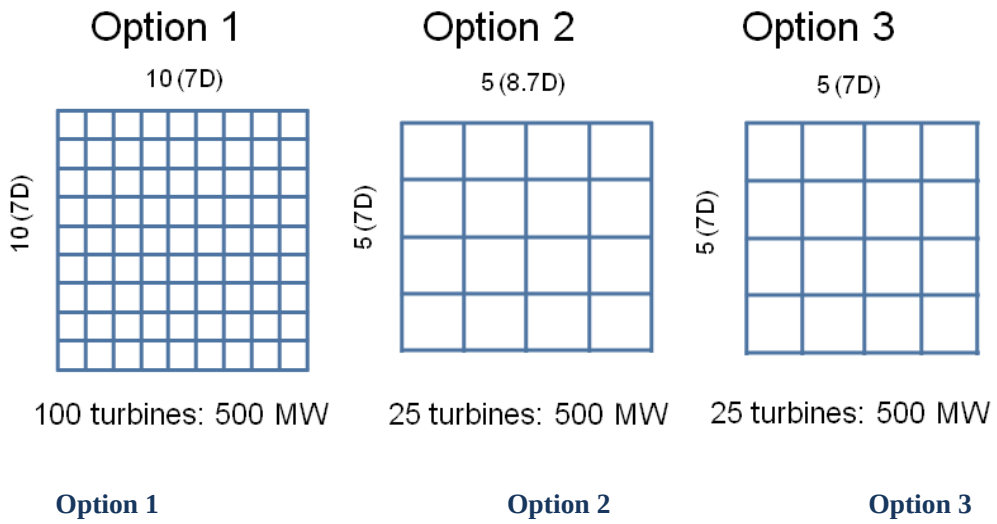

Figure 11: Layouts considered: Left 100 turbines with a rated power of 5MW, middle and right 25 turbines with a rated power of 20 MW

1.6 Lifetime loads

The principle goal of the designer of a commercial wind farm will be to make that wind farm as profitable as possible. This is not as straightforward as simply establishing the layout of turbines which generates the highest energy yield. The energy yield represents the income generated by the farm, but to understand its profitability it is also necessary to understand the costs involved in its construction and operation.

Many costs are easy to model – the procurement price of a turbine is a known quantity, for example. Others are much harder to establish. For example, the maintenance cost of a wind farm will depend on many factors, such as the wind conditions, operational strategy, turbine design and build quality and so on.

As part of UPWIND Work Package 8, a cost modelwas developed to illustrate how a financial analysis of a wind farm layout should be performed. This cost model considers the lifetime economics of the farm, including both the capital investment and operational costs.

It is aimed at helping the wind farm designer establish the optimum turbine layout. For this reason it can safely be restricted to analysing only those costs which will vary with the layout. The procurement costs of the turbines, for example, have been ignored since for a fixed number of turbines they will not change, regardless of where on the site the turbines are installed.

A central part of this cost model has been to analyse the costs incurred as a result of turbulence induced fatigue loading on the turbines. This is arguably the most complex part of the analysis, since it involves calculation of wake induced turbulence, fatigue loading and consequent repair and maintenance costs.

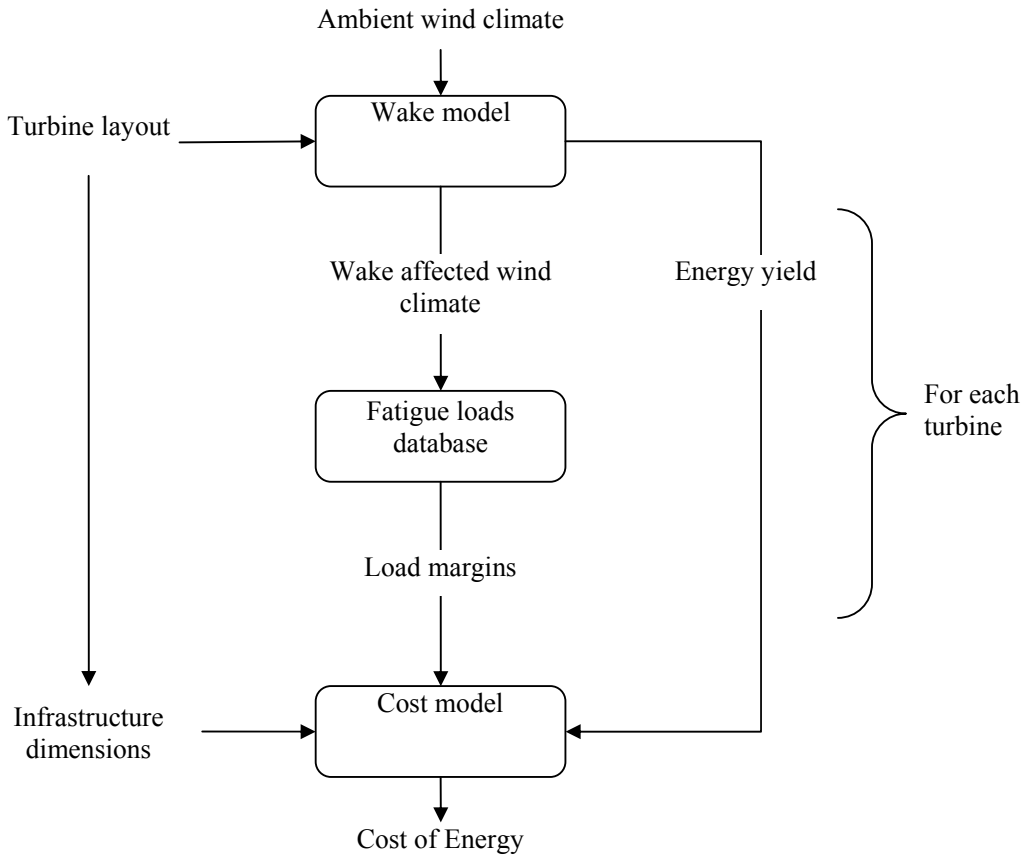

Figure 12. Cost optimisation flow diagram

Costs which vary with turbine layout, both capital and infrastructure, have been included in the cost model. Development of the fatigue loads database has created a technique for rapidly establishing the site specific loading on critical components, at speeds which are fast enough to be usable in an optimisation routine.

Preliminary testing has shown that the use of Cost of Energy as the target for layout optimisation gives different results from the use of energy yield. This will be valuable to wind farm developers, for whom economic performance is ultimately of prime importance.

Considerable further work is required to refine the cost model. Its structure is currently purely illustrative. The process of establishing the relationship between maintenance costs and fatigue loading in particular is currently little understood, and needs to be further investigated

1.7 References

Barthelmie RJ, Hansen K, Frandsen ST, Rathmann O, Schepers JG, Schlez W, Philips J, Rados K, Zervos A, Politis ES, Chaviaropoulos PK (2009) Modelling and measuring flow and wind turbine wakes in large wind farms offshore. Wind Energy 12:431-444. DOI: 410.1002/we.1348

Barthelmie RJ, Jensen LE (2010) Evaluation of power losses due to wind turbine wakes at the Nysted offshore wind farm. Wind Energy DOI: 10.1002/we.408

Barthelmie RJ, Pryor SC, Frandsen ST, Hansen K, Schepers JG, Rados K, Schlez W, Neubert A, Jensen LE, Neckelmann S (2010) Quantifying the impact of wind turbine wakes on power output at offshore wind farms. Journal of Atmospheric and Oceanic Technology 27:1302-1317

Hansen KH, Barthelmie RJ, Jensen LE, Sommer A (2010) The impact of turbulence intensity and atmospheric stability on power deficits due to wind turbine wakes at Horns Rev wind farm. Wind Energy Submitted 8 September 2010. WE-10-0149.

Prospathopoulos J.M, Politis ES, Chaviaropoulos PK (2008): Modelling wind turbine wakes in complex terrain. Proceedings of the 2008 European Wind Energy Conference & Exhibition, Brussels, 31/3-3/4/2008, Edited by P. K. Chaviaropoulos, pp. 42-46

Prospathopoulos J.M, Politis ES, Rados K, Chaviaropoulos PK (2010a): Evaluation of the effects of turbulence model enhancements on wind turbine wake predictions. Wind Energy, to appear (DOI: 10.1002/we.419)

Prospathopoulos J.M, Cabezon D, Politis ES, Chaviaropoulos PK, Rados KG, Schepers JG., Hansen KS, Barthelmie RJ (2010b): Simulation of wind farms in flat and complex terrain using CFD. Proceedings of 'The Science of Making Torque from Wind' Conference, Heraklion, Greece, 28-30/6/2010, Edited by S. Voutsinas and P. K. Chaviaropoulos, pp. 359-370, 2010

Machielse LAH, Eecen PJ, Korterink H., van der Pijl SP, Schepers, JG (2007): ECN test farm measurements for validation of wake models", Proceedings of the 2007 European Wind Energy Conference & Exhibition, Milan 7-10/5/2007, Edited by P. K. Chaviaropoulos, pp. 98-102

Schepers, G., Barthelmie, R.J. and Politis, E.S.: 2010, 'Wake reducing concepts. Upwind WP8 Deliverable 8.5', ECN, Petten, p. 30.

List of papers and presentations

Papers

1. Barthelmie, R.J., Frandsen, S.T., Nielsen, N.M., Pryor, S.C., Rethore, P.E. and H.E. Jørgensen, 2007: Modelling and measurements of power losses and turbulence intensity in wind turbine wakes at Middelgrunden offshore wind farm, Wind Energy doi: 10.1002/we.238. **10**, 217-228.

2. Frandsen, S.T., Jørgensen, H.E., Barthelmie, R.J., Rathmann, O., Badger, J., Hansen, K., Ott, S., Rethore, P.-E., Larsen, S.E., Jensen, L.E. 2009: The making of a second-generation wind farm efficiency model-complex, Wind Energy, **12(5),** 445-458. DOI: 10.1002/we.351.

3. Barthelmie, R.J., Hansen, K., Frandsen, S.T., Rathmann, O., Schepers, J.G., Schlez, W., Philips, J., Rados, K., Zervos, A., Politis, E.S. and Chaviaropoulos, P.K. 2009: Modelling and measuring flow and wind turbine wakes in large wind farms offshore, Wind Energy, **12(5)**, 431–444. DOI: 10.1002/we.348.

4. Barthelmie, R.J., Pryor, S.C., Frandsen, S.T., Hansen, K.S., Schepers, J.G., Rados, K., Schlez, W., Neubert, A., Jensen, L.E. and Neckelmann, S. 2009: Quantifying the impact of wind turbine wakes on power output at offshore wind farms. *Journal of Atmospheric and Oceanic Technology*, **27(8),** 1302-1317. doi: 10.1175/2010JTECHA1398.1.

5. Barthelmie, R.J. and Jensen, L.E. 2010: Evaluation of power losses due to wind turbine wakes at the Nysted offshore wind farm, *Wind Energy*, **13**, 573–586, DOI: 10.1002/we.408.

6. Politis, E., Prospathopoulos, J. and Chaviaropoulos, P.K., Cabezon, D., Hansen, K. and Barthelmie, R.J. 2010: Modelling wake effects in large complex terrain wind farms: the problem, the methods and the issues, *Wind Energy* (submitted WE-10-0103 2-July-2010).

7. Hansen, K.S., Barthelmie, R.J., Jensen, L.E. and Sommer. A. 2010: The impact of turbulence intensity and atmospheric stability on power deficits due to wind turbine wakes at Horns Rev wind farm, *Wind Energy* (WE-10-0103, submitted 7 September 2010).

8. J.G. Schepers, J.G. and Obdam, T.G. 2010: Analysis of wake measurements from the ECN Wind Turbine Test Site Wieringermeer, EWTW, *Wind Energy* (Submitted October 2010).

Presentations or posters with papers

1. Rathmann, O., Frandsen, S.T. and Barthelmie, R.J. 2007: Wake modelling for intermediate and large wind farms. *European Wind Energy Conference and Exhibition,* Milan, May 2007 (poster). 8pp.

2. Barthelmie, R.J., Schepers, J.G., van der Pijl, S., Rathmann, O., Frandsen, S.T., Cabezon, D., Politis, E., Prospathopoulos, J., Rados, K.,. Hansen, K., Schlez, W., Phillips, J. and Neubert, A. 2007: Flow and wakes in complex terrain and offshore: model development and verification in UPWIND. *European Wind Energy Conference and Exhibition,* Milan, May 2007 (poster). 10pp.

3. Barthelmie, R.J., Rathmann, O., Frandsen, S.T., Hansen, K., Politis, E., Prospathopoulos, J., Rados, K., Cabezon, D., Schlez, W., Phillips, J., Neubert, A., Schepers, J.G. and van der Piljl, S., Rados 2007: Modelling and measurements of wakes in large offshore wind farms, *Conference on the science of making torque from wind*, Danish Technical University, August 2007. 8 pp. Journal of Physics Conference Series, Vol. 75, 012049.

4. Barthelmie, R.J., E.S. Politis, Prospathopoulos, J., Hansen, K.S., Rados, K.,' Frandsen, S.T., Rathmann, Schlez, W., Phillips, J., Schepers, G. and van der Pijl, S. and Cabezón, D. 2007: Wakes in large offshore wind farms; model evaluation in Upwind. *European Offshore Wind conference*, Berlin, December 2007.

5. Barthelmie, R.J., Frandsen, S.T., Rathmann, O., Hansen, K., Politis, E.S., Propspathpoulos, J., Hansen, Cabezón, D. , Rados, K., van der Pijl, S. and Schepers, G., Schlez, W., Phillips, J. and Neubert, A., 2008: Flow and wakes in large wind farmsin complex terrain and offshore. *European Wind Energy Association Conference*, Brussels, March 2008 (Scientific track).

6. J. M. Prospathopoulos, E. S Politis and P. K. Chaviaropoulos : Modelling Wind Turbine Wakes in Complex Terrain. *European Wind Energy Association Conference*, Brussels, March 2008. (Scientific track).

7. Barthelmie, R.J., Frandsen, S.T., Rathmann, O., Politis, E., Propspathpoulos, J., Rados, K., Hansen, K., Cabezon, D., Schlez, W., Phillips, J., Neubert, A., van der Pijl, S. and Schepers, G. 2008: Flow and wakes in large wind farms in complex terrain and offshore. *American Wind Energy Association Conference*, Houston, Texas, June 2008.

8. Barthelmie, R.J. Politis, E., Prospathopoulos, J., Frandsen, S.T., Rathmann, O., Hansen, K., van der Pijl, S., Schepers, G., Rados, K., Cabezón, D., Schlez, W., Phillips, J., Neubert, A. 2008: Power losses due to wakes in large wind farms, *World Renewable Energy Congress X*, Glasgow, July 2008.

9. Rados, K.G., Prospathopoulos, J.M., Stefanatos, N.Ch., Politis, E.S., Chaviaropoulos, P.K. and Zervos, A. 2009: CFD Modeling Issues of Wind Turbine Wakes under Stable Atmospheric Conditions, *European Wind Energy Conference, Marseilles*, March 2009 (Poster).

10. Barthelmie, R.J., Hansen, K., Frandsen, S.T., Rathmann, O., Jensen, L.E., Neckelmann, S., Schlez, W., Rados, K. and Schepers, J.G. 2009: Modelling the impact of wakes on power output at Nysted and Horns Rev. *European Wind Energy Conference and Exhibition 2009*, Marseilles, March 2009.

11. Schlez, W., Neubert, A. and Prakesh, C. 2009: New developments in large wind farm modelling. *European Wind Energy Conference and Exhibition 2009*, Marseilles, March 2009 (Poster).

12. Cabezón D., Sanz J., Martí I., Crespo A. 2009: CFD modelling of the interaction between the Surface Boundary Layer and rotor wake. Comparison of results obtained with different turbulence models and mesh strategies. *European Wind Energy Conference and Exhibition 2009*, Marseille, March 2009.

13. Ott, S. 2009. Applying flow models of different complexity for estimation of wind turbine wakes. *European Wind Energy Conference and Exhibition 2009*, Marseille, March 2009 (Poster).

14. Rathmann, O. 2009: A fast parameterized wake-model for large wind farms. *European Wind Energy Conference and Exhibition 2009*, Marseille, March 2009 (Poster).

15. Barthelmie, R.J., Frandsen, S.T., Hansen, K., Schepers, J.G., Rados, K., Schlez, W., Neubert, A., Jensen, L.E. and Neckelmann, S. 2009: Modelling the impact of wakes on power output in large offshore wind farms. *Offshore Wind Energy in Mediterranean and Other European Seas 2009*, Brindisi, May 2009, 12 pp.

16. Prospathopoulos, J., Politis, E.P., Chaviaropoulos, P.K., Rados, K.G. Rados, Schepers, G.S. Cabezon-Martinez, D., Hansen, K.S. and Barthelmie, R.J. 2010: CFD modelling of wind farms in complex terrain. *European Wind Energy Conference*, Warsaw, April 2010, 9 pp.

17. Cabezón, D., Hansen, K. and Barthelmie, R.J 2010: Analysis and validation of CFD wind farm models in complex terrain. Effects induced by topography and wind turbines. *European Wind Energy Conference*, Warsaw, April 2010, 7pp.

18. Rathmann, O., Frandsen, S. and Nielsen, M. 2010: Wake decay constant for the infinite turbine array. *European Wind Energy Conference*, Warsaw, April 2010, 9pp.

19. J. Phillips, S. Cox , A Henderson, J Gill "Wake effects within and between large wind projects: The challenge of scale, density and neighbours – onshore and offshore", EWEC 2010, Warsaw, Poland.

20. A Henderson, J Clayton, A Neubert, W Schlez, "Impact of Neighbouring Wind Farm Wakes on Energy Yield of Offshore Wind Farms", DEWEK2010 Bremen, Germany.

21. Cabezón, D., Hansen, K. and Barthelmie, R.J 2010: Linearity analysis of wake effects induced by complex terrain and wind turbines through CFD wind farm models. *Fifth European Conference on Computational Fluid Dynamics, ECCOMAS CFD 2010,* Lisbon, June 2010. (Submitted).

22. Prospathopoulos, J., Cabezón, D., Politis, E.P., Chaviaropoulos, P.K., Rados, K.G., Schepers, G.S., Hansen, K.S. and Barthelmie, R.J. 2010: Simulation of wind farms in flat and complex terrain using CFD, The Science of Making Torque from Wind, Crete, June 2010. 12 pp.

23. Hansen, K.S., Barthelmie, R.J., Jensen, L.E. and Sommer, A. 2010: Simulation of wind farms in flat and complex terrain using CFD, The Science of Making Torque from Wind, Crete, June 2010. 6 pp.

Presentations or posters (without proceedings).

1. Jørgensen, H.E., Rathmann, O., Frandsen, S.T., Barthelmie, R.J., Badger, J., Ott, S., Rethore, P.E., Larsen, S.E. and Jensen, L.E. 2008: The making of a second generation wind farm efficiency model-complex. *European Wind Energy Association Conference*, Brussels, March 2008. (Scientific track)

2. Barthelmie, R.J., Frandsen, S.T., Rathmann, O., Hansen, K., Sørensen, J.N., Schepers, J.G., van der Pijl, S., Rados, K., Politis, E., Philips, J. and I. Marti and D. Cabezon 2007: Power losses from wakes in large offshore wind farms. ERE1-1FR2P-0281. European Geosciences Union Annual *Meeting*, Vienna, 15-20 April 2007 (poster).

3. Barthelmie, R.J., Frandsen, S.T., Rathmann, O., Hansen, K., Cabezon, D., Politis, E., Prospathpoulos, J., Rados, K., van der Pijl, S. and Schepers, G., Schlez, W., Phillips, J., Neubert, A. 2008: Wake modelling and measurements in Upwind. *European Geophysical Union Annual Conference*, Vienna, April 2008. (Poster).

4. Barthelmie, R.J. Optimising wind farm layouts. WIndiana, Indianapolis, June 17-18 2008. (Poster).

5. Barthelmie, R.J., Pryor, S.C., Frandsen, S.T., Hansen, K., Schepers, J.G., Rados, K., Schlez, W., Neubert, A., Jensen, L.E. and Neckelmann, S. 2009: Improved modelling of power output in large offshore wind farms based on data from Nysted and Horns Rev. *European Offshore Conference 2009*, Stockholm, 14-16 September 2009.

6. Barthelmie, R.J., Frandsen, S.T. and Pryor, S.C. 2009: Energy dynamics of an infinitely large wind farm. *European Offshore Conference 2009*, Stockholm, 14-16 September 2009 (Poster).

7. Barthelmie, R.J., Frandsen, S.T., Hansen, K., Schepers, J.G., Rados, K., Schlez, W., Neubert, A., Jensen, L.E. and Neckelmann, S. 2009: Modelling the impact of wakes on power output in large offshore wind farms. *EUROMECH 2009 Colloquium 508 on Wind Turbine Wakes*, Madrid, October 2009.

8. J. M. Prospathopoulos, E. S. Politis, K. G. Rados and P. K. Chaviaropoulos, 2009: Enhanced CFD Modelling of Wind Turbine Wakes, *EUROMECH Colloquium 508 on Wind Turbine Wakes*, Madrid, October 2009.

9. Barthelmie, R.J., Moriarty, P. and Frandsen, S.T. 2009: Universal benchmarks for wind turbine wake and wind farm models. *European Wind Energy Conference*, Warsaw, March 2010 (Poster).

Appendix 1: Deliverable 8.1 Data

Project funded by the European Commission under the 6th (EC) RTD Framework Programme (2002- 2006) within the framework of the specific research and technological development programme "Integrating and strengthening the European Research Area"

Project UpWind

Contract No.:
019945 (SES6)

"Integrated Wind Turbine Design"

Wp8: Flow

Deliverable D8.1 Data

AUTHOR:	Kurt S. Hansen
AFFILIATION:	Technical University of Denmark
ADDRESS:	Nils Koppels Allé, B403-DTU, DK-2800 Lyngby
TEL.:	+45 4525 4318
EMAIL:	ksh@mek.dtu.dk
FURTHER AUTHORS:	R.Barthelmie
REVIEWER:	WP8 Project members
APPROVER:	

Document Information

DOCUMENT TYPE	Deliverable D8.1
DOCUMENT NAME:	WP8Flow8.1D1.doc
REVISION:	
REV.DATE:	
CLASSIFICATION:	
STATUS:	

Abstract: Three wind farm flow cases with turbine different spacing have been defined for validating the wake deficit calculations inside an offshore wind farm. The measured wake deficit is determined for a number of flow directions in the 160MW Horns Rev wind farm.

Contents

STATUS, CONFIDENTIALITY AND ACCESSIBILITY									
Status				**Confidentiality**				**Accessibility**	
S0	Approved/Released			**R0**	General public			Private web site	
S1	Reviewed			**R1**	Restricted to project members			Public web site	
S2	Pending for review			**R2**	Restricted to European. Commission			Paper copy	
S3	Draft for commends			**R3**	Restricted to WP members + PL	**x**			
S4	Under preparation	**x**		**R4**	Restricted to Task members +WPL+PL				

PL: *Project leader* **WPL:** *Work package leader* **TL:** *Task leader*

1 Introduction

It is evident that wake or wind farm models have not been evaluated for very large wind farms. Since the combination of single wakes is the current approach to modeling wakes within offshore wind farms, there is major uncertainty in these predictions of wake interactions. For very large wind farms single wake or local momentum balance approaches may be insufficient, since the wind farm must be expected to interact with the wind climate, giving rise to a complicated flow pattern. One way of viewing/simplifying the problem is that on the larger scale the wind farm adds to the terrain surface roughness and thus resulting in a wind speed reduction on top of the reduction stemming from the individual wakes. i.e. determining the extent of the macro-scale effect. Presently, no solid empirical information is available to assess accuracy of the industry standards in software for GW-size wind farms. However, it is known that ignoring the large-scale effect (interaction with the boundary-layer) will result in optimistic estimates of the necessary separation distance for large wind farms. Present engineering codes suggest that 1-2km of separation will allow the flow to regenerate whereas roughness change models indicate that an order of magnitude larger separation is needed for the wind speed to recover.

This document defines three basic offshore flow cases, which can be identified from existing wind farm measurements, and used for validation modeled wakes within offshore wind farms.

1.1 Types of measurements

There are essentially two types of measurements; meteorological and wind farm data. Some wind farms retain the meteorological mast(s) that was/were established for the resource determination and if these data are available in addition to wind farm data it is an added bonus particularly with regard to questions such as ‘What is the wind farm power curve?’ (depending on the mast location). At few offshore wind farms such as Vindeby, Bockstigen, Horns Rev and Nysted one or more meteorological masts were added after construction to aid research.

Meteorological data can also be divided into two types – mast and remotely sensed data. Examples of wind farms supported by meteorological mast data include Nørrkær Enge, Vindeby, Horns Rev and Nysted. The advantage of meteorological mast data is that it is usually available for a long period, it is typically accurate (although this can depend on the mast structure) and wind speed, direction and turbulence profiles to hub-height are usually available at a good time resolution and with high data capture. The most obvious disadvantage is that the location of the measurements is fixed so from a wake perspective the wake distance is fixed. However, wake analysis has to be made for specific directional sectors and the wake distances can vary according to the layout of the wind farm and the position of the mast. Measurements are rarely made above hub-height.

Remote sensing is providing additional types of information for use in wind energy. We exclude here satellite data although these have been used both for wind resource and for wakes estimation. Both sodar and doppler lidar are able to measure wind speed profiles both beyond and above hub-height and may be particularly useful offshore due to the expense of erecting tall meteorological masts in this environment. Data from both instruments requires additional processing and maybe subject to some accuracy or operational limitations but progress has been made to the point where Doppler lidar in particular may become a standard instrument. As yet, there have been limited studies using sodar or lidar in wake studies. Obviously for wake studies in large wind farms, wind farm data are needed. Parameters required would typically be the power output, nacelle direction and yaw misalignment and additional operational information such as a status signal. These data are routinely collected using Supervisory Control And Data Acquisition (SCADA) systems although storage and retrieval of these data for research purposes may be a time consuming process. A more significant issue is that all wind farm data are typically confidential and developers are reticent to share raw data. This is a big issue in model evaluation exercises where data are necessary and also by the nature of the exercise many different groups are involved. Nevertheless it is clear that access to data is critical at this point while the wind farm model evaluation for more challenging environments is conducted.

1.2 Issues comparing models and measurements

There are some major issues in wind farm model validation studies which will be discussed below. As stated above we concentrate here on power loss modelling which should encompass the whole range of wind speeds and directions and we also consider that the range of wind farm/wake model extends from engineering through to full CFD models. In general, computing requirements for CFD models means we are restricted to examining a number of specific wind speed and direction cases and only a moderate number of turbines rather than wind farms with ~100 turbines which can easily be done by WindFarmer and WAsP. On the other hand it can be difficult to extract reasonable simulations from some of the wind farm models for very specific cases. For example, WAsP relies on having a Weibull fit to wind speed distributions and fairly large directional sectors (30°). Therefore for specific wind speeds and narrow directional bins models like WAsP are never going to produce very exact solutions because they are being used beyond their operational windows. In addition to this there are a number of specific issues:

- Establishing the freestream flow. The major issues in determining the freestream flow are the displacement of the measurement mast from the array (assuming there is a mast), adjustments in the flow over this distance especially in coastal areas and differences in height between the measurement and the turbine hub-height. If there is no mast or the mast is in the wake of turbines or subject to coastal flow then the turbine(s) in the freestream flow may be used. If power measurements are used to determine wind speed they will be subject to any errors in the site specific power curve.
- Wind direction, nacelle direction and yaw misalignment. Because of the difficulty in establishing true north when erecting wind vanes (especially offshore where landmarks may not be determinable) it can be difficult to establish a true freestream direction. Even a well maintained wind vane may have a bias of up to 5° and it is important to understand this because the total width of a wake may be of the order 10-15° at typical turbine spacing. In a large wind farm, each turbine may have a separate bias on the direction, which is very difficult to determine. Analysis must be undertaken to calibrate the maximum wake direction to within 1° and to check for bias of the yaw angle on each wind turbine in the array.
- If there is a gradient of wind speeds across the wind farm as there may be e.g. in coastal areas, near a forest or caused by topography these variations will need to be accounted for before wake calculations are undertaken.
- In terms of modelling wakes both the power curve and thrust coefficients must be known but these will vary according to the specific environment. A power curve must be calculated for the site. For modelling, the question of whether the thrust coefficient should be set to one value for the wind farm or at each individual turbine in each simulation is still an open one. The state-of-the-art is to validate the individual power and pitch curves with reference to the

nacelle anemometer, which seems to be a rather robust method to determine changes in the system setup.

- Comparing the modelled standard deviation of power losses in a row with the measured standard deviation raises a number of issues. The two most important are ensuring that the time averaging is equivalent between models and measurements and taking into account that there will be natural fluctuations in the wind speed and direction in any period. Models are typically run for specific directions but it may be necessary to include the standard deviation of the wind direction in the model simulations.
- In the large wind farm context the time scale of wake transport must be considered. A large wind farm with 100 turbines in a 10 by 10 array with an 80 m diameter rotor and a space of 7 rotor diameters has a length of nearly 6 km. At a wind speed of 8 m/s the travel time through the array is more than 10 minutes. As mentioned above the wind direction will be subject to natural fluctuations in addition to possible wake deflection but there will also be natural variations in the wind speed over this time scale.
- Determining turbulence intensity and stability may be critical. Turbulence intensity is a key parameter in many models. Using either mast data to determine this information or deriving it from turbine data is subject to fairly large errors for the reasons discussed above and because the accuracy of temperature measurements used to derive stability parameters is often inadequate.

2 Horns Rev Wind farm measurements

2.1 Definition of offshore wind farm flow cases

Due to an agreement with DONG Energy A/S (formerly ELSAM Engineering A/S) it has been possible to obtain access to one year of offshore recordings from the Horns Rev wind farm recorded during 2005. The dataset from Horns Rev offshore wind farm includes 10-minute mean values of power, nacelle position, pitch angle and yaw misalignment from each wind turbine together with wind speeds and wind directions on the near by three metrological mast. The data set represents a full operational year with very high park availability.

During the WP8 kick-off meeting is was decided to define three basic flow cases according to the discussions listed in the minutes [2].

The flow cases represent three different wind turbine spacing, which are a fundamental parameter when validating the wake deficit. The spacing, which is determined by the wind farm layout, cannot be changed, is defining three basic flow cases with uniform inflow representing a long velocity fetch distance:

Case	Spacing	Wind direction	V_{hub}
1:	7.0×D	270 deg.	6 ± 0.5, 8 ± 0.5 & 10 ± 0.5 m/s
2:	9.4×D	221 deg.	6 ± 0.5, 8 ± 0.5 & 10 ± 0.5 m/s
3:	10.4×D	312 deg.	6 ± 0.5, 8 ± 0.5 & 10 ± 0.5 m/s

The downwind power deficit and the derived speed deficit are determined for each flow case during different flow conditions e.g. atmospheric stability classes, wind directional sectors and wind speed bins in the following chapter.

2.2 Park layout

Horns Rev Wind Farm consists of an 8 row (east to west) by 10 column (north to south) matrix of 80 turbines. The vertical columns are aligned approximately 7.2° West of North - forming a parallelogram. The spacing between turbines in both the rows and columns is 7D (=560m). The spacing between turbines in the south-west to north-east diagonal (221°) is 9.4D (appr.750m) and in the north-west diagonal (312°) is 10.4D (appr.840m) as indicated on Figure 1. Further information about the park layout is given in [1] and the location of the three meteorological masts outside the park is shown in Appendix A.

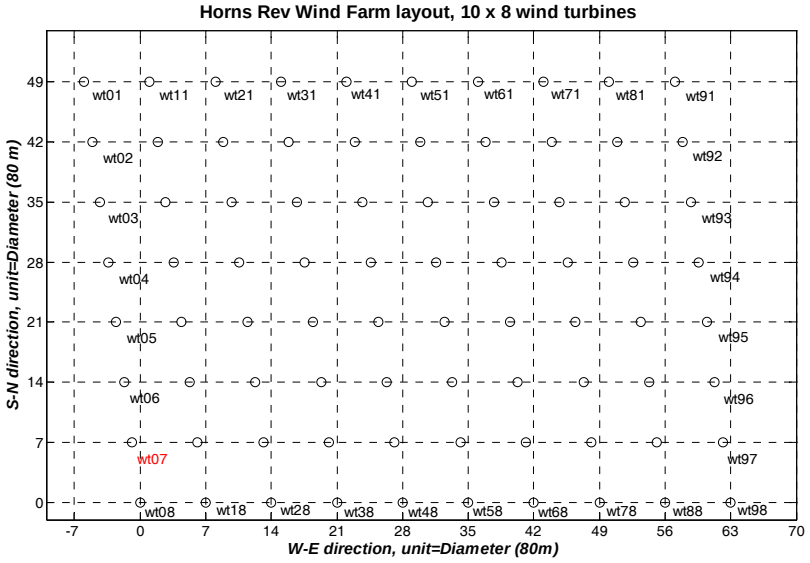

Figure 1: Layout of Horns Rev Wind Farm, where the reference wind turbine (wt07) is located in the SW corner of the park.

2.3 Data screening

The Horns Rev data set contains a number of representative 10-minute statistical values from each wind turbine e.g. electrical power, pitch angle, wind speed and direction measured on nacelle, nacelle position and the turbine run counter.

All the measurements have been validated according to a proper power signal level compared to nacelle wind speed and mean pitch angle. Furthermore all events like idling, start and stop sequences and reduced power levels have been marked with a index, which has been included the selection of measurements for the flow cases.

The meteorological properties have been recorded and stored as 10 minute mean values from 3 masts near the wind turbines as indicated in [3] and Appendix A. All measurements are checked during inter-comparison and outliners have been marked with a (quality) index.

2.3.1 Atmospheric stability.

The atmospheric stability at Horns Rev during 2005 is based on the difference between water and air temperatures at the wake mast M7 located between park and land due to good signal availability. The Richardson number (*Ri*) is calculated according to (1)

$$Ri = 9.81/(273.15+T_u)\times((T_u - T_l)/\Delta h_T)/sqr((V_{70} - V_{20})/\Delta h_V) \qquad (1)$$

Sensor	Air/water	Air/air
T_u - degC	h = 64 m (asl)	h = 64 m
T_l - degC	h = -3 m (bsl)	h = 64 m
V_{70}	h = 70 m	h = 70 m
V_{16}	h = 20 m	h = 20 m
z'	31 m	37.5 m

Note the wake situations with reduced wind speed at hub height have not been eliminated.
The atmospheric stability (z/L) with a reference height z' is defined according to:

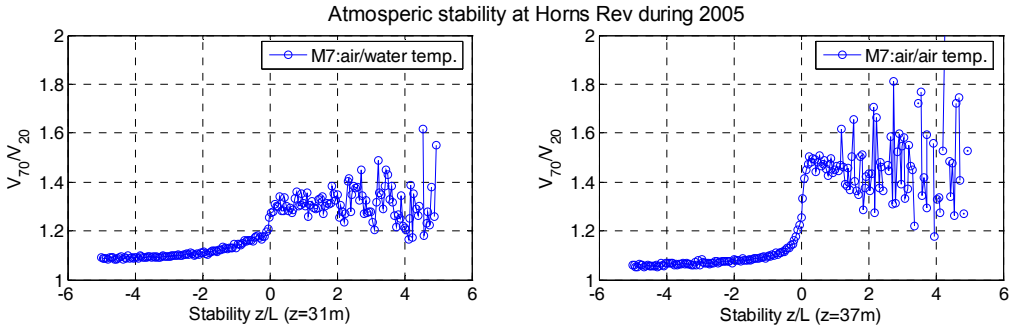

Figure 2: Distribution of atmospheric stability measured at Horns Rev during 2005; a) air/water difference and b) air/air temperature difference.

The available periods covers 8.606 hours during 2005, as shown on Figure 2, are classified in stability classes as listed in Table 1. The main part of wind farm measurements used the analysis have been recorded during (slightly) unstable atmospheric stratification (-12 <z'/L <-2) with reference to air/air stability.

Table 1: Stability classes for Horns Rev measurements during 2005, based on air/air temperature measurements.

Very unstable; z/L < -12	1920 hours
Unstable, -12< z/L<-2	1881 hours
Near neutral, -2 < z/L < +2	2618 hours
Stable; z/L> 2	2187 hours
Total	8606 hours

While all temperatures from Horns rev are recorded with absolute thermometers and undocumented calibration and low resolution, the resolution of the temperature difference is low. All analysis performed on the Horns Rev measurements in the following chapters are based on the air/air stability.

2.3.2 Power curves

The electrical power curve has been determined for 5 turbines, during unstable conditions and in two distinct, free sectors. The main purpose of validating the power curves for a number of turbines with free undisturbed inflow is to determine a reference power curve. The reference power curve is based on the curves for wind turbine wt01, wt07, wt09, wt95 and wt98 respectively.

1) Eletrical power from wind turbine wt01, wt05 & wt07 combined with wind speed from mast M2, 67 m, from a 45 degree western sector.
2) Eletrical power from wind turbine wt95 & wt97 combined with the wind speed from mast M7, 70 m, from a 45 degree eastern sector.

The variation between the power curves on Figure 3 is small and this result in a robust derived [mean] curve, especially in the area of interest between 5.5 – 10.5 m/s. The reference power curve values (below rated power) are listed in Table 3 and reflect operation with a pitch angle of approximately -1°.

The reference power curve is assumed to be representative for each of the 80 wind turbines in the wind farm.

Table 2: V80 power and thrust curves from [3].

wind speed	power,kW	thrust coeff.
4	66.6	0.818
5	154	0.806
6	282	0.804
7	460	0.805
8	696	0.806
9	996	0.807
10	1341	0.793
11	1661	0.739
12	1866	0.709
13	1958	0.409
14	1988	0.314
15	1997	0.249
16	1999	0.202
17	2000	0.167
18	2000	0.140
19	2000	0.119
20	2000	0.102
21	2000	0.088
22	2000	0.077
23	2000	0.067
24	2000	0.060
25	2000	0.053

Please note that the power and thrust coefficient curves listed in Table 2 are specific to the turbines delivered for the Horns Rev Wind farm and may not apply to V80 turbines delivered for other projects.

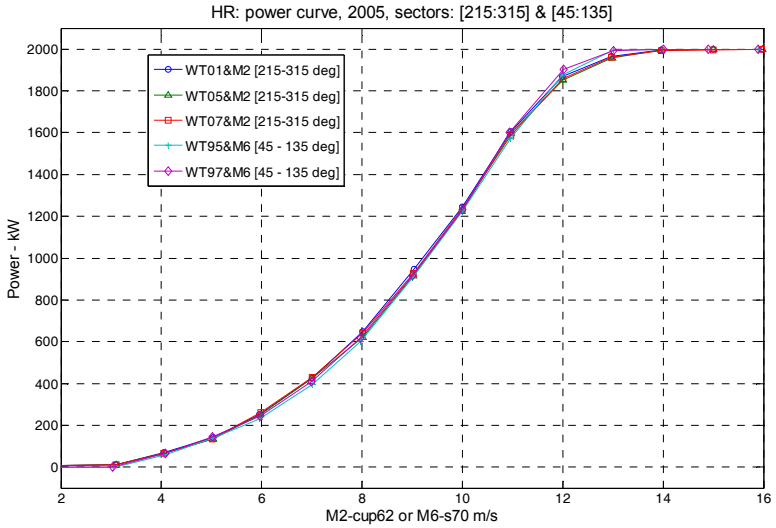

Figure 3: Power curves during unstable conditions.

Table 3: Reference power curve for V80 -
located at Horns Rev, during unstable atmospheric conditions.

V_{hub} (m/s)	Power (kW)
5.5	184.8
6.5	324.8
7.5	511.7
8.5	751.0
9.5	1048.4
10.5	1409.5

2.3.3 Definition of reference wind direction

The wind direction is measured both at the three masts and as the nacelle position of each individual wind turbine. According to [1], it is rather difficult to use one of these values and based on this reference it was decided to use an upstream wind turbine as reference. The nacelle position of wt07 has been used as a reference with a mean offset correction of 21 degrees.

2.3.4 Methodology

The data query has been performed on the 10 minute mean electrical power values where:

- $5.5<V_{hub}\leq 6.5$ m/s equals 185<El.Power≤325 kW for the upwind wind turbine
- $7.5<V_{hub}\leq 8.5$ m/s equals 510<El.Power≤750 kW for the upwind wind turbine
- $9.5<V_{hub}\leq 10.5$ m/s equals 1050<El.Power≤1410 kW for the upwind wind turbine

The resulting mean power output from both upwind and downwind turbines are transformed to wind speed by use of the reference power curve given in Table 3.

2.3.5 Conditions used for the data selection

A number of predefined conditions have been applied to the data search criteria for each of the three flow cases defined in section 2.1:

1. The power from the upwind column of wind turbines have been used to determine the wind speed level, while there is no free, undisturbed wind speed signals available nearby.
2. The atmospheric stability (z/L) is based on only an air/air temperature difference, measured at wake mast M7, due to lack of valid observations from other masts.
3. The directional bin size is 2 degrees, with reference to the nacelle direction wt07.
4. The number of required, online wind turbines in each row has been limited to 8 (e.g. wt0x, wt1x, wt2x, wt3x, wt4x, wt5x, wt6x & wt7x), where x is the row number.
5. The number of online wind turbines in each diagonal is 5 (e.g. wt07, wt16, wt25, wt34 & wt43).

2.3.6 Turbulence intensity

Unfortunately the turbulence intensity measured at hub height on a free, undistrubed mast (M2), was not available during the period. The mean turbulence intensity measured during 2 previous years has been extracted, corresponding to each flow case and wind speed bin, as shown on Figure 4, but the turbulence intensity is not sorted according to atmospheric stability.

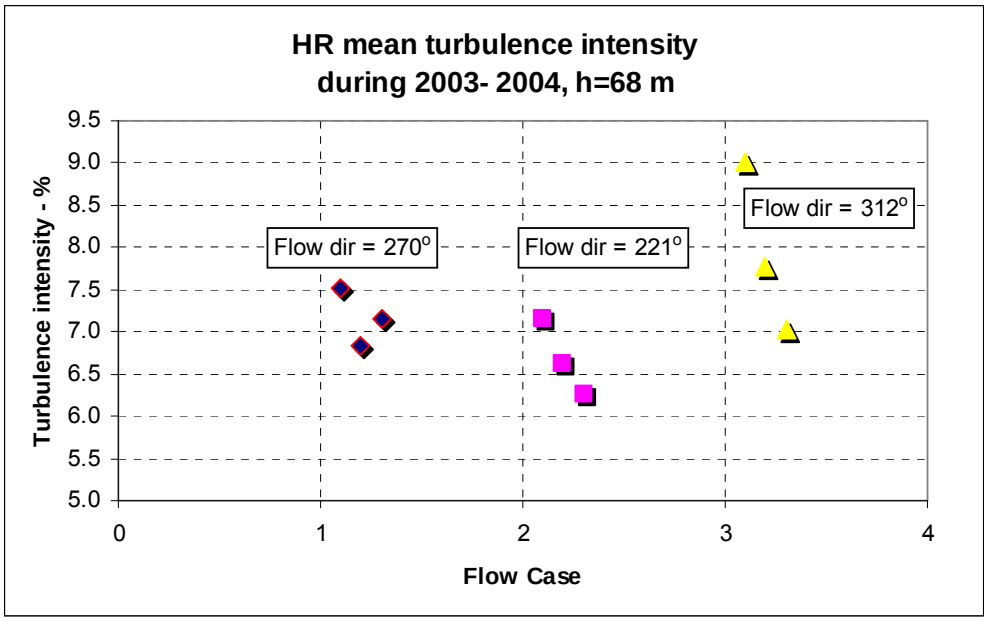

Figure 4: Turbulence intensity at Horns Rev as function of wind speed bin and wind direction recorded during 2003 - 2004.

2.4 Case 1: flow direction 270 degrees with a 7D spacing.

The flow direction 270 degrees is along rows of 10 wind turbines with 7D spacing, but only 8 upwind turbines in each row have been included in the wake deficit determination.

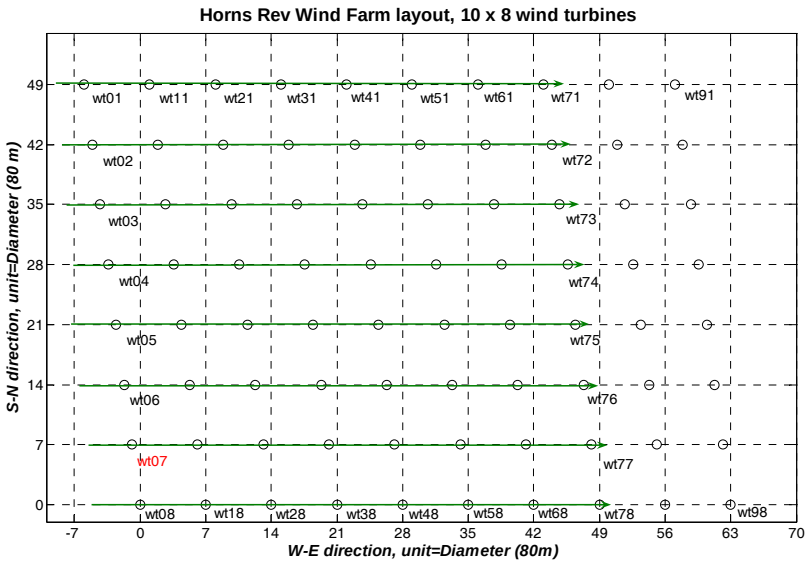

Figure 5: Flow direction in case 1; 8x8 rows of online turbines are used in this flow case, with reference to turbine wt07.

Table 4: Definition of Case 1.

Case	Speed	Direction	Stratification	Valid periods
1.6.1	6 ±0.5 m/s	270°±1	-12<z/L≤-2	8/row
1.6.2	6 ±0.5 m/s	270°±5	z/L≤-12	8/row
1.6.3	6 ±0.5 m/s	270°±5	-12<z/L≤-2	45/row
1.6.4	6 ±0.5 m/s	270°±5	-2<z/L≤+2	15/row
1.6.5	6 ±0.5 m/s	270°±5	2<z/L	6/row
1.6.6	6 ±0.5 m/s	270°±10	-12<z/L≤-2	64/row
1.6.7	6 ±0.5 m/s	270°±15	-12<z/L≤-2	120/row
1.8.1	8 ±0.5 m/s	270°±1	-12<z/L≤-2	8.6/row
1.8.2	8 ±0.5 m/s	270°±5	-12<z/L≤-2	54/row
1.8.3	8 ±0.5 m/s	270°±10	-12<z/L≤-2	113/row
1.8.4	8 ±0.5 m/s	270°±15	-12<z/L≤-2	156/row
1.10.1	10 ±0.5 m/s	270°±1	-12<z/L≤-2	3.5/row
1.10.2	10 ±0.5 m/s	270°±5	-12<z/L≤-2	16/row
1.10.3	10 ±0.5 m/s	270°±10	-12<z/L≤-2	25/row
1.10.4	10 ±0.5 m/s	270°±15	-12<z/L≤-2	36/row

Comments: Only a limited number of available observations have been identified for each wind speed bin and stability class. Unstable and neutral stratification is dominating, as indicated on Figure 2, se Case 1.6.3 and 1.6.4. Table 4 includes 2, 10, 20 & 30 degree sector results suitable for WAsP flow

modeling. The flow deficit is presented both as a power deficit ratio and as a derived speed deficit with reference to the upwind turbine. The deficits are listed in Appendix C.

Flow profiles for case 1

Case 1.6; wind speed bin at 6 m/s results in 15 x 8 periods = 120 periods distributed on 8 rows, which corresponds to approximately 2 hour of valid measurements along each row for a 2 degree sector. The mean wind speed deficit along a row is presented as function of the distance between upwind and downwind wind turbine for each case. The error bars represents the standard deviation of the mean row deficits (8 rows).

Case 1.6.1, 1.6.3, 1.6.6 and 1.6.7 are plotted together for comparison and the deficits are listed in Appendix C.

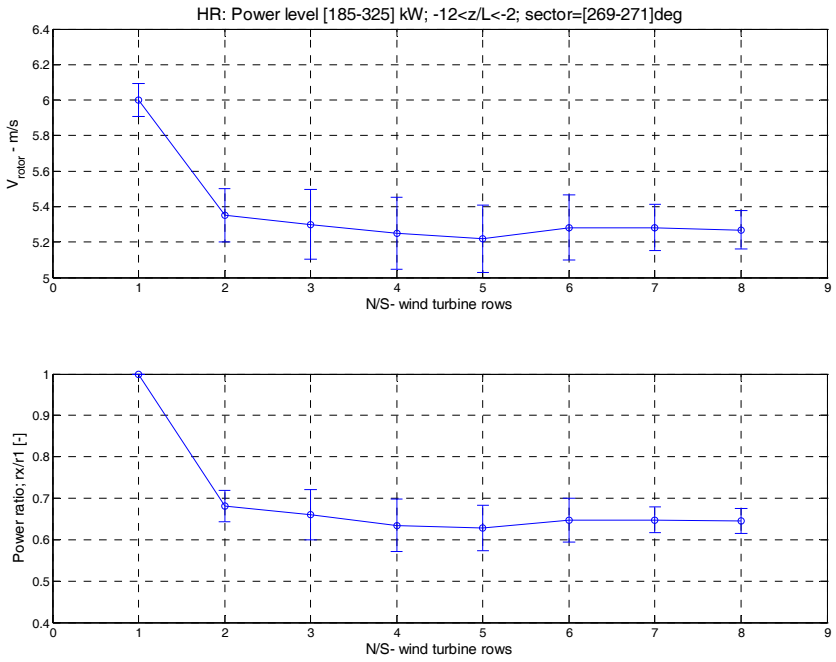

Figure 6: Case 1.6.1; Speed and power deficit at 6 m/s during unstable conditions, sector=2 deg.

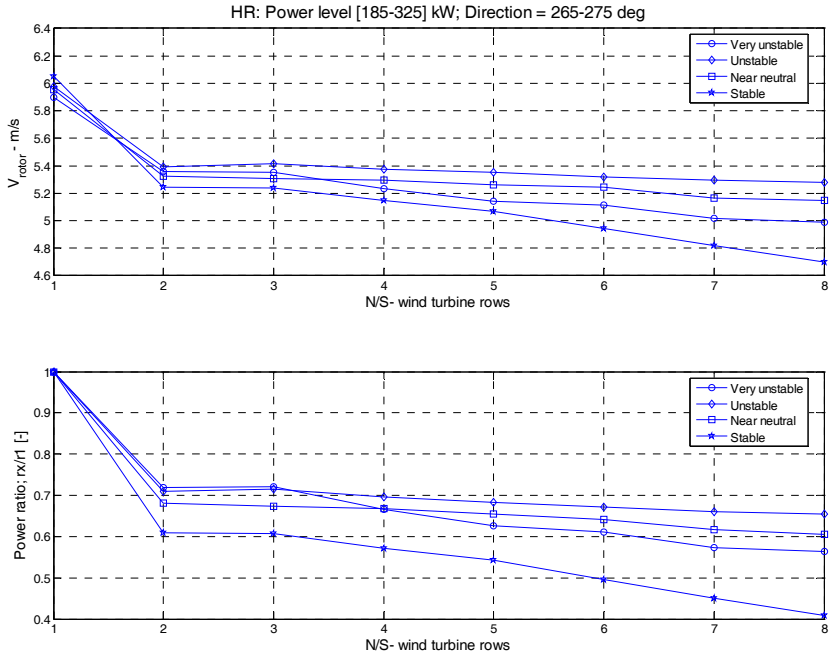

Figure 7: Speed and power deficit at 6 m/s during very unstable, unstable, neutral and stable conditions, sector=10 deg.

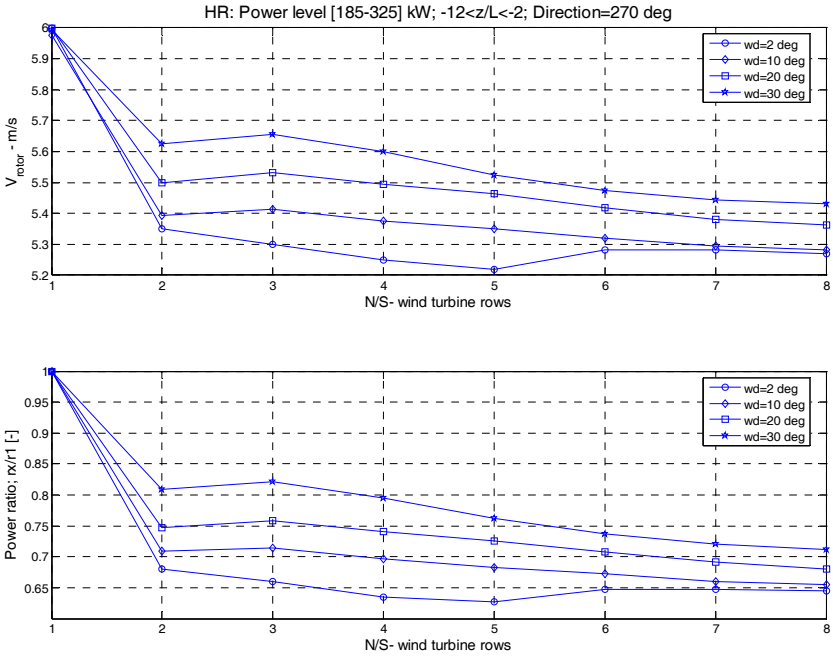

Figure 8: Speed and power deficit at 6 m/s during unstable conditions, for sectors = 2, 10, 20 & 30 deg.

Case 1.8; wind speed bin at 8 m/s results in 20 x 8 periods = 160 periods distributed on 8 rows, which corresponds to approximately 3 hour of valid measurements along each row for a 2 degree sector. The mean wind speed deficit along a row is presented as function of the distance between upwind and downwind wind turbine for each case.

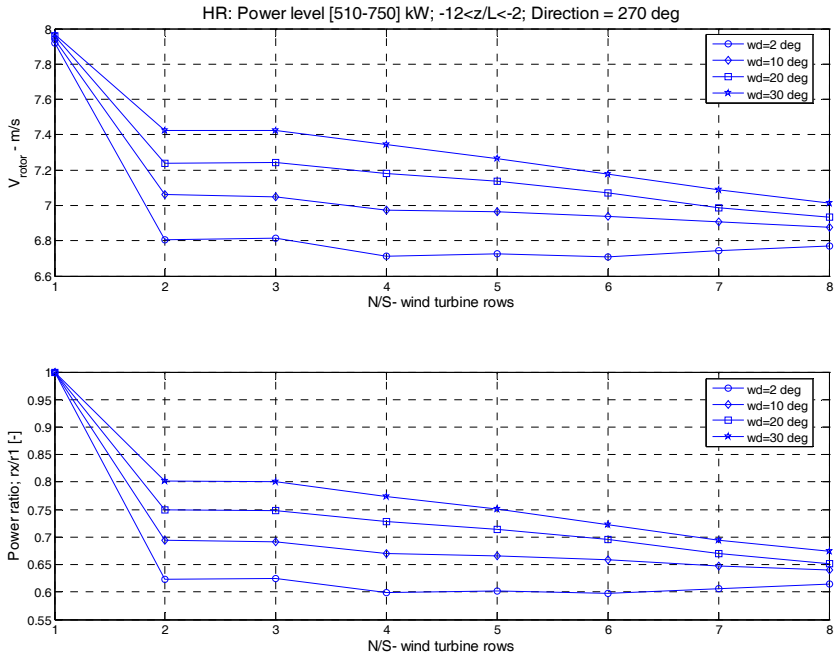

Figure 9: Speed and power deficit at 8 m/s during unstable conditions, sectors = 2, 10, 20 & 30 deg.

A detailed directional sensitivity analysis has been performed for 2 degree sector observations covering both unstable and near neutral conditions. The figure, which is shown in Appendix B, demonstrates how sensitive the speed deficit is to the "pure" wake situation (sector = 169-271 deg.).

Case 1.10; wind speed bin at 10 m/s results in 16.5 x 8 periods = 138 periods distributed on 8 rows, which corresponds to approximately 3 hours of valid measurements along each row for a 2 degree sector. The mean wind speed deficit along a row is presented as function of the distance between upwind and downwind wind turbine for each case.

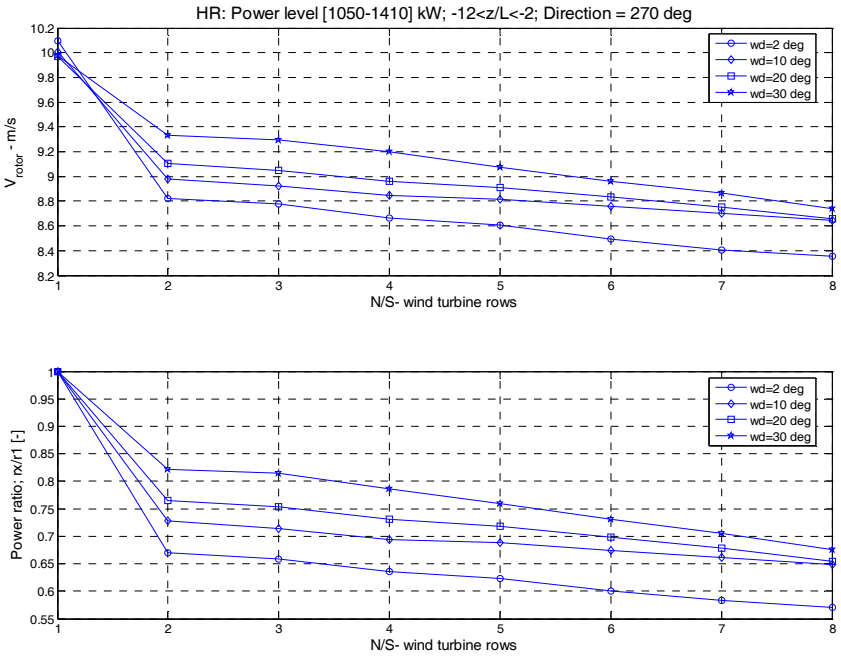

Figure 10: Speed and power deficit at 10 m/s during unstable conditions, sectors = 2, 10, 20 and 30 deg.

2.5 Case 2: flow direction 221 degrees diagonal through the wind farm with 9.4D spacing.

The flow direction 221 degrees is along rows of 5-10 wind turbines with 9.4D spacing, where 5 turbines in each row are included in the wake deficit determination.

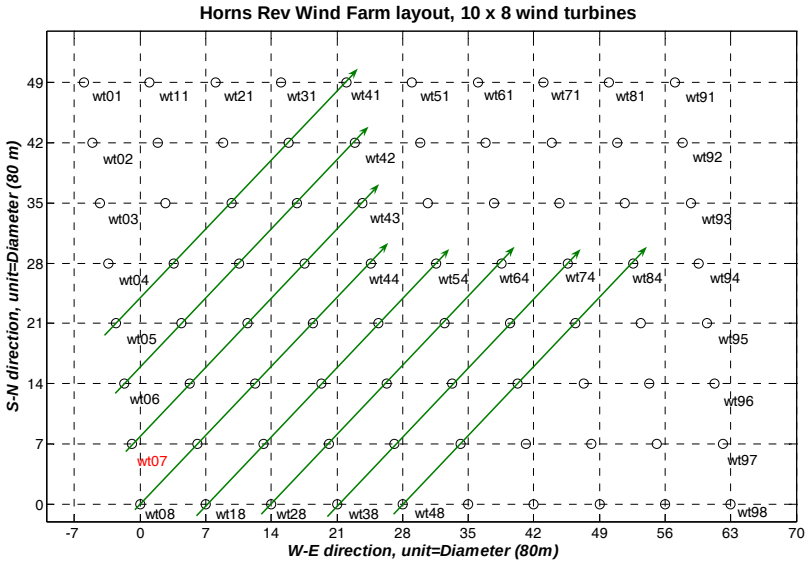

Figure 11: Flow direction in Case 2, 8x 5 rows of online turbines are used in this case, with reference to wt07.

The wake deficits determined in Case 2 is based on measurements from 8 diagonal rows each consisting of 5 wind turbines, as indicated on Figure 11.

Table 5: Definition of Case 2.

Case	Speed	Direction	Stratification	Valid periods
2.6.1	6 ±0.5 m/s	221°±1	z/L≤-12	0.6/row
2.6.2	6 ±0.5 m/s	221°±1	-12<z/L≤-2	3/row
2.6.3	6 ±0.5 m/s	221°±1	-2<z/L≤+2	5/row
2.6.4	6 ±0.5 m/s	221°±1	+2<z/L	6/row
2.6.5	6 ±0.5 m/s	221°±5	-12<z/L≤-2	18/row
2.6.6	6 ±0.5 m/s	221°±10	-12<z/L≤-2	32/row
2.6.7	6 ±0.5 m/s	221°±15	-12<z/L≤-2	49/row
2.8.1	8 ±0.5 m/s	221°±1	-12<z/L≤-2	12/row
2.8.2	8 ±0.5 m/s	221°±5	-12<z/L≤-2	48/row
2.8.3	8 ±0.5 m/s	221°±10	-12<z/L≤-2	84/row
2.8.4	8 ±0.5 m/s	221°±15	-12<z/L≤-2	106/row
2.10.1	10 ±0.5 m/s	221°±1	-12<z/L≤-2	1/row
2.10.2	10 ±0.5 m/s	221°±5	-12<z/L≤-2	4.6/row
2.10.3	10 ±0.5 m/s	221°±10	-12<z/L≤-2	8.6/row
2.10.4	10 ±0.5 m/s	221°±15	-12<z/L≤-2	16/row

Table 5 defines 2, 10, 20 and 30 degree flow sectors suitable for WAsP flow modeling and the deficits are listed in Appendix C.

Flow profiles for case 2

Case 2.6; wind speed bin at 6 m/s results in 13 x 8 periods =104 periods distributed on 8 rows, which corresponds to approximately 2 hours of valid measurements along each row for a 2 degree sector. The mean wind speed deficit along a row is presented as function of the distance between upwind and downwind wind turbine for each case.

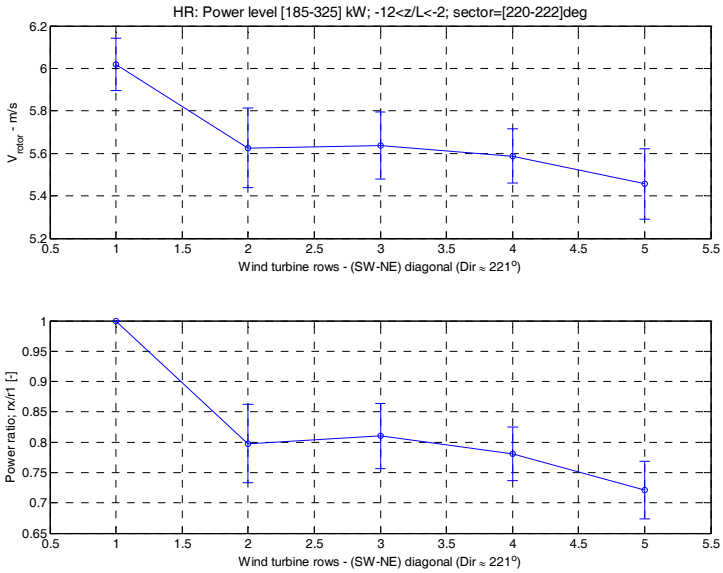

Figure 12: Case 2.6.2; Speed and power deficit at 6 m/s during unstable conditions, sector=2 deg.

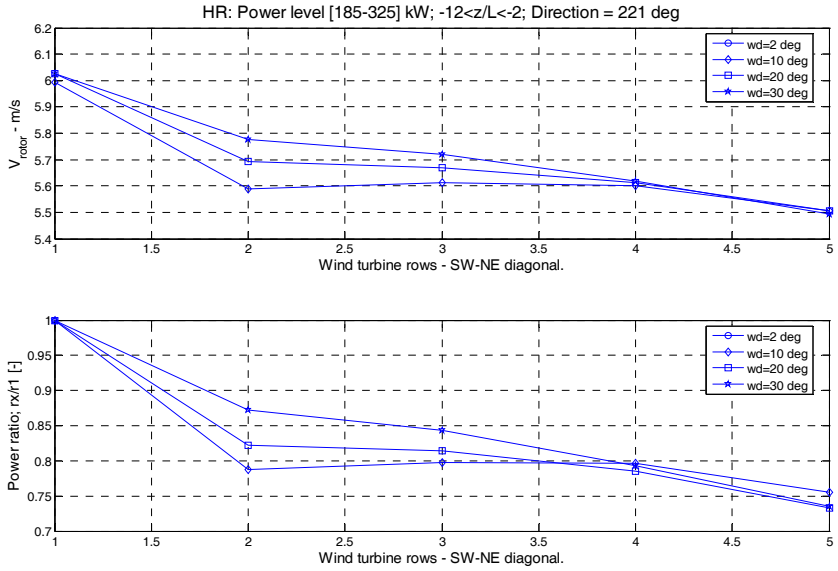

Figure 13: Speed and power deficit at 6 m/s during unstable conditions, sector=10, 20 & 30 deg.

Case 2.8; wind speed bin at 8 m/s results in 22 x 8 periods =176 periods distributed on 8 rows, which corresponds to approximately 3½ hours of valid measurements along each row for a 2 degree sector. The mean wind speed deficit along a row is presented as function of the distance between upwind and downwind wind turbine for each case.

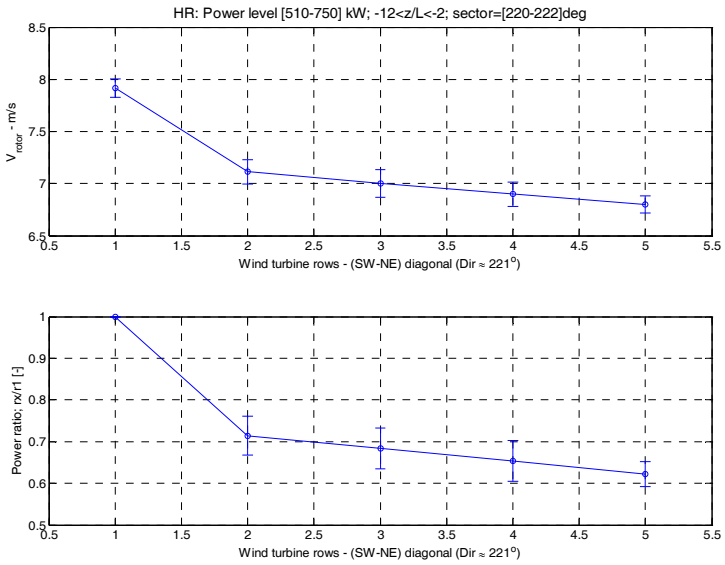

Figure 14: Case 2.8.1; Speed and power deficit at 8 m/s during unstable conditions, sector=2 deg, based on 12 periods.

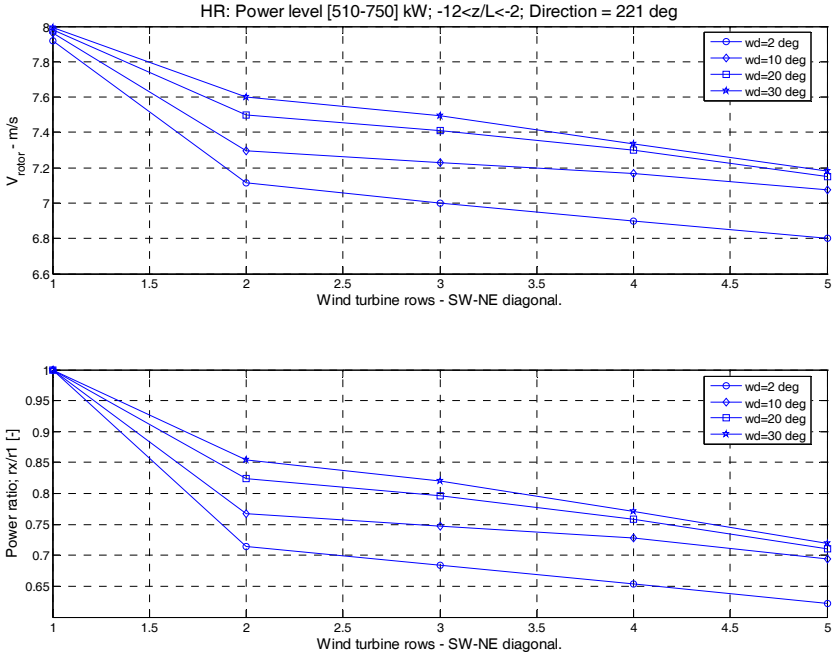

Figure 15: Speed and power deficit at 8 m/s during unstable conditions, sector= 2, 10, 20 & 30 deg.

Case 2.10; wind speed bin at 10 m/s results in 23 x 8 periods =184 periods distributed on 8 rows, which corresponds to 4 hours of valid measurements along each row for a 2 degree sector. The mean wind speed deficit along a row is presented as function of the distance between upwind and downwind wind turbine for each case.

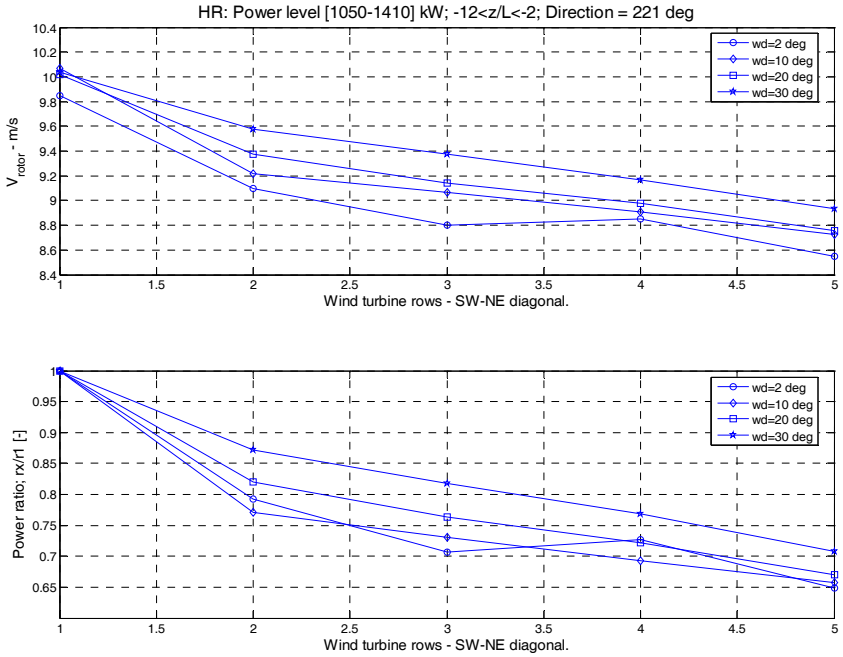

Figure 16: Speed and power deficit at 10 m/s during unstable conditions, sector=2, 10, 20 & 30 deg.

2.6 Case 3: flow direction 312 degrees with 10.4D spacing.

The flow direction 312 degrees is along a row of 5-10 wind turbines with a 10.4D spacing, where 5 turbines in each row are included in the wake deficit determination.

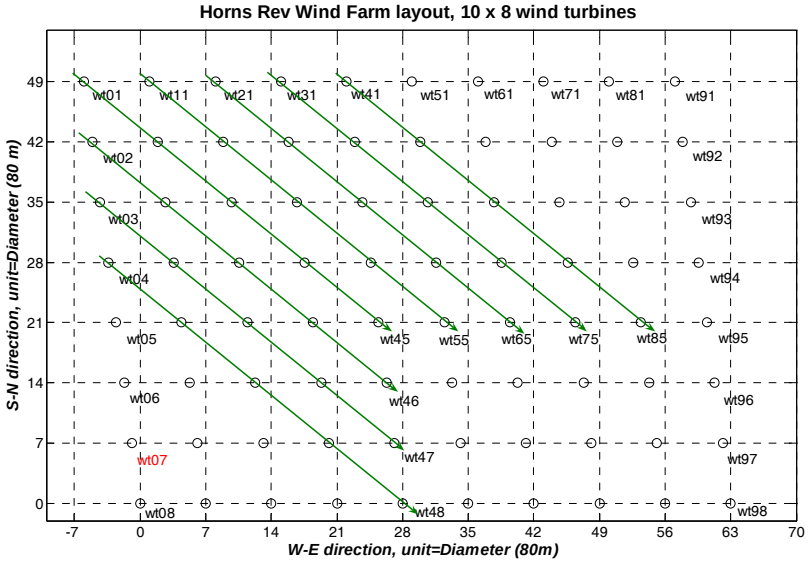

Figure 17: Flow directions used in case 2, 7x 5 online turbines are used with reference to wt07.

The wake deficits determined in Case 3 is based on measurements from 8 diagonal rows each consisting of 5 wind turbines, as indicated on Figure 17.

Table 6: Definition of Case 3.

Case	Speed	Direction	Stratification	Valid periods
3.6.1	6 ±0.5 m/s	312°±1	z/L≤-12	0/row
3.6.2	6 ±0.5 m/s	312°±1	-12<z/L≤-2	16/row
3.6.3	6 ±0.5 m/s	312°±1	-2<z/L≤2	1/row
3.6.4	6 ±0.5 m/s	312°±1	z/L>2	2/row
3.6.5	6 ±0.5 m/s	312°±5	-12<z/L≤-2	70/row
3.6.6	6 ±0.5 m/s	312°±10	-12<z/L≤-2	120/row
3.6.7	6 ±0.5 m/s	312°±15	-12<z/L≤-2	171/row
3.8.1	8 ±0.5 m/s	312°±1	-12<z/L≤-2	5/row
3.8.2	8 ±0.5 m/s	312°±5	-12<z/L≤-2	26/row
3.8.3	8 ±0.5 m/s	312°±10	-12<z/L≤-2	54/row
3.8.4	8 ±0.5 m/s	312°±15	-12<z/L≤-2	94/row
3.10.1	10 ±0.5 m/s	312°±1	-12<z/L≤-2	2/row
3.10.2	10 ±0.5 m/s	312°±5	-12<z/L≤-2	9/row
3.10.3	10 ±0.5 m/s	312°±10	-12<z/L≤-2	22/row
3.10.4	10 ±0.5 m/s	312°±15	-12<z/L≤-2	28/row

Table 6 includes 2, 10, 20 and 30 degree sector results, suitable for WAsP flow modeling and the deficits are listed in Appendix C.

Flow profiles for case 3

Case 3.6; wind speed bin at 6 m/s results in 20 x 8 periods =160 periods distributed on 8 rows, which corresponds to approximately 3 hours of valid measurements along each row for a 2 degree sector. The mean wind speed deficit along a row is presented as function of the distance between upwind and downwind wind turbine for each case.

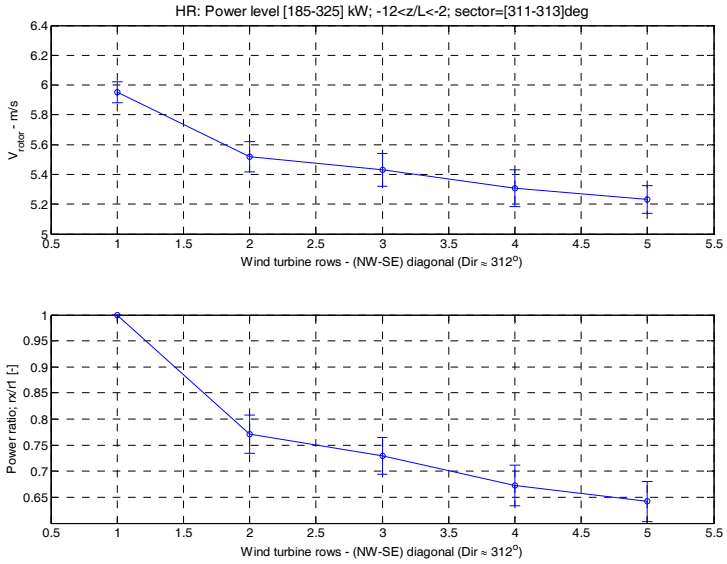

Figure 18: Case 3.6.2, Speed and power deficit at 6 m/s during unstable conditions, sector=2 deg.

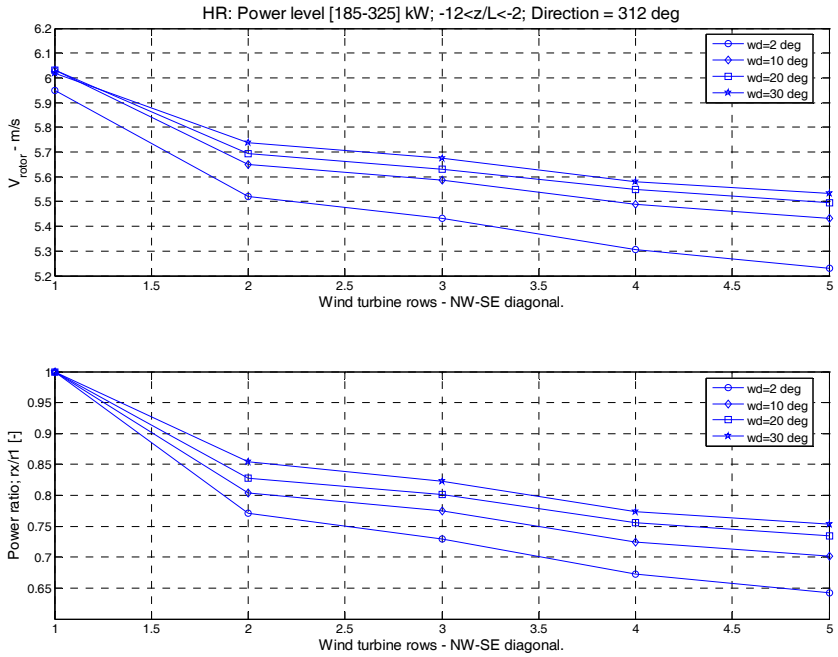

Figure 19: Speed and power deficit at 6 m/s during unstable conditions, sector = 2, 10, 20 and 30 deg.

Case 3.8; wind speed bin at 8 m/s results in 13 x 8 periods =104 periods distributed on 8 rows, which corresponds to 2 hours of valid measurements along each row for a 2 degree sector. The mean wind speed deficit along a row is presented as function of the distance between upwind and downwind wind turbine for each case.

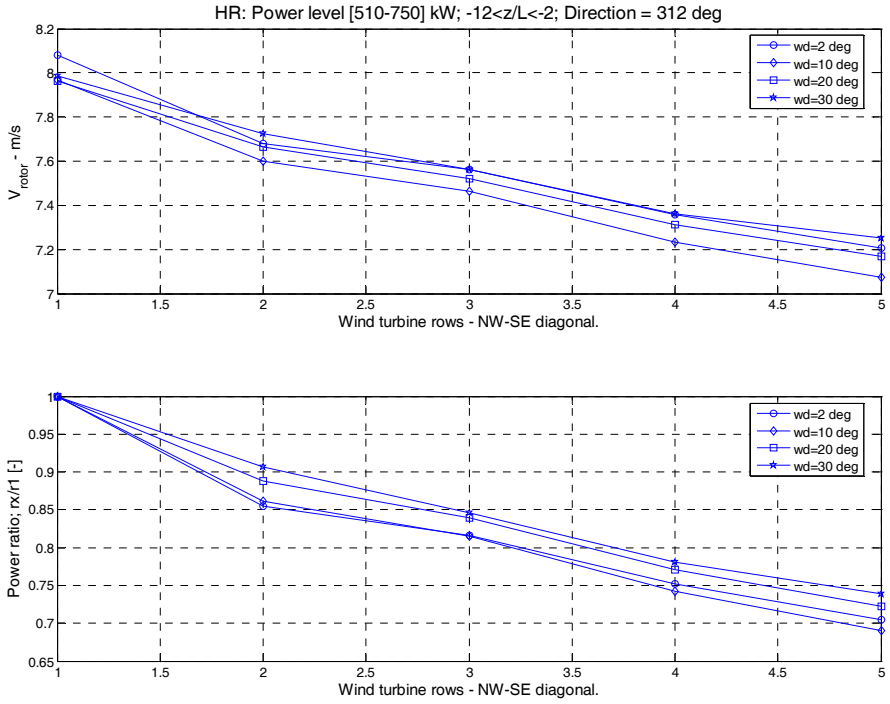

Figure 20: Speed and power deficit at 8 m/s during unstable conditions, sector = 2, 10, 20 & 30 deg.

Case 3.10; wind speed bin at 10 m/s results in 26.6 x 8 periods =213 periods distributed on 8 rows, which corresponds to approximately 5 hours of valid measurements along each row for a 2 degree sector. The mean wind speed deficit along a row is presented as function of the distance between upwind and downwind wind turbine for each case.

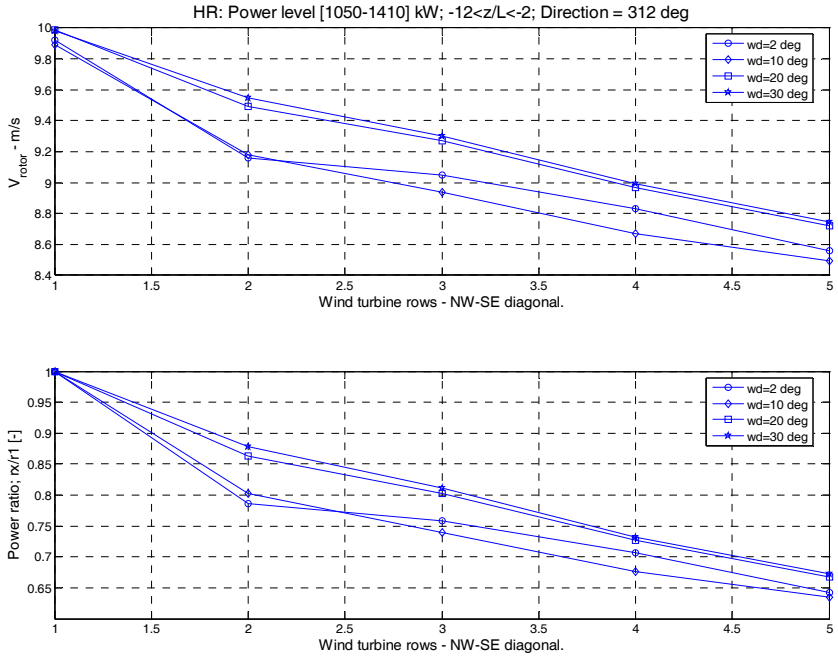

Figure 21: Speed and power deficit at 10 m/s during unstable conditions, sector = 2, 10, 20 & 30 deg.

2.7 Discussion

The finding from basic flow cases have been presented above both as power deficit ratios and as derived wind speed deficits. The major findings are:

- The smallest sector size of 2° represents an almost "pure" wake situation where all downwind turbines are covered by the wake, which is demonstration by a very low (<0.5°) mean yaw misalignment of the down wind turbines.
- The uncertainty of the nacelle position value is rather low, which influences the quality resulting mean deficit. Furthermore all nacelle position registrations are uncorrected due to an individual varying offset.
- Increased sector size of 10, 20 and 30 degrees decreases the deficit due to increased mixing and meandering wakes.
- The uncertainty of the power measurements is unknown, while there is now available documentation on sensor calibration, measurement chain setup,...
- Due to high uncertainty both on the temperature difference recordings and wind speed differences inside the wind farm wake, the derived stability measure is rather uncertain, which influences the deficit determination as function of stability.
- Several sub-cases contain only a limited number of valid observations, which influences the contents of the final flow cases matrix.

3 Wake modelling in complex terrain

3.1 Overview

Models of the engineering type have been developed and calibrated for flat terrain applications. However, in complex terrain applications, the assumptions made in those models are no longer valid. More advanced methods should be applied taking into account the effect of the atmospheric boundary layer including flow separation and streamlining. In this respect the adoption of Navier-Stokes solvers seems to be the most accurate approach and the only one capable of simulating the interaction of wind turbine wake with the wind velocity shear and the shape of the complex terrain.

There are several issues, which need to be investigated regarding wake modelling in complex terrain:

- Complex topography results in the narrowing of the wind rose and the decrease the Weibull-k values. How does the narrowing behave with the increase in the hub height? The effect on the power curve should be quantified.
- The effect of topography on the wake geometry has to be investigated. Does the wake follow the streamlines? How does the terrain affect the wake opening?
- The reference wind velocity should be correctly assigned for modelling purposes. This is not obvious for steep slopes and wind parks with machine-wake interaction. In the context of an actuator disk modelling of the wind turbines, the combination of a BEM method with a Navier-Stokes solver could overcome the issue of the reference velocity definition by directly calculating the blade forces.

By answering these issues, it is expected to develop relationships for the maximum wind velocity deficit, the turbulence intensity and the wake geometry, which would complete the wake modelling along with those existing in flat terrain.

3.2 Complex terrain cases: The Gaussian Hill

The idealized simulation of a single wake in the case of a Gaussian hill will constitute the basis for the comparison of the wake characteristics between flat and complex terrain. The conclusions deduced from the analysis of the 3D and 2D Gaussian hill can be extended to more complex terrain where the irregularities of the topography are seen as separate hills.

The Gaussian 2D hill geometry is defined by the relationship

$$z = h\, e^{\left[-0.5\left(\frac{x}{\sigma}\right)^2\right]},\ \sigma = L/1.1774, \qquad (1)$$

here x, z are the horizontal and vertical coordinates, h is the height of the hill and L is defined as $x(z = h/2)$. In the 3D hill, $\sqrt{x^2 + y^2}$ replaces x in Eq.(1). The 3D and 2D hill terrain derived from Eq.(1) for $L = 1750$ are shown in Fig.1. Two configurations corresponding to different hill slopes will be examined: $h = 700m$, $L = 1750m$ (steep slope) and $h = 700m$, $L = 3000m$ (gentle slope).

The different configurations will be simulated with one wind turbine at hilltop and without the wind turbine. The simulations without the wind turbine are needed to provide the value of wind speed at the wind turbine position for the calculation of the actuator disk force as well as the reference velocity field for the evaluation of the wind speed deficit. The machine is the 5 MW reference turbine used in Upwind WP2 with 126 m diameter (D=126 m) and 90 m hub height. Note, that the lengths in Figure 1 have been dimensionalized with the wind turbine diameter. The input wind velocity profile is assumed logarithmic with 500 m boundary layer height and 10m/s velocity at hub height. Three different levels of turbulence intensity (5%, 13% and 15%) and six different wind directions (0, ±15°, ±30°) will be examined.

The variations of wind speed deficit and turbulence intensity at hub height above ground level and the vertical profiles behind the wind turbine must be estimated and compared to the respective ones in flat terrain, so that basic guidelines are derived for the effect of the hill on the wake characteristics.

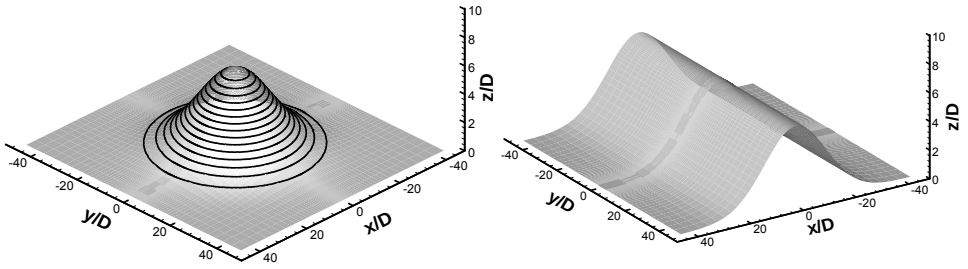

Figure 1: Terrain of the 3D and 2D Gaussian hill ($L = 1750$).

3.3 Complex terrain cases: Five turbines in flat terrain

In flat terrain wind parks, wind turbines are often aligned in parallel rows, which means that one machine can be partially or completely situated in the wake of a neighbouring wind turbine. In order to estimate the effect of a neighbouring wake on the wind turbine efficiency, multi-wake simulations for the worst (in terms of efficiency) case will be examined.

The simulation of five subsequent wind turbines in flat terrain is considered to well cover this case. A parametric analysis will be done for different values of the distance between the wind turbines (3, 5 and 7D) and different values of Ct (0.3, 0.5 and 0.7). The level of turbulence intensity will be set equal to 13%.

The wind speed deficit and wake radius variations at hub height will indicate the significance of the wake effect of the previous wind turbines and how this effect decays as the distance from the first machine increases. The vertical and lateral profiles of the wind deficit along with the xz and yz contour plots can represent the evolution of the wake geometry.

3.4 Complex terrain cases: The complex terrain wind farm

A real wind farm located in a moderately complex terrain is proposed for the comparison and validation of wake models. The wind farm, installed in 2001, is constituted by 43 wind turbines separated 1.5 diameters in the adjacent direction and approximately 11 diameters between rows. The layout is formed by 5 alignments oriented towards the prevailing wind directions (NW-SE).

Two meteorological masts are located upstream of the wind farm on the wind directions mentioned above. The masts registered 10 minutes averages of wind speed, wind direction and standard deviation of wind speed at 20 m and 40 m high. In addition, the air temperature is measured at 10 m height. Regarding power data, the output energy as well as the nacelle wind speed for every wind turbine is recorded on an hourly basis. Furthermore, a specific status signal is also registered in order to filter the unavailability of the wind turbines. Overall, a 2 year period of simultaneous data (meteorological and wind farm) is available.

The location of the meteorological masts allows the upstream flow in the prevailing wind direction to be characterised in order to analyse situations of far wake. Other non-prevailing sectors (W-WSW) corresponding to near wake scenarios are known to contain enough frequency of data and some information could also be extracted. Yaw angle at the wind turbines was not registered so that only wind direction at the meteorological masts could be used at the filtering process.

The study represents a first attempt of comparing and validating the existing wake models on a real moderately complex site and according to real field data.

4 Acknowledgement

We would like to acknowledge DONG Energy A/S (formerly ELSAM Engineering A/S) and Vattenfall AB, owners of the Horns Rev wind farm for allowing use of Horns Rev data,) and owners of the wind farm in complex terrain and the five turbines in flat terrain for allowing use of their data.

5 References.

[1] "Investigation of Observed and Modeled Wake Effect on Horns Rev", using WindPro; Master thesis made by David Ryan Van Luvanee; MEK, DTU 2006,

[2] Upwind WP8 kick-off meeting 17.10.2006, Aristo, Amsterdam

[3] Leo E. Jensen et.al."Wake measurements from the Horns Rev Wind farm", presented at EWEC 2004, London, November 2004

Appendix A: Location of meteorological mast at the Horns Rev wind farm.

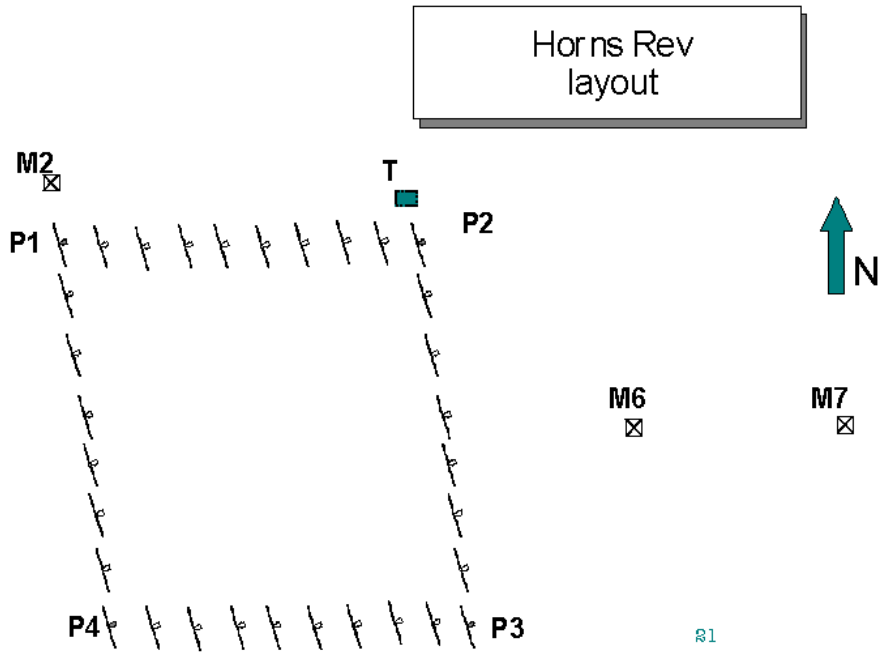

Position of main objects:

- The park corners turbines are P1 (=wt01), P2 (=wt91), P3 (=wt98) and P4 (=wt08)
- Transformer stations T, is located NW of P2
- Mast M2 is located NW of the P1,
- Mast M6 is located 2 km east of the park
- Mast M7 is located 6 km east of the park

	Coordinates	
M2	423.41	6153.3
P1	423.97	6151.4
P2	429.01	6151.4
P3	429.45	6147.6
P4	424.45	6147.6
T	428.95	6152.0
M6	431.25	6149.5
M7	435.25	6149.5

Direction between main objects

directions, deg	M2	M6	M7
P1	163	285	280
P2	109	311	287
P3	134	227	251
T	104	317	292
M6	116	0	270
M7	108	90	0
M2	0	296	288

Free inflow sectors to masts

	Mast	
M2	0°	90°
M2	180°	360°
M6	-20°	200°
M7	-40°	220°

Appendix B: Directional sensitivity analysis for Case 1.8.2

The wake deficit as function of wind direction for a number of 2 degrees sectors has been determined for the 7D flow case, where each curve represents approximately 3 hours of measurements.

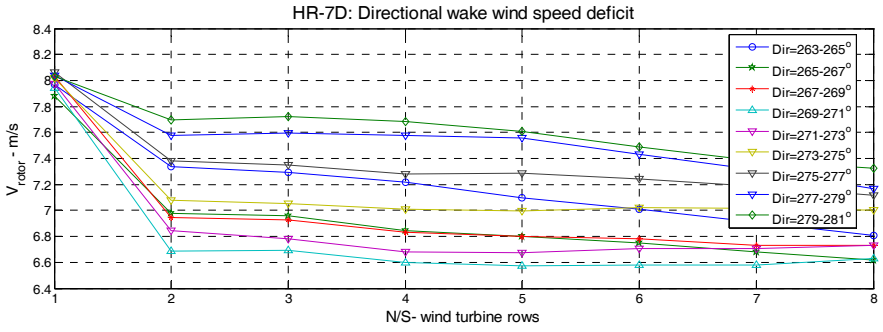

Figure 22: Directional wake deficits during unstable and near neutral conditions, V_{hub}=8 ±0.5 m/s.

Appendix C: Calculated speed and power deficit values

	CASE:1.6 - Figure 8							
	speed deficit				**power deficit ratio**			
row	*dw=2°*	*dw=10°*	*dw=20°*	*dw=30°*	*dw=2°*	*dw=10°*	*dw=20°*	*dw=30°*

1	6.00	5.97	6.00	5.99	1.000	1.000	1.000	1.000
2	5.35	5.39	5.50	5.62	0.681	0.709	0.747	0.808
3	5.30	5.41	5.53	5.66	0.660	0.715	0.759	0.822
4	5.25	5.37	5.49	5.60	0.634	0.696	0.741	0.795
5	5.22	5.35	5.46	5.52	0.627	0.682	0.725	0.762
6	5.28	5.32	5.42	5.47	0.648	0.672	0.708	0.737
7	5.28	5.29	5.38	5.44	0.648	0.659	0.691	0.720
8	5.27	5.28	5.36	5.43	0.645	0.654	0.680	0.712

	CASE:1.8 - Figure 9							
	speed deficit				**power deficit ratio**			
row	*dw=2°*	*dw=10°*	*dw=20°*	*dw=30°*	*dw=2°*	*dw=10°*	*dw=20°*	*dw=30°*
1	7.92	7.94	7.96	7.97	1.000	1.000	1.000	1.000
2	6.81	7.06	7.24	7.42	0.623	0.694	0.750	0.802
3	6.81	7.05	7.24	7.42	0.625	0.691	0.749	0.801
4	6.71	6.97	7.18	7.34	0.599	0.671	0.728	0.774
5	6.72	6.96	7.14	7.26	0.601	0.665	0.714	0.750
6	6.71	6.94	7.07	7.17	0.598	0.659	0.695	0.723
7	6.74	6.91	6.99	7.09	0.607	0.647	0.670	0.694
8	6.77	6.87	6.93	7.01	0.615	0.640	0.652	0.675

	CASE:1.10 - Figure 10							
	speed deficit				**power deficit ratio**			
row	*dw=2°*	*dw=10°*	*dw=20°*	*dw=30°*	*dw=2°*	*dw=10°*	*dw=20°*	*dw=30°*
1	10.09	10.01	9.97	9.98	1.000	1.000	1.000	1.000
2	8.82	8.98	9.11	9.33	0.669	0.728	0.765	0.822
3	8.77	8.92	9.05	9.29	0.659	0.714	0.754	0.814
4	8.66	8.84	8.96	9.20	0.636	0.694	0.731	0.787
5	8.61	8.81	8.91	9.07	0.623	0.688	0.719	0.759
6	8.49	8.76	8.83	8.96	0.600	0.674	0.698	0.731
7	8.41	8.70	8.75	8.86	0.584	0.662	0.678	0.706
8	8.36	8.64	8.66	8.74	0.571	0.649	0.654	0.676

	CASE 2.6 - Figure 13							
	speed deficit				**power deficit ratio**			
row	*dw=2°*	*dw=10°*	*dw=20°*	*dw=30°*	*dw=2°*	*dw=10°*	*dw=20°*	*dw=30°*
1		5.99	6.02	6.02		1.000	1.000	1.000
2		5.59	5.69	5.77		0.788	0.822	0.873
3		5.61	5.67	5.72		0.797	0.814	0.844
4		5.60	5.61	5.62		0.797	0.785	0.793
5		5.51	5.51	5.49		0.756	0.732	0.735

	CASE 2.8 - Figure 15							
	speed deficit				**power deficit ratio**			
row	*dw=2°*	*dw=10°*	*dw=20°*	*dw=30°*	*dw=2°*	*dw=10°*	*dw=20°*	*dw=30°*
1	7.92	7.96	7.98	7.99	1.000	1.000	1.000	1.000
2	7.11	7.29	7.50	7.60	0.715	0.768	0.824	0.854
3	7.00	7.23	7.41	7.49	0.683	0.747	0.797	0.820
4	6.90	7.17	7.30	7.34	0.654	0.728	0.759	0.771
5	6.80	7.07	7.15	7.18	0.622	0.694	0.711	0.719

	CASE 2.10 - Figure 16							
	speed deficit				**power deficit ratio**			
row	*dw=2°*	*dw=10°*	*dw=20°*	*dw=30°*	*dw=2°*	*dw=10°*	*dw=20°*	*dw=30°*
1	9.85	10.07	10.02	10.04	1.000	1.000	1.000	1.000
2	9.10	9.22	9.38	9.58	0.792	0.771	0.820	0.872
3	8.80	9.06	9.14	9.38	0.706	0.730	0.763	0.817
4	8.85	8.91	8.97	9.17	0.726	0.693	0.721	0.768
5	8.55	8.72	8.76	8.93	0.648	0.658	0.670	0.708

	CASE 3.6 - Figure *19*							
	speed deficit				**power deficit ratio**			
row	*dw=2°*	*dw=10°*	*dw=20°*	*dw=30°*	*dw=2°*	*dw=10°*	*dw=20°*	*dw=30°*
1	5.95	6.03	6.03	6.02	1.000	1.000	1.000	1.000
2	5.52	5.65	5.69	5.74	0.771	0.804	0.827	0.855
3	5.43	5.59	5.63	5.67	0.729	0.774	0.802	0.822
4	5.31	5.49	5.55	5.58	0.673	0.724	0.755	0.774
5	5.23	5.43	5.49	5.53	0.642	0.701	0.734	0.753

	CASE 3.8 - Figure *20*							
	speed deficit				**power deficit ratio**			
row	*dw=2°*	*dw=10°*	*dw=20°*	*dw=30°*	*dw=2°*	*dw=10°*	*dw=20°*	*dw=30°*
1	8.08	7.97	7.96	7.99	1.000	1.000	1.000	1.000
2	7.68	7.60	7.66	7.72	0.854	0.862	0.888	0.907
3	7.56	7.46	7.52	7.56	0.816	0.815	0.840	0.846
4	7.36	7.23	7.31	7.36	0.752	0.742	0.771	0.781
5	7.21	7.07	7.17	7.25	0.705	0.691	0.722	0.739

	CASE 3.10 - Figure *21*							
	speed deficit				**power deficit ratio**			
row	*dw=2º*	*dw=10º*	*dw=20º*	*dw=30º*	*dw=2º*	*dw=10º*	*dw=20º*	*dw=30º*
1	9.92	9.89	9.99	9.98	1.000	1.000	1.000	1.000
2	9.16	9.18	9.49	9.55	0.786	0.802	0.863	0.878
3	9.05	8.94	9.27	9.30	0.758	0.739	0.803	0.812
4	8.83	8.67	8.97	8.99	0.707	0.677	0.726	0.732
5	8.56	8.49	8.72	8.74	0.642	0.634	0.668	0.673

Appendix C: Calculated speed and power deficit values

	CASE:1.6 - Figure 8							
	speed deficit				**power deficit ratio**			
row	*dw=2º*	*dw=10º*	*dw=20º*	*dw=30º*	*dw=2º*	*dw=10º*	*dw=20º*	*dw=30º*
1	6.00	5.97	6.00	5.99	1.000	1.000	1.000	1.000
2	5.35	5.39	5.50	5.62	0.681	0.709	0.747	0.808
3	5.30	5.41	5.53	5.66	0.660	0.715	0.759	0.822
4	5.25	5.37	5.49	5.60	0.634	0.696	0.741	0.795
5	5.22	5.35	5.46	5.52	0.627	0.682	0.725	0.762
6	5.28	5.32	5.42	5.47	0.648	0.672	0.708	0.737
7	5.28	5.29	5.38	5.44	0.648	0.659	0.691	0.720
8	5.27	5.28	5.36	5.43	0.645	0.654	0.680	0.712

	CASE:1.8 - Figure 9							
	speed deficit				**power deficit ratio**			
row	*dw=2º*	*dw=10º*	*dw=20º*	*dw=30º*	*dw=2º*	*dw=10º*	*dw=20º*	*dw=30º*
1	7.92	7.94	7.96	7.97	1.000	1.000	1.000	1.000
2	6.81	7.06	7.24	7.42	0.623	0.694	0.750	0.802
3	6.81	7.05	7.24	7.42	0.625	0.691	0.749	0.801
4	6.71	6.97	7.18	7.34	0.599	0.671	0.728	0.774
5	6.72	6.96	7.14	7.26	0.601	0.665	0.714	0.750
6	6.71	6.94	7.07	7.17	0.598	0.659	0.695	0.723
7	6.74	6.91	6.99	7.09	0.607	0.647	0.670	0.694
8	6.77	6.87	6.93	7.01	0.615	0.640	0.652	0.675

	CASE:1.10 - Figure 10							
	speed deficit				**power deficit ratio**			
row	*dw=2º*	*dw=10º*	*dw=20º*	*dw=30º*	*dw=2º*	*dw=10º*	*dw=20º*	*dw=30º*
1	10.09	10.01	9.97	9.98	1.000	1.000	1.000	1.000
2	8.82	8.98	9.11	9.33	0.669	0.728	0.765	0.822

3	8.77	8.92	9.05	9.29	0.659	0.714	0.754	0.814
4	8.66	8.84	8.96	9.20	0.636	0.694	0.731	0.787
5	8.61	8.81	8.91	9.07	0.623	0.688	0.719	0.759
6	8.49	8.76	8.83	8.96	0.600	0.674	0.698	0.731
7	8.41	8.70	8.75	8.86	0.584	0.662	0.678	0.706
8	8.36	8.64	8.66	8.74	0.571	0.649	0.654	0.676

	CASE 2.6 - Figure 13							
	speed deficit				**power deficit ratio**			
row	*dw=2°*	*dw=10°*	*dw=20°*	*dw=30°*	*dw=2°*	*dw=10°*	*dw=20°*	*dw=30°*
1		5.99	6.02	6.02		1.000	1.000	1.000
2		5.59	5.69	5.77		0.788	0.822	0.873
3		5.61	5.67	5.72		0.797	0.814	0.844
4		5.60	5.61	5.62		0.797	0.785	0.793
5		5.51	5.51	5.49		0.756	0.732	0.735

	CASE 2.8 - Figure 15							
	speed deficit				**power deficit ratio**			
row	*dw=2°*	*dw=10°*	*dw=20°*	*dw=30°*	*dw=2°*	*dw=10°*	*dw=20°*	*dw=30°*
1	7.92	7.96	7.98	7.99	1.000	1.000	1.000	1.000
2	7.11	7.29	7.50	7.60	0.715	0.768	0.824	0.854
3	7.00	7.23	7.41	7.49	0.683	0.747	0.797	0.820
4	6.90	7.17	7.30	7.34	0.654	0.728	0.759	0.771
5	6.80	7.07	7.15	7.18	0.622	0.694	0.711	0.719

	CASE 2.10 - Figure 16							
	speed deficit				**power deficit ratio**			
row	*dw=2°*	*dw=10°*	*dw=20°*	*dw=30°*	*dw=2°*	*dw=10°*	*dw=20°*	*dw=30°*
1	9.85	10.07	10.02	10.04	1.000	1.000	1.000	1.000
2	9.10	9.22	9.38	9.58	0.792	0.771	0.820	0.872
3	8.80	9.06	9.14	9.38	0.706	0.730	0.763	0.817
4	8.85	8.91	8.97	9.17	0.726	0.693	0.721	0.768
5	8.55	8.72	8.76	8.93	0.648	0.658	0.670	0.708

	CASE 3.6 - Figure *19*							
	speed deficit				**power deficit ratio**			
row	*dw=2°*	*dw=10°*	*dw=20°*	*dw=30°*	*dw=2°*	*dw=10°*	*dw=20°*	*dw=30°*
1	5.95	6.03	6.03	6.02	1.000	1.000	1.000	1.000
2	5.52	5.65	5.69	5.74	0.771	0.804	0.827	0.855
3	5.43	5.59	5.63	5.67	0.729	0.774	0.802	0.822
4	5.31	5.49	5.55	5.58	0.673	0.724	0.755	0.774

5	5.23	5.43	5.49	5.53	0.642	0.701	0.734	0.753

	CASE 3.8 - Figure *20*							
	speed deficit				**power deficit ratio**			
row	*dw=2°*	*dw=10°*	*dw=20°*	*dw=30°*	*dw=2°*	*dw=10°*	*dw=20°*	*dw=30°*
1	8.08	7.97	7.96	7.99	1.000	1.000	1.000	1.000
2	7.68	7.60	7.66	7.72	0.854	0.862	0.888	0.907
3	7.56	7.46	7.52	7.56	0.816	0.815	0.840	0.846
4	7.36	7.23	7.31	7.36	0.752	0.742	0.771	0.781
5	7.21	7.07	7.17	7.25	0.705	0.691	0.722	0.739

	CASE 3.10 - Figure *21*							
	speed deficit				**power deficit ratio**			
row	*dw=2°*	*dw=10°*	*dw=20°*	*dw=30°*	*dw=2°*	*dw=10°*	*dw=20°*	*dw=30°*
1	9.92	9.89	9.99	9.98	1.000	1.000	1.000	1.000
2	9.16	9.18	9.49	9.55	0.786	0.802	0.863	0.878
3	9.05	8.94	9.27	9.30	0.758	0.739	0.803	0.812
4	8.83	8.67	8.97	8.99	0.707	0.677	0.726	0.732
5	8.56	8.49	8.72	8.74	0.642	0.634	0.668	0.673

Appendix C: Calculated speed and power deficit values

	CASE:1.6 - Figure 8							
	speed deficit				**power deficit ratio**			
row	*dw=2°*	*dw=10°*	*dw=20°*	*dw=30°*	*dw=2°*	*dw=10°*	*dw=20°*	*dw=30°*
1	6.00	5.97	6.00	5.99	1.000	1.000	1.000	1.000
2	5.35	5.39	5.50	5.62	0.681	0.709	0.747	0.808
3	5.30	5.41	5.53	5.66	0.660	0.715	0.759	0.822
4	5.25	5.37	5.49	5.60	0.634	0.696	0.741	0.795
5	5.22	5.35	5.46	5.52	0.627	0.682	0.725	0.762
6	5.28	5.32	5.42	5.47	0.648	0.672	0.708	0.737
7	5.28	5.29	5.38	5.44	0.648	0.659	0.691	0.720
8	5.27	5.28	5.36	5.43	0.645	0.654	0.680	0.712

	CASE:1.8 - Figure 9							
	speed deficit				**power deficit ratio**			
row	*dw=2°*	*dw=10°*	*dw=20°*	*dw=30°*	*dw=2°*	*dw=10°*	*dw=20°*	*dw=30°*
1	7.92	7.94	7.96	7.97	1.000	1.000	1.000	1.000
2	6.81	7.06	7.24	7.42	0.623	0.694	0.750	0.802
3	6.81	7.05	7.24	7.42	0.625	0.691	0.749	0.801
4	6.71	6.97	7.18	7.34	0.599	0.671	0.728	0.774
5	6.72	6.96	7.14	7.26	0.601	0.665	0.714	0.750
6	6.71	6.94	7.07	7.17	0.598	0.659	0.695	0.723
7	6.74	6.91	6.99	7.09	0.607	0.647	0.670	0.694
8	6.77	6.87	6.93	7.01	0.615	0.640	0.652	0.675

	CASE:1.10 - Figure 10							
	speed deficit				**power deficit ratio**			
row	*dw=2°*	*dw=10°*	*dw=20°*	*dw=30°*	*dw=2°*	*dw=10°*	*dw=20°*	*dw=30°*
1	10.09	10.01	9.97	9.98	1.000	1.000	1.000	1.000
2	8.82	8.98	9.11	9.33	0.669	0.728	0.765	0.822
3	8.77	8.92	9.05	9.29	0.659	0.714	0.754	0.814
4	8.66	8.84	8.96	9.20	0.636	0.694	0.731	0.787
5	8.61	8.81	8.91	9.07	0.623	0.688	0.719	0.759
6	8.49	8.76	8.83	8.96	0.600	0.674	0.698	0.731
7	8.41	8.70	8.75	8.86	0.584	0.662	0.678	0.706
8	8.36	8.64	8.66	8.74	0.571	0.649	0.654	0.676

	CASE 2.6 - Figure 13	
	speed deficit	**power deficit ratio**

row	*dw=2°*	*dw=10°*	*dw=20°*	*dw=30°*	*dw=2°*	*dw=10°*	*dw=20°*	*dw=30°*
1		5.99	6.02	6.02		1.000	1.000	1.000
2		5.59	5.69	5.77		0.788	0.822	0.873
3		5.61	5.67	5.72		0.797	0.814	0.844
4		5.60	5.61	5.62		0.797	0.785	0.793
5		5.51	5.51	5.49		0.756	0.732	0.735

	CASE 2.8 - Figure 15							
	speed deficit				**power deficit ratio**			
row	*dw=2°*	*dw=10°*	*dw=20°*	*dw=30°*	*dw=2°*	*dw=10°*	*dw=20°*	*dw=30°*
1	7.92	7.96	7.98	7.99	1.000	1.000	1.000	1.000
2	7.11	7.29	7.50	7.60	0.715	0.768	0.824	0.854
3	7.00	7.23	7.41	7.49	0.683	0.747	0.797	0.820
4	6.90	7.17	7.30	7.34	0.654	0.728	0.759	0.771
5	6.80	7.07	7.15	7.18	0.622	0.694	0.711	0.719

	CASE 2.10 - Figure 16							
	speed deficit				**power deficit ratio**			
row	*dw=2°*	*dw=10°*	*dw=20°*	*dw=30°*	*dw=2°*	*dw=10°*	*dw=20°*	*dw=30°*
1	9.85	10.07	10.02	10.04	1.000	1.000	1.000	1.000
2	9.10	9.22	9.38	9.58	0.792	0.771	0.820	0.872
3	8.80	9.06	9.14	9.38	0.706	0.730	0.763	0.817
4	8.85	8.91	8.97	9.17	0.726	0.693	0.721	0.768
5	8.55	8.72	8.76	8.93	0.648	0.658	0.670	0.708

	CASE 3.6 - Figure *19*							
	speed deficit				**power deficit ratio**			
row	*dw=2°*	*dw=10°*	*dw=20°*	*dw=30°*	*dw=2°*	*dw=10°*	*dw=20°*	*dw=30°*
1	5.95	6.03	6.03	6.02	1.000	1.000	1.000	1.000
2	5.52	5.65	5.69	5.74	0.771	0.804	0.827	0.855
3	5.43	5.59	5.63	5.67	0.729	0.774	0.802	0.822
4	5.31	5.49	5.55	5.58	0.673	0.724	0.755	0.774
5	5.23	5.43	5.49	5.53	0.642	0.701	0.734	0.753

	CASE 3.8 - Figure *20*							
	speed deficit				**power deficit ratio**			
row	*dw=2°*	*dw=10°*	*dw=20°*	*dw=30°*	*dw=2°*	*dw=10°*	*dw=20°*	*dw=30°*
1	8.08	7.97	7.96	7.99	1.000	1.000	1.000	1.000
2	7.68	7.60	7.66	7.72	0.854	0.862	0.888	0.907
3	7.56	7.46	7.52	7.56	0.816	0.815	0.840	0.846
4	7.36	7.23	7.31	7.36	0.752	0.742	0.771	0.781

5	7.21	7.07	7.17	7.25	0.705	0.691	0.722	0.739

	CASE 3.10 - Figure *21*							
	speed deficit				**power deficit ratio**			
row	*dw=2°*	*dw=10°*	*dw=20°*	*dw=30°*	*dw=2°*	*dw=10°*	*dw=20°*	*dw=30°*
1	9.92	9.89	9.99	9.98	1.000	1.000	1.000	1.000
2	9.16	9.18	9.49	9.55	0.786	0.802	0.863	0.878
3	9.05	8.94	9.27	9.30	0.758	0.739	0.803	0.812
4	8.83	8.67	8.97	8.99	0.707	0.677	0.726	0.732
5	8.56	8.49	8.72	8.74	0.642	0.634	0.668	0.673

Appendix 2: Deliverable 8.2 Offshore

Project funded by the European Commission under the 6th (EC) RTD Framework Programme (2002- 2006) within the framework of the specific research and technological development programme "Integrating and strengthening the European Research Area"

Project UpWind

Contract No.:
019945 (SES6)

"Integrated Wind Turbine Design"

Wp8: Flow

Deliverable D8.2 Comparing existing wake models with CFD offshore

AUTHOR:	Rebecca Barthelmie
AFFILIATION:	University of Edinburgh/Risø National Laboratory
ADDRESS:	
TEL.:	
EMAIL:	r.barthelmie@ed.ac.uk
FURTHER AUTHORS:	W. Schlez, J. Phillips, A. Neubert Garrad Hassan and Partners (Germany) K. Hansen, DTU (Denmark) K. Rados, NTUA (Greece) O. Rathmann and S.T. Frandsen Risø National Laboratory/DTU (Denmark) J.G. Schepers, S.P. van der Pijl ECN (Netherlands)
REVIEWER:	
APPROVER:	

Document Information

DOCUMENT TYPE	Deliverable 8.2
DOCUMENT NAME:	Comparing existing wake models with CFD offshore
REVISION:	1
REV.DATE:	
CLASSIFICATION:	RE
STATUS:	Draft

Abstract: This deliverable presents an overview of research conducted in the Flow workpackage of the EU funded UPWIND project which focuses on improving models for flow within and downwind of large offshore wind farms. The main activity is modelling the behaviour of wind turbine wakes in order to improve power output predictions.

For the first time, wind farm models have run simulations for comparison with data from an offshore wind farm. These have been compared with a CFD and a parabolised model. General results indicate wind farm models without modification under-estimate wake losses while CFD-type codes over-estimate wake losses. The main difficulty comparing the models and measurements is that the CFD type models run specific simulations while wind farm models are designed to run over a range of conditions and use average results. This means that they typically need wider direction sectors while the CFD models need narrow sectors. Further simulations are being run to evaluate the impact of the simulation specifications.

Contents

STATUS, CONFIDENTIALITY AND ACCESSIBILITY									
Status				**Confidentiality**				**Accessibility**	
S0	Approved/Released			**R0**	General public			Private web site	x
S1	Reviewed			**R1**	Restricted to project members	x		Public web site	
S2	Pending for review			**R2**	Restricted to European. Commission			Paper copy	
S3	Draft for commends			**R3**	Restricted to WP members + PL				
S4	Under preparation			**R4**	Restricted to Task members +WPL+PL				

PL: *Project leader* **WPL:** *Work package leader* **TL:** *Task leader*

1 Introduction

As wind farms and wind turbines grow larger there is an increasing need to describe accurately the wind speed, wind shear and turbulence climate at the wind farm site. In addition, each wind turbine generates a wake and the neighbouring wind turbine in the array which is exposed to the wake will experience a lower wind speed and higher turbulence than the unobstructed turbine. In other words, the energy yield of the wind farm will be lower and the loads higher than for an equivalent number of single turbines.

The central core of most wind farm models was developed in the 1980's for small wind farms in simple or moderately complex terrain. Wind farms being developed today are larger and often in complex terrain, close to forests or offshore. Thus there is a need for further research, to examine the performance of wind farm and wake models in these more difficult environments. In ideal circumstances, wind and turbulence would be predicted on a fine mesh (horizontal and vertical) for the whole wind farm over a range of wind speeds and directions. There is a gap between engineering solutions and computational fluid dynamics (CFD) models and a bridge is needed between these types of models in order to provide more detailed information for modelling power losses, for better wind farm and turbine design and for more sophisticated control strategies and load calculations. This is the focus of our work within the EU funded UPWIND project that aims to develop the next generation of wind turbines in the 5-12 MW range.

2 Issues comparing models and measurements

Measurements made at Horns Rev are detailed in Deliverable 8.1.

There are some major issues in wind farm model validation studies which will be discussed below. As stated above we concentrate here on power loss modelling which should encompass the whole range of wind speeds and directions and we also consider that the range of wind farm/wake model extends from engineering through to full CFD models. In general, computing requirements for CFD models means we are restricted to examining a number of specific wind speed and direction cases and only a moderate number of turbines rather than wind farms with ~100 turbines which can easily be done by WindFarmer and WAsP. On the other hand it can be difficult to extract reasonable simulations from some of the wind farm models for very specific cases. For example, WAsP relies on having a Weibull fit to wind speed distributions and fairly large directional sectors (30°). Therefore for specific wind speeds and narrow directional bins models like WAsP are never going to produce very exact solutions because they are being used beyond their operational windows. In addition to this there are a number of specific issues:

- Establishing the freestream flow. The major issues in determining the freestream flow are the displacement of the measurement mast from the array (assuming there is a mast), adjustments in the flow over this distance especially in coastal areas and differences in height between the measurement and the turbine hub-height. If there is no mast or the mast is in the wake of turbines or subject to coastal flow then the turbine(s) in the freestream flow may be used. If power measurements are used to determine wind speed they will be subject to any errors in the site specific power curve.
- Wind direction, nacelle direction and yaw misalignment. Because of the difficulty in establishing true north when erecting wind vanes (especially offshore where landmarks

may not be determinable) it can be difficult to establish a true freestream direction. Even a well maintained wind vane may have a bias of up to 5° and it is important to understand this because the total width of a wake may be of the order 10-15° at typical turbine spacing. In a large wind farm, each turbine may have a separate bias on the direction, which is very difficult to determine. Analysis must be undertaken to calibrate the maximum wake direction to within 1° and to check for bias of the yaw angle on each wind turbine in the array.

- If there is a gradient of wind speeds across the wind farm as there may be e.g. in coastal areas, near a forest or caused by topography these variations will need to be accounted for before wake calculations are undertaken.
- In terms of modelling wakes both the power curve and thrust coefficients must be known but these will vary according to the specific environment. A power curve must be calculated for the site. For modelling, the question of whether the thrust coefficient should be set to one value for the wind farm or at each individual turbine in each simulation is still an open one. The state-of-the-art is to validate the individual power and pitch curves with reference to the nacelle anemometer, which seems to be a rather robust method to determine changes in the system setup.
- Comparing the modelled standard deviation of power losses in a row with the measured standard deviation raises a number of issues. The two most important are ensuring that the time averaging is equivalent between models and measurements and taking into account that there will be natural fluctuations in the wind speed and direction in any period. Models are typically run for specific directions but it may be necessary to include the standard deviation of the wind direction in the model simulations.
- In the large wind farm context the time scale of wake transport must be considered. A large wind farm with 100 turbines in a 10 by 10 array with an 80 m diameter rotor and a space of 7 rotor diameters has a length of nearly 6 km. At a wind speed of 8 m/s the travel time through the array is more than 10 minutes. As mentioned above the wind direction will be subject to natural fluctuations in addition to possible wake deflection but there will also be natural variations in the wind speed over this time scale.
- Determining turbulence intensity and stability may be critical. Turbulence intensity is a key parameter in many models. Using either mast data to determine this information or deriving it from turbine data is subject to fairly large errors for the reasons discussed above and because the accuracy of temperature measurements used to derive stability parameters is often inadequate.

3 Wake modelling

Models describing wind turbine wakes were developed mainly in the 1980's e.g. (Ainslie, 1988) and were used in wind farm models to approximate losses due to wakes e.g. (Mortensen et al., 2000). By necessity the wake models had to be fairly straightforward, building on relatively few wake measurements and not requiring too much computing power. However, for single wakes or small wind farms in fairly straightforward environments these tended to give results which were not strongly in disagreement with the available data (e.g. ((Barthelmie et al., 2006); (Crespo et al., 1999); (Magnusson and Smedman, 1999)). It should be emphasised that this discussion mainly concerns power losses due to wakes. Modelling of turbulence in wakes for load calculations tends to focus on for specific cases while power loss modelling has to encompass the full range of wind speeds and directions ((Frandsen and Thøgersen, 1999); (Quarton and Ainslie, 1990); (Thomsen and Sørensen, 1999)).

It has recently become clear that wake modelling for large offshore wind farms is inadequate (Mechali et al., 2006) and also that wake modelling in complex terrain needs to be significantly

improved. Therefore the focus of our work is in these two areas. A major shift has occurred in terms of computing resources which means that wake modelling is no longer confined to engineering approximations and that CFD modelling of the whole wind farm can be undertaken. This brings a new dimension to wake model in terms of the detailed temporal and spatial variation that can be modelled but a new complexity to wake model evaluation since measurements are not available on a finely spaced mesh over the wind farm, nor (typically) at high time resolution. CFD also brings new detail to near-wake studies which are not (typically) considered in wind farm studies. Below we describe some of the issues involved in wake model evaluation using the range of wake/wind farm models from the most straightforward like WAsP, through the moderately complex (Ainslie based e.g. WindFarmer) to the more complex (e.g. Wakefarm based on UPM) to complete CFD models.

A comparison of the main wake/wind farm models was undertaken as part of the ENDOW project (e.g. (Schlez et al., 2002), (Rados et al., 2002)) for small offshore wind farms. From this and a further experiment at Vindeby (Barthelmie et al., 2003a; Barthelmie et al., 2006) it was not possible to distinguish any particular model or group of models as outperforming the others in terms of the accuracy of prediction of single wakes. The main issue for the current project is that there appears to be a fundamental difference between the behaviour of wakes in small wind farms where standard models perform adequately (Barthelmie et al., 2007) and those in large multi-row wind farms where current wind farm models appear to under-predict wake losses (Mechali et al., 2006). It can be postulated that this is due to the interaction of turbulence generated by wind turbines wakes with the overlying atmosphere (Frandsen, 2005) and that a new generation of models is required to deal with this complex interaction of wakes with each other and the boundary-layer (Frandsen et al., 2006). The main objective of our research in this regard is to evaluate and improve wake/wind farm models in comparison with data from large (multi-row) offshore wind farms.

3.1 Definition of flow cases for offshore wind farms based on Horns Rev data

A number of flow cases have been defined for the Horns Rev offshore wind farm. The Horns Rev wind farm is a Danish 160 MW wind farm, owned by DONG Energy A/S and Vattenfall AB, consisting of 80 Vestas V80 wind turbines located in a 8 by 10 grid, with a basic spacing of 7D as shown in Figure 4. See (Jensen, 2004) for more detail about the wind farm and wake measurements.

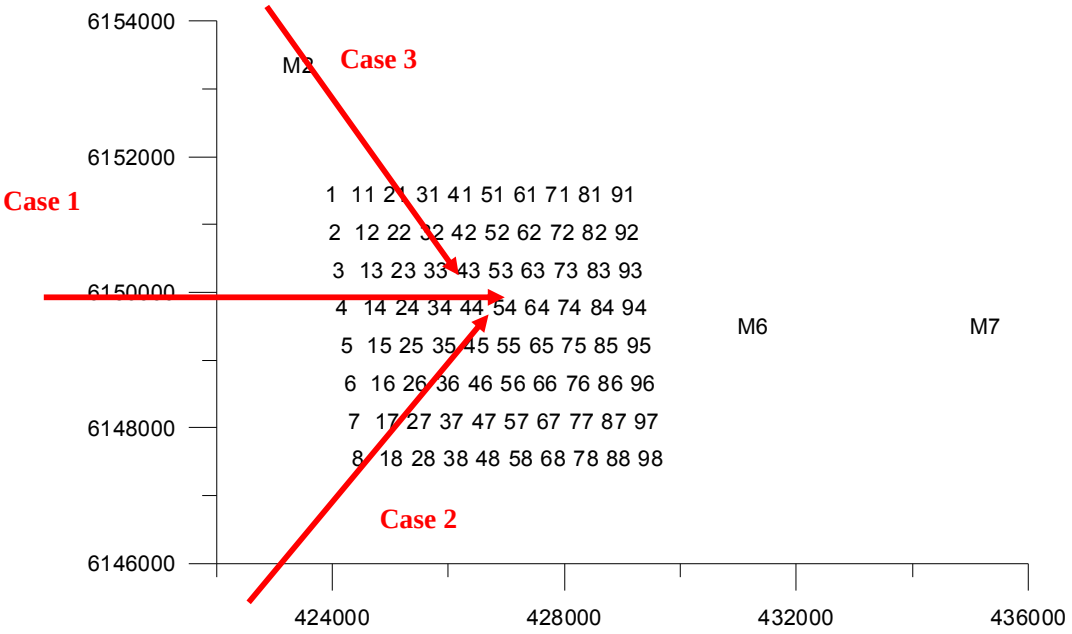

Figure 4: Horns Rev layout including definition of 7D, 9.4D and 10.5D flow directions.

Electrical power, nacelle position and wind turbine status signals have been extracted from the SCADA system with a reference period of 10-minutes and merged with meteorological measurements from three masts (M2, M6 and M7). The undisturbed power values are used to define 3x3 flow cases, corresponding to wind speeds levels of 6±0.5, 8±0.5 and 10±0.5 m/s, which are combined with three different spacings 7 D, 9.4 D and 10.5 D. The mean deficit along a row of turbines has been calculated and presented on Figure 5 for 3 different spacings. More details of the data can be found in Deliverable 8.1.

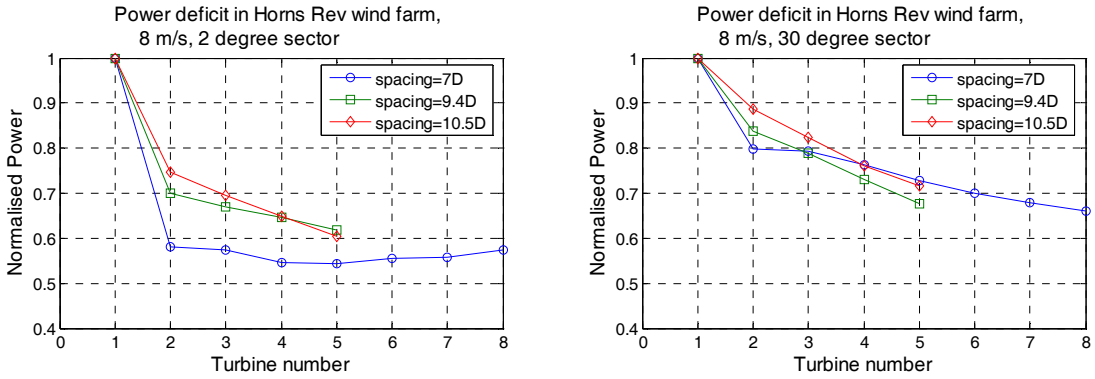

Figure 5: Power deficit inside Horns Rev wind farm for V=8±0.5 m/s inflow for different spacing.

3.2 Models used in the comparison

ECN

ECN's WAKEFARM model is based on the UPMWAKE code which originally was developed by the Universidad Polytecnica de Madrid. It is based on the parabolized Navier-Stokes equations. Turbulence is modelled by means of the k-epsilon turbulence model. Through the parabolization of the governing equations it is assumed that there exists a predominant direction of flow and that (among others) the downstream pressure field has little influence on the upstream flow conditions. In other words, the axial pressure gradients are neglected. These assumptions are plausible some distance away from the turbine and allows for a rapidh numerical solution procedure. In the near wake, however, the wake expands, the flow decelerates and pressure gradients are eminent. Obviously, the assumptions no longer hold in the near wake and additional modelling is necessary to account for the near wake.

In the ENDOW project (Schepers, 2003) this was accomplished by excluding the near wake and the solution procedure started at a fixed distance behind the rotor. A Gaussian velocity-deficit profile was prescribed that acts as a boundary condition for the far wake. This initial profile is based on experiments. Hence the near-wake physics are not accounted for explicitly and rely on tuning with experimental data. In the present project a hybrid method is used which is still based on the WAKEFARM model but the near wake expansion and flow-deceleration is accounted for directly. This is achieved by an analogy with the boundary-layer equations. The (axial) pressure gradients are prescribed as external forces and enforce the flow to decelerate and the wake to expand in the near wake. A free vortex wake method is used to compute these pressure gradient terms a priori.

GH

The ambient wind speed distribution and boundary layer profile is calculated by an external wind flow model, WAsP is used in this project. The wind turbine wake model then makes use of this data superimposing the effect of the offshore wind farm. We use an empirical representation of the wind turbine as suggested by Ainslie (Ainslie, 1988). The initial wake is in this model a function of the wind turbine dimensions, thrust coefficient and local ambient wind speed and turbulence. The eddy viscosity wake model in GH WindFarmer is a CFD calculation representing the development of the velocity deficit using a finite-difference solution of the Navier-Stokes equations in axis-symmetric co-ordinates. The eddy viscosity model thus automatically observes the conservation of mass and momentum in the wake. An eddy viscosity turbulence closure scheme is used to relate the shear stress to gradients of velocity deficit. Empirical expressions are used to model the wake turbulence (Quarton and Ainslie, 1990) and the superposition of several wakes that are impacting on one single location. Multiple wakes are calculated by consecutive downstream modelling of individual wakes. Due to the empirical components in GH WindFarmer it is possible to model typically 7200 wind speed and directional scenarios needed for a complete energy assessment of a wind farm in reasonable time. The model has performed well in all environments, including small offshore wind farms (Barthelmie et al., 2003b).

WAsP

The Wind Atlas Analysis and Application Program (WAsP) is based on a linearised model used in the European Wind Atlas and is the most widely used wind resource/wind farm model in the world. The WAsP program (Mortensen et al., 2005) uses meteorological data from a measurement station to generate a local wind climate from which the effects of obstacles, roughness and complex terrain have been removed. To produce a wind climate for a nearby wind farm or wind turbine site these local effects are reintroduced. In terms of wind farm modelling the wake model in the commercial version is based on (Katic et al., 1986). A new version of the wake model is being developed (see below). The main advantage of the program

is that it is fast and robust. It does not model flow in complex terrain if flow separation occurs although there are methods for improving its predictions in complex terrain which are given in (Bowen and Mortensen, 1996). Also it is not intended for single simulations. The program utilises the station data by fitting it to a two parameter Weibulll distribution. For the complex terrain simulations discussed below it is important to note that the program is being used in a way which is not recommended.

As described in Section 4.2 the WAsP model is designed to use the Weibull distribution of wind speeds in a number of direction sectors. To perform specific simulations for small wind speed and directions bins approximations have to be made which limits the accuracy of the results. For example, here a Weibull distribution for wind speeds was assumed with a shape factor of 2 which is reasonable offshore and with the scale parameter adjusted to give the required mean wind speed. However, a large number of wind speeds will be above or below the mean, giving quite different results from performing a simulation at one specific wind speed. Similarly, the wind speed distribution by direction cannot be limited to having all wind speeds in one sector. Results are shown here to give a general guide as to how WAsP performs. A new wake model is being developed for WAsP and this is described below.

The new WAsP wake model

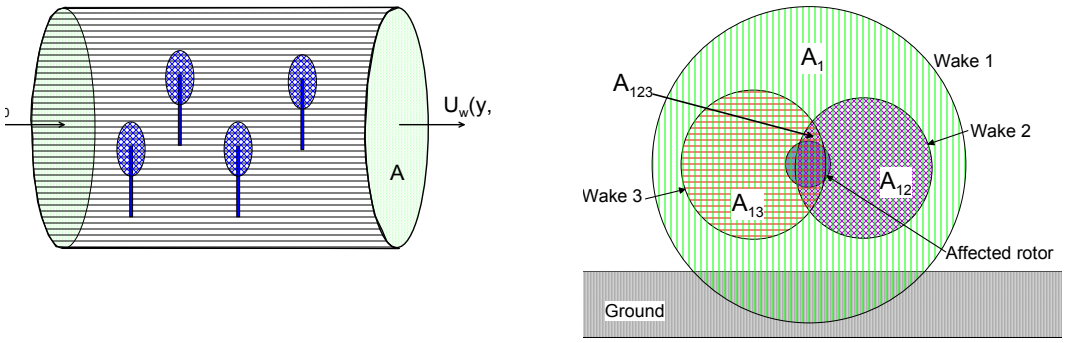

Figure 6: Left. Cylindrical control volume around a set of turbines. Cut-off of the control volume at the ground level has been left out for graphical reasons. Right: Overlapping wakes example. The wake structure is composed of a number of "mosaic tiles", each with one or more overlapping individual wakes.

The model aims at wind farm production estimates in engineering software like WAsP. Thus the wake model must be computationally fast while having the most important wind flow features adequately represented. The model is based on balance equations for volume and momentum in a control-volume as illustrated in Figure 6. The relative speed deficit $\delta \equiv (U_w - U_0)/U_0$ at the exit plane of the control volume is then related to the thrusts on the turbine rotors. The individual wakes are assumed to develop according to a power-law expansion with an exponent of 1/3 to 1/2. In the model, the speed deficit distribution at a certain downwind (turbine) position is assumed to be a pattern of one or more overlapping wakes areas, "mosaic tiles" as illustrated in Figure 6, each assumed to have constant relative speed deficit. The wake model will be calibrated and tested against relevant off-shore wind farm data (Rathmann et al., 2007).

NTUA

NTUA CFD model solves the 3D Reynolds averaged incompressible Navier-Stokes equations with second order spatial accuracy. The model (Magnusson et al., 1996) (see also (Rados et al., 2002)) assumes Cartesian grids, uses the k-ε turbulence closure model and accommodates wind turbines embedded in its grid as momentum sinks representing the force applied on the rotor disk that is in turn

evaluated from the local Ct thrust coefficient. NTUA has performed preliminary offshore wake calculations for the Horns Rev Wind Farm. Due to the extensive cpu effort and memory requirements, only Case 1.8.2 (see below) was initially simulated and model results were compared with observations.

3.3 Comparison of models and measurements

The preliminary evaluation shown in Figure 7 is for a westerly wind direction with flow exactly along the rows as shown in Figure 7. The wind speed bins shown are for 6, 8 and 10 m/s. At these low to moderate wind speeds, the thrust coefficient is relatively high. Thus the wake losses shown are likely to be the most severe but wind directions in the relatively narrow wind direction bins will also occur relatively seldom. As shown in Figure 7, using a narrow wake sector power output drops at the second turbine to about 65% but then remains approximately constant. This is because the centre of the wake is captured. Using a wider sector likely encompasses multiple wake interactions. As expected wake losses decrease as wind speed increases. These limited scenarios indicate a general tendency for unmodified wind farm models to underpredict wake losses while the CFD type models overpredict them and more work is needed to understand this. In the first instance this will focus on wake losses at intermediate sector widths.

Figures 8 and 9 illustrates wake losses for flow at either 315°or 345° which is equivalent to flow down the row but with longer turbine spacing. There is a general tendency to the same behaviour in the different sector widths. Major differences between the observed behaviour in different wind speeds in Case 3 is likely a data issue.

4 Conclusions

Within the Upwind project research in support of upscaling of wind turbines to the 12 MW size and beyond is underway. The research presented in this paper focuses on a comparison of wake models with measurements for a large offshore wind farm. It is clear that further research is needed to understand why the unmodified wind farm models under-estimate wake losses while the

5 Acknowledgements

Research funded in part by EU project UPWIND reference SES6 019945. RB acknowledges the Scottish Funding Council for their support of the Joint Research Institute with the Heriot-Watt University as a component part of the Edinburgh Research Partnership. We would like to acknowledge DONG Energy A/S and Vattenfall AB, owners of the Horns Rev wind farm for allowing use of Horns Rev data.

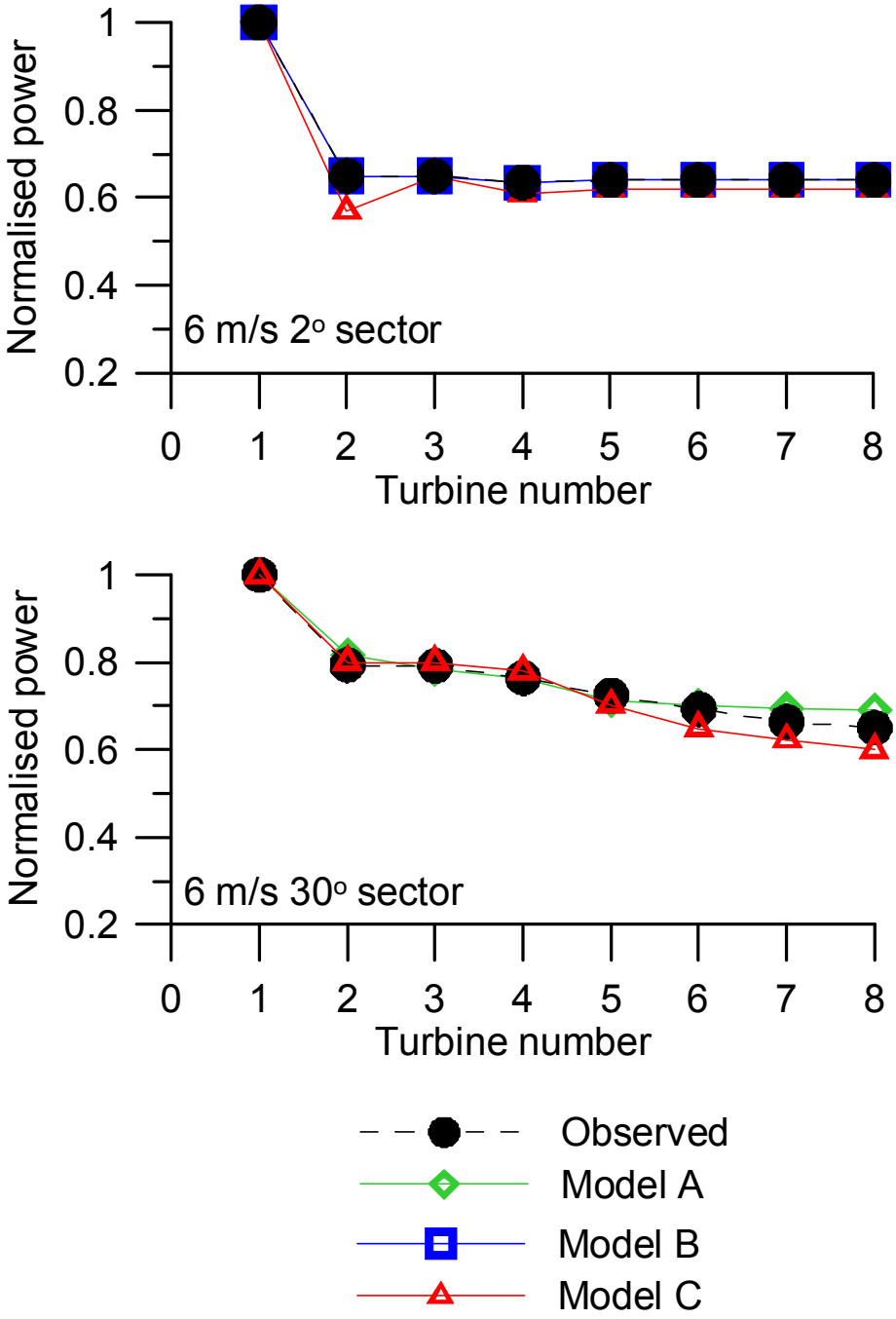

Figure 7: Preliminary comparison of models and measurements for three wind speed scenarios at Horns Rev (direction 270°, case 1 in Figure 4).

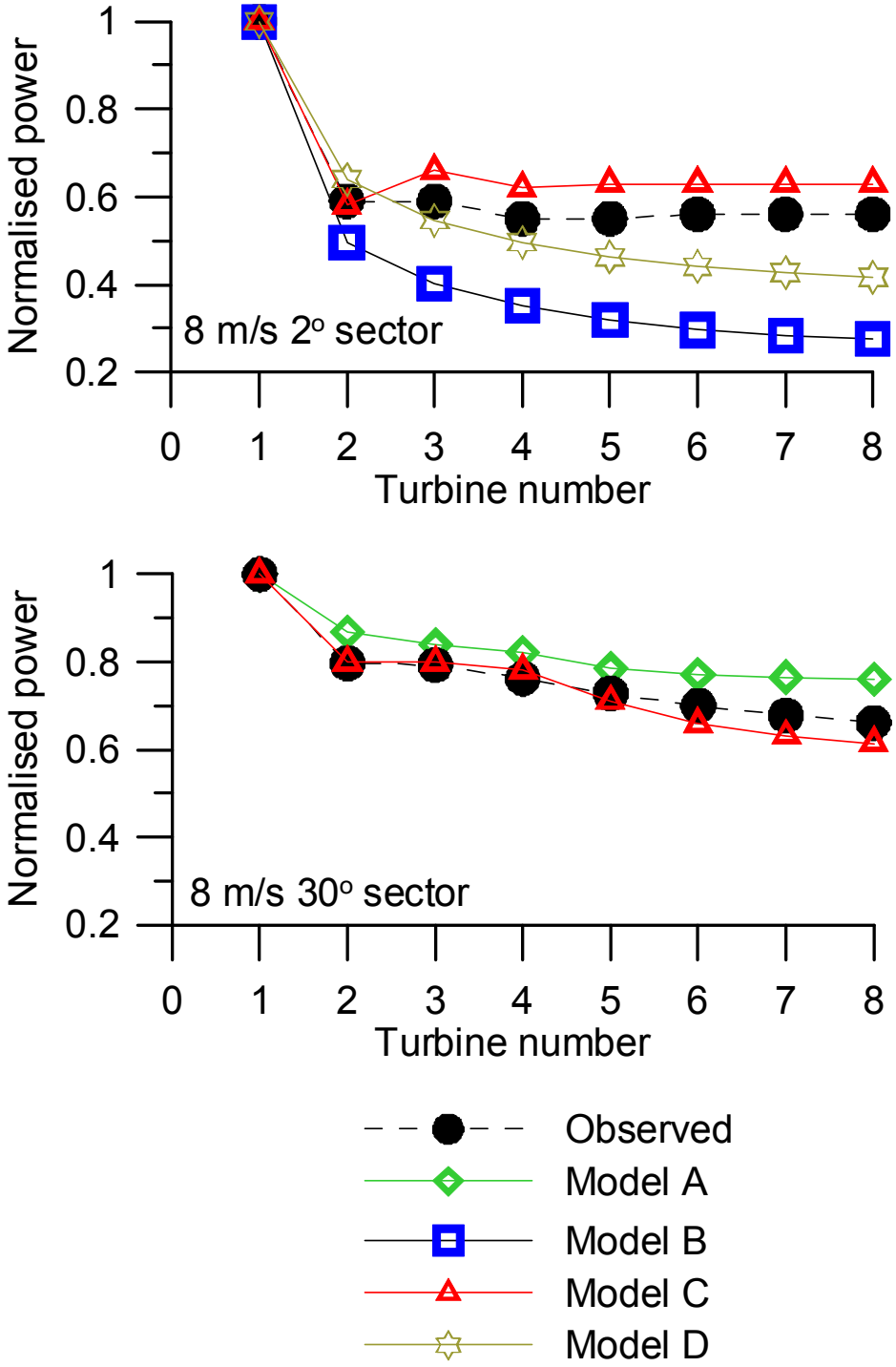

Figure 7: Preliminary comparison of models and measurements for three wind speed scenarios at Horns Rev (direction 270°, case 1 in Figure 4). (Continued)

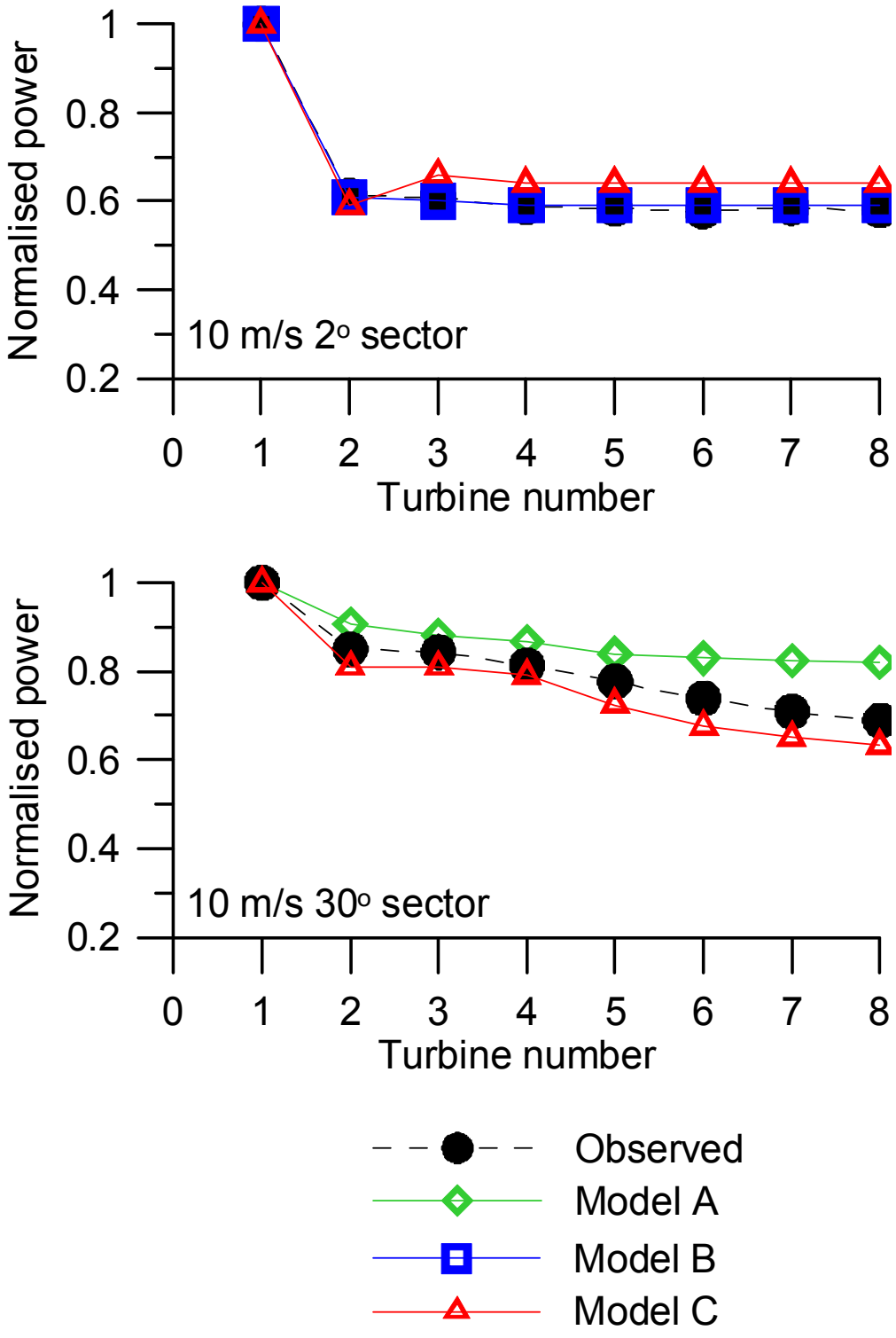

Figure 7: Preliminary comparison of models and measurements for three wind speed scenarios at Horns Rev (direction 270°, case 1 in Figure 4). (Continued).

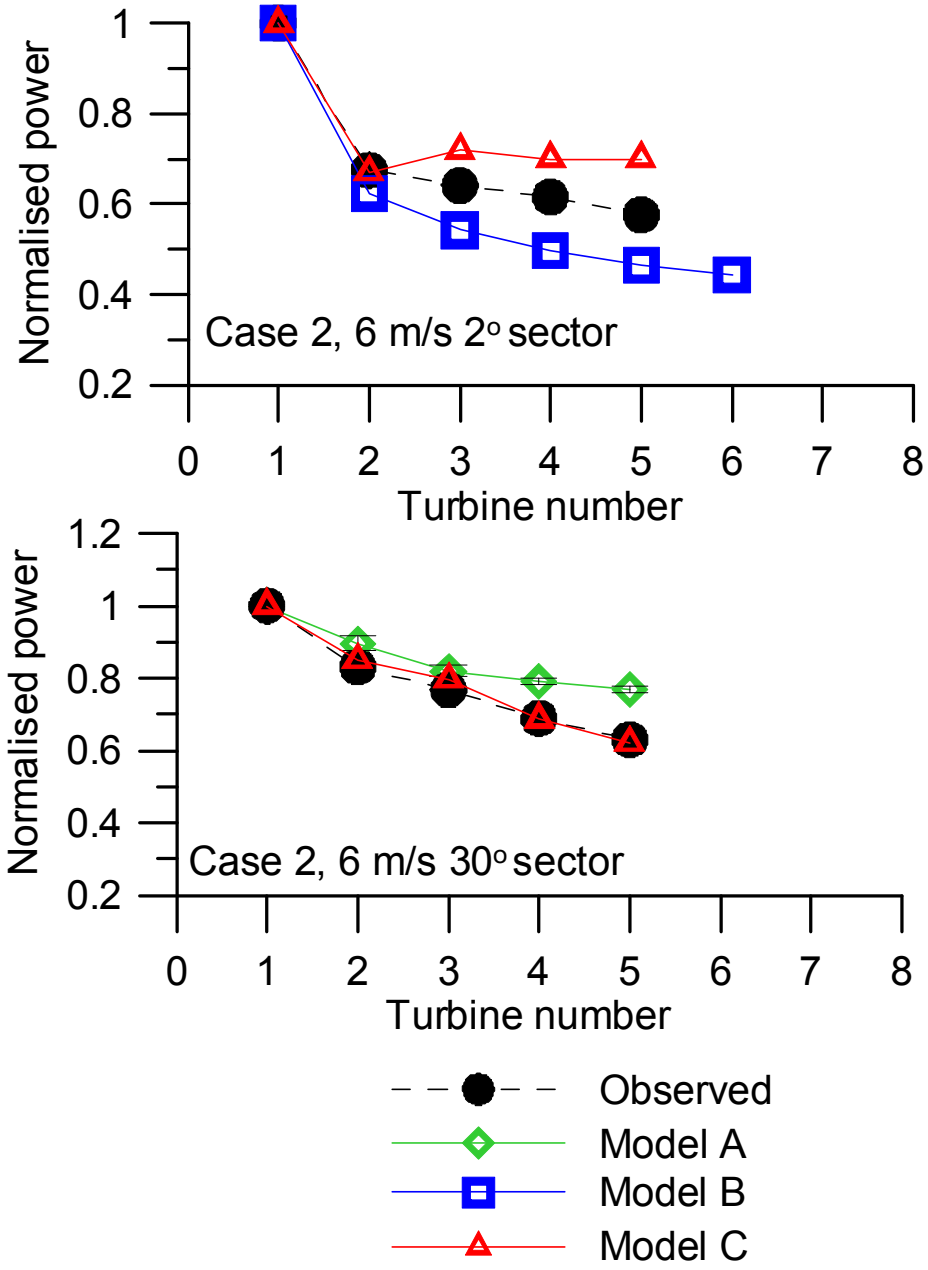

Figure 8: Preliminary comparison of models and measurements for three wind speed scenarios at Horns Rev (direction 315°, case 2 in Figure 4). (Continued).

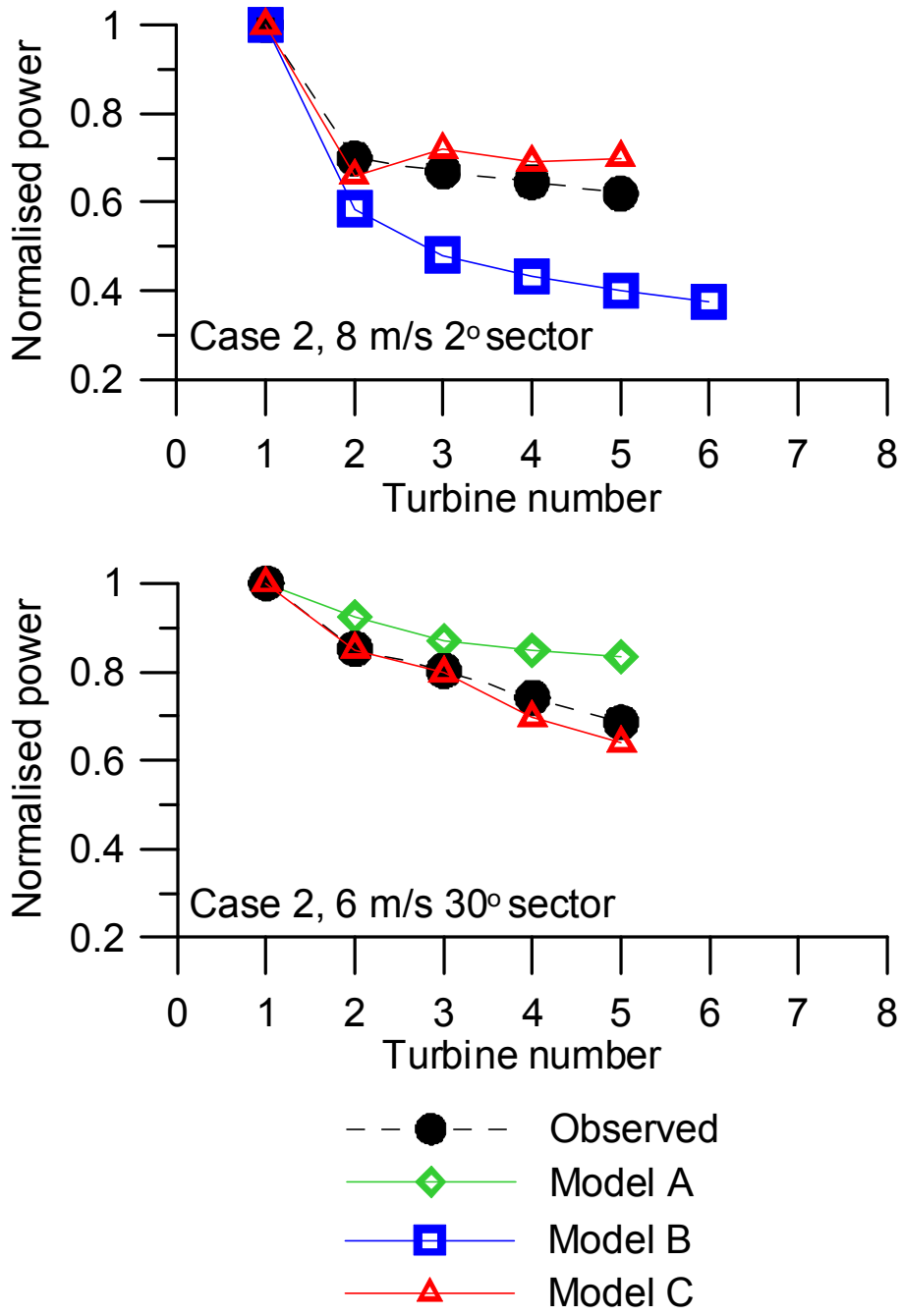

Figure 8: Preliminary comparison of models and measurements for three wind speed scenarios at Horns Rev (direction 315°, case 2 in Figure 4). (Continued).

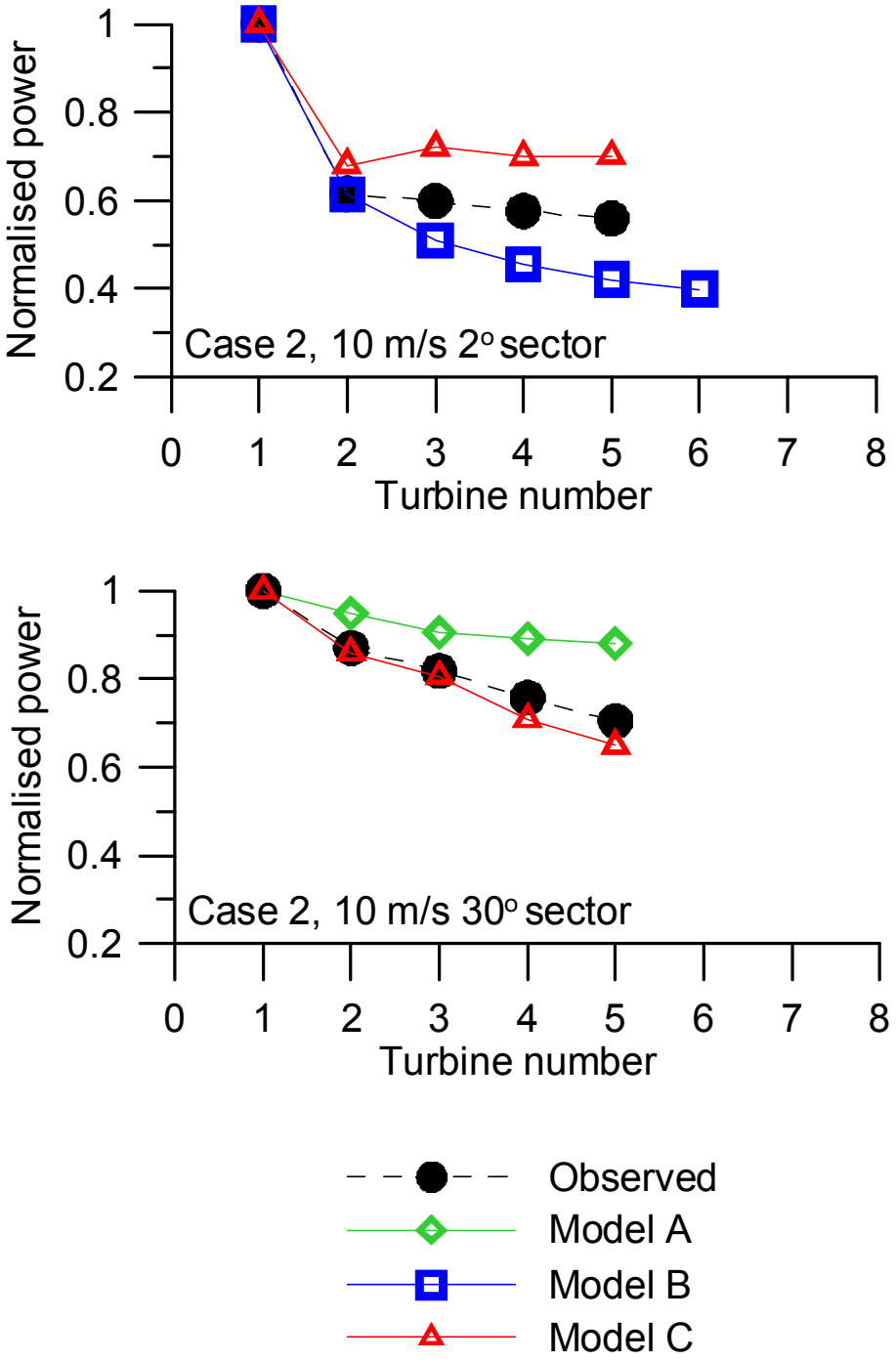

Figure 8: Preliminary comparison of models and measurements for three wind speed scenarios at Horns Rev (direction 315°, case 2 in Figure 4). (Continued).

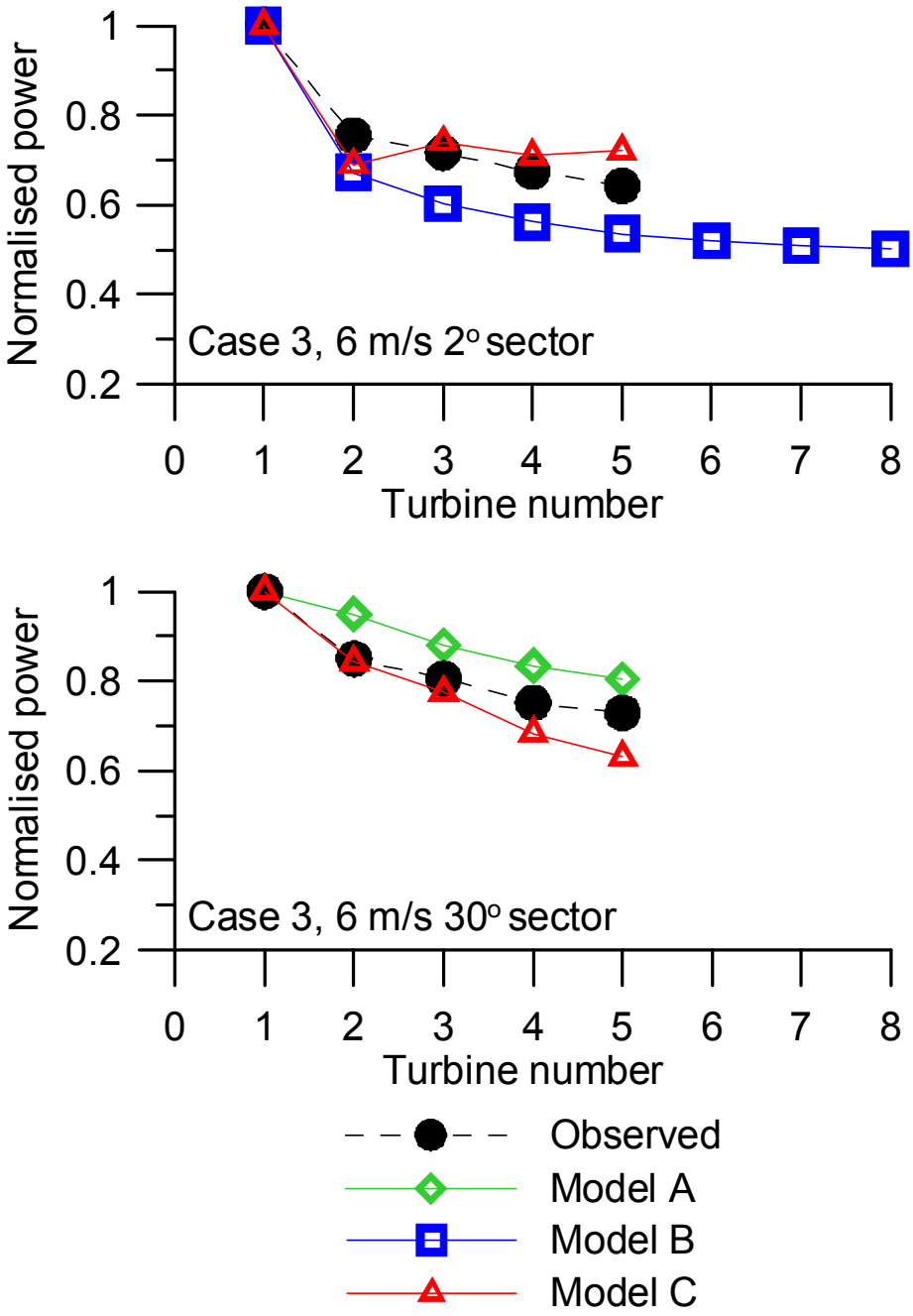

Figure 9: Preliminary comparison of models and measurements for three wind speed scenarios at Horns Rev (direction 345°, case 3 in Figure 4).

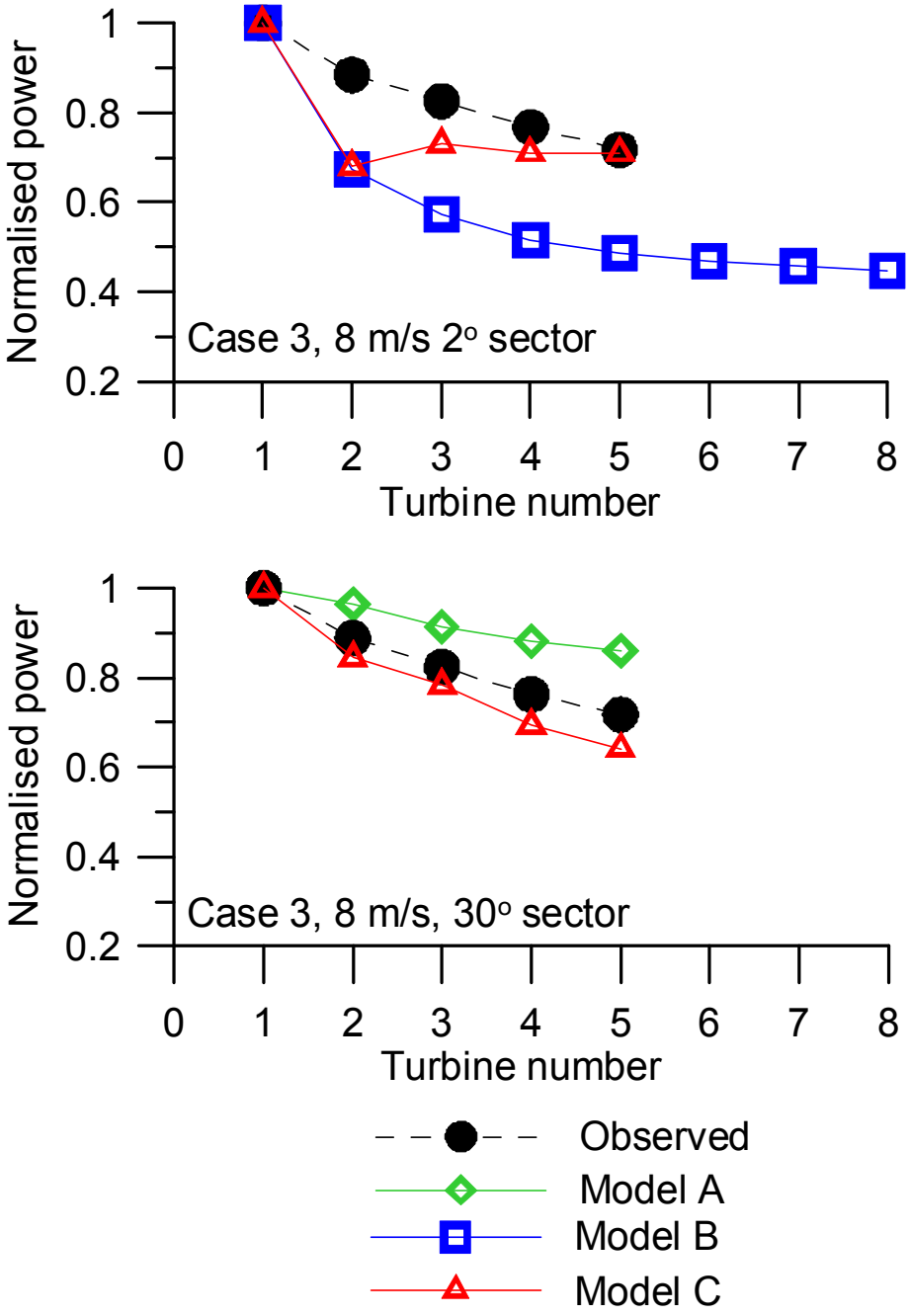

Figure 9: Preliminary comparison of models and measurements for three wind speed scenarios at Horns Rev (direction 345°, case 3 in Figure 4). (Continued).

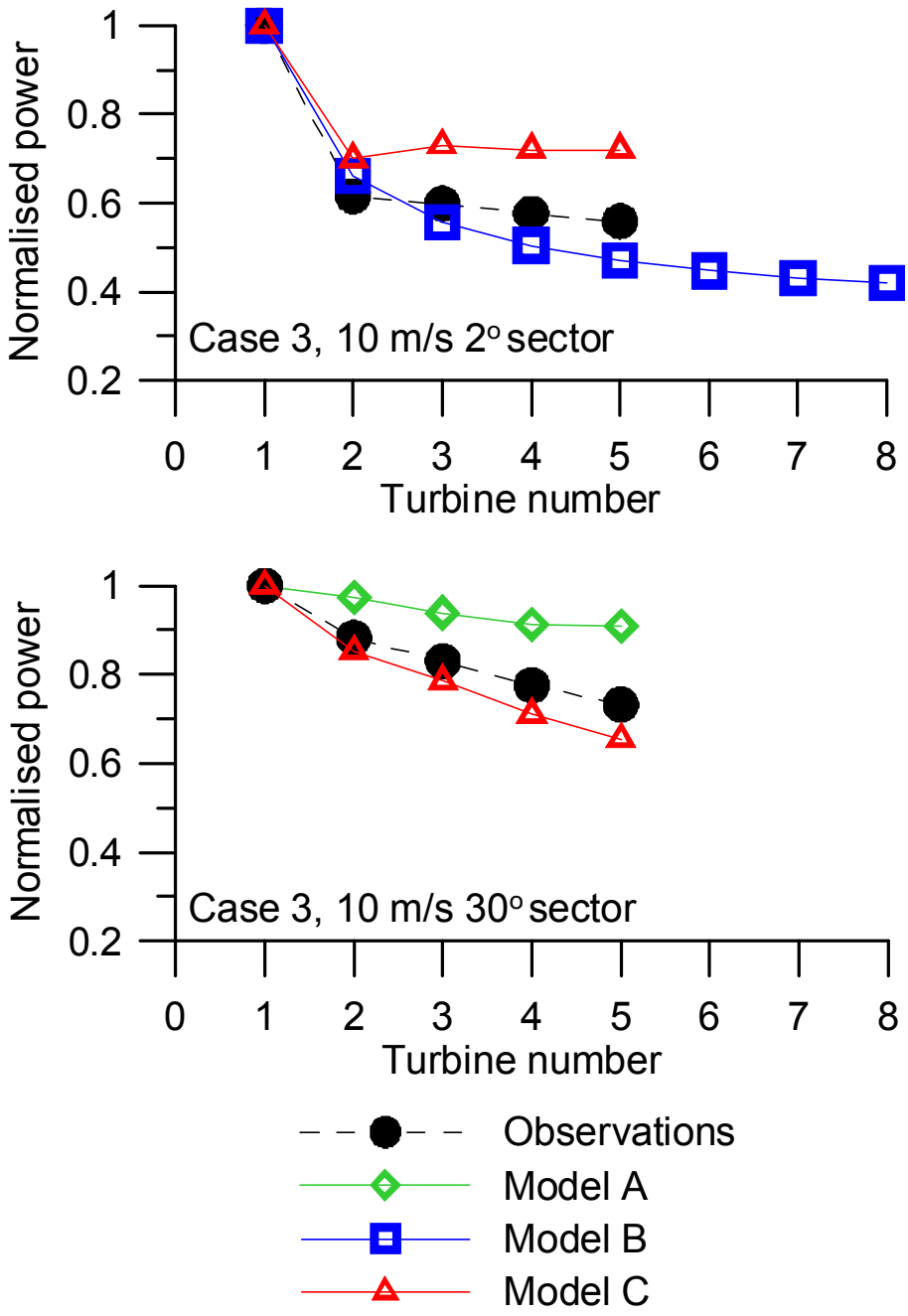

Figure 9: Preliminary comparison of models and measurements for three wind speed scenarios at Horns Rev (direction 345°, case 3 in Figure 4). (Continued).

6 References

1. Barthelmie, R.J., S.C. Pryor, S. Frandsen, et al. Analytical and empirical modelling of flow downwind of large wind farm clusters. in The science of making torque from wind. 2004. Delft.

2. Ainslie, J.F., Calculating the flow field in the wake of wind turbines. Journal of Wind Engineering and Industrial Aerodynamics, 1988. 27: p. 213-224.
3. Mortensen, N.G., D. Heathfield, L. Landberg, et al. (2000) Getting started with WASP 7.0. Risø-I-1532(EN). p. 60. http://www.wasp.dk/Download/DownloadFiles/WAsP/WAsP7/Getting%20Started%20with%20WAsP%207.pdf.
4. Barthelmie, R.J., L. Folkerts, K. Rados, et al., Comparison of wake model simulations with offshore wind turbine wake profiles measured by sodar. Journal of Atmospheric and Oceanic Technology, 2006. 23(7): p. 888-901.
5. Crespo, A., J. Hernandez, and S. Frandsen, Survey and modelling methods for wind turbine wakes and wind farms. Wind Energy, 1999. 2: p. 1-24.
6. Magnusson, M. and A.S. Smedman, Air flow behind wind turbines. Journal of Wind Engineering and Industrial Aerodynamics, 1999. 80: p. 169-189.
7. Frandsen, S. and M.L. Thøgersen, Integrated fatigue loading for wind turbines in wind farms by combining ambient turbulence and wakes. Wind Engineering, 1999. 23: p. 327-339.
8. Quarton, D. and J. Ainslie, Turbulence in wind turbine wakes. Wind Engineering, 1990. 14(1).
9. Thomsen, K. and P. Sørensen, Fatigue loads for wind turbines operating in wakes. Journal of Wind Engineering and Industrial Aerodynamics, 1999. 80(121-136).
10. Mechali, M., L. Jensen, R. Barthelmie, et al. Wake effects at Horns Rev and their influence on energy production. in European Wind Energy Conference and Exhibition. 2006. Athens, Greece: p. 10.
11. Hasager, C.B., R. Barthelmie, M. Christiansen, et al., Quantifying offshore wind resources from satellite maps: study area the North Sea. Wind Energy, 2006. 9(1-2): p. 63-74.
12. Christiansen, M.B. and C. Hasager, Wake effects of large offshore wind farms identified from SAR. Remote Sensing of Environment, 2005. 98: p. 251-268.
13. Antoniou, I., H. Jørgensen, T. Mikkelsen, et al. Offshore wind profile measurements from remote sensing instruments. in European Wind Energy Association Conference. 2006. Athens, Greece, February 2006: 10 pp.
14. Barthelmie, R.J., L. Folkerts, F. Ormel, et al., Offshore wind turbine wakes measured by SODAR. Journal of Atmospheric and Oceanic Technology, 2003. 30: p. 466-477.
15. Wilcox, D.C. (1993) Turbulence modelling for CFD. DCW Industries Inc., IBSN 0-9636051-0-0.
16. Mortensen, N.G., D.N. Heathfield, L. Myllerup, et al. (2005) Wind Atlas Analysis and Application Program: WAsP 8 Help Facility. Risø National Laboratory, Roskilde, Denmark. 335 topics. ISBN 87-550-3457-8. http://www.risoe.dk/vea/projects/nimo/WAsPHelp/Wasp8.htm.
17. Katic, I., J. Højstrup, and N.O. Jensen. A simple model for cluster efficiency. in European Wind Energy Association. 1986. Rome: p. 407-409.
18. Bowen, A.J. and N.G. Mortensen. Exploring the limits of WASP: the wind analysis and application programme. in European Union Wind Energy Conference. 1996. Goteborg: H.S. Stephens and Associates, Bedford, UK.
19. Schlez, W., A.E. Umaña, R. Barthelmie, et al., ENDOW: Improvement of wake models within offshore windfarms. Wind Engineering, 2002. 25: p. 281-287.
20. Rados, K., G. Larsen, R. Barthelmie, et al., Comparison of wake models with data for offshore windfarms. Wind Engineering, 2002. 25: p. 271-280.
21. Barthelmie, R.J., S.T. Frandsen, M.N. Nielsen, et al., Modelling and measurements of power losses and turbulence intensity in wind turbine wakes at Middelgrunden offshore wind farm. Wind Energy (in review), 2007.
22. Frandsen, S. (2005) Turbulence and turbulence-generated fatigue loading in wind turbine clusters. Risø-R-1188(EN). p. 128 http://www.risoe.dk/rispubl/VEA/ris-r-1188.htm.
23. Frandsen, S., R. Barthelmie, S. Pryor, et al., Analytical modelling of wind speed deficit in large offshore wind farms. Wind Energy 2006. 9(1-2): p. 39-53.

24. Jensen, L. Wake measurements from the Horns Rev wind farm. in European Wind Energy Conference. 2004: EWEA (on CD): 9 pp.
25. Schepers, J.G. (2003) ENDOW: Validation and improvement of ECN's wake model. ECN, ECN-C--03-034 (March 2003): p. 113.
26. Barthelmie, R.J., G.C. Larsen, S.C. Pryor, et al. (2003) Efficient development of offshore windfarms (ENDOW): Final report to the European Commission., Risø National Laboratory, Risø-R-1407(EN): 30 pp.
27. Rathmann, O., S.T. Frandsen, and R.J. Barthelmie. Wake modelling for intermediate and large wind farms. in European Wind Energy Conference and Exhibition. 2007. Milan.
28. Magnusson, M., K.G. Rados, and S.G. Voutsinas, A study of the flow down stream of a wind turbine using measurements and simulations. Wind Engineering, 1996. 20(2): p. 389-403.
29. Tetzlaff G. et al. (1984) Meteorologische Messungen zur Standortwahl für Windenergieanlagen im Küstengebiet., Institut für Meteorologie und Klimatologie der Universität Hannover: p. BMFT-FB-T 84-017.
30. Schlez, W., A. Neubert, and G. Smith. New developments in precision wind farm modelling. in Deutsche Windenergie Konferenz. 2006. Bremen: 5 pp.

Appendix 3: Deliverable 8.3 Complex Terrain

Project funded by the European Commission under the 6th (EC) RTD Framework Programme (2002- 2006) within the framework of the specific research and technological development programme "Integrating and Strengthening the European Research Area"

Project UpWind
Contract No.: 019945 (SES6)

"Integrated Wind Turbine Design"

Evaluating Wake Models for Use in Complex Terrain

Deliverable 8.3

AUTHOR:	John Prospathopoulos[1] & Evangelos S. Politis[1]
AFFILIATION:	[1]Centre for Renewable Energy Sources
ADDRESS:	19th km Marathonos Ave., GR19009, Pikermi, Greece
TEL.:	(+30) 2106603300
EMAIL:	jprosp@cres.gr
FURTHER AUTHORS:	Rebecca J. Barthelmie[2] and Daniel Cabezón[3]
AFFILIATION:	[2]University of Edinburgh, [3]National Renewable Energy Centre (Spain)
REVIEWER:	
APPROVER:	

Document Information

DOCUMENT TYPE	Deliverable
DOCUMENT NAME:	D8.3
REVISION:	01
REV. DATE:	February 29, 2008
CLASSIFICATION:	R3: Restricted to WP members
STATUS:	Final

Abstract: This report is the third deliverable of Work Package 8 of the UpWind project. The report deals with the modeling of the wind turbine wakes using a Navier–Stokes solver along with the k-ω turbulence model, where wind turbines are modelled as momentum absorbers. Application is made for two ideal Gaussian hill configurations, one axisymmetric 3D and one quasi-3D, for various turbulence intensity and wind direction conditions. Simulations are made with one wind turbine placed at hilltop and without. The simulations without wind turbine are needed to provide the value of wind speed at the rotor position for the calculation of the actuator disk force, as well as the reference velocity field for the evaluation of the wind speed deficit. Results are presented separately for the cases with and without wind turbine in the form of streamwise wind speed variations at hub height, vertical profiles and wind speed contours. The predictions of the wind speed deficit for the axisymmetric 3D and the quasi-3D hills using two Navier–Stokes algorithms and one commercial software are compared with those in flat terrain for the various levels of turbulence intensity.

Contents

STATUS, CONFIDENTIALITY AND ACCESSIBILITY									
Status				**Confidentiality**				**Accessibility**	
S0	Approved/Released	x		**R0**	General public	x		Private web site	
S1	Reviewed			**R1**	Restricted to project members			Public web site	x
S2	Pending for review			**R2**	Restricted to European. Commission			Paper copy	
S3	Draft for commends			**R3**	Restricted to WP members + PL				
S4	Under preparation			**R4**	Restricted to Task members +WPL+PL				

PL: *Project leader* **WPL:** *Work package leader* **TL:** *Task leader*

1 Introduction

This report is the third deliverable of Work Package 8 of the project "Integrated Wind Turbine Design" (UpWind) partially funded by the European Commission under the contract 019945 (SES6). The partners involved in this work package are Risø National Laboratory (Risø, Denmark), Technical University of Denmark (DTU, Denmark), Energy Research Centre of the Netherlands (ECN), Centre for Renewable Energy Sources (CRES, Greece), National Technical University of Athens (NTUA, Greece), Garrad Hassan & Partners Ltd. (GH, England), University of Edinburgh (UEDIN, Scotland) and National Renewable Energy Centre (CENER, Spain).

The overall objective of this work package is to develop a basis for modelling the wake effects in both large off-shore and complex terrain wind farms. The existing engineering type models have been developed and calibrated for flat terrain applications, so their use in complex terrain applications has not been thoroughly validated yet. Taking into account the difficulty to conduct full scale measurements in complex terrain, Navier–Stokes flow modelling can be used for numerical simulations, since, apart from being able of modelling the complex topography, it is capable of taking into account the interaction of a wind turbine (W/T) wake with the wind shear and the narrowing of the wind rose, and therefore can constitute a sound basis for evaluating the features of the wakes in complex terrain and evaluate the existing engineering-type models. The first step towards this direction is to simulate some ideal complex terrain test cases and to compare the predicted wake characteristics with those in flat terrain. To this end, four reference terrain cases have been defined: a 3D axisymmetric and a quasi-3D Gaussian hill, each one with two different mean slopes.

This report deals with the simulation of the 3D axisymmetric and quasi-3D Gaussian hill for the case of the steepest slope. In Chapter 2, the terrain geometry is defined and the test cases are selected for various levels of turbulence intensity and wind direction. In Chapter 3, a short description of the methodology is provided, focusing on the numerical part concerning grid construction and boundary conditions.

Three partners have contributed to the report; CRES, CENER and UEDIN. Numerical predictions of the wind speed and turbulence intensity are presented in Chapter 4, in the form of streamwise variations, vertical profiles and contours, and are distinguished into three sections. The first one refers to the simulations without W/T, which are necessary to estimate the reference wind speed field. The second presents the respective predictions when a reference paper case 5 MW W/T is included in the computation, modelled as an actuator disk at the hill top. Finally, in the third section, the predictions of the wake deficit, calculated as the wind speed difference between the two previous simulations are presented and compared to those in flat terrain for the various cases.

2 Definition of test cases: the Gaussian hill

The idealized simulation of a single wake in the case of a Gaussian hill has been selected as the basis for the comparison of the wake characteristics between flat and complex terrain. The conclusions deduced from the analysis of the axisymmetric and quasi-3D Gaussian hill can be extended to more complex terrain where the irregularities of the topography are seen as separate hills.

The Gaussian quasi-3D hill geometry is defined by the relationship:

$$z = h\, e^{\left[-0.5\left(\frac{x}{\sigma}\right)^2\right]},\ \sigma = L/1.1774, \quad (1)$$

where x and z are the horizontal and vertical coordinates, h is the height of the hill and L is defined as $x(z = h/2)$. In the case of the axisymmetric hill, $\sqrt{x^2 + y^2}$ replaces x in Eq. (1). The axisymmetric and quasi-3D hill terrain derived from Eq. (1) for $L = 1750$ are shown in Figure 23. The configuration investigated corresponds to $h = 700\,m$ and $L = 1750\,m$ (steep slope with a mean value of 0.4).

The different configurations are simulated with one W/T placed at hilltop and without. The simulations without W/T are needed to provide the value of wind speed at the W/T position for the calculation of the actuator disk force, as well as the reference wind speed field for the evaluation of the wind speed deficit. The machine is the reference 5 MW turbine established in WP 1A1 that features a diameter (*D*) of 126 m and 90 m hub height. The inflow wind speed profile is assumed logarithmic with 500 m boundary layer height and 10 m/s wind speed at hub height. Three different levels of inlet turbulence intensity TI_{in} at hub height, 5, 13 and 20%, are examined. The different levels of TI_{in} correspond to different values of roughness length ($2.29\ 10^{-7}$, 0.0445 and 0.639 *m*, respectively, see Appendix A) and subsequently to different inflow wind speed profiles. All computations are initially carried out for flat terrain using the same grid size to allow for a reliable comparison. For the quasi-3D hill case, three different wind directions, 0, 15° and 30° are also investigated.

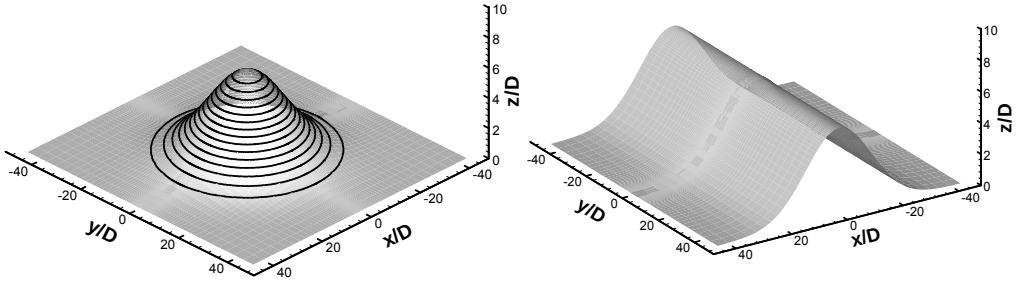

Figure 23: **Layout of the terrain for the axisymmetric and the quasi-3D Gaussian hills.**

3 The Methodology

For the purposes of this report, two Navier–Stokes solvers (one in-house developed in CRES and one commercial, FLUENT, employed by CENER as CFDWake), as well as one commercial, linear software (WAsP) are employed. They are all briefly presented below.

3.1 The Navier–Stokes solver of CRES (CRES–FlowNS)

1.1.1. The algorithm

The governing equations are numerically integrated by means of an implicit pressure correction scheme, where W/Ts are modelled as momentum absorbers by means of their thrust coefficient [1]. A matrix-free algorithm for pressure updating is introduced, which maintains the compatibility of the velocity and pressure field corrections, allowing for practical unlimited large time steps within the time integration process. Spatial discretization is performed on a computational domain, resulting from a body-fitted coordinate transformation, using finite difference/finite volume techniques. The convection terms in the momentum equations are handled by a second order upwind scheme bounded through a limiter. Centred second order schemes are employed for the discretization of the diffusion terms. The Cartesian velocity components are stored at grid-nodes while pressure is computed at mid-cells. This staggering technique allows for pressure field computation without any explicit need of pressure boundary conditions. A linear fourth order dissipation term is added into the continuity equation to prevent the velocity-pressure decoupling. To accommodate the large computational grids needed in most applications for a fair discretization of the topography at hand, a multi-block version of the implicit solver has been developed. Turbulence closure is achieved using the k–ω model [2], with, suitably modified for atmospheric flows, coefficients:

$$\alpha = 0.3706, \quad \beta = 0.0275, \quad \beta_* = 0.033, \quad \sigma = 0.5, \quad \sigma_* = 0.5 \qquad (2)$$

1.1.2. Computational domain and grid

Since all computations are run in non-dimensional form, the dimensionalization of lengths and wind speeds has been made with the W/T rotor diameter, D, and the ambient wind speed, U_∞, respectively. The dimensions of the computational domain have been extended sufficiently so that the flow is not restricted. For the flat terrain cases, the x dimension of the computational domain ranges from $-10D$ to $20D$, the y dimension ranges from $-10D$ to $10D$ and its height is $11D$. For the Gaussian hill cases, the horizontal dimensions x and y range approximately from $-75D$ to $75D$ and the height is $80D$. In each case, the W/T is positioned at the origin of the axes. The distribution of grid-lines is kept the same for all cases. In the horizontal directions, the grid size is constant, equal to $0.05D$, from $-0.55D$ to $0.55D$ (around the W/T), and increases outwards, following a geometrical progression, until the maximum dimension of the domain is reached (see Figure 24). In the vertical direction, the first three grid-lines are positioned close to the ground at heights 0.01, 0.03 and $0.05D$ respectively. From $0.05D$ up to a height of $1.55D$ the grid size is kept constant, equal to $0.05D$, and then increases following a geometrical progression up to the maximum height of the domain. In this way, a fine mesh is constructed in the area of the W/T (see Figure 25).

If the wind direction is not parallel to the x-axis, the disk rotor is rotated by a yaw angle to remain perpendicular to the flow. This angle is the wind speed direction at the W/T's rotor centre, as calculated from the simulation without W/T. In such a case, the horizontal grid mesh is modified, as shown in Figure 26, so that the grid lines are aligned with the plane of the yawed disk rotor.

1.1.3. Boundary conditions

The inflow wind wind speed profile follows the logarithmic law:

$$U_x = \frac{u_*}{K}\ln\left(\frac{z}{z_0}\right), \quad (3)$$

where u_* is the friction velocity, $K = 0.41$ is the von-Karmann constant and z_0 is the roughness length. In the case of inflow not aligned with x direction, Eq. (2) takes the form:

$$U_x = \frac{u_*}{K}\ln\left(\frac{z}{z_0}\right)\cos(a_w), \quad U_y = \frac{u_*}{K}\ln\left(\frac{z}{z_0}\right)\sin(a_w), \quad (4)$$

where a_w is the wind direction relative to x-axis.

The friction velocity is related to the roughness through:

$$u_* = \frac{K}{\ln(\delta / z_0)}, \quad (5)$$

with δ being the atmospheric boundary layer thickness and $U_x(\delta) = 1$. The inflow k and ω profiles are given by the relationships:

$$k = u_*^2 / \sqrt{\beta_*}, \quad \omega = \frac{u_*}{\sqrt{\beta_*}Kz} \quad (6)$$

On the lower surface, the non-slip condition yields zero wind speed. The Cartesian wind speed components are specified at the upper far-field boundary ($U_x = 1, U_y = 0, U_z = 0$). Neumann wind speed conditions are imposed at the outflow and the side boundaries. For the boundary conditions of k and ω, a similar approach is followed. It must be noted that Neumann conditions are imposed at the inlet plane as well, allowing k and ω to adapt themselves to the prescribed boundary conditions.

3.2 The Navier–Stokes solver of CENER (CFDWake)

The model is based on the commercial CFD code Fluent, adapted for the calculation of the local effects on complex terrain in the neutral atmospheric boundary layer. Wind is considered as 3D incompressible steady flow and the Coriolis force as well as the heat effects are omitted.

The modified Navier–Stokes equations are averaged by decomposing the instantaneous velocity into a mean and a fluctuating value, solved through the Reynolds stress tensor. The model is based on the standard k–ε turbulence closure scheme, which includes the Boussinesq hypothesis in order to relate the Reynolds Stress Tensor to the velocity gradients through the eddy viscosity concept.

The inlet boundary conditions are based on the profiles of wind speed, turbulent kinetic energy and turbulent dissipation rate, as solution of the k–ε model in the turbulent surface boundary layer considering local equilibrium at the wall.

The terrain is parameterized as a rough wall according to the local aerodynamic roughness length and it is solved by using modified wall functions adapted to the logarithmic wind speed profile of the atmospheric boundary layer.

The mesh is created through a semi-automatic grid generator based on block topologies in order to generate structured meshes projected onto the surface of the terrain.

The wake model is based on the actuator-disk concept. The turbine is represented by an actuator disk upon which a distribution of forces, defined as axial momentum sources, are applied on the incoming flow at a rate defined by the work that the rotor extracts from the fluid. The rotor is supposed to be uniformly loaded, with the exerted forces as a function of the incident wind speed, the thrust coefficient and the rotor diameter.

3.3 The WAsP algorithm

The Wind Atlas Analysis and Application Program (WAsP) is based on a linearised model used in the European Wind Atlas [3]. The WAsP program [4] uses meteorological data from a measurement station to generate a local wind climate from which the effects of obstacles, roughness and complex terrain have been removed. To produce a wind climate for a nearby wind farm or wind turbine site these local effects are reintroduced.

WAsP utilises the 'BZ-model' of Troen [5] to calculate the wind velocity perturbations induced by orographic features such as single hills or more complex terrain. The BZ-model belongs to a family of models related to the Jackson and Hunt theory for flow over hills [6][7]. The model was developed with the specific purpose of detailed wind energy siting in mind and has the following general features:

It employs a high-resolution, zooming, polar grid. This is coupled with a map analysis routine in order to calculate the potential flow perturbation profile at the central point of the model.

It integrates the roughness conditions of the terrain surface into the spectral or scale decomposition. The 'inner-layer' structure is calculated using a balance condition between surface stress, advection and the pressure gradient.

It uses an atmospheric boundary layer thickness of approx. 1 km to force the large scale (say, more than a few kilometres) flow around high-elevation areas.

The main advantage of the program is that it is fast and robust. It does not model flow in complex terrain if flow separation occurs although there are methods for improving its predictions in complex terrain [8]. For the simulations discussed below it is important to note that the program is being used in a way which is not recommended. WAsP does not treat the near-wake (less than 3-4 rotor diameters) downstream and these results should be disregarded. Also, the programm is being run with a standard wake decay coefficient of 0.075 regardless of the turbulence intesity (which in turn is set by changing the roughness length). The wake decay coefficient defines wake expansion which is related to turbulence intensity so using one standard value for all simulations has an impact on the final results.

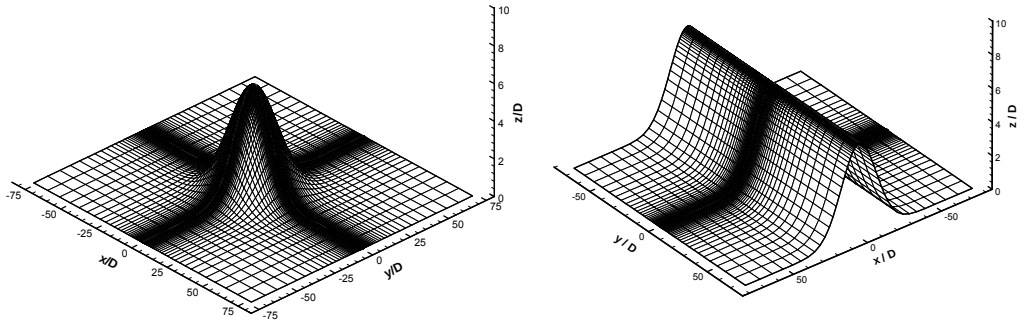

Figure 24: **Layout of the generated surface grids for the axisymmetric and the quasi-3D Gaussian hills**

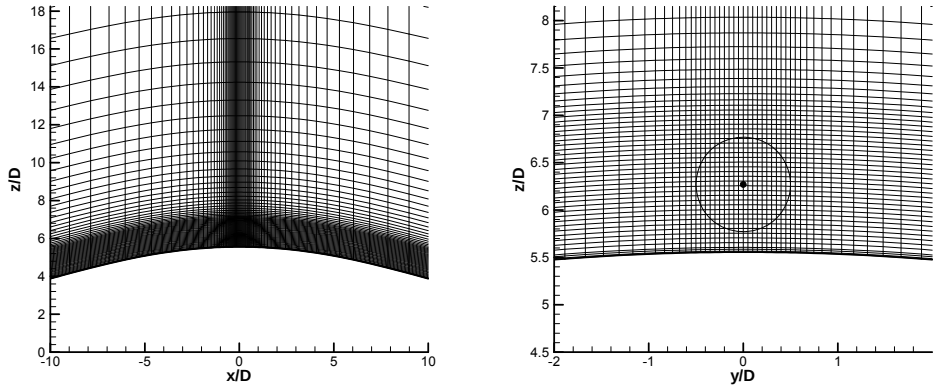

(a) (b)

Figure 25: **Layout of the grid focusing on the W/T region for the axisymmetric Gaussian hill: (a) at plane y=0 and (b) at plane x=0**

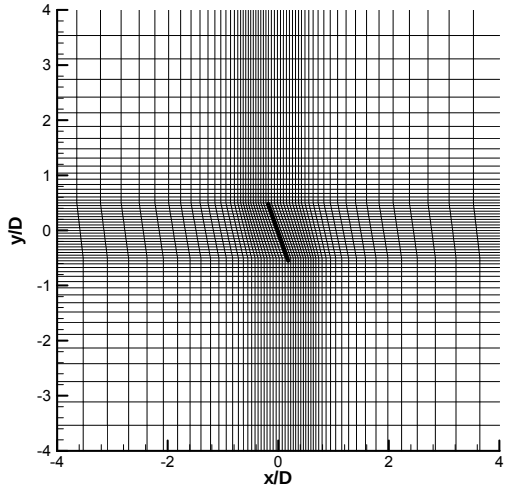

Figure 26: **Ground plan of the xy plane at hub height focusing on the region of the yawed disk rotor**

4 Results and discussion

4.1 Flow over the hill without wind turbines

The configuration of the hill without W/T is used as a datum test case, since it provides the reference wind speed for the calculation of the deficit and the estimation of the thrust coefficient (C_t) value of the W/T rotor and illustrates the basic flow features in complex terrain. In the following, numerical predictions of the wind speed and the turbulence intensity (TI) are presented. The relationship for the calculation of TI is derived in Appendix B, in connection with [9].

Streamwise variations at hub height

The streamwise variation of the normalized streamwise wind speed (U_x) at hub height for the 3D axisymmetric and the quasi-3D hill is shown in Figure 27a and b, respectively. It is observed that the increase in TI_{in}, which is equivalent to an increase in roughness, results in a higher flow acceleration on the hill top and also a higher deceleration in the lee side of the hill.

It should be noted that for all cases the inflow wind speed at hub height is 10 m/s. However, the variation of roughness modifies the shape of the boundary layer and, consequently, the value of the free stream wind speed. In Table 7, the values of the free stream wind speed U_∞, along with the corresponding TI_{in} and roughness lengths, are quoted. Dimensionalization with U_∞ explains the different values of inlet wind speed appearing in Figure 27.

Table 7: **Dependence of the free stream wind speed on TI_{in}**

TI_{in}	z_0 (m)	U_∞ (m/s)
5%	$2.29 \cdot 10^{-7}$	10.90
13%	0.0445	12.47
20%	0.639	13.80

The predicted accelerations and decelerations are higher for the quasi-3D hill. For the quasi-3D case the effect of changing wind direction from 0^o to 15^o and then 30^o is also examined. The presence of the hill changes the initial wind direction leading to a successive decrease by 5^o and 10^o at the W/T rotor centre. The predicted directions of 10^o and 20^o at the rotor centre define the axes along which the wind speed variations are calculated. As depicted by Figure 28, there is a small decrease of the predicted accelerations and decelerations when the wind direction changes to 30^o. This is a result of the fact that the flow follows a slightly smoother effective terrain course with the change in wind direction.

The predicted variation of turbulence intensity is shown in Figure 29 and Figure 30. Turbulence intensity decreases on the hill top and then reaches its peak in the region of highest wind speed deceleration. For high roughness values ($TI_{in} = 20\%$), the peak in the lee side of the hill reaches more than twice the inlet value. These values become even higher in the quasi-3D case (see Figure 29b). The change in the wind direction from 0^o to 30^o results in a decrease of the turbulence intensity in the lee side of the hill because of the flow following a smoother course as mentioned in the previous paragraph (Figure 30). This effect becomes significant for high values of roughness ($TI_{in} = 20\%$, see Figure 30c).

The predictions of CRES (Navier–Stokes) and UEDIN (WAsP) for the wind speed at hub height are compared in Figure 31. Normalization of wind speed refers to the velocity at the hill top. As expected WAsP predicts higher flow acceleration at the hill top than the Navier–Stokes code. Both codes agree that flow acceleration increases with TI_{in}, however flow deceleration is not so well reproduced by WAsP at the lee side of the hill.

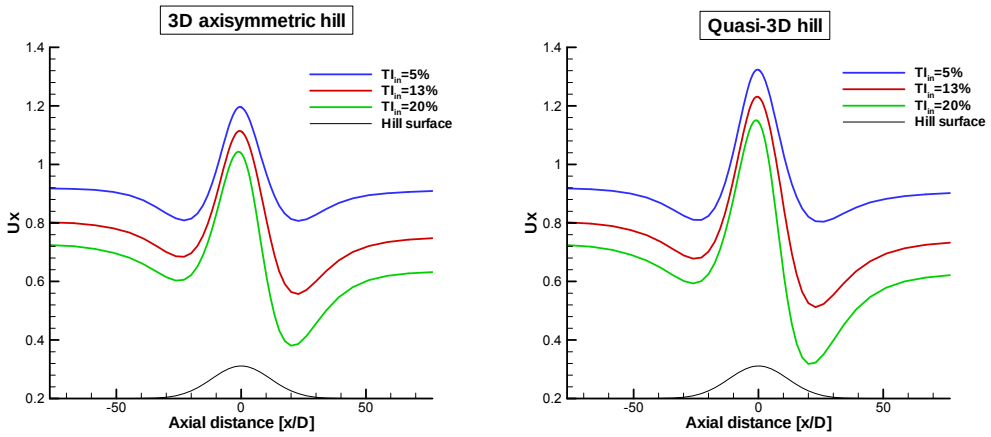

(a) (b)

Figure 27: **Variation of the streamwise wind speed at the hub height of the symmetry plane ($y = 0$) for various values of TI_{in}. Wind direction is 0°.**

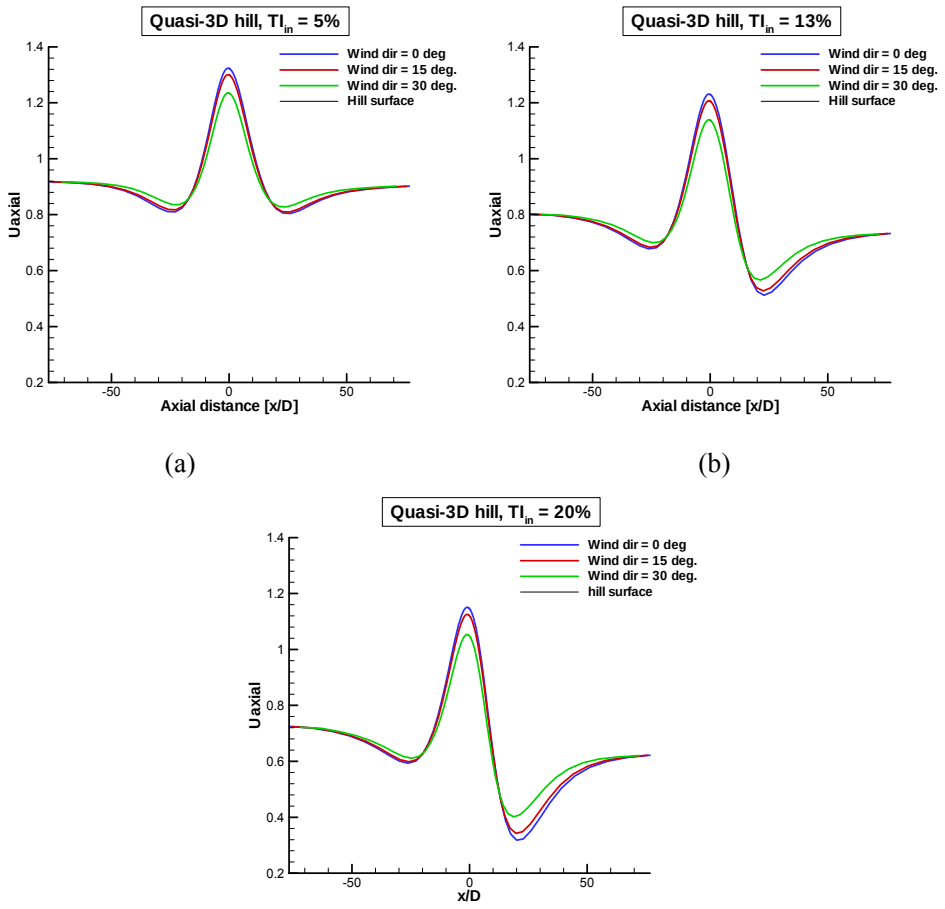

Figure 28: **Variation of the streamwise wind speed at the hub height of the symmetry plane ($y = 0$) for various wind directions and TI_{in} values: (a) 5%, (b) 13% and (c) 20%.**

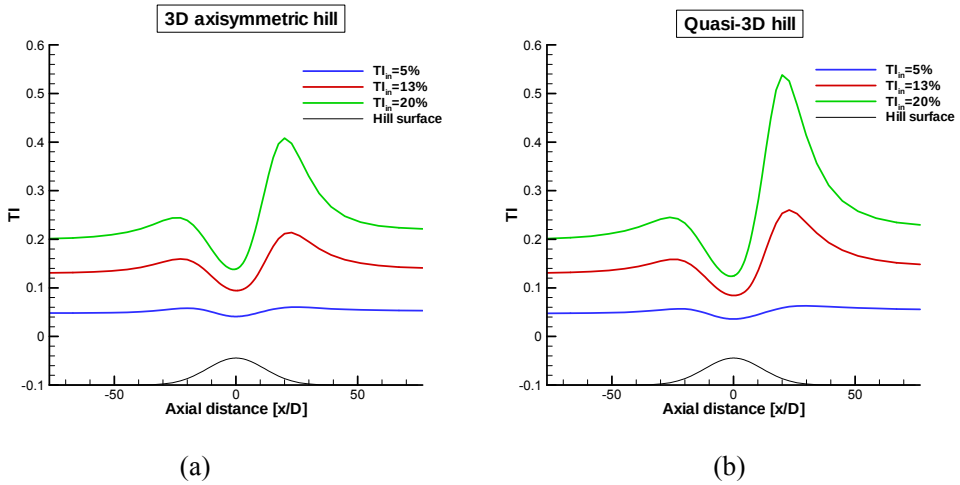

Figure 29: *Variation of the turbulence intensity at the hub height of the symmetry plane ($y = 0$) for various values of TI_{in} values. Wind direction is 0^o.*

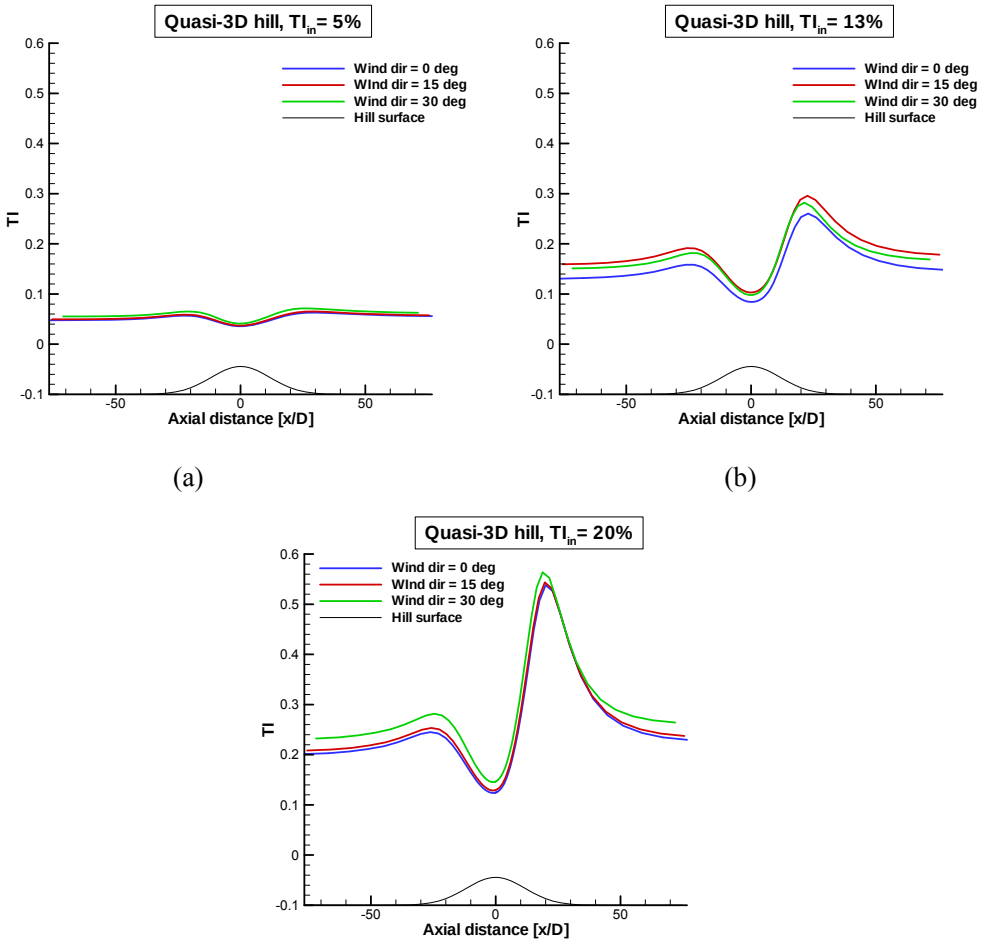

Figure 30: **Variation of the turbulence intensity at the hub height of the symmetry plane ($y = 0$) for various wind directions and TI_{in} values: (a) 5%, (b) 13% and (c) 20%.**

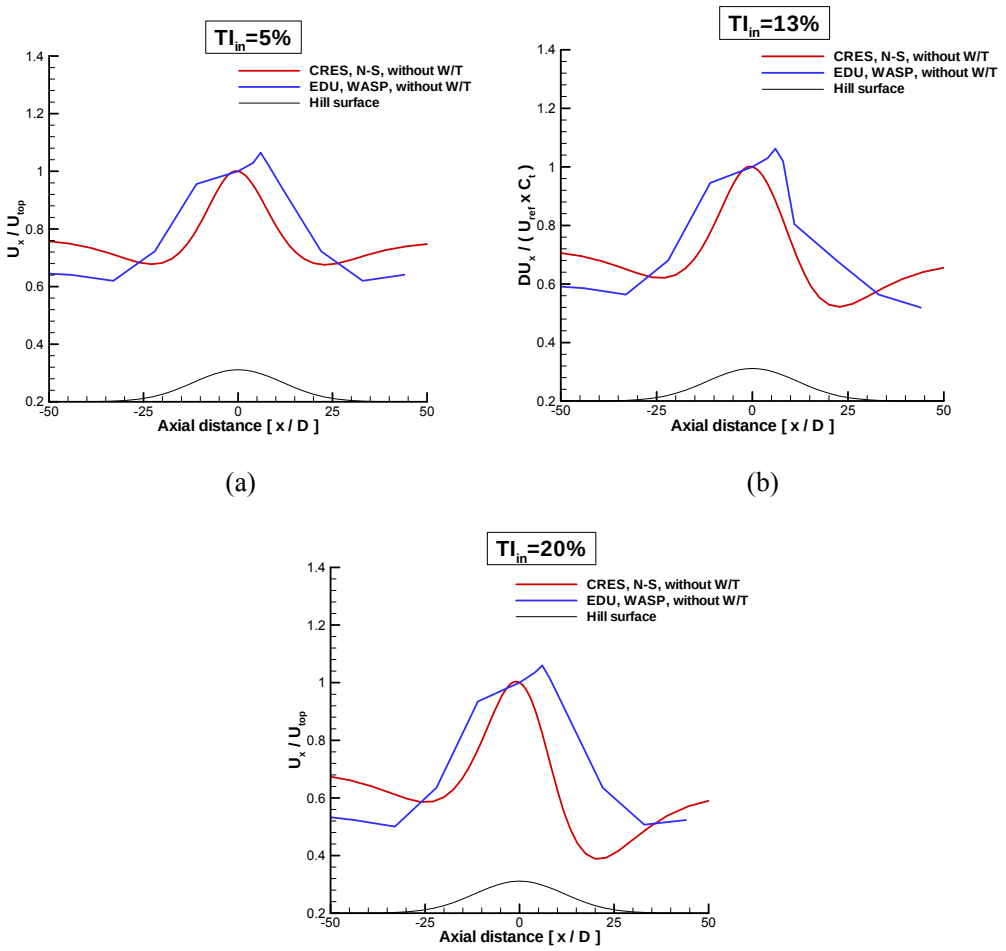

Figure 31: **3D axisymmetric hill - *Streamwise* wind speed variation at the hub height of the symmetry plane ($y = 0$) for various TI_{in} values: (a) 5%, (b) 13% and (c) 20%. Normalization has been done with the predicted velocity at the hill top (hub height) without W/T.**

Vertical profiles

The vertical profiles of U_x component of the wind speed vector are shown in Figure 33 for various distances downstream the hill top. Plotting positions have been selected to cover regions of near and far wake in the presence of a W/T. In the absence of a W/T, the first three positions, $x = 1$, 3 and $5D$ are located in the region of highest flow acceleration, $x = 10D$ is an intermediate position, $x = 20D$ is the position of the highest flow deceleration and $x = 40D$ is located at the hill base, where the terrain has become flat.

The conclusions drawn from the streamwise variations presented in the previous paragraph are also confirmed from the vertical profiles. As depicted by Figure 32 the flow acceleration is observed near the hill top ($1-5D$) and the maximum flow deceleration occurs at $x = 20D$. The deceleration is higher for $TI_{in} = 20\%$. At $x = 40D$, the boundary layer has recovered its

logarithmic shape (with higher thickness though) for the lowest $TI_{in} = 5\%$, but it is still in deceleration for $TI_{in} = 20\%$. The comparison of the vertical profiles between axisymmetric and quasi-3D hill indicates the higher acceleration and deceleration for the second case.

The change in wind direction does not significantly affect the wind speed profiles. The slight decrease of the maximum flow acceleration observed in the streamwise variations of Figure 28 is also observed in the vertical profiles of Figure 33 for $x = 1$, 3 and $5D$. The vertical profiles of turbulence intensity presented in Figure 34 and Figure 35 show the significant increase of turbulence in the region of flow deceleration. The level of turbulence intensity remains well above its inlet value even at $40D$ downstream the hill top.

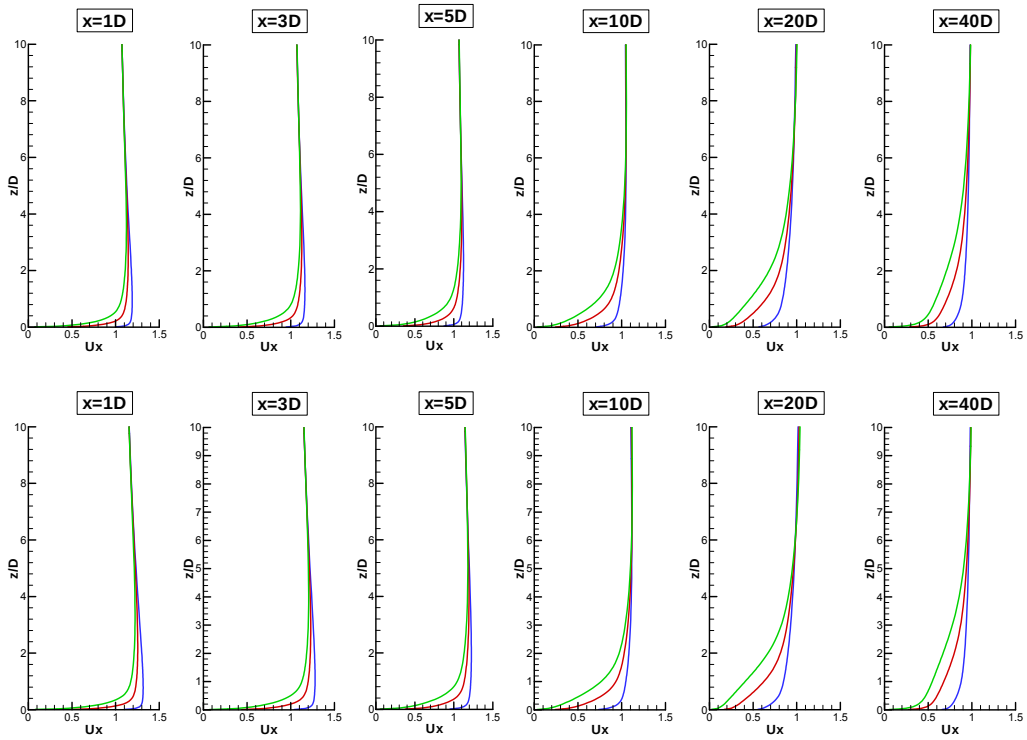

Figure 32: *Vertical profiles of the streamwise wind speed downstream the hill top for various values of TI_{in} : 5%, 13%, 20%. Upper: 3D axisymmetric hill. Lower: Quasi-3D hill (wind direction 0^o).*

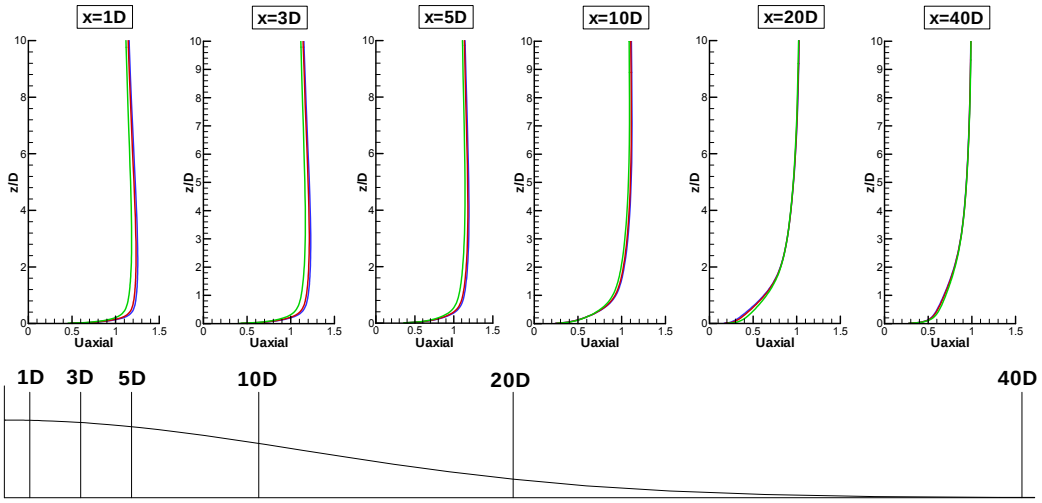

Figure 33: *Vertical profiles of the streamwise wind speed downstream the hill top of the quasi-3D hill for various wind directions:* ——— *0°,* ——— *15°,* ——— *30°. TI_{in} is 13%.*

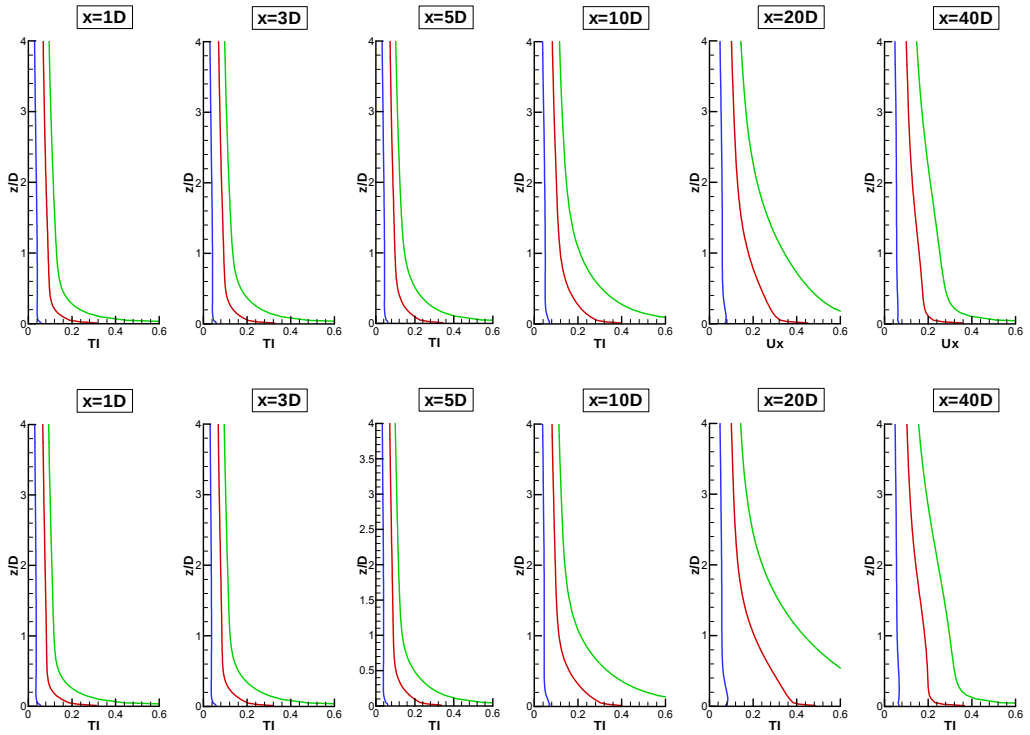

Figure 34: **Vertical profiles of the turbulence intensity downstream the hill top for various values of TI_{in} : ——— 5%, ——— 13%, ——— 20%.**

Upper: 3D axisymmetric hill. Lower: Quasi-3D hill (wind direction is 0°).

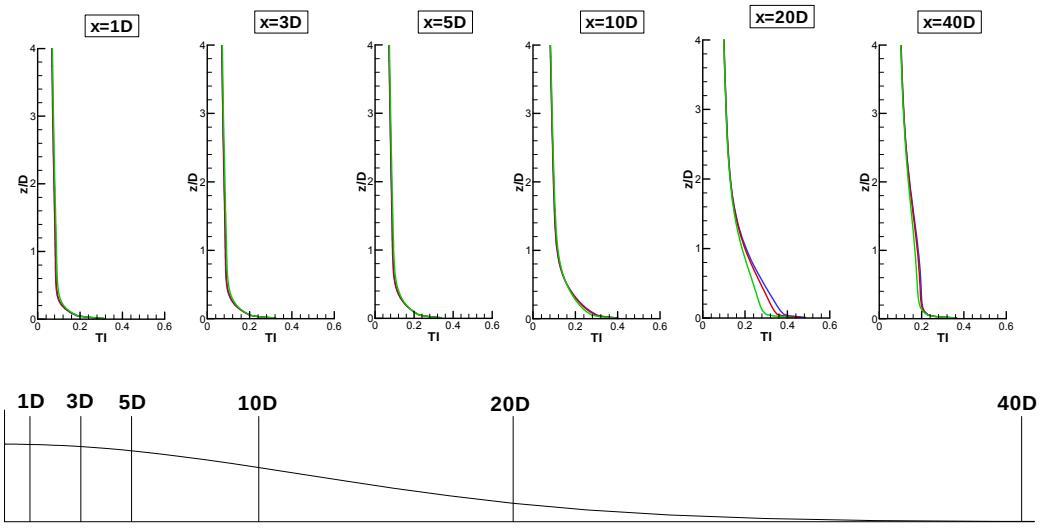

Figure 35: *Vertical profiles of the turbulence intensity downstream the hill top of the quasi-3D hill for various wind directions:* ——— *0°,* ——— *15°,* ——— *30°.* TI_{in} *is 13%.*

The predictions between CRES and UEDIN for the vertical streamwise velocity profiles downstream of the hill top are compared in Figure 36. Normalization of velocity refers to the hill top velocity at hub height. The results at distances 6-11D confirm that WAsP predicts lower flow deceleration at the lee side of the hill. The agreement on the profile gradients can be considered good at all distances.

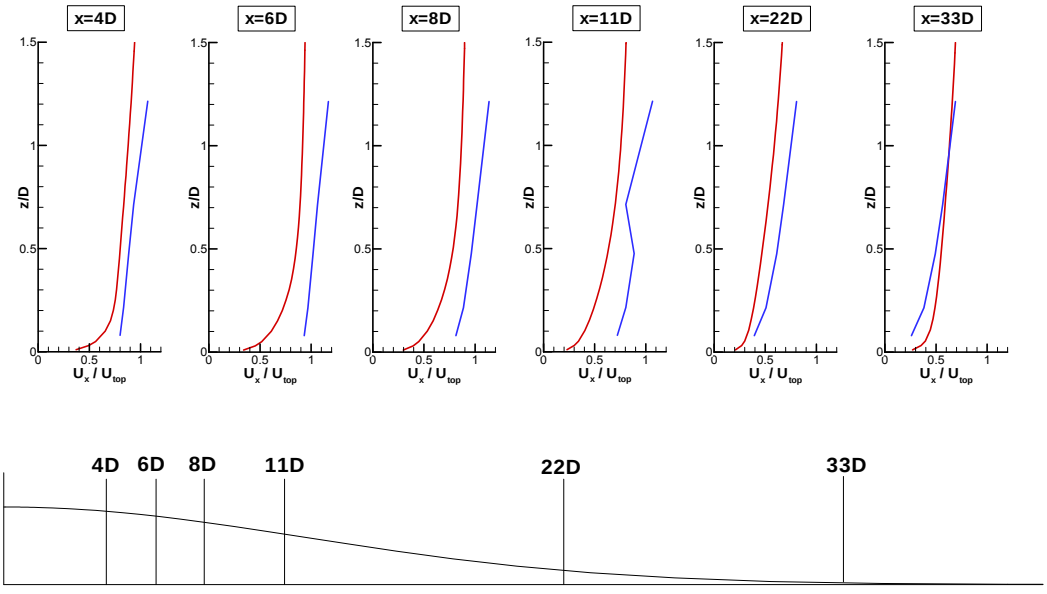

Figure 36: *Vertical profiles of the streamwise velocity downstream the hill top of the 3D axisymmetric hill for various distances.* ——— *UEDIN (WAsP),* ——— *CRES (N-S).* TI_{in} *is 13%. Normalization has been done with the predicted velocity at the hill top (hub height).*

Wind speed contours

The wind speed contours of the streamwise wind speed at the plane $y = 0$ are compared between the axisymmetric and the quasi-3D hill in Figure 37 for the three TI_{in} levels considered. The comparison confirms that the wind speed around the hill top are higher in the quasi-3D case than the axisymmetric one. The symmetry of the wind speed pattern around the hill top indicates the full convergence of the numerical code. In Figure 38, the same comparison is made for the U_x wind speed contours at the hub height plane a. g. l. A symmetrical and a 2D-like patterns are clearly observed in the axisymmetric and quasi-3D cases, respectively. The higher accelerations and decelerations in the quasi-3D case are also clearly presented here.

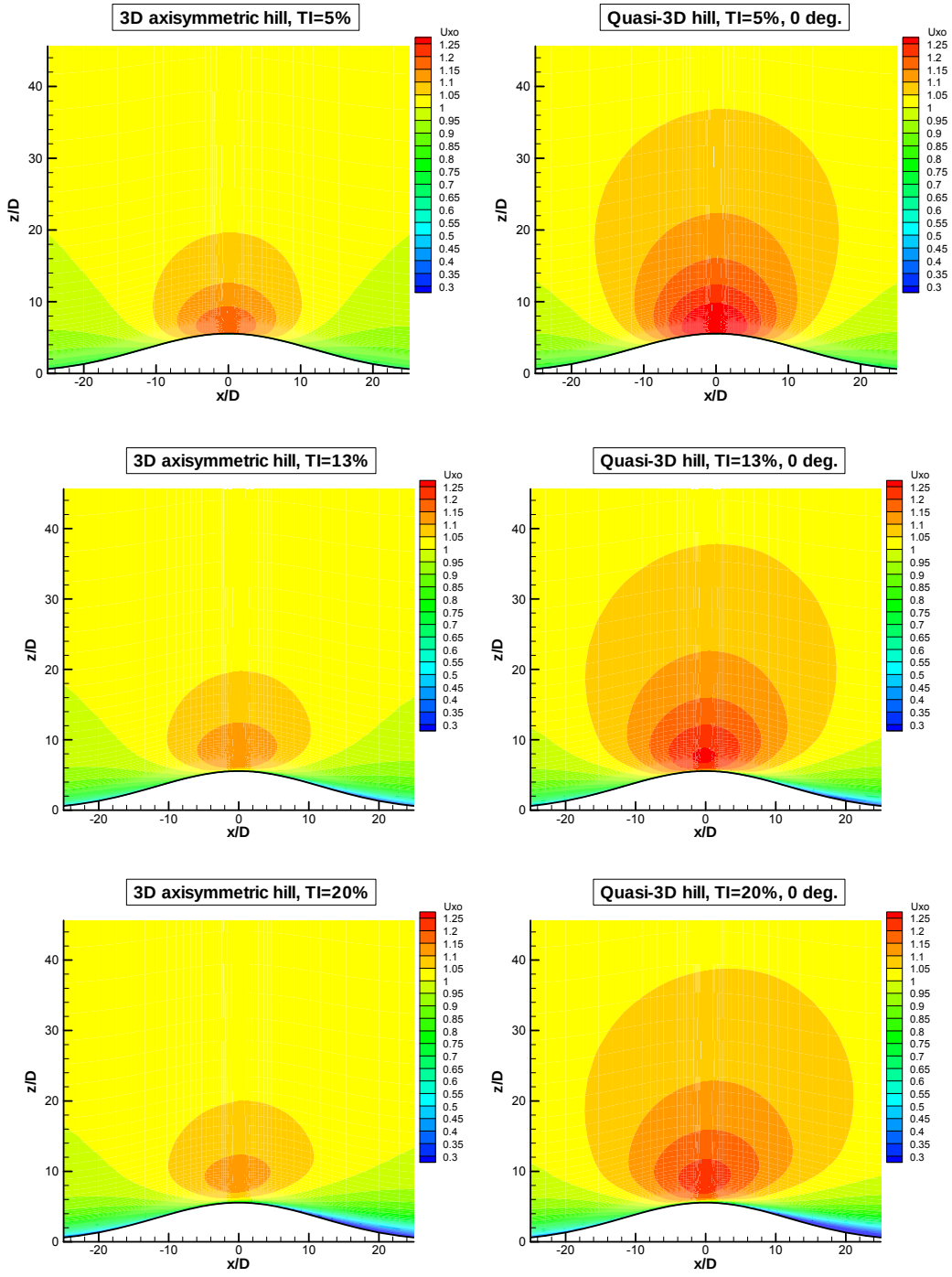

Figure 37: **Streamwise wind speed contours for the axisymmetric and quasi-3D hill at the symmetry plane ($y = 0$). Upper: TI_{in} = 5%. Middle: TI_{in} = 13%. Lower: TI_{in} = 20%.**

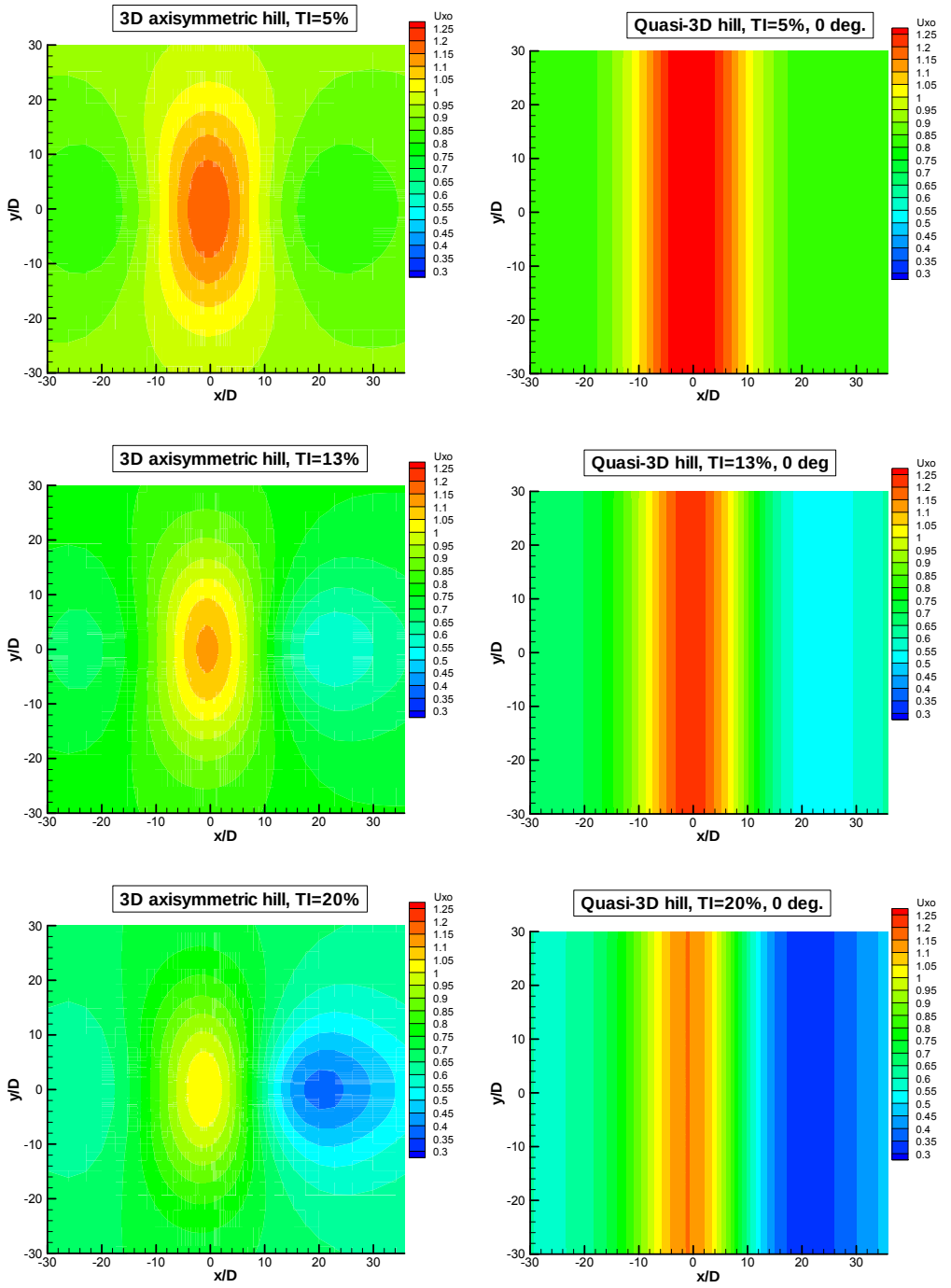

Figure 38: **Streamwise wind speed contours for the axisymmetric and quasi-3D hill at hub height a. g. l. Upper: TI_{in} = 5%. Middle: TI_{in} = 13%. Lower: TI_{in} = 20%.**

4.2 Flow over the hill with one wind turbine at the top

The presence of the W/T is simulated as a momentum sink at the grid cells that correspond to the disk rotor surface. The source term added to the right hand-side of the momentum equation in x-axis expresses the force exerted on the fluid by the disk rotor:

$$F_{disk} = -\frac{1}{2}\rho U_{disk}^2 C_t A, \quad (7)$$

where ρ is the air density, A is the disk rotor surface, U_{disk} is the reference wind speed at hub height (which obtained from the respective case without W/T) and C_t is the thrust coefficient that corresponds to U_{disk} through the $C_t = f(U)$ curve of the W/T. In Eq. (7), U_{disk} and C_t have been approximated as constant across the disk surface. In Table 8, the predicted reference velocities U_{disk} for the various cases without W/T and the corresponding C_t values are quoted. The values of U_∞ for the different TI_{in} values are also included in Table 8.

Table 8: **Reference velocities and thrust coefficients for the calculation of the W/T force in the various cases examined**

TI_{in}	U_∞	Axisymmetric hill	Quasi-3D hill		
			0°	15°	30°
5%	10.90 m/s	$U_{disk}=1.19\,U_\infty$ $C_t=0.392$	$U_{disk}=1.32\,U_\infty$ $C_t=0.281$	$U_{disk}=1.3\,U_\infty$ $C_t=0.296$	$U_{disk}=1.23\,U_\infty$ $C_t=0.354$
13 %	12.47 m/s	$U_{disk}=1.11\,U_\infty$ $C_t=0.317$	$U_{disk}=1.23\,U_\infty$ $C_t=0.230$	$U_{disk}=1.20\,U_\infty$ $C_t=0.246$	$U_{disk}=1.14\,U_\infty$ $C_t=0.317$
20 %	13.80 m/s	$U_{disk}=1.04\,U_\infty$ $C_t=0.286$	$U_{disk}=1.15\,U_\infty$ $C_t=0.210$	$U_{disk}=1.12\,U_\infty$ $C_t=0.225$	$U_{disk}=1.05\,U_\infty$ $C_t=0.278$

4.2.1 Streamwise variations at hub height

The impact of TI_{in} and hill geometry on the development of the streamwise wind speed are similar to those observed in the case without W/T. However, the W/T presence causes an abrupt drop of the wind speed at the disk rotor position, as seen in Figure 39. In the quasi-3D hill case, the differences in acceleration and deceleration produced by changing the wind direction are reinforced with the presence of W/T (see Figure 40). The same applies for the turbulence intensity variations (see Figure 41 and Figure 42). It must be noted that in Figure 40, the U_{axial} has been calculated along the axis defined by the predicted flow direction at rotor's centre in the respective case without W/T. In Figure 43, the streamwise wind speed and turbulence variations are compared for the cases with and without W/T. Apart from the expected differences in the W/T region, an increase in the flow deceleration combined with an increase in turbulence intensity are observed at the lee side of the hill. This effect is more pronounced for the cases with low TI_{in} and weakens as the level of TI_{in} increases.

The predictions of the streamwise wind speed at hub height are compared between CRES and UEDIN ın Figure 22. Normalization refers to the predicted velocity at hill top without W/T.

Both codes predict the abrupt velocity reduction due to the actuator disk. However, the coarse discretization in WAsP results does not permit an accurate comparison of the predicted velocity reductions. The comparison of the predictions behind the W/T is similar to that of Figure 9, without the W/T, indicating the dominant effect of the terrain on the velocity variation.

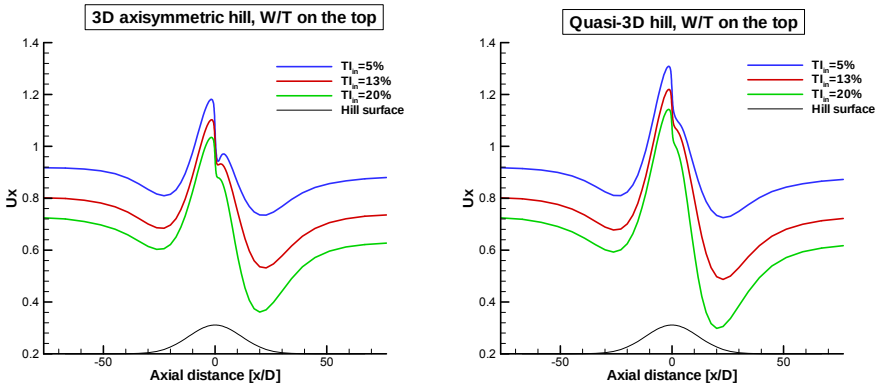

(a) (b)

Figure 39: **Variation of the streamwise wind speed at the hub height of the symmetry plane ($y = 0$) for various values of TI_{in} . Wind direction is 0°.**

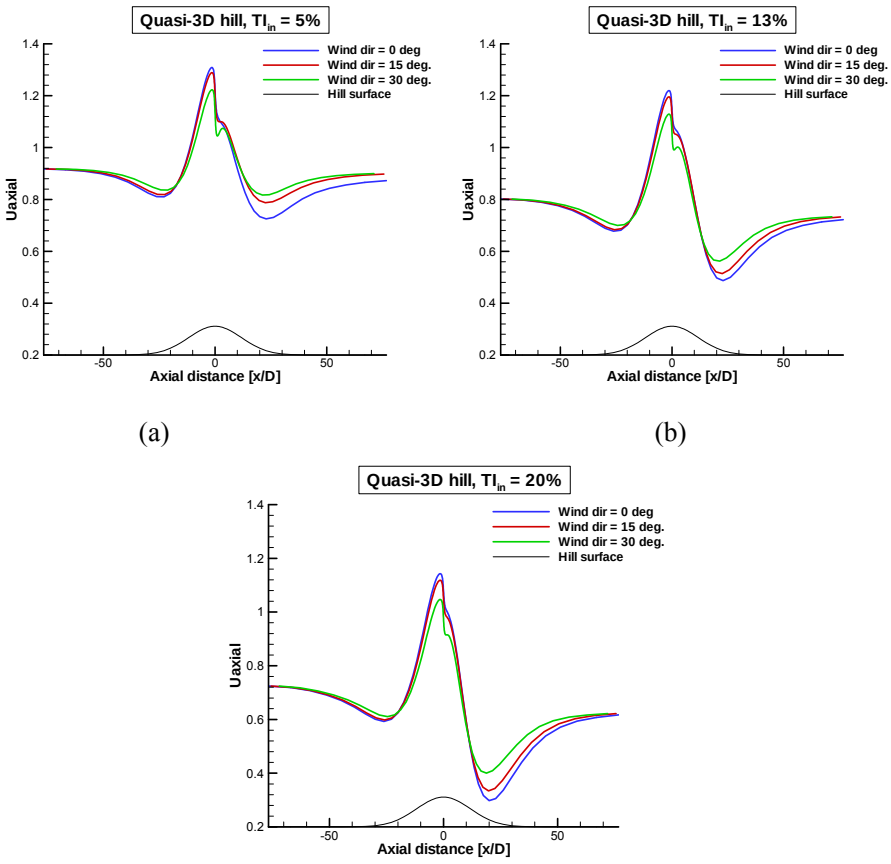

(a) (b)

(c)

Figure 40: **Variation of the streamwise wind speed at the hub height of the symmetry plane ($y = 0$) for various wind directions and TI_{in} values: (a) 5%, (b) 13% and (c) 20%.**

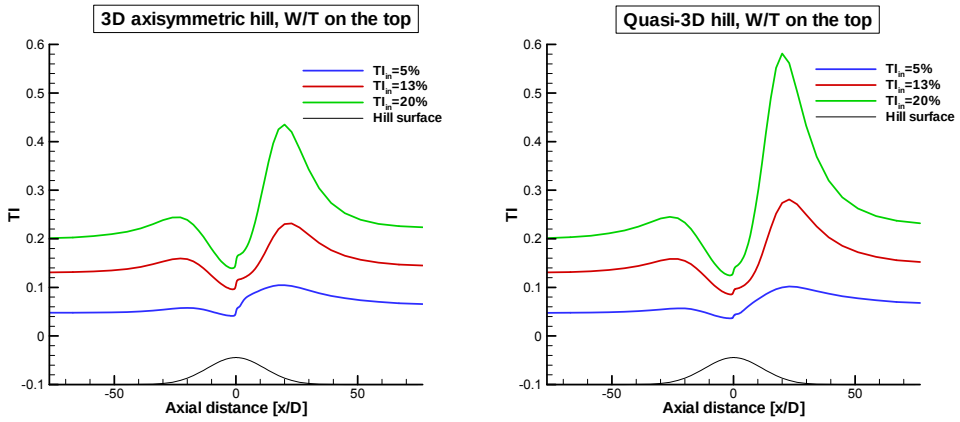

(a) (b)

Figure 41: **Variation of the turbulence intensity at the hub height of the symmetry plane ($y = 0$) for various values of TI_{in} . Wind direction is 0°.**

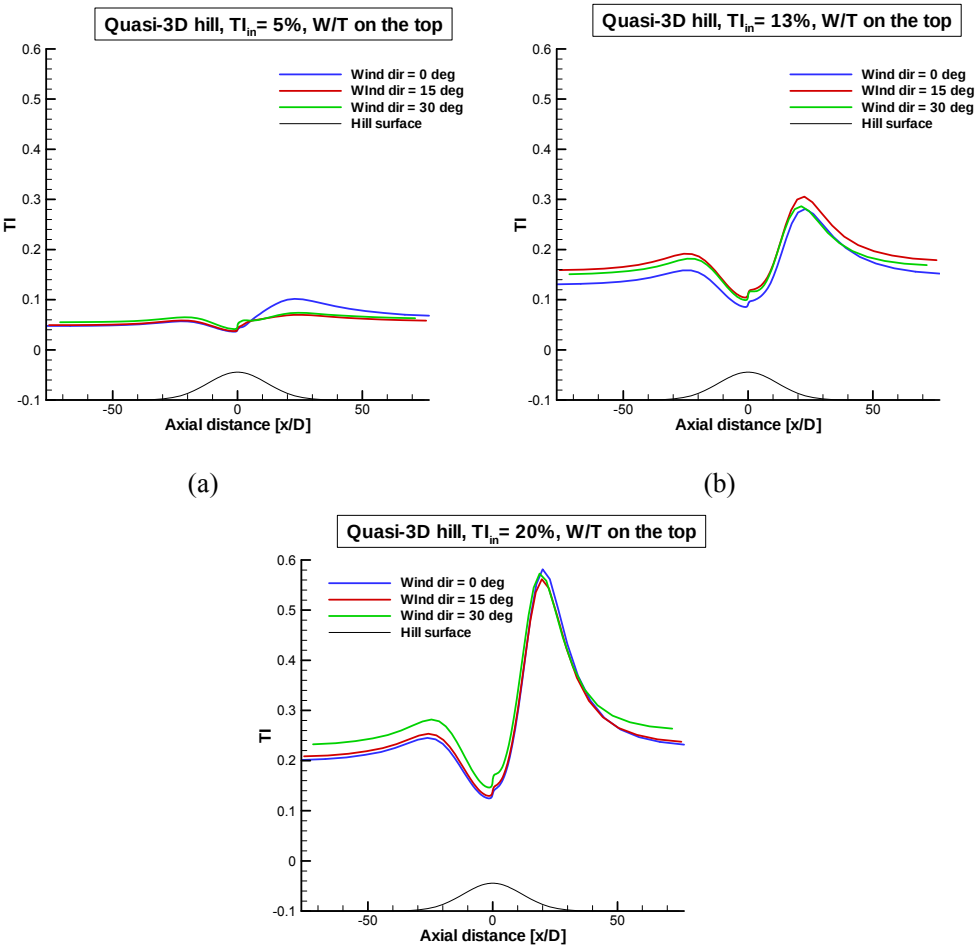

(a) (b)

(c)

Figure 42: **Variation of the turbulence intensity at the hub height of the symmetry plane ($y = 0$) for various wind directions and TI_{in} values: (a) 5%, (b) 13% and (c) 20%.**

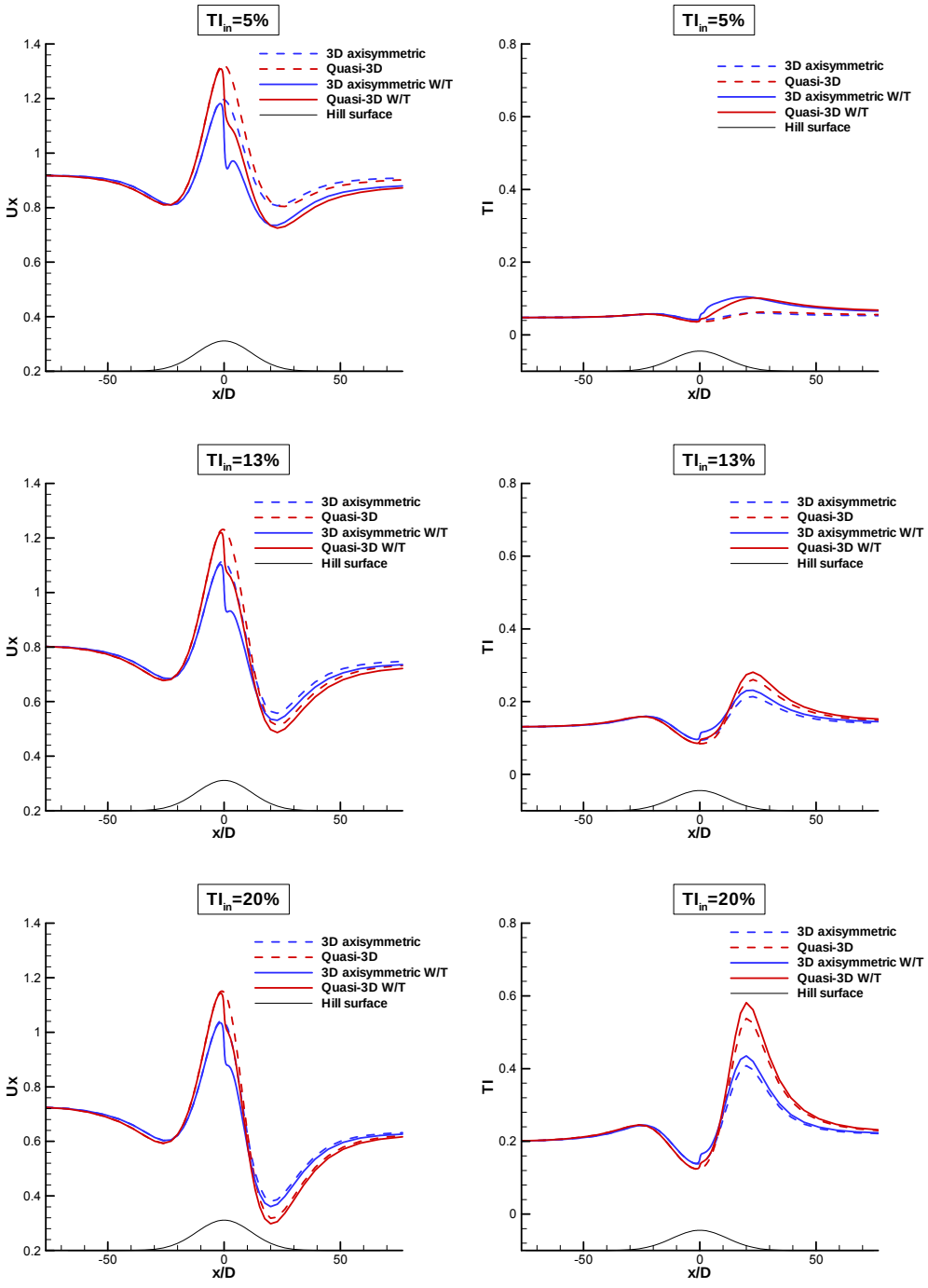

Figure 43: **Comparison of the streamwise wind speed and turbulence intensity variation at the hub height of the symmetry plane ($y = 0$) for the axi-symmetric and quasi-3D hills with and without W/T. Upper: TI_{in} = 5%. Middle: TI_{in} = 13%. Lower: TI_{in} = 20%.**

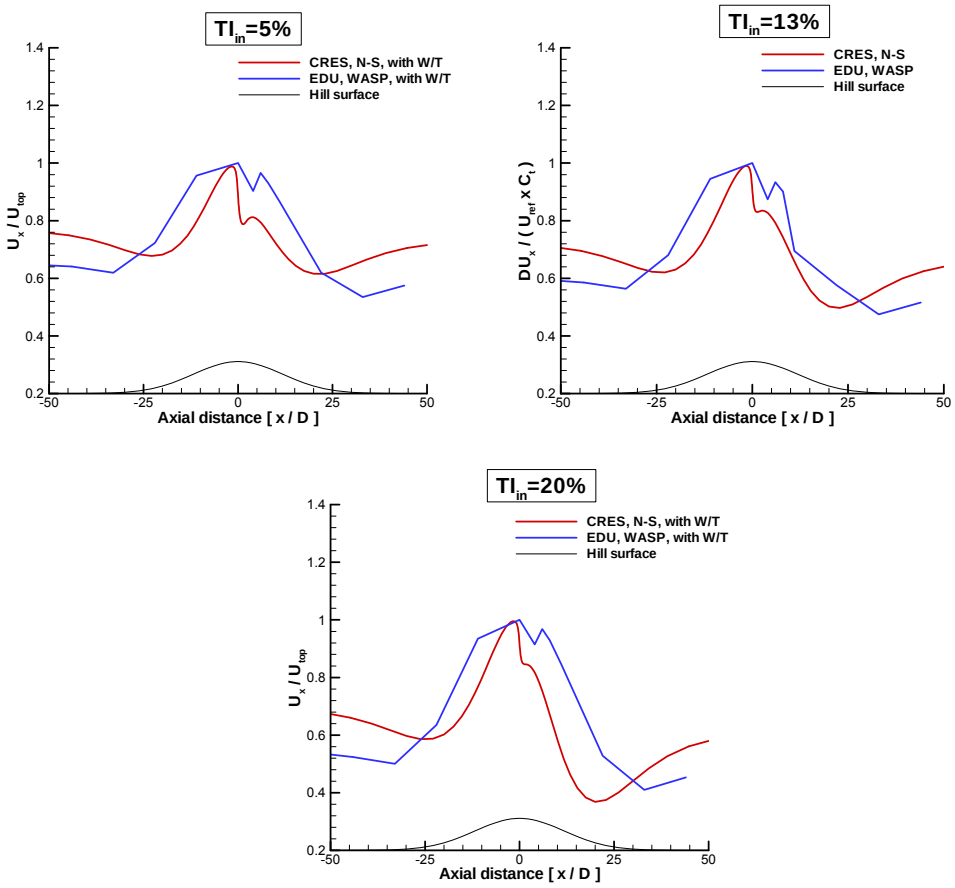

Figure 44: ***Streamwise*** **wind speed variation at the hub height of the symmetry plane ($y = 0$) for 3D axisymmetric hill for various TI_{in} values: (a) 5%, (b) 13% and (c) 20%. Normalization has been done with the predicted velocity at the hill top (hub height) without W/T.**

4.2.2. Vertical profiles

The W/T induced wake changes the wind speed profile, as depicted by Figure 45 and Figure 46. The change in the shape of the wind speed profile is more pronounced for low turbulence (5%). After 5 D, the distortion of the profile disappears; however there is a delay in the flow recovery compared to the case without W/T. This difference in wind speed between the cases with and without W/T expresses the wind speed deficit in the presence of a W/T. A relative distortion appears in the turbulence intensity profiles (see Figure 47 and Figure 48). As expected, the W/T presence increases the turbulence level behind the machine.

In Figure 49, the predictions of the vertical profiles of the streamwise wind speed are depicted for both CRES and UEDIN. Normalization refers to the velocity at hill top without W/T. The good agreement between the velocity profiles at the distance of 4 D shows that the simulation of the W/T effect is equivalent in both codes. The comparison of the profile gradients is still satisfactory in the presence of the W/T, although the coarse discretization of the WAsP results is not proper for accurate conclusions. At the distance of 33 D, the comparison of the velocity profiles indicates that the Navier–Stokes code predicts a faster flow recovery.

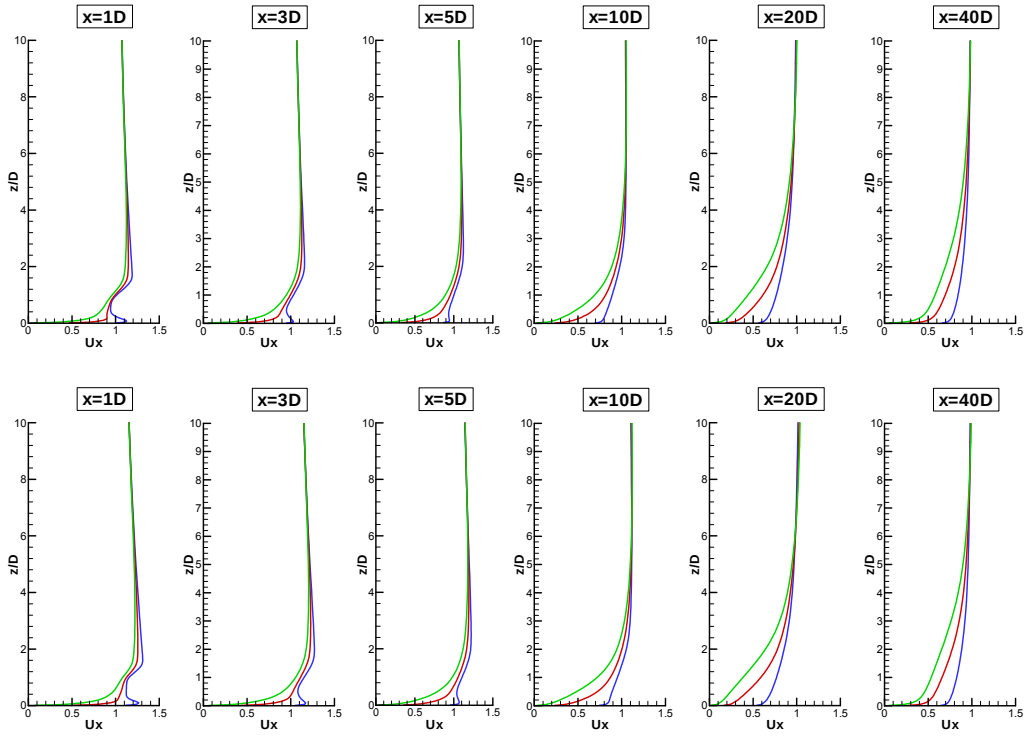

Figure 45: *Vertical profiles of the streamwise wind speed downstream of the hill top in the presence of a W/T for various values of TI_{in} : 5%, 13%, 20%. Upper: 3D axisymmetric hill. Lower: Quasi-3D hill (wind direction 0^o).*

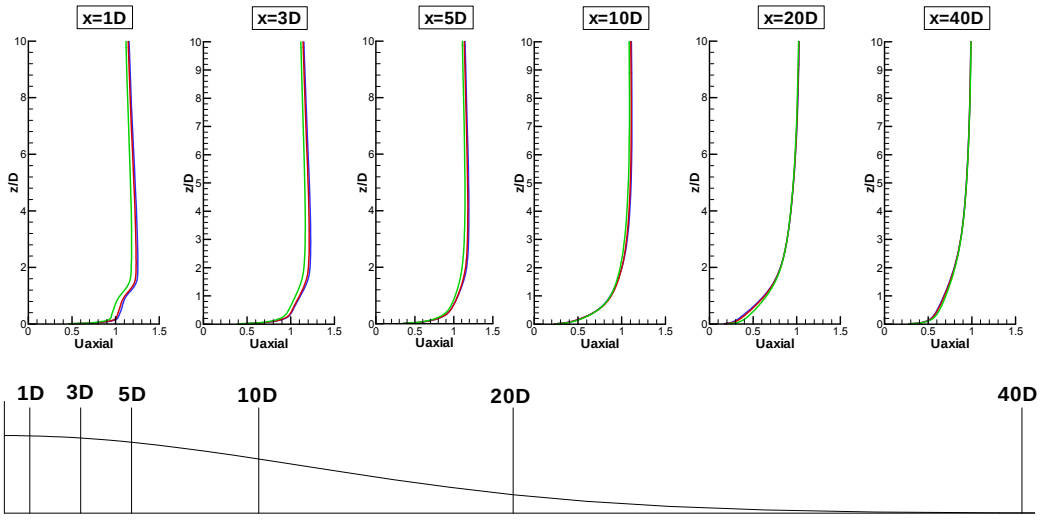

Figure 46: *Vertical profiles of the turbulence intensity downstream the hill top of the quasi-3D hill for various wind directions: 0^o, 15^o, 30^o. TI_{in} is 13%.*

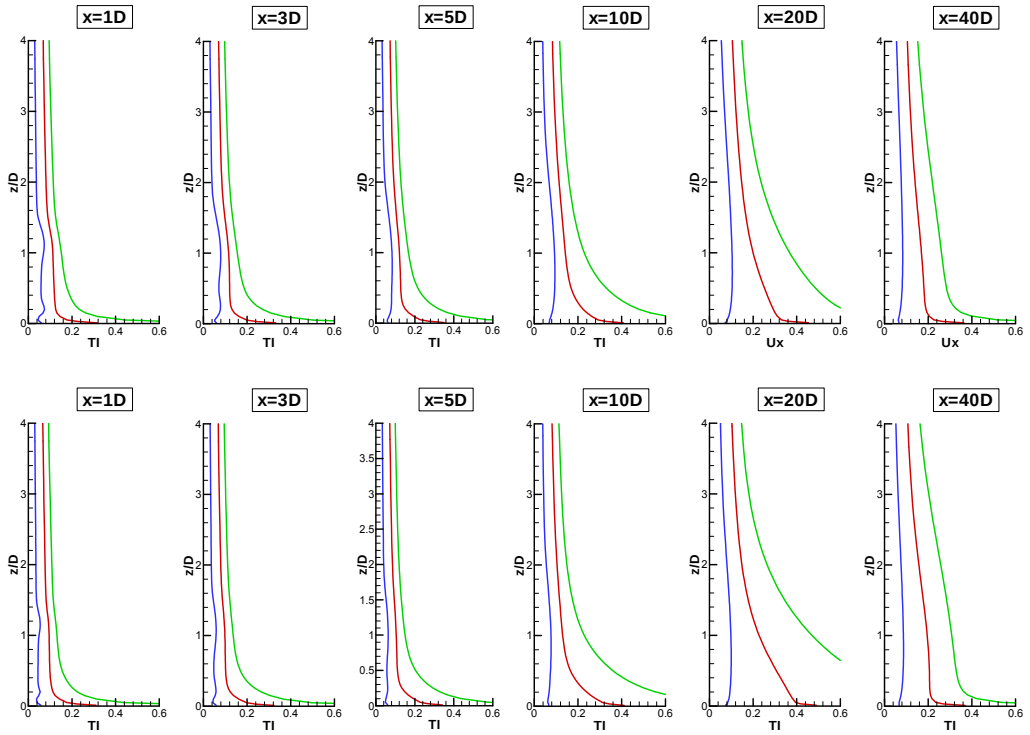

Figure 47: **Vertical profiles of the turbulence intensity downstream the hill top in the presence of a W/T for various values of TI_{in} : 5%, 13%, 20%.**

Upper: 3D axisymmetric hill. Lower: Quasi-3D hill (wind direction 0°).

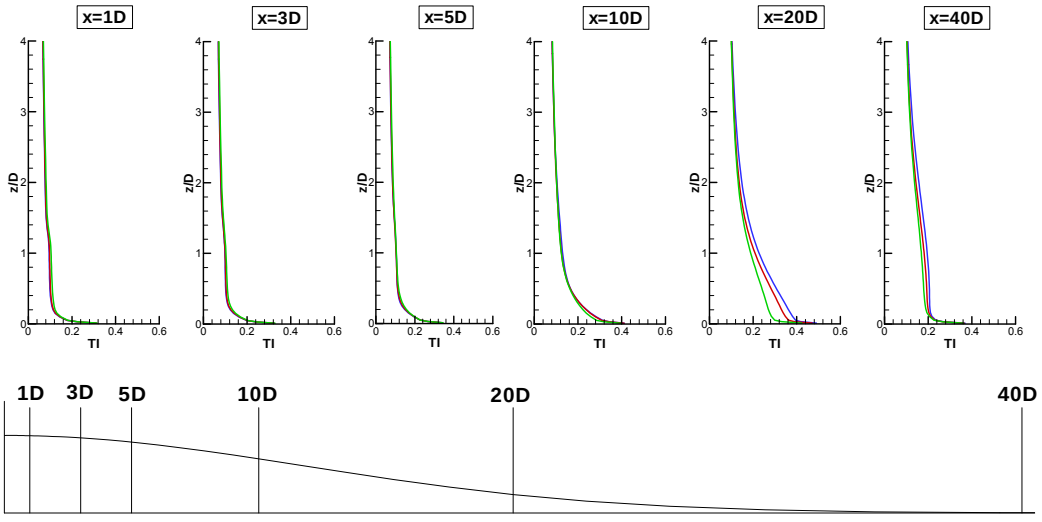

Figure 48: **Vertical profiles of the turbulence intensity downstream the hill top of the quasi-3D hill for various wind directions: 0°, 15°, 30°. TI_{in} is 13%.**

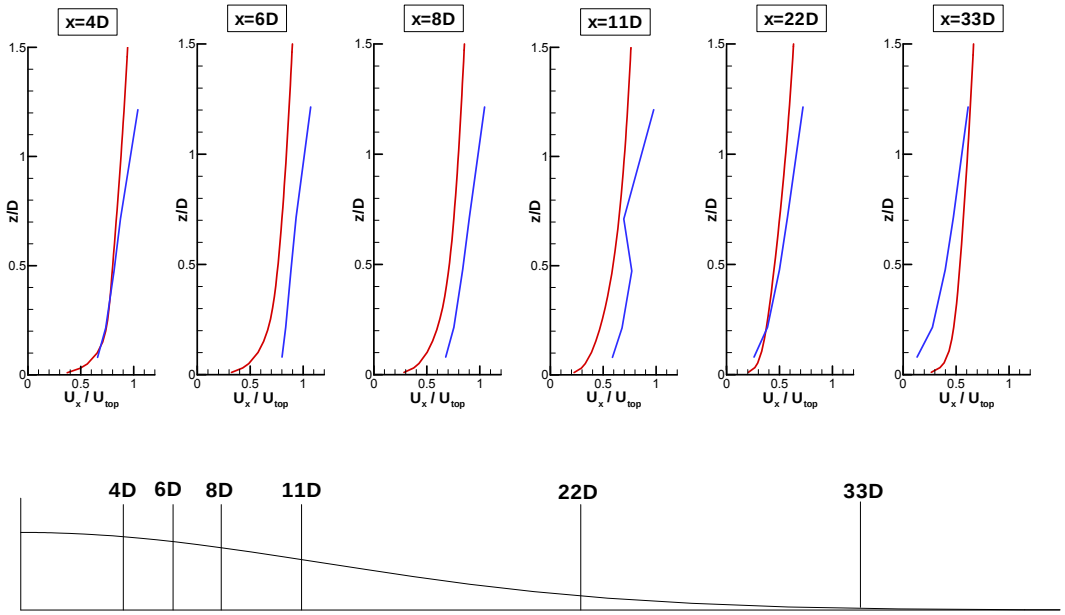

Figure 49: *Vertical profiles of the streamwise velocity downstream the hill top of the 3D axisymmetric hill for various distances.* ——— *UEDIN (WAsP),* ——— *CRES (N-S).* TI_{in} *is 13%. Normalization has been done with the predicted velocity at the hill top (hub height).*

4.2.3 Wind speed contours

In Figure 50 the streamwise wind speed contours at the symmetry plane ($y = 0$) are plotted and compared between the axisymmetric and the quasi-3D hill. The discontinuity of the contours in the W/T region depicts the fact that the disk rotor operates as a momentum sink. This discontinuity is more pronounced for $TI_{in} = 5\%$ and weakens as TI_{in} increases, in agreement with the observations made in the streamwise variations and the wind speed profiles. This effect is more clearly represented in the wind speed contours at hub height a. g. l. (see Figure 51). In these contours, it can also be observed that the effect of the W/T presence is visible at long distances (more than $30D$) downstream the W/T.

In Figure 52, the streamwise wind speed contours are plotted at the transversal plane at $1D$ from the W/T for the two hill cases and for the various values of the inlet turbulence intensity studied. A scale-up has been made in the region of the disk rotor, the perimeter of which is drawn along with the computational grid. For $TI_{in} = 5\%$ a stronger effect of the rotor disk in the wake is observed, which is in agreement with the abrupt wind speed drop observed in Figure 43a and the wind speed profiles shown in Figure 45. In both hill cases, the wake centre is below the disk rotor centre. As the level of TI_{in} increases, the W/T effect on the wake diminishes, as also observed in the wind speed profiles. Finally, the wind speed contours for the total horizontal wind speed $U_{tot} = \sqrt{U_x^2 + U_y^2}$ at hub height a. g. l. are presented in Figure 53 for the wind directions of 15^o and 30^o. The lower accelerations and decelerations predicted for the 30^o wind direction case are due to the fact that the flow follows a relatively smoother terrain. Figure 53 also shows that the wind speed deficit occurs in the direction of the flow at the rotor centre

which is 10^{o} and 20^{o}, respectively, as the disk rotor has been rotated during the generation of the grid by an equal yaw angle, so that its surface remains perpendicular to the flow.

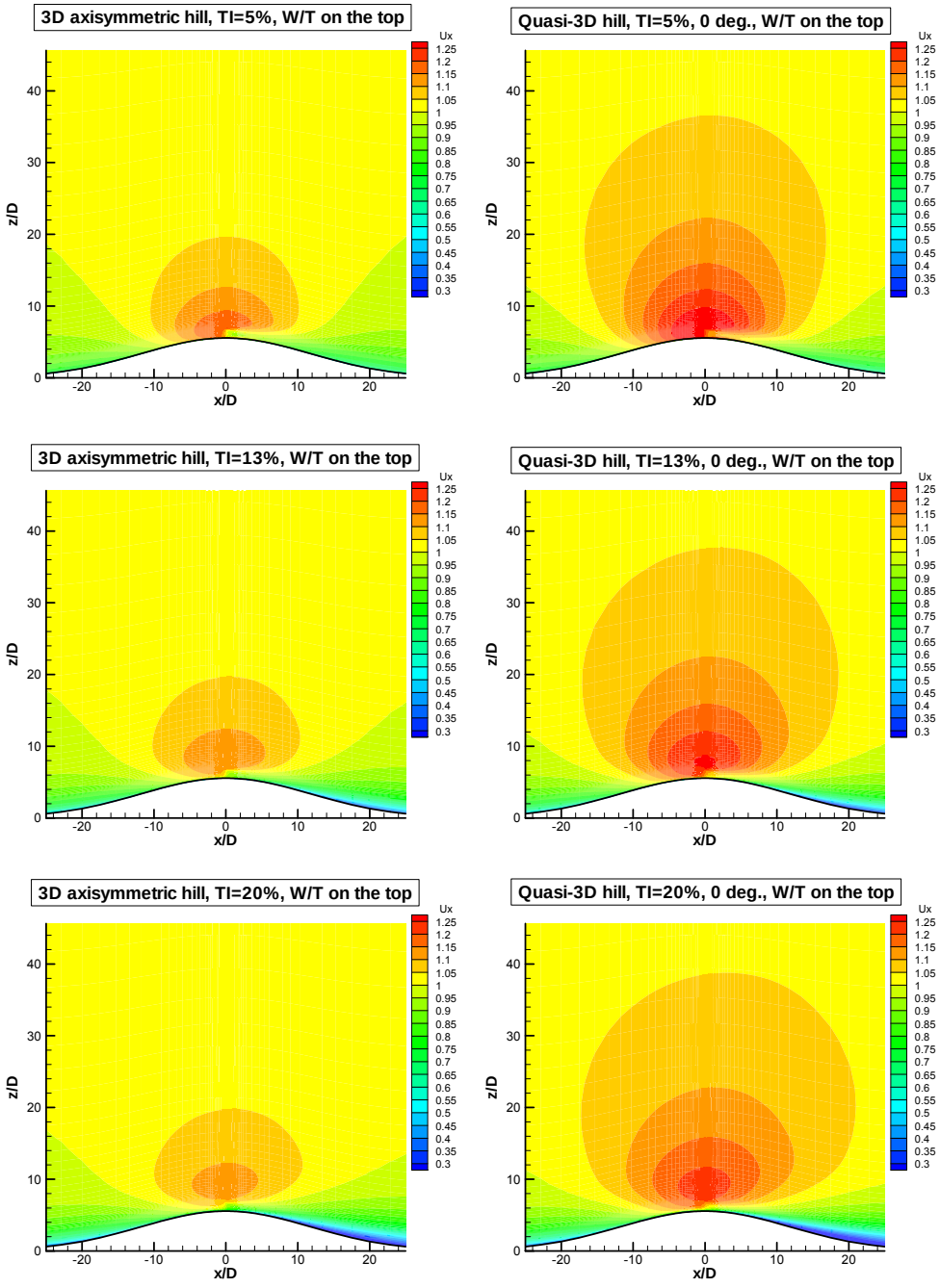

Figure 50: **Streamwise wind speed contours for the axisymmetric and quasi-3D hill at the symmetry plane ($y = 0$). Upper: TI_{in} = 5%. Middle: TI_{in} = 13%. Lower: TI_{in} = 20%.**

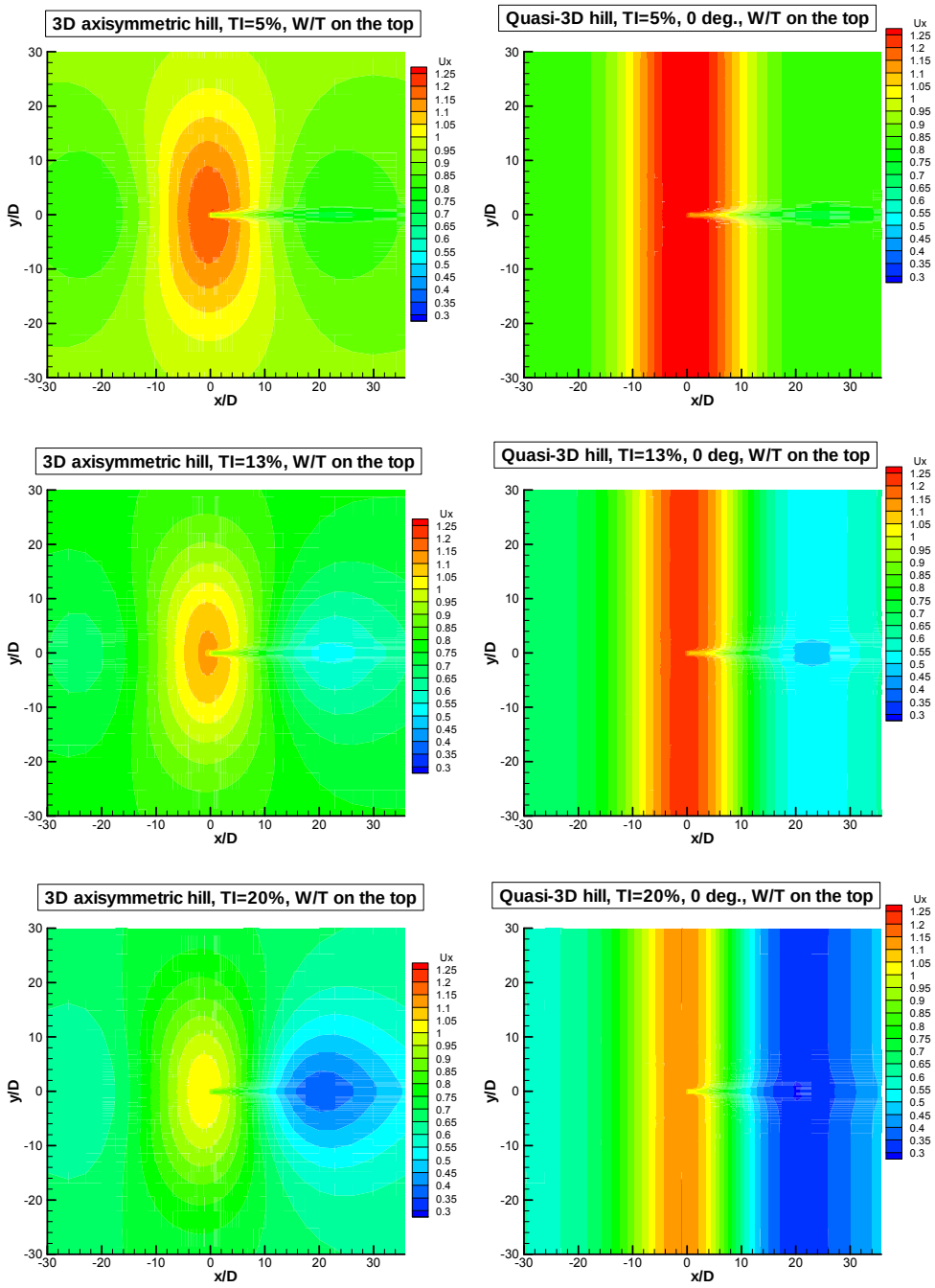

Figure 51: **Streamwise wind speed contours for the axisymmetric and quasi-3D hill at hub height a. g. l. Upper: TI_{in} = 5%. Middle: TI_{in} = 13%. Lower: TI_{in} = 20%.**

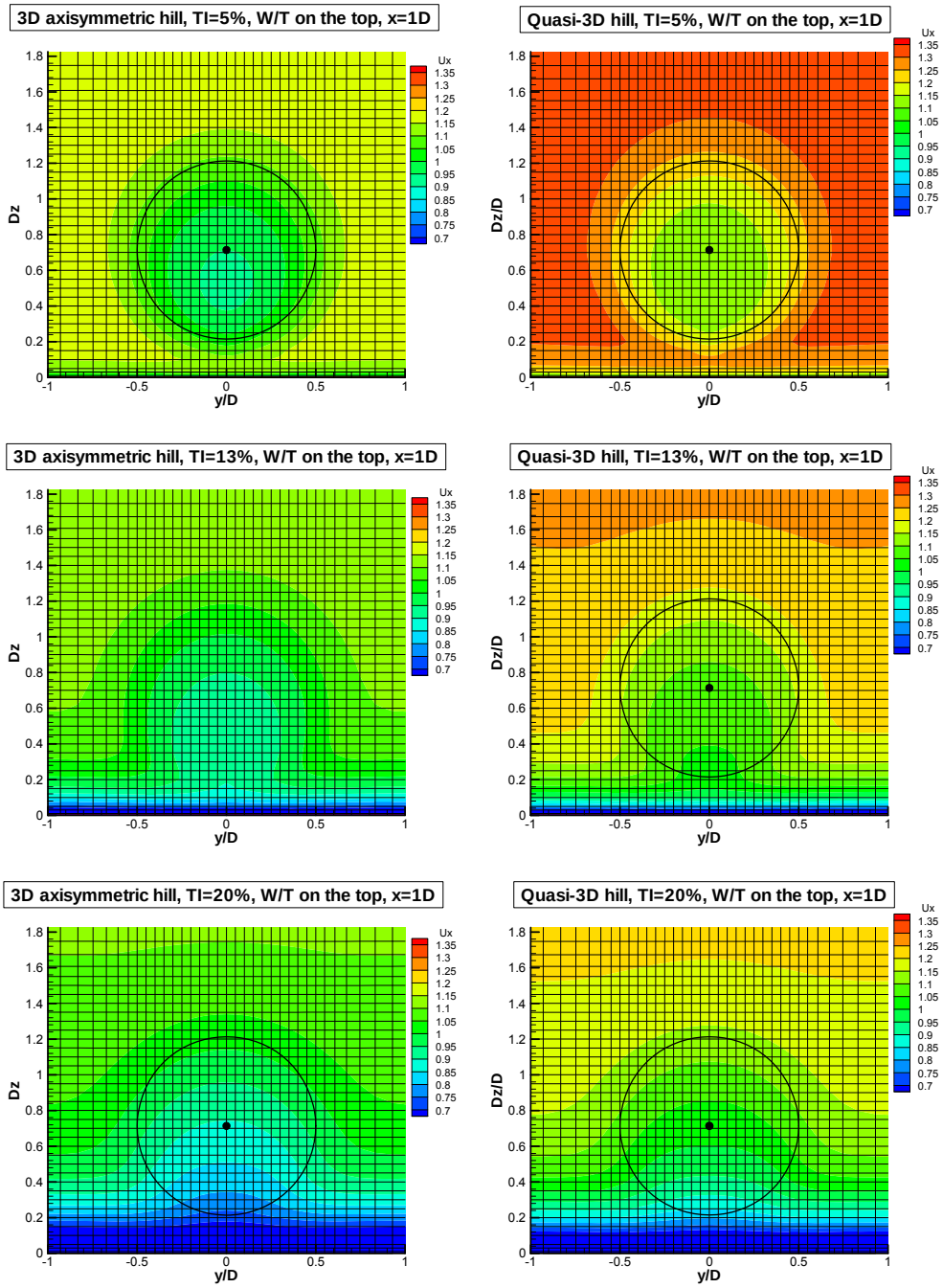

Figure 52: **Streamwise wind speed contours for the axisymmetric and quasi-3D hill at plane $x = 1D$ downstream the W/T. Upper: TI_{in} = 5%. Middle: TI_{in} = 13%. Lower: TI_{in} = 20%.**

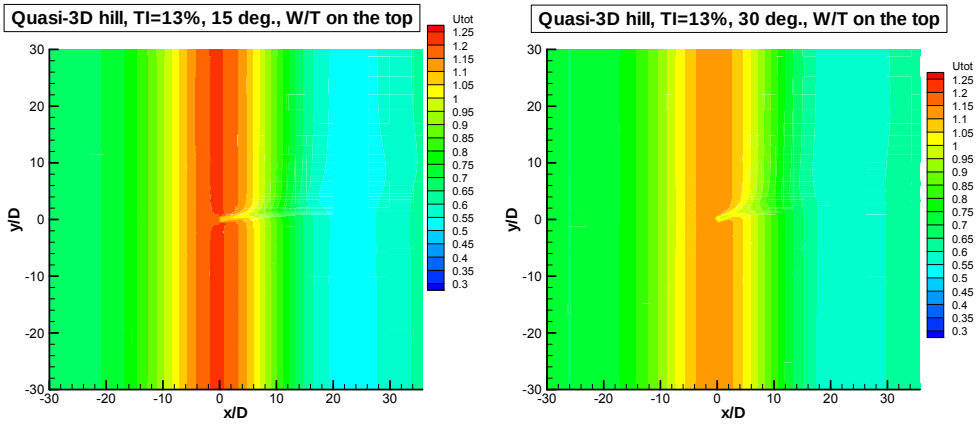

Figure 53: **Streamwise wind speed contours above the quasi-3D hill at hub height a. g. l. for wind directions of 15° and 30° for TI_{in} = 13%.**

4.3 Wind speed deficit prediction

The wind speed deficit ΔU in the presence of a wind turbine is calculated with reference to the flow field without W/T, using the relationship:

$$\Delta U = \frac{DU_x}{U_{ref} \times C_t} = \frac{U_{axial}(without\ W/T) - U_{axial}(with\ W/T)}{U_{axial}(without\ W/T) \times C_t}.$$

In the above definition, U_{axial} is the U_x wind speed for 0° wind direction or the total horizontal wind speed $U_{tot} = \sqrt{U_x^2 + U_y^2}$ when the wind direction is 15° or 30°.

4.3.1 Deficit at hub height

In Figure 54, the wind speed deficit is presented for the 3D axisymmetric hill, the quasi-3D hill and the flat terrain case for different levels of TI_{in}. One important conclusion is that in both hill cases the deficit remains significant at long distances (even greater than $40D$) downstream the W/T. On the contrary, in the flat terrain case, the deficit is already practically negligible at $20\,D$. The decay rate is even slower for the quasi-3D hill. The comparison between hill and flat terrain cases is better shown in Figure 58. The increase of the turbulence level results in a faster flow recovery at long distances as expected. However, it is noticeable that the wind speed deficit at hub height is not always monotonously decreasing. This is mainly observed in the quasi-3D case and is more pronounced for the $TI_{in} = 20\%$ case (Figure 54b, Figure 58).

The wind speed deficit predictions between CRES and CFDWake are compared in Figure 55. The reference C_t used for the calculation of the disk rotor force is higher in the CFDWake predictions, indicating that lower velocities have been predicted in the case without W/T. For $TI_{in} = 5\%$, CRES and CFDWake calculated $C_t = 0.39$ and 0.383 respectively, whereas for $TI_{in} = 13\%$ the respective values are 0.317 and 0.27. CRES predicts a faster decay rate which is a result of the higher C_t predicted value or equivalently of the lower predicted velocity at the hill top. The comparison of wind speed deficit predictions between CRES, CFDWake and UEDIN is presented in Figure 56. UEDIN predicts a slower wind speed deficit decay in the far wake, especially for $TI_{in} = 13\%$ and $TI_{in} = 20\%$, than the two Navier–Stokes codes. For $TI_{in} = 5\%$ and $TI_{in} = 20\%$ a close agreement is observed between CRES and UEDIN up to the distance of $10D$. However, at that distance UEDIN predicts a rather peculiar increase in the

deficit, which leads to divergence of the predictions at longer distances. Regarding the turbulence intensity predictions (Figure 57), the agreement between CRES and CFDWake is very good for $TI_{in} = 13\%$, whereas small differences are observed in the wake region for the $TI_{in} = 5\%$ case.

Another important remark is the drastic effect of the wind direction on the decay rate of deficit. In Figure 59, it is observed that the change of the wind direction from 0^o to 30^o significantly increases the decay rate. At 30^o wind direction, the decay rate of deficit is comparable to that of flat terrain.

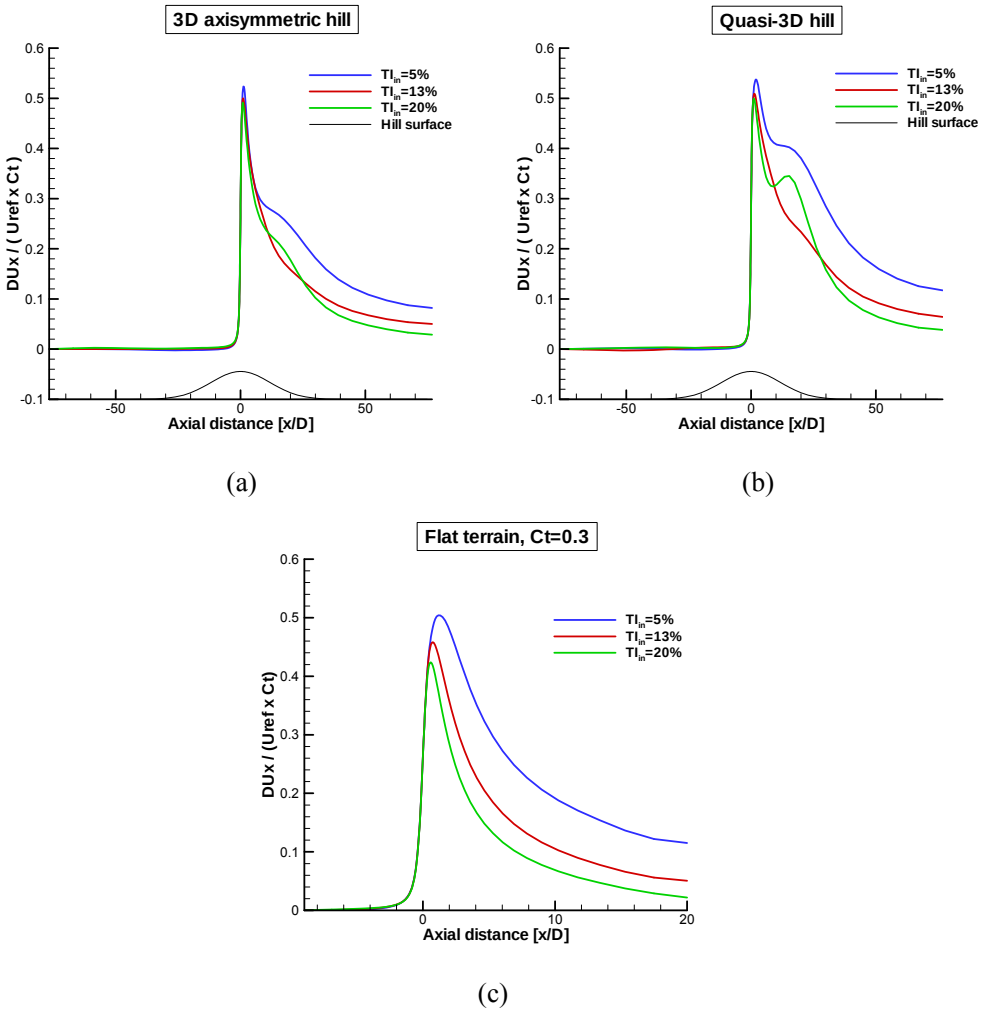

Figure 54: **Wind speed deficit along $y = 0$ line at hub height a. g. l. for various values of TI_{in}. (a) axisymmetric hill, (b) quasi-3D and (c) flat terrain. Wind direction is 0^o.**

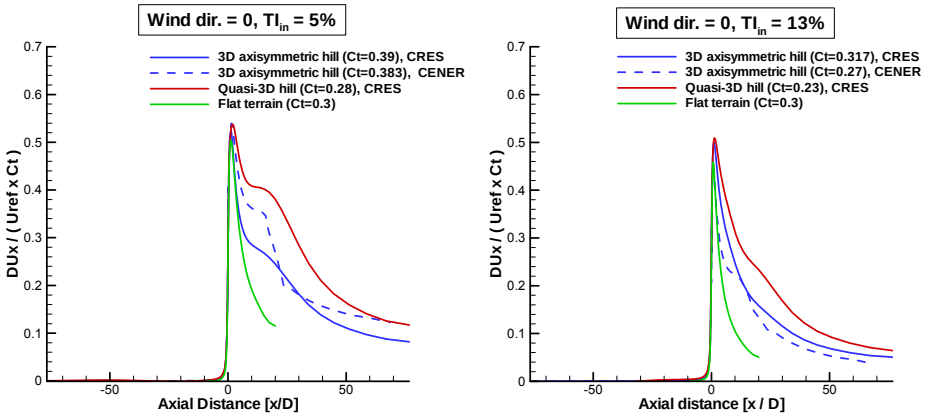

(a) (b)

Figure 55: **Wind speed deficit for (a) TI_{in} = 5% and (b) TI_{in} = 13%.**

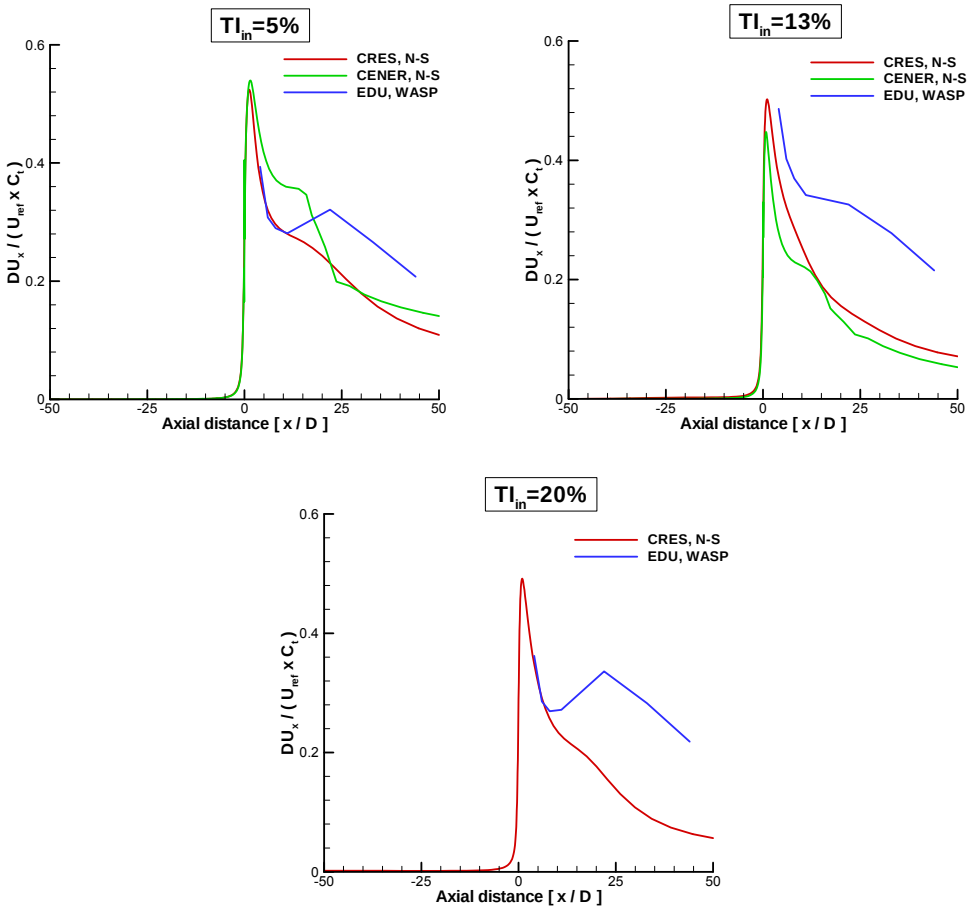

Figure 56: **Wind speed deficit for (a) TI_{in} = 5%, (b) TI_{in} = 13% and (b) TI_{in} = 20%. Comparison between CRES (N-S), CFDWake (N-S) and UEDIN (WAsP).**

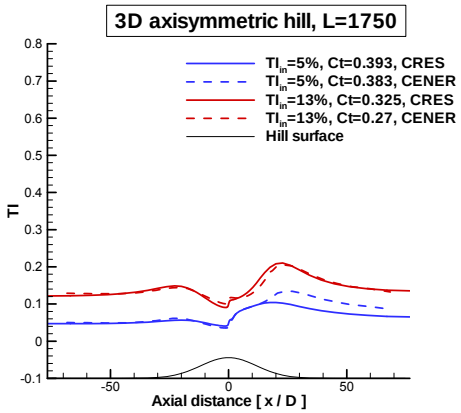

Figure 57: **Turbulence intensity along $y = 0$ line at hub height a. g. l. for TI_{in} 5% and 13%.**

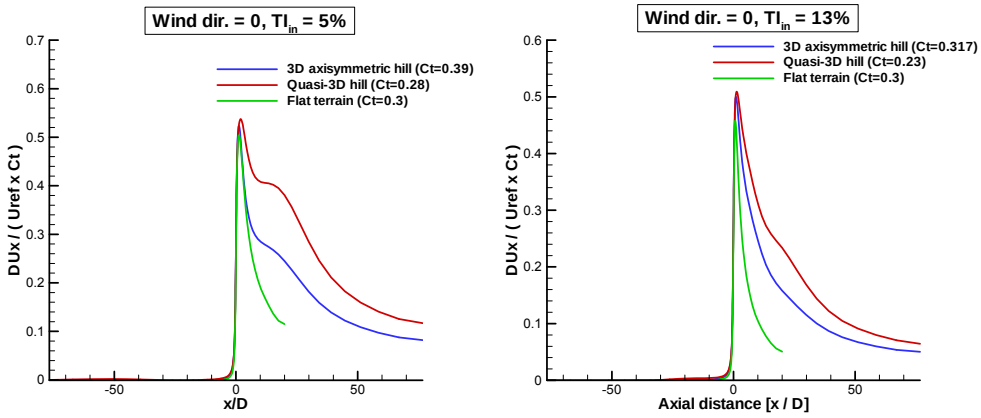

(a) (b)

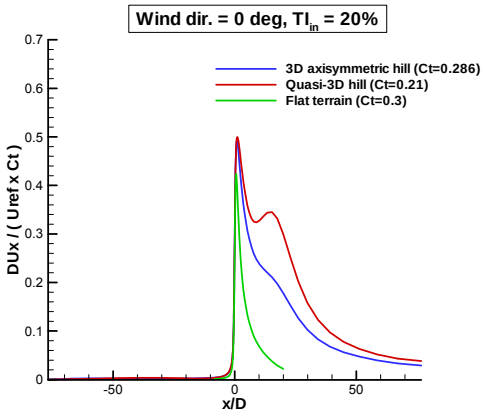

(c)

Figure 58: **Wind speed deficit at the hub height a. g. l. for axisymmetric hill, quasi-3D hill and flat terrain. TI_{in} is (a) 5%, (b) 13% and (c) 20%. Wind direction is 0^o.**

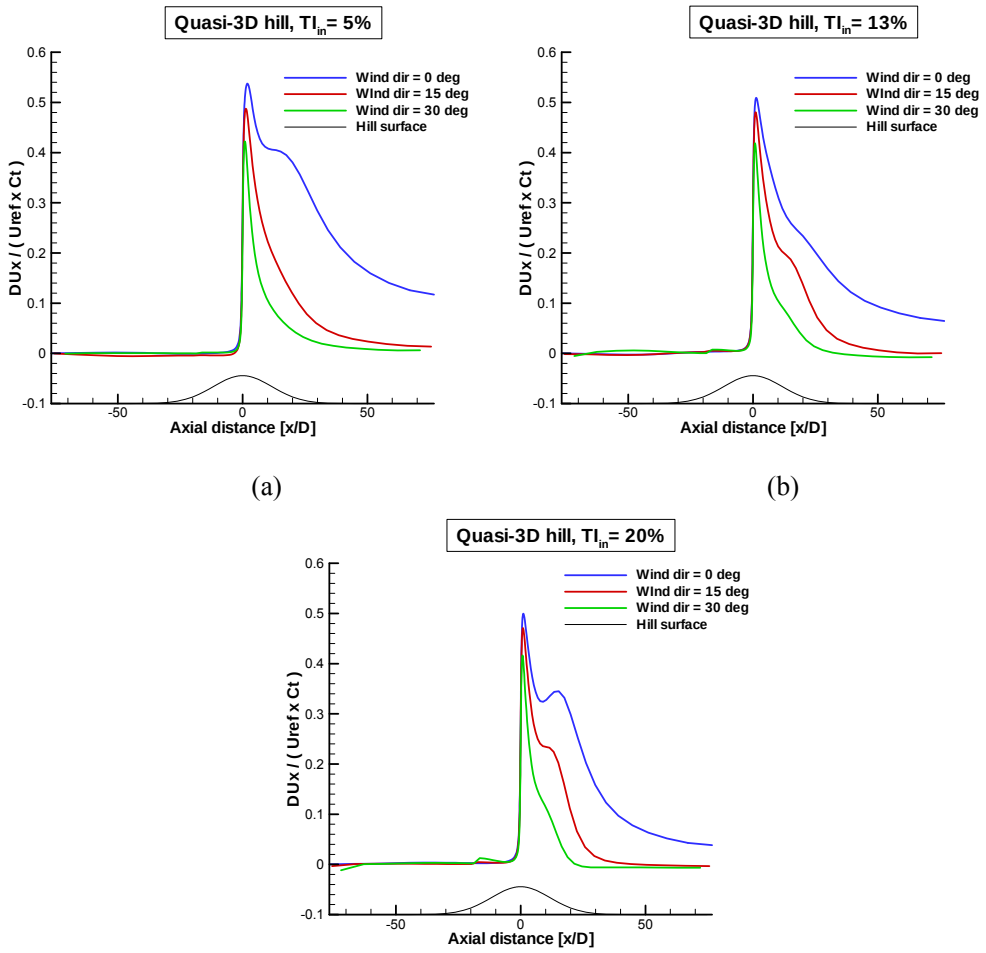

Figure 59: **Wind speed deficit at hub height along the W/T orientation for quasi-3D hill and various wind directions.** TI_{in} **is: (a) 5%, (b) 13% and (c) 20%.**

4.3.2 Vertical profiles

In Figure 60 the vertical deficit profiles are plotted at increasing distance downstream the hill top. A straightforward observation is the modification of the wake geometry with turbulence, especially in the $TI_{in} = 20\%$ case, which is responsible for the aforementioned non-monotonous variation of the deficit in the stream-wise direction. The height of the maximum deficit reduces with increasing TI_{in} and for $TI_{in} = 20\%$ is located close to the ground. Another remark is that the predicted deficit maintains higher values in the quasi-3D hill case, denoting a slower decay rate, which was also seen in the stream-wise variations. The deficit values remain significant after $20D$ and in some cases even after $40D$ ($TI_{in} = 5\%$).

The significant effect of the wind direction on the deficit is confirmed by the profiles shown in Figure 61. The height of the maximum deficit remains constant denoting similar wake geometry; its level, however, attenuates fast as the wind direction changes from 0 to 30°. For the latter case, the wind speed deficit is practically negligible after $20D$.

In Figure 62, the deficit profiles for the axisymmetric and the quasi-3D hill cases are compared with those predicted in the flat terrain case. The increase of deficit in level and size, as well as its slower decay rate for the hill cases are clearly shown. In the flat terrain case, the position of maximum deficit remains almost constant, a little lower than hub height. In both hill cases, the position of maximum deficit moves downwards up to a certain distance which depends on the inlet level of turbulence, and then it is gradually elevated until the wake vanishes.

In Figure 63, the comparison of the predicted velocity deficit and turbulence intensity profiles between CRES and CFDWake is presented. The agreement between the turbulence intensity profiles is good, with the exception of small heights for the $TI_{in} = 5\%$ case, at which CFDWake predicts higher values. This difference, which could be attributed to the wall function treatment on the ground, could be responsible for the higher velocity deficit predicted by CFDWake at all positions up to $20D$ distance. For the $TI_{in} = 13\%$ case, CFDWake predicts slightly lower velocity deficit at the same positions. The overall good agreement on the TI predictions indicates that the velocity deficit difference is not caused from the different turbulence models, k–ω (CRES) and k–ε (CFDWake).

The large differences in wind speed deficit between Navier–Stokes and WAsP predictions is also depicted in the vertical profiles of Figure 64. The comparison of the profiles at distances greater than $11D$ shows that the WAsP predictions retain higher deficit values in the far wake.

4.3.3 Deficit contours

In

Figure 65 and Figure 66 the deficit contours at the plane $y = 0$ are compared for the two hills and the flat terrain case. The wake evolution at long distances in both hill cases, and particularly in the quasi-3D case, contrasts the quick vanishing in the flat terrain case. It also clearly depicted that the increase of TI_{in} favours a faster wake deficit attenuation.

Similar remarks can be made by observing the contour plots at constant hub height a. g. l. in Figure 67 and Figure 68. In this plane, however, a wider spreading of the wake is also visible as the turbulence level increases. A more detailed illustration of the wake geometry can be made by focusing on the region behind the W/T at a plane parallel to the rotor disk. In Figure 69, Figure 70 and Figure 71 the deficit contours are presented at 1 and $5D$ downstream the W/T for various TI_{in} values (5%, 13% and 20%). In the flat terrain case, the wake centre is located about $0.05D$ lower than hub height at $1D$ downstream. This height difference becomes about $0.1D$ at $5D$ downstream. In the axisymmetric and the quasi-3D hill cases, the height difference between wake centre and hub is about $0.15D$ at $1D$ downstream and becomes about $0.2D$ at $5D$ downstream. In Figure 69b, it seems that for the $TI_{in} = 20\%$ case, the circular shape of the wake geometry has already been distorted at $5D$ downstream. Finally, the effect of wind direction on the wake geometry is shown in Figure 72. As the wind direction changes from 0 to 30^{o}, a faster attenuation and a wider spreading of the wake occurs.

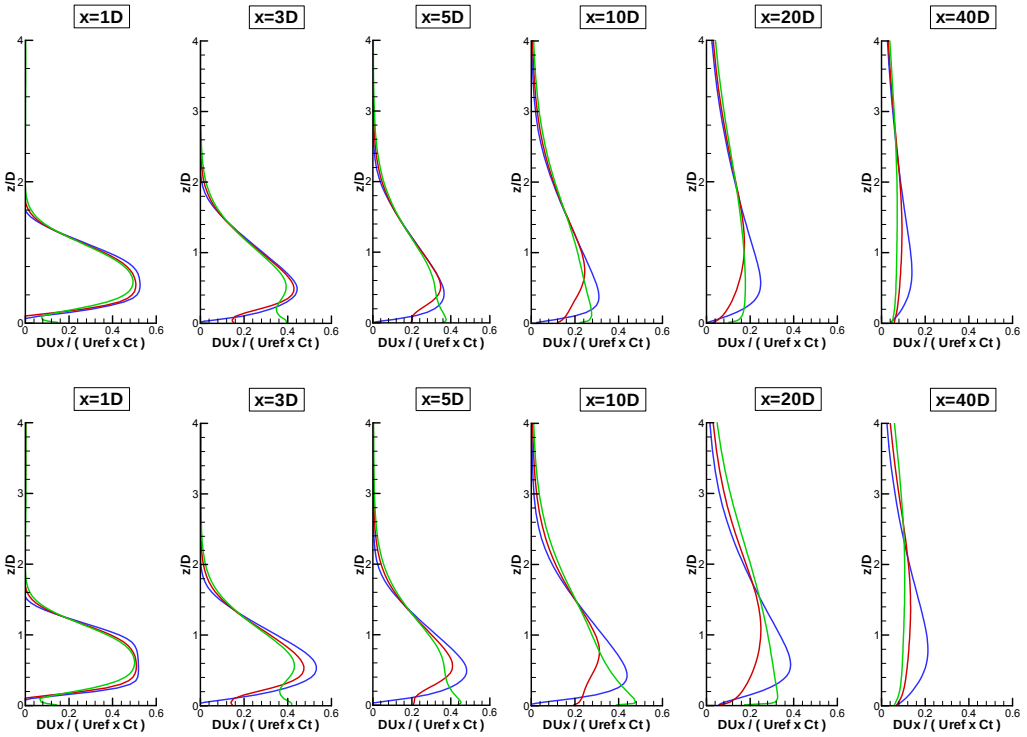

Figure 60: **Quasi-3D hill – Vertical profiles of wind speed deficit downstream the hill top in the presence of W/T for axisymmetric (upper) and quasi-3D (lower) hills and various values of TI_{in}: 5%, 13%, 20%.**

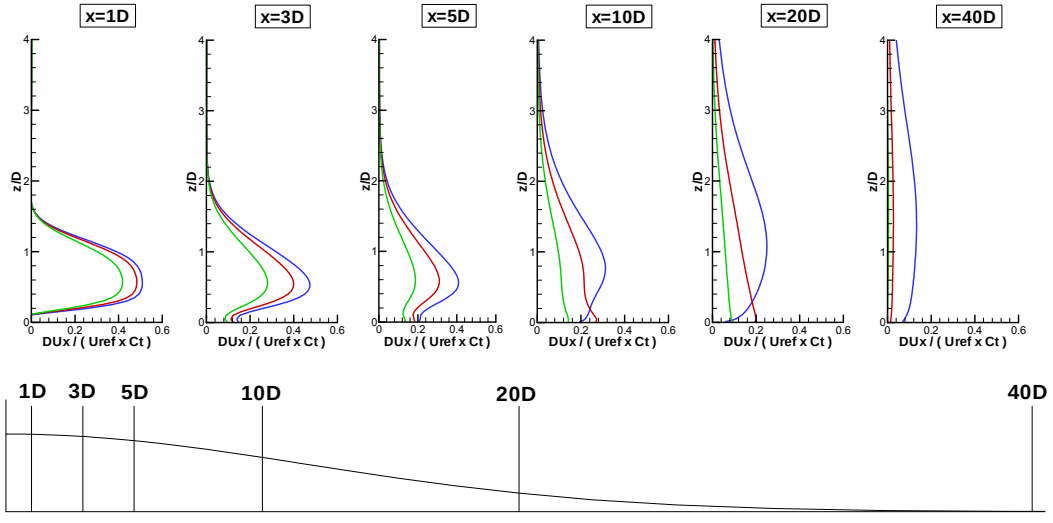

Figure 61: **Quasi-3D hill – Vertical profiles of wind speed deficit downstream the hill top in the presence of W/T for various wind directions: 0°, 15°, 30°. TI_{in} = 13%.**

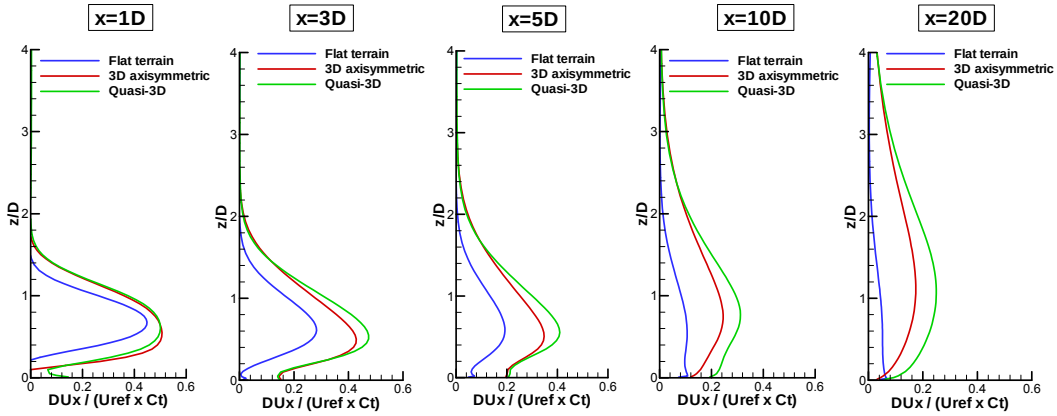

Figure 62: **Comparison of wind speed deficit vertical profiles among 3D axisymmetric hill, quasi-3D hill and flat terrain at increasing distance downstream the W/T. TI_{in} = 13%**

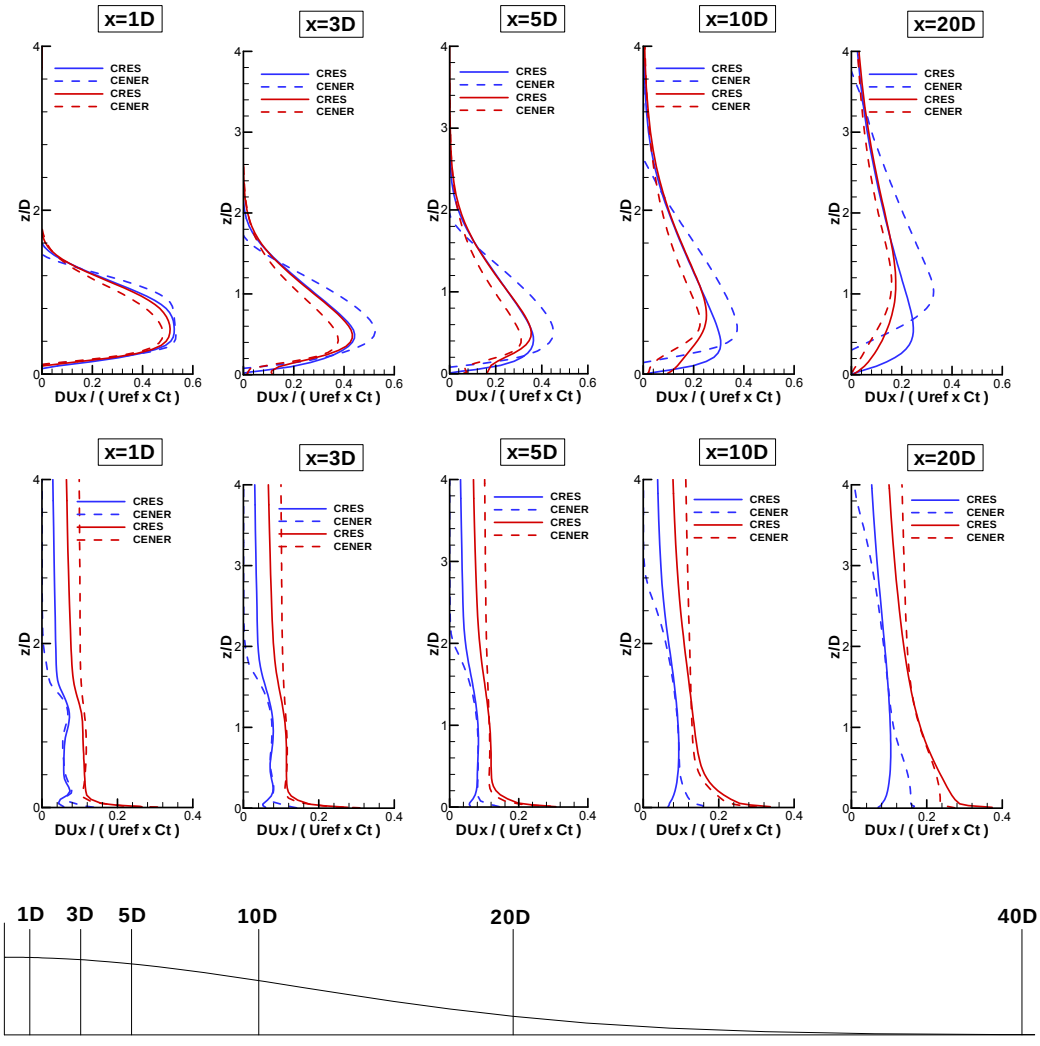

Figure 63: **Comparison of wind speed deficit and turbulence intensity vertical profiles between CRES and CFDWake at increasing distance downstream the W/T. TI_{in} : 5%, 13%**

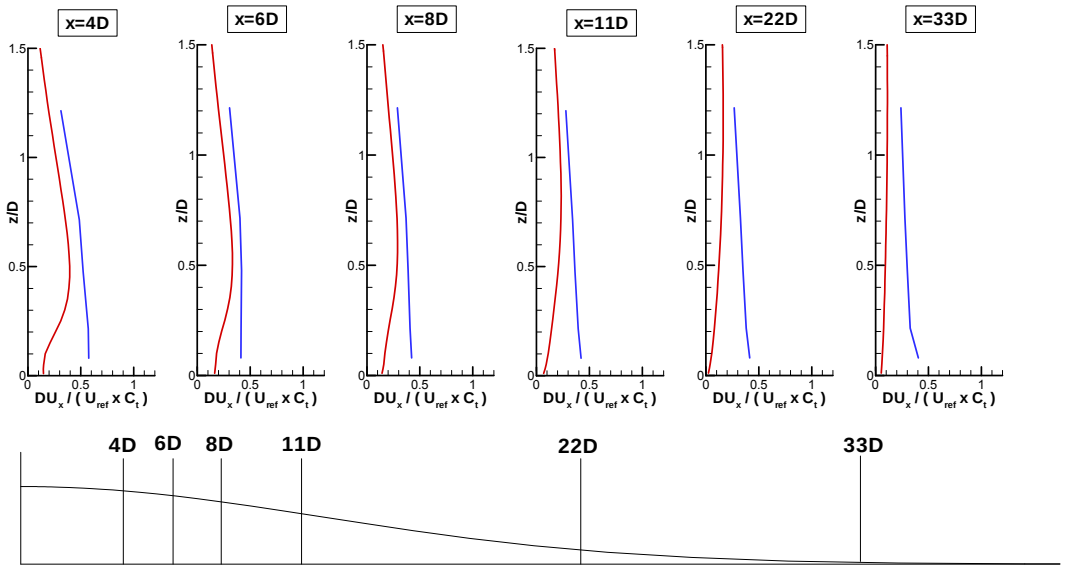

Figure 64: **Comparison of wind speed deficit vertical profiles between CRES (N-S) and UEDIN (WasP) at increasing distance downstream the W/T. TI_{in} is 13%.**

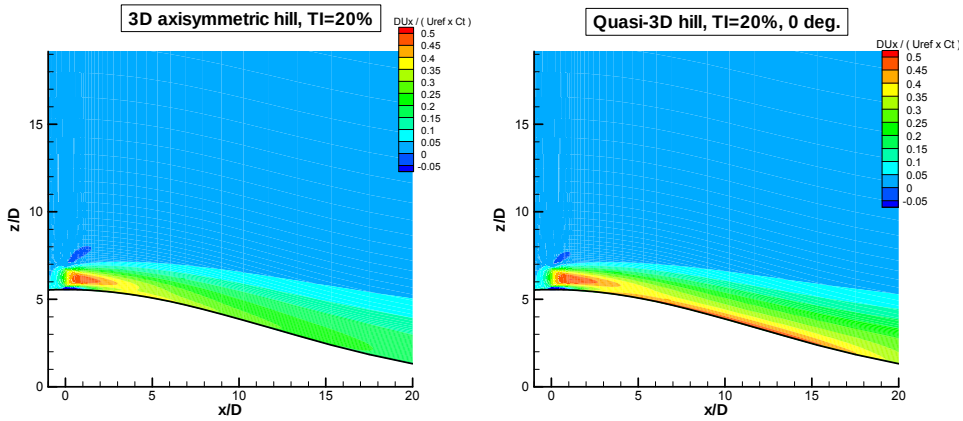

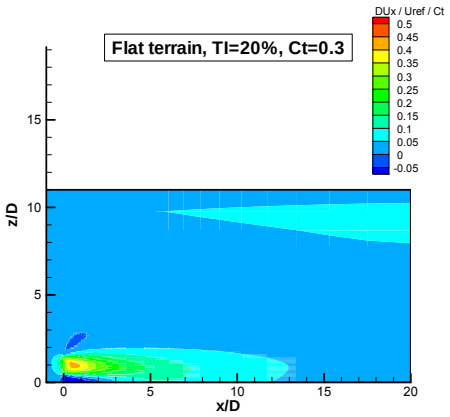

Figure 65: ***Comparison of wind speed deficit contours at the symmetry plane ($y = 0$) among flat terrain, 3D axisymmetric hill and quasi-3D hill. TI_{in} = 20%.***

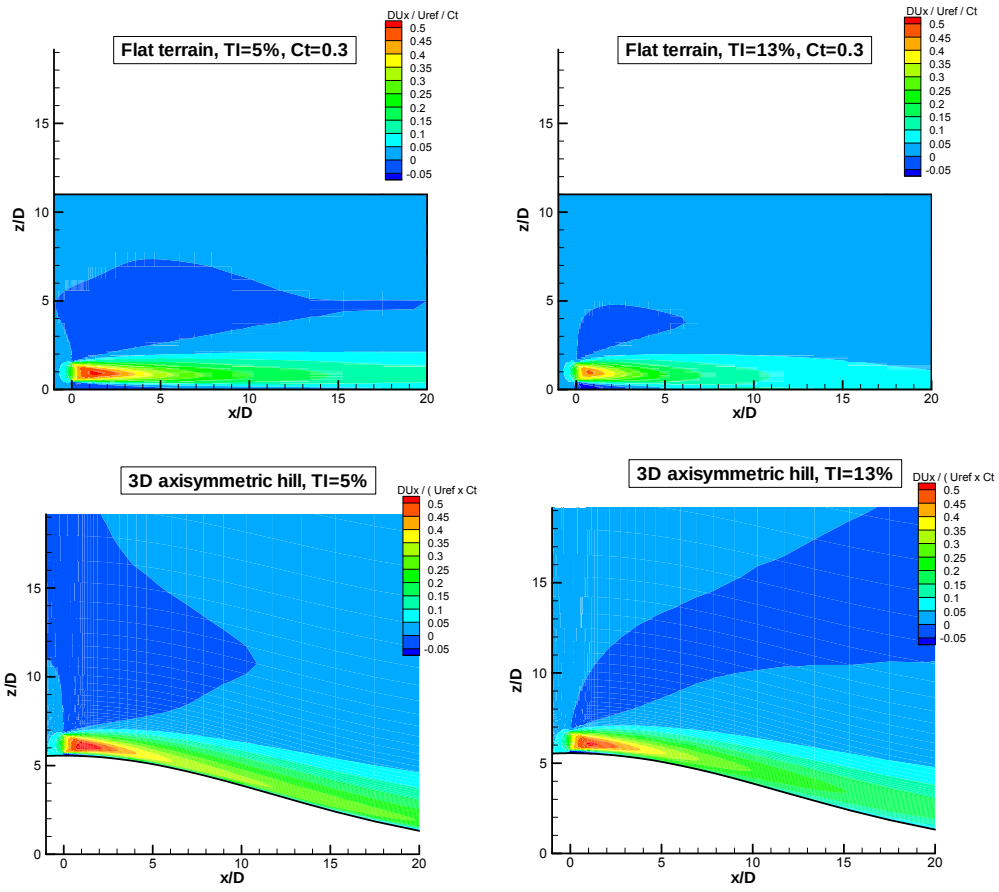

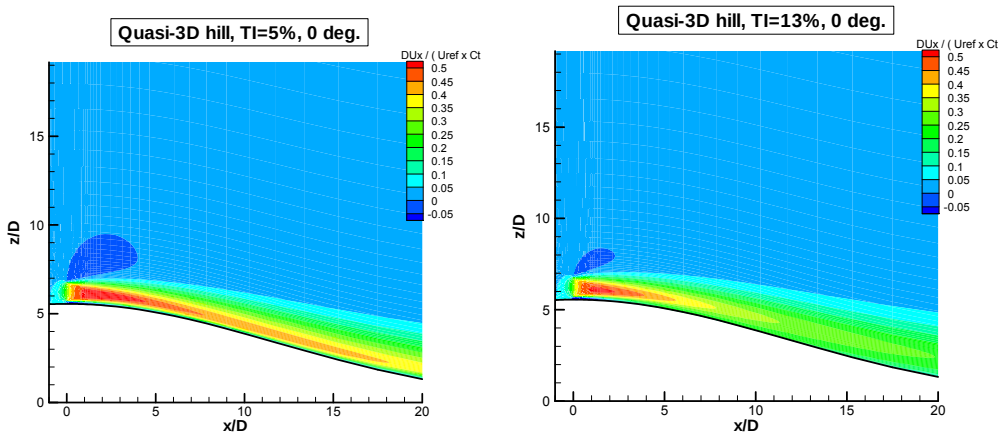

(a) (b)

Figure 66: **Comparison of wind speed deficit contours at the symmetry plane ($y = 0$) among flat terrain, 3D axisymmetric and quasi-3D hill. TI_{in} is (a) 5% and (b) 13%.**

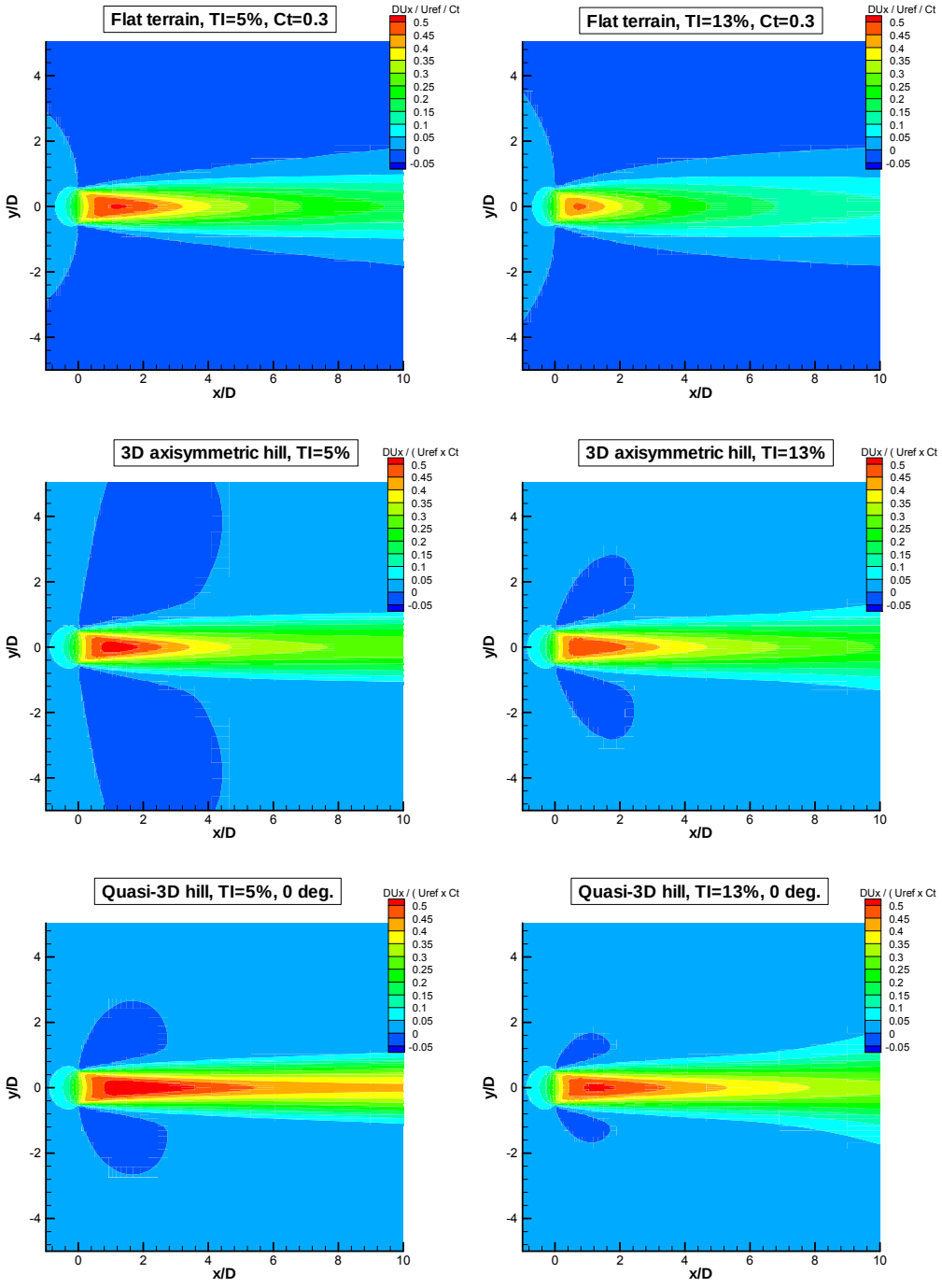

(a) (b)

Figure 67: **Comparison of wind speed deficit contours at hub height a. g. l. among flat terrain, 3D axisymmetric hill and quasi-3D hill. TI_{in} is (a) 5% and (b) 13%.**

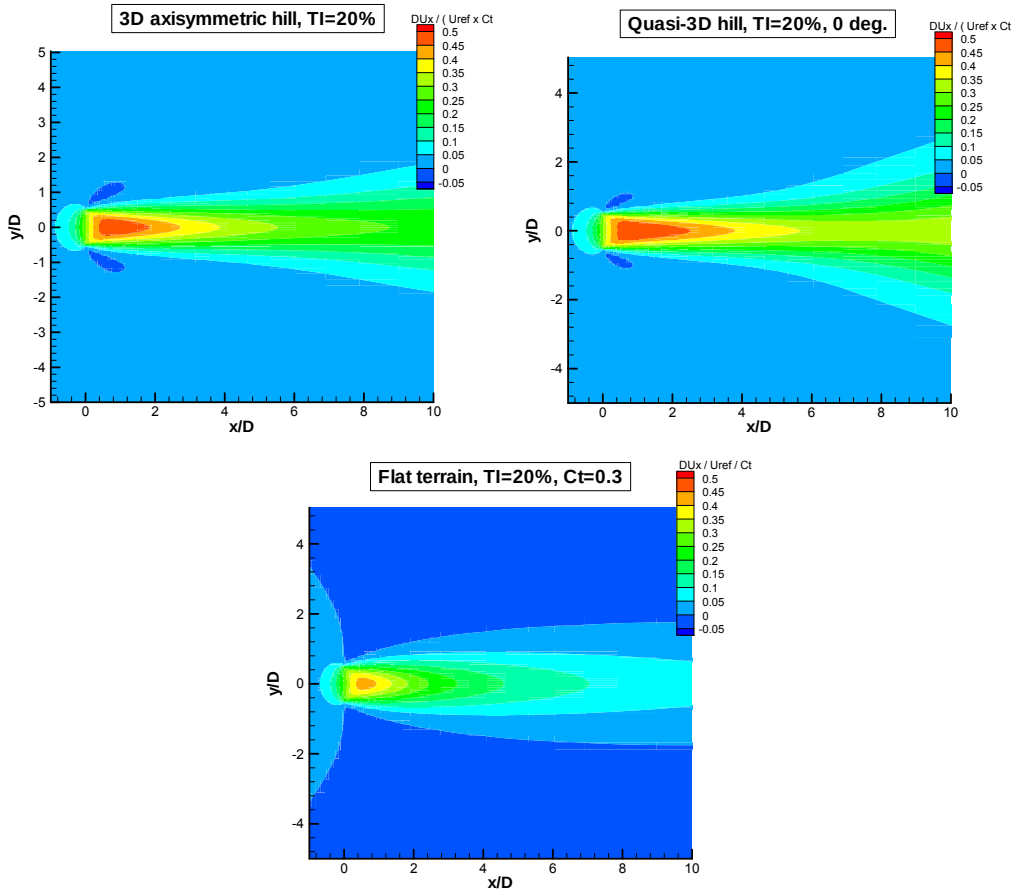

Figure 68: **Comparison of wind speed deficit contours at hub height a. g. l. among flat terrain, 3D axisymmetric hill and quasi-3D hill for TI_{in} = 20%.**

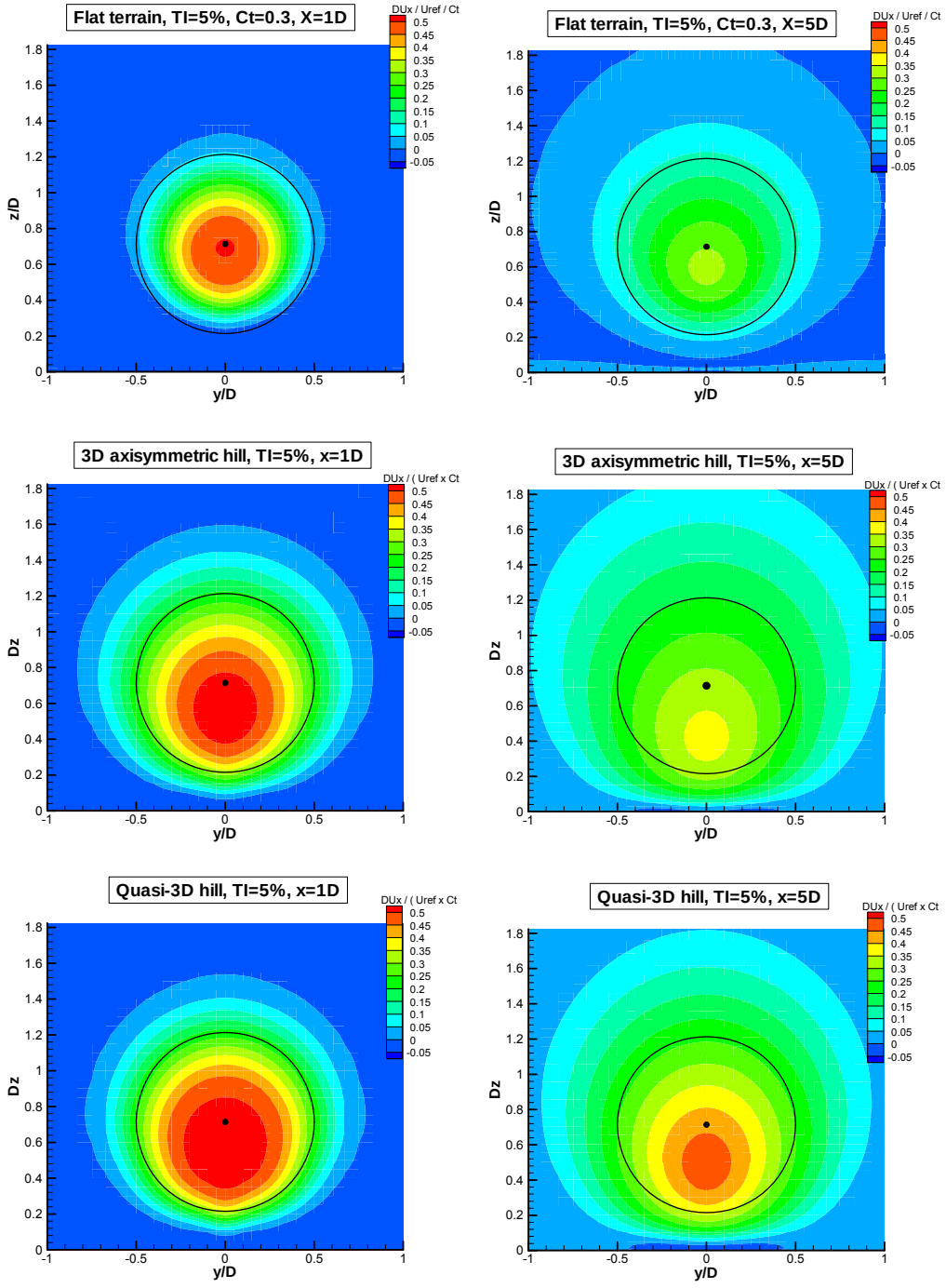

(a) (b)

Figure 69: **Comparison of wind speed deficit contours at (a) $x = 1D$ and (b) $x = 5D$ downstream the hill top among flat terrain, 3D axisymmetric hill and quasi-3D hill. $TI_{in} = 5\%$.**

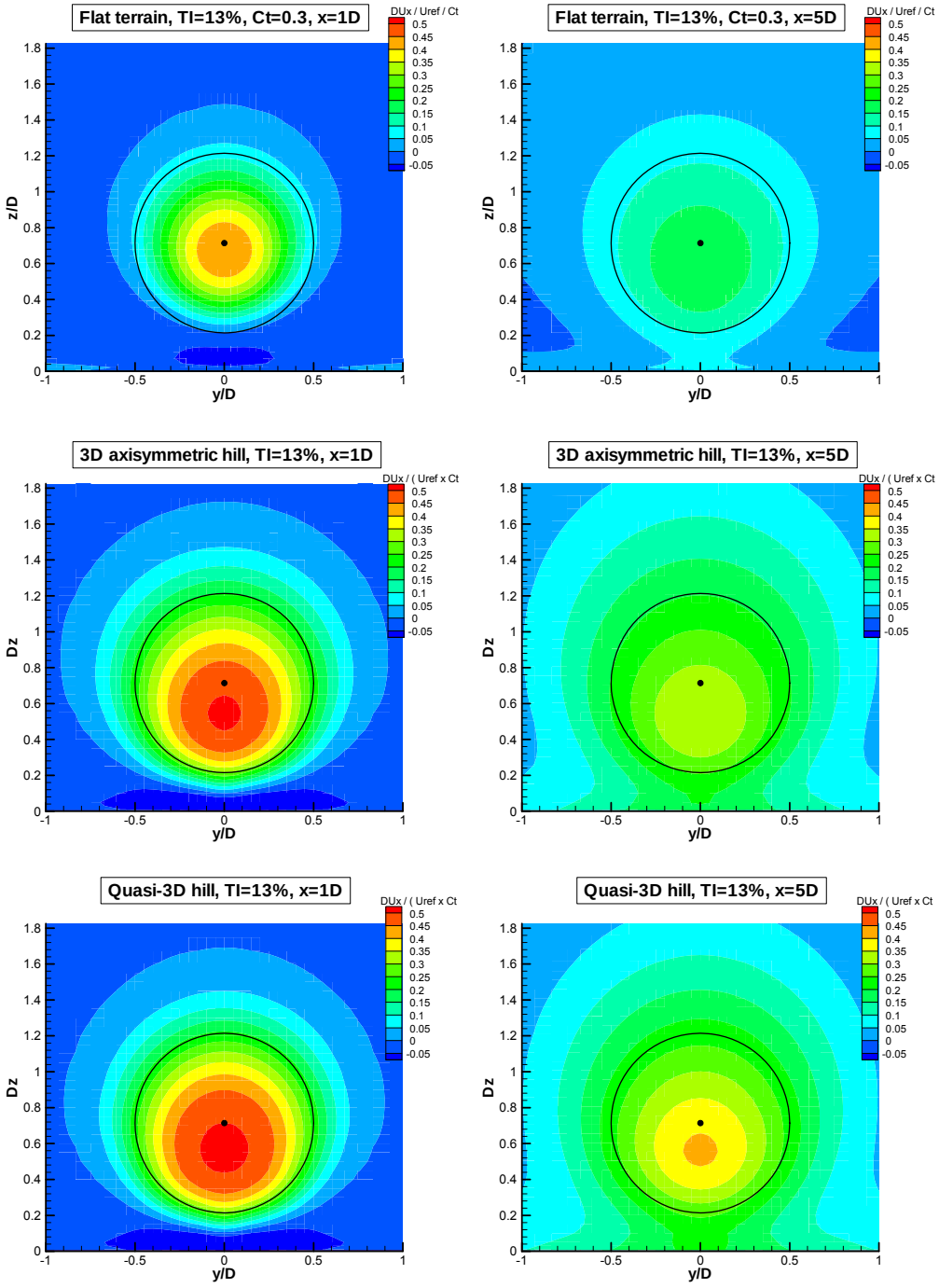

Figure 70: **Comparison of wind speed deficit contours at (a) $x = 1D$ and (b) $x = 5D$ downstream the W/T among flat terrain, 3D axisymmetric hill and quasi-3D hill. TI_{in} is 13%.**

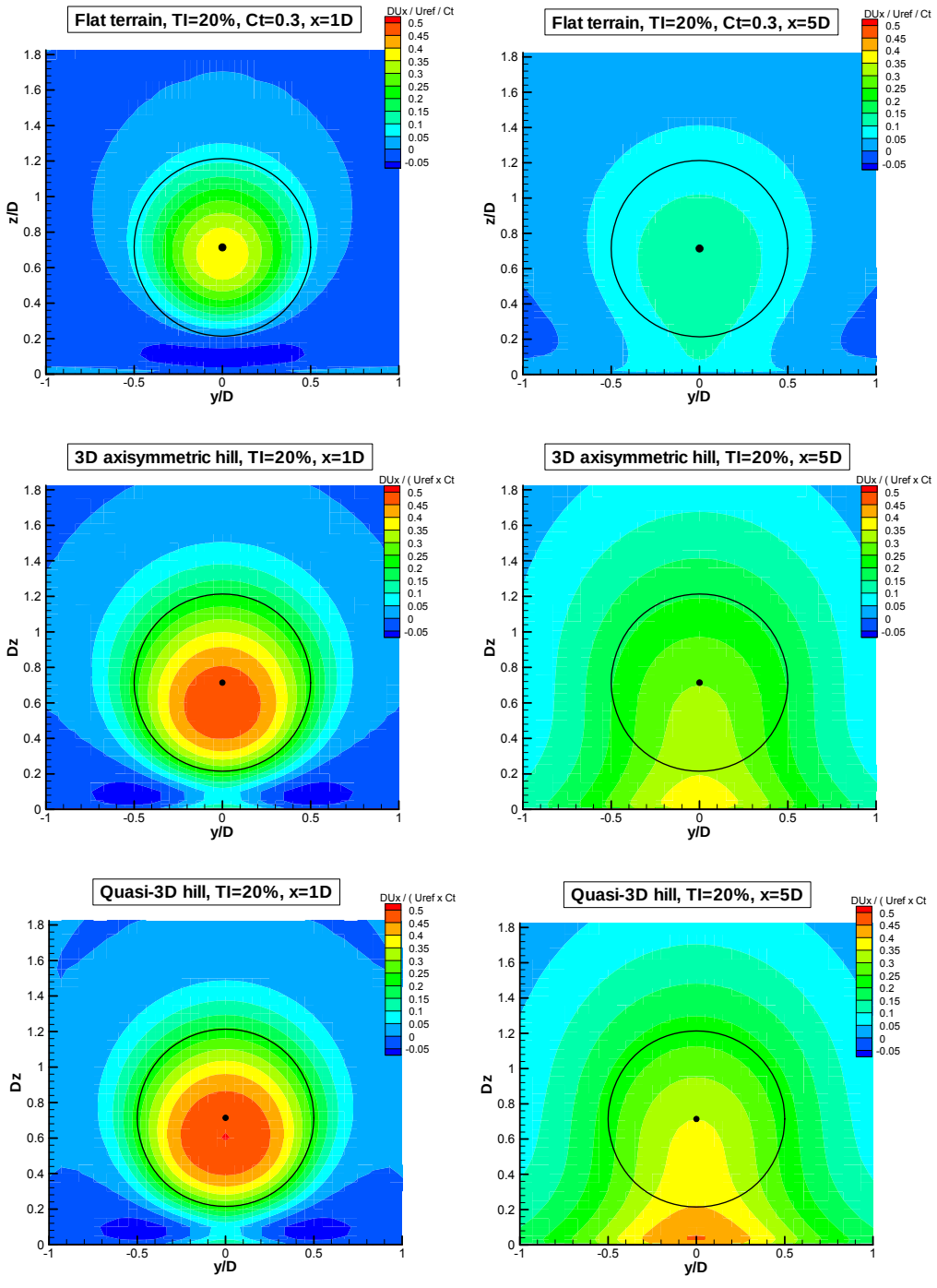

(a) (b)

Figure 71: **Comparison of wind speed deficit contours at (a) $x = 1D$ and (b) $x = 5D$ downstream the W/T among flat terrain, 3D axisymmetric hill and quasi-3D hill. TI_{in} = 20%.**

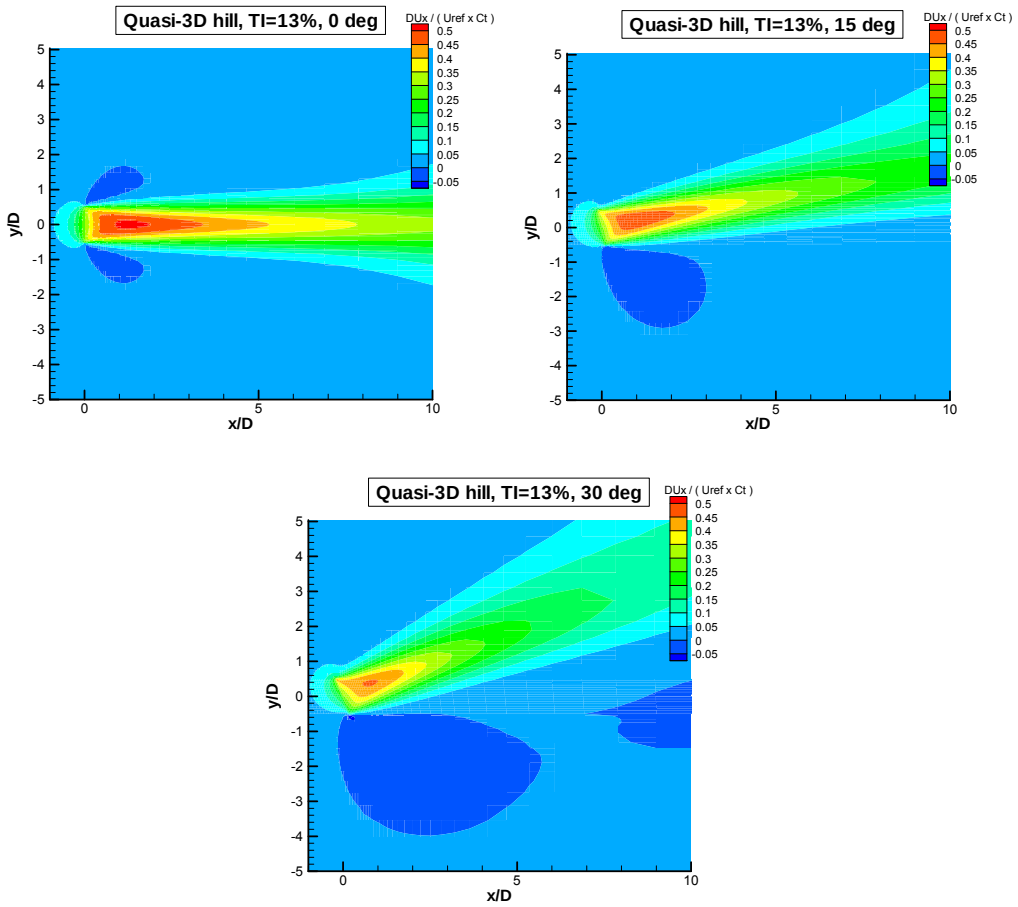

Figure 72: **Wind speed deficit contours at hub height for quasi-3D hill for 0, 15 and 30^o wind directions. Yaw angle is 0, 10 and 20^o, respectively. TI_{in} = 13%.**

5 Conclusions

The wake characteristics of a paper case 5 MW wind turbine situated on the top of a Gaussian hill were investigated through a Navier–Stokes based analysis in this report and compared with the respective characteristics in flat terrain. Two different hill geometries were examined, a 3D axisymmetric and a quasi-3D one. The effects of the hill terrain, the turbulence intensity and the wind direction on the wake characteristics were assessed. For the sake of completeness, wind speed and turbulence intensity predictions were first presented for the reference cases without W/T. The basic conclusions drawn from the numerical analysis can be summarized below.

The change of the inlet turbulence intensity, which is equivalent to a change in roughness, affects the shape of the wind speed boundary layer. An increase in the inlet turbulence produces higher accelerations at the hill top and higher decelerations at the lee side of the hill. This effect is reinforced by the W/T presence and is more pronounced in the quasi-3D hill. As a result, the increase of the TI_{in} causes a decrease in the C_t value of the W/T, implying a weaker effect on the wind speed deficit.

The presence of the hill increases significantly the turbulence intensity downstream the W/T. The maximum values occur in the region of highest flow deceleration, about $20D$ downstream the W/T. In a flat terrain, any increase in turbulence is caused only by the W/T presence.

In both hill cases the deficit remains significant at $20D$ from the W/T, and in some cases even at $40D$ (for the lower turbulence intensity value examined, $TI_{in} = 5\%$). On the contrary, in the flat terrain case, the deficit has already been practically negligible at $20D$. The decay rate is even slower for the quasi-3D hill.

The increase of the turbulence level results in a faster flow recovery at long distances as expected. However, the wind speed deficit at hub height is not always monotonously decreasing. This is a result of the wake geometry modification when the turbulence level changes, which is more pronounced in the quasi-3D geometry for the $TI_{in} = 20\%$ case.

In the flat terrain case, the wake centre is about $0.05D$ lower than hub height at $1D$ downstream and about $0.1D$ at $5D$ downstream. In the axisymmetric and the quasi-3D hill cases, the height difference between wake centre and hub is larger, about $0.15D$ and $0.2D$ at $1D$ and $5D$ downstream, respectively. For the $TI_{in} = 20\%$ case, the circular shape of the wake geometry has already been distorted at $5D$ downstream.

The effect of the wind direction on the decay rate of deficit is drastic. A change in the wind direction from 0 to 30^o increases the decay rate in such a degree that it becomes comparable to that of flat terrain. For the 30^o case, the wind speed deficit is practically negligible after $20D$. The height of the maximum deficit remains constant denoting similar wake geometry in the near wake. As the wind direction changes from 0 to 30^o, a wider spreading of the wake is observed at long distances.

The predictions for the 3D axisymmetric hill with steep slope were also compared to those of two other models: Another Navier–Stokes model using k–ε turbulence closure and the WAsP model. The comparison in the velocity deficit and turbulence intensity between the two Navier–Stokes models can be considered good, whereas the WAsP predicts reasonable velocity profile gradients and satisfactory deficit values for distances up to $11D$.

6 References

[1] Chaviaropoulos, P. K. and Douvikas, D. I., (1998), “Mean-flow-field Simulations over Complex Terrain Using a 3D Reynolds Averaged Navier–Stokes Solver”, Proceedings of ECCOMAS ’98, Vol. I, Part II, pp. 842-848

[2] Wilcox, D. C., (1993), Turbulence Modelling for CFD, DCW Industries Inc., La Canada, California, IBSN 0-9636051-0-0

[3] Troen, I., Petersen, E. L., (1989), ”European Wind Atlas,” Risø National Laboratory, Roskilde, Denmark p 656

[4] Mortensen, N. G., Heathfield, D. N., Myllerup, L., Landberg, L., Rathmann, O., (2005), “Wind Atlas Analysis and Application Program: WAsP 8 Help Facility,” Risø National Laboratory, Roskilde, Denmark

[5] Troen, I., (1990), “A high resolution spectral model for flow in complex terrain”, Ninth Symposium on Turbulence and Diffusion, Roskilde, April 30 – May 3, pp.417-420.

[6] Jackson, P.S. and Hunt, J.C.R., (1975), “Turbulent flow over a low hill”, *Q. J. Meteorol. Soc.* 101, pp.929-955.

[7] Taylor, P.A., Walmsley, J.L., and Salmon, J.R., (1983), “A Simple Model of Neutrally Stratified Boundary-Layer Flow over Real Terrain Incorporating Wavenumber-Dependent Scaling”, *Boundary-Layer Meteorol.* 26, pp.169-189.

[8] Bowen, A. J., Mortensen, N. G., (1996), “Exploring the limits of WASP: the wind analysis and application programme”, European Union Wind Energy Conference, H.S. Stephens and Associates, Bedford, UK, Goteborg.

[9] Schepers, J. G., (2003), ENDOW: Validation and Improvement of ECN’s Wake Model, Technical Report ECN-C-03-034, Energy Research Centre of the Netherlands

Appendix A

Derivation of the Relationship between the Inflow Turbulence Intensity at Hub Height and the Roughness Length

The turbulent kinetic energy, k, is defined as:

$$k = 0.5\left(\sigma_x^2 + \sigma_y^2 + \sigma_z^2\right), \tag{A-1}$$

where σ_x, σ_y and σ_z are the standard deviations of the wind speed fluctuations in directions x, y, z respectively. Taking into account the anisotropy of turbulence, $\sigma_y / \sigma_x = 0.8$ and $\sigma_z / \sigma_x = 0.5$, Eq. (A-1) becomes:

$$k = \sigma_x^2 f, \tag{A-2}$$

with $f = 0.5(1 + (\sigma_y / \sigma_x)^2 + (\sigma_z / \sigma_x)^2) = 0.945$. Combination of Eq. (6) with Eq. (A-2) results in the relationship:

$$\sigma_x = 2.4135\, u_*. \tag{A-3}$$

The inflow turbulence intensity at hub height, TI_{in}, is defined as $TI_{in} = \sigma_x / U_{in}$, with U_{in} being the local inflow wind speed. Using this definition, Eq. (A-3) can be written as:

$$\frac{U_{in}}{u_*} = \frac{2.4135}{TI_{in}}. \tag{A-4}$$

By substituting Eq. (A-4) into the logarithmic inflow wind speed profile given by Eq. (3), it follows that:

$$\frac{2.4135}{TI_{in}} = \frac{1}{K}\ln\left(\frac{z_{hub}}{z_0}\right) \qquad \text{or} \qquad z_0 = z_{hub}\, e^{-0.9895 / TI_{in}}, \tag{A5}$$

which relates the inflow turbulence intensity TI_{in} at hub height z_{hub} with the roughness length z_0.

Appendix B

Derivation of the Relationship between Turbulent Kinetic Energy and Turbulence Intensity

For the free stream flow, the turbulent intensity in x-direction is given by:

$$TI_x(z) = \sigma_x / U_x(z) \ , \tag{B-1}$$

where σ_x is the standard deviation of the wind speed fluctuations in x-direction and U_x is a function of height only, See Eq. (3).

In the wake region, the turbulence intensity is given by:

$$TI_{x,w}(y,z) = \sigma_{xw}(y,z) / U_x(z) \ , \tag{B-2}$$

namely the standard deviation of the wind speed fluctuations is again normalized with the free stream wind speed and not the local wake wind speed. Thus, added turbulence intensity is defined, which is a measure for the increase in standard deviation:

$$TI_{add,x}(y,z) = \sqrt{TI_{w,x}(y,z)^2 - TI_x(z)^2} = 1/U_x \sqrt{\sigma_{w,x}(y,z)^2 - \sigma_x(z)^2} \tag{B-3}$$

Considering the anisotropy of turbulence for the basic atmosphere, Eq. (A-2) is valid and can be rewritten as:

$$TI_x(z) = 1.026\sqrt{k(z)} / U_x(z), \tag{B-4}$$

where $k(z)$ is the turbulent kinetic energy in the free stream. The turbulent kinetic energy in the wake region has been increased by the added turbulence:

$$k_w(y,z) = k(z) + k_{add}(y,z) \tag{B-5}$$

If the added turbulence was also anisotropic, the turbulence intensity in the wake should be given by Eq. (B-4) with $k_w(y,z)$ instead of $k(z)$. However, measurements in wakes have shown lower values for turbulence intensity in x-direction than those obtained considering Eq. (A-2). Therefore, a fully isotropic turbulence is assumed in the wake. Thus, turbulence intensity in x-direction is decreased improving the agreement with measurements. The isotropic assumption implies that $k = 1.5\sigma_x^2$, $\sigma_x = \sigma_y = \sigma_z = 0.82\sqrt{k}$ and is adopted only for the added turbulence:

$$TI_{add,x}(y,z) = 0.82\sqrt{k_{add}(y,z)} / U_x(z) \tag{B-6}$$

The combination of equations (B-3) through (B-6) results in:

$$TI_{w,x}(y,z) = 1/U_x(z)\sqrt{0.6724\ k_w(y,z) + 0.3803\, k(z)} \ , \tag{B-7}$$

which is the relationship providing the turbulent intensity in the wake using the predicted turbulent kinetic energy $k_w(y,z)$. In this report, Eq. (B-7) is also used for the cases without W/T, so that the relation between the predicted turbulent kinetic energy and the turbulence intensity is uniform.

Appendix 4: Deliverable 8.4 Offshore clusters

Project funded by the European Commission under the 6th (EC) RTD Framework Programme (2002- 2006) within the framework of the specific research and technological development programme "Integrating and strengthening the European Research Area"

Project UpWind
Contract No.:
019945 (SES6)

"Integrated Wind Turbine Design"

Wp8: Flow

Deliverable D8.4

Report on planetary boundary layer model including wind farm feedback focusing on the performance of the wind farm as a unit

AUTHOR:	Sten Frandsen
AFFILIATION:	Risø National Laboratory/ Technical University of Denmark
ADDRESS:	Frederiksborgvej 399, 4000 Roskilde, Denmark
TEL.:	+45 46 77 50 72
EMAIL:	Sten.Frandsen@risoe.dk
FURTHER AUTHORS:	R.Barthelmie, Ole Rathmann, Hans E. Jørgensen, Jake Badger, Kurt Hansen, Søren Ott, Pierre-Elouan Rethore, Søren E. Larsen, Leo E. Jensen, Wolfgang Schlez, Anja Neubert and Gillian Smith
REVIEWER:	WP8 Project members
APPROVER:	

Document Information

DOCUMENT TYPE	Deliverable D8.4
DOCUMENT NAME:	WP8Flow8.1D1.doc
REVISION:	
REV.DATE:	
CLASSIFICATION:	
STATUS:	

Abstract: It was the goal of the project – by means of data from the demonstration wind farms Horns Rev and Nysted, analyses of these data and modelling – to facilitate prediction of the power losses from a wind farm should a new wind farm be built upwind relative to the prevailing wind direction. Or conversely, predict with adequate accuracy the production of a new wind farm built downwind of an existing wind farm.

The project should be seen in the perspective of the two existing demonstration wind farms that extend 5-10 km in each direction. In order to e.g. use the existing electrical infrastructure it may appropriate to build new wind farms rather close to the existing wind farms. A relevant question is therefore how far away new wind farms must be placed to avoid too large power losses.

Measurements have been carried out for several years at the two sites, and databases have been prepared. The databases – one for each site – include production and operational statistics for the wind turbines and statistics for the meteorological measurements carries out in the vicinity of the wind farms.

Several different modelling activities were carried out, which *intentionally* to some extent are redundant. Thus, if different modelling efforts results in comparable results, the quality of the models will be tested outside the physical range where data are available.

The main achievements of the project are:

- Measurements were carried out at the Nysted and Horns Rev demonstration wind farms for several years. Doing so included design, installation and operation of the measurement system
- A data base was built from the incoming data. The data have been organized to facilitate verification of the models developed as part of the project
- 6-7 different models have been developed and compared

Contents

STATUS, CONFIDENTIALITY AND ACCESSIBILITY									
Status				**Confidentiality**				**Accessibility**	
S0	Approved/Released			**R0**	General public			Private web site	
S1	Reviewed			**R1**	Restricted to project members			Public web site	
S2	Pending for review			**R2**	Restricted to European. Commission			Paper copy	
S3	Draft for commends	**x**		**R3**	Restricted to WP members + PL	**x**			
S4	Under preparation			**R4**	Restricted to Task members +WPL+PL				

PL: *Project leader* **WPL:** *Work package leader* **TL:** *Task leader*

7 Executive summary

7.1 Project objectives

It is the goal of the this work – by means of data from the demonstration wind farms Horns Rev and Nysted, analyses of these data and modelling – to facilitate prediction of the power losses from a wind farm should a new wind farm be built upwind relative to the prevailing wind direction. Or conversely, predict with adequate accuracy the production of a new wind farm built downwind of an existing wind farm.

The project should be seen in the perspective of the two existing demonstration wind farms that extend 5-10 km in each direction. In order to e.g. use the existing electrical infrastructure it may appropriate to build new wind farms rather close to the existing wind farms. Relevant questions are therefore how far away new wind farms must be placed to avoid too large power losses and how these losses should be quantified by models or measurement in case of conflicting commercial interests.

7.2 Issues comparing models and measurements

There are some major issues in wind farm model validation studies which will be discussed below. As stated above we concentrate here on power loss modelling which should encompass the whole range of wind speeds and directions and we also consider that the range of wind farm/wake model extends from engineering through to full CFD models. In general, computing requirements for CFD models means we are restricted to examining a number of specific wind speed and direction cases and only a moderate number of turbines rather than wind farms with ~100 turbines which can easily be done by WindFarmer and WAsP. On the other hand it can be difficult to extract reasonable simulations from some of the wind farm models for very specific cases. For example, WAsP relies on having a Weibull fit to wind speed distributions and fairly large directional sectors (30□). Therefore for specific wind speeds and narrow directional bins models like WAsP are never going to produce very exact solutions because they are being used beyond their operational windows. In addition to this there are a number of specific issues:

- Establishing the freestream flow. The major issues in determining the freestream flow are the displacement of the measurement mast from the array (assuming there is a mast), adjustments in the flow over this distance especially in coastal areas and differences in height between the measurement and the turbine hub-height. If there is no mast or the mast is in the wake of turbines or subject to coastal flow then the turbine(s) in the freestream flow may be used. If power measurements are used to determine wind speed they will be subject to any errors in the site specific power curve.
- Wind direction, nacelle direction and yaw misalignment. Because of the difficulty in establishing true north when erecting wind vanes (especially offshore where landmarks may not be determinable) it can be difficult to establish a true freestream direction. Even a well maintained wind vane may have a bias of up to 5□ and it is important to understand this because the total width of a wake may be of the order 10-15□ at typical turbine spacing. In a large wind farm, each turbine may have a separate bias on the direction, which is difficult to determine. Analysis must be undertaken to calibrate the

maximum wake direction to within 1□ and to check for bias of the yaw angle on each wind turbine in the array.

- If there is a gradient of wind speeds across the wind farm as there may be e.g. in coastal areas, near a forest or caused by topography these variations will need to be accounted for before wake calculations are undertaken.
- In terms of modelling wakes both the power curve and thrust coefficients must be known but these will vary according to the specific environment. A power curve must be calculated for the site. For modelling, the question of whether the thrust coefficient should be set to one value for the wind farm or at each individual turbine in each simulation is still an open one. The state-of-the-art is to validate the individual power and pitch curves with reference to the nacelle anemometer, which seems to be a rather robust method to determine changes in the system setup.
- Comparing the modelled standard deviation of power losses in a row with the measured standard deviation raises a number of issues. The two most important are ensuring that the time averaging is equivalent between models and measurements and taking into account that there will be natural fluctuations in the wind speed and direction in any period. Models are typically run for specific directions but it may be necessary to include the standard deviation of the wind direction in the model simulations.
- In the large wind farm context the time scale of wake transport must be considered. A large wind farm with 100 turbines in a 10 by 10 array with an 80 m diameter rotor and a space of 7 rotor diameters has a length of nearly 6 km. At a wind speed of 8 m/s the travel time through the array is more than 10 minutes. As mentioned above the wind direction will be subject to natural fluctuations in addition to possible wake deflection but there will also be natural variations in the wind speed over this time scale.
- Determining turbulence intensity and stability may be critical. Turbulence intensity is a key parameter in many models. Using either mast data to determine this information or deriving it from turbine data is subject to fairly large errors for the reasons discussed above and because the accuracy of temperature measurements used to derive stability parameters is often inadequate.

7.3 Measurements and data analyses

Measurements have been carried out for several years at the two sites, and databases have been prepared. The databases – one for each site – include production and operational statistics for the wind turbines and statistics for the meteorological measurements carries out in the vicinity of the wind farms.

Having the considerations of Section 7.2 in mind, the data have been analyzed in various ways by members of the project team. One particularly important type of result is the wind-speed-drop curves: by mean of the (inverse) power curve of the wind turbines the mean wind speed at each wind turbine position is derived and together with the met mast measurements, the development of wind speed through and downwind of the wind farm is estimated for Westerly winds. These wind-speed-drop curves are the main experimental results, which are paramount to the verification of the numerical and analytical models.

Also turbulence and vertical mean wind speed profiles are derived from the measurements and applied in connection with the modelling work.

In addition, so-called laser-lidar measurements have been performed, though with less conclusive result.

The measurements are reported in more details in Section 8.

A separate report on the measurements and basic data analysis will be issued within the next few months

7.4 Modelling

Although extremely valuable the data from the two demonstration projects, the data themselves are not sufficient to document the operational model(s) that is intended to emerge from this project.

Therefore, we started several different modelling activities, which *intentionally* to some extent are redundant. Thus, if different modelling efforts results in comparable results, the quality of the models will be tested outside the physical range where data are available.

The engineering models presently applied for calculating production losses due to wake effects from neighbouring wind turbines are based on local unit-by-unit momentum equations, disregarding a two-way interaction with the atmosphere, Frandsen et al. (2006). On the other hand, another group of models, which did not reach engineering maturity, predict the array efficiency of very large wind farms by viewing the wind turbines as roughness elements. A third option is to apply CFD[1] schemes. These models encompass the individual wind turbines and thus track and integrate the momentum and energy budget for the whole wind farm, but has hitherto not been applied for the two way interaction with the atmosphere.

A total of 6-7 different modelling approaches have been applied.

These are described in Section 9.

7.5 Conclusions

All considered the project participants find that the project has been immensely successful. The main achievements of the project are:

- Measurements were carried out at the Nysted and Horns Rev demonstration wind farms for several years. Doing so included design, installation and operation of the measurement system
- A data base was built from the incoming data. The data have been organized to facilitate verification of the models developed as part of the project
- 6-7 different models have been developed and compared. It is found that the modelling work already done forms a sufficient and adequate basis for prediction of production from one or more large wind farms

Although we find that the available data and the modelling work already done are sufficient as scientific basis, the user software – anticipated in the project proposal – remains to be

1 Computational Fluid Dynamics – numerical solutions to the equations of motion of the fluid.

designed and produced. The task of integrating the small-scale and large-scale models proved more difficult than anticipated. However, we are confident that solutions will be found in the near future.

8 Data from Horns Rev and Nysted wind farms

The two demonstration wind farms were owned by ELSAM and E2, respectively, when the project was initiated. Presently, the Horns Rev wind farm is jointly owned by the power companies DONG Energy and Vattenfall, and the Nysted wind farm is owned by DONG Energy.

A separate report on the measurements and basic data analysis will be issued within the next few months.

8.1 Description of sites

The basic wind farms layout is described below.

1.1.4. a) Horns Rev

The wind farm layout is a 10 times 8 matrix forming a slightly oblique rectangle, Figure 73. The distance between the turbines is 560 meters in both directions, corresponding to 7 rotor diameters. The Vestas V80 wind turbine units have a rotor diameter of R=80m, and hub height H=70m.

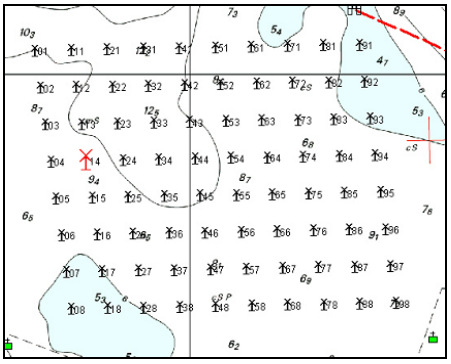

Figure 73 The turbines are numbered so that the westernmost column is numbered from 01 to 08 with 01 being the turbine in the northwest corner, and the easternmost column being numbered 91 through 98. This may lead to the wrongful assumption that there are actually 98 turbines, but as several numbers are unused, the number of turbines is still only 80.

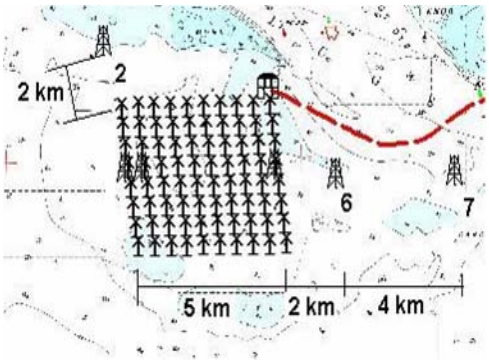

Figure 74 The position of the meteorological towers. The "downwind" met masts are off-line relative to the West-East wind turbine rows – placed on a line in the middle of two rows.

For the wake measurement, the most interesting turbine data are the diameter, the hub height and the thrust coefficient. Since the Vestas V80 turbine is a pitch-variable speed machine, running with constant tip-speed ratio at low to medium wind speeds, the thrust coefficient is fairly constant. This is very convenient for the scientific work as e.g. relative wind speed deficits can be expected to be fairly constant for a large wind speed range.

The power and thrust coefficient curves are specific to the turbines delivered for the Horns Rev wind farm and may not apply to V80 turbines delivered for other projects.

The wind farm is located in the North Sea, approximately 30 km west of Esbjerg. The distance to the nearest point on shore (Blåvands Huk) is approximately 13 km.

Around the wind farm three met masts are installed, Figure 74. The oldest mast is called M2. This mast was installed before construction of the wind farm and is the one that was used to determine the wind resource at the site. Several other papers have described and analysed measurements from that mast.

In the summer of 2003 two more masts (called M6 and M7) were installed, Figure 74. The purpose of these masts is to study the recovery of the shaddow flow behind the wind farm for westerly winds, and support the development of new scientific and engineering models for calculation of external wake effects from large offshore wind farms.

M2 is located 2 km north-northwest of the northwest corner turbine (01). M6 and M7 are located 2 and 6 km east of the wind farm respectively on a line that passes right through the middle of the fourth and fifth row.

In addition to the wind flow measurements in the met mast, statistics of power and other operational parameters from all wind turbine units were recorded.

b) Nysted

Nysted wind farm was commissioned in 2004 by Energi E2 and is now owned by DONG Energy. It has the largest installed capacity in an offshore wind farm, 165.6 MW. It is located approximately 11 km to the south of the island of Lolland, Denmark. There are 72 turbines laid out in nine rows, with west-to-east spacing of 10.5 rotor diameters (i.e. an inter-turbine distance of 857 m) and eight columns north to south with a spacing of 5.8 D (481 m), see Figure 75.

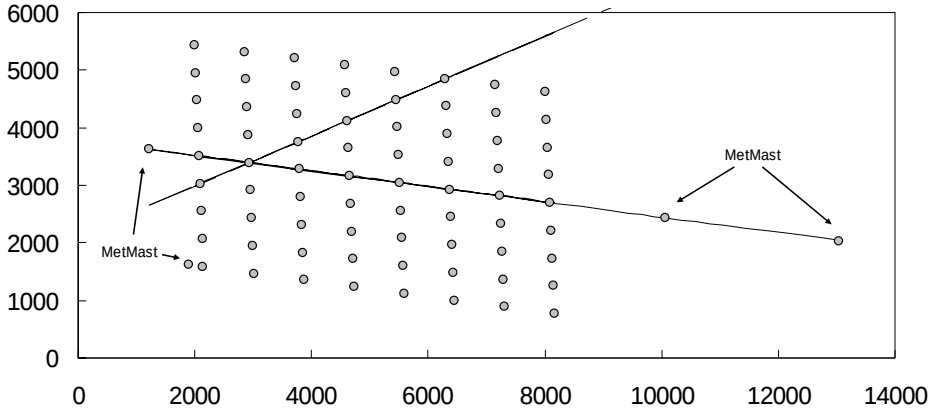

Figure 75. Layout of the Nysted wind farm. Different wind directions offer different wind turbine separations for model verification. The "downwind" met masts are in line with wind turbine row.

The turbines are Bonus 2.3 MW with a hub height of 68.8 m and a rotor diameter of 82.4 m. Prior to construction, two 50 m meteorological masts were erected to provide site wind assessment, one on-site, the other approximately 11 km east on the island of Falster (Gedser land mast). After wind farm construction, four additional 70 m masts were erected. Two of these are close to or upwind of the wind farm in the prevailing south-westerly wind direction. The remaining masts are downwind of the array in the prevailing wind direction at distances of 2 and 6 km. Ten-minute averages of power, yaw and status signal from each turbine are available from June 2004 and onwards. Meteorological data were utilised from all four post-construction masts where wind speed profiles, direction and temperature measurements were selected from the SCADA database. Data collection within the SCADA system ensures that all data are time synchronised.

8.2 Measurements made

Globally, the amount of information available is satisfying. The data are stored as 10-minute statistics and some one-second statistical data was available on request. In both cases the relevant sensors available were the wind speed anemometers and wind vanes on the met masts and the wind turbine anemometers, the thermometers on the met masts, the power production sensors and the yaw direction sensors of the turbines. In addition, the pitch angle of the wind turbine blades and the rotor rotational velocity were used as quality filters.

While the whole data set at Nysted including additional parameters such as humidity were available, supplied data from Horns Rev were solely the requested variables described

above. The data available from Horns Rev cover the year of 2005 (>50.000 data points), while Nysted data were available from June 2004 onwards (>150.000 data points).

The wind turbines were in both cases operating more than 97% of the time, which provides a fairly large amount of useable data. Nonetheless, the cases when the whole wind farms were operating at full capacity (all the turbine are working) are more limited (less than 10% of the time). This amount of data is not enough for making wake statistics, as it requires, on top of this condition, additional conditions over the wind direction and wind speed. In order to overcome this problem, the condition where a full row of turbines are working was used instead, which provide a much larger amount of data (>70%).

The two data sets were first available in two different data format: a SCADA database for Nysted, updated in real time, and a raw ASCII file format for Horns Rev. This required gathering the two formats in a new SQL database format.

8.3 Data quality

The quality of the two data sets is generally good. Globally, the amount of information available is satisfying in both cases. However, during the data analysis campaign, several types of data corruption were encountered.

In Nysted database, some of the mast wind vane sensors kept indicating the same wind direction during a relatively long period of time (sometimes several days), while the other wind direction sensors were all agreeing on a completely different wind direction. This seems to indicate that the wind vane could have been blocked physically during those periods, or that the data was corrupted, and reproducing the same values over and over. If it is the second explanation is the right one, it implies that there might be a similar corruption of data in other sensors, which was – however – not spotted during the data analysis.

In Horns Rev database,

- The yaw sensors of the wind turbines were in general of rather poor reliability. It seems that after a shut down, the yaw sensor is not working properly for a relatively long period of time (sometimes several hours).
- The mast 2, located north west of the wind farm, is equipped with 3 wind vanes, but during most of the year 2005, only one was working. During the second half of the year 2005, this sensor was indicating a wind direction covering just a fraction of the direction angles, while the two other masts were covering the full range of directions. This seems to indicate that the wind vane was physically blocked between two directions, or that the algorithm used to extract the data was deficient.
- The top anemometers at all the three met masts are all indicating a wind speed higher that it would be expected from a logarithmic profile. While it's a commonly observed problem, several interpretations can be found in the literature, arguing that the top anemometers are the only one to be trusted, or the opposite. According to a parallel study over a comparison between a LIDAR measurement located on the platform, and the met mast measurements, done at Risø DTU, the top anemometer seems to be over predicting the wind speed. Following these observations, the top anemometers were not considered in the data analysis.

- At least one wind turbine (WT93) seemed to have an offset of time (at least 30 min) during a relatively long period of time (at least a day). This was apparent on the power production, where the turbine was following the rest of its neighbouring turbines, with a small delay. This kind of data corruption is difficult to identify and it is possible that other cases of timestamp corruption have gone unnoticed.
- The wind farm was sometimes under power regulation, which means that the power output of the turbines did not follow the regular power curve. In order to exclude those cases from the data analysis, the timestamps when it occurred were referenced in a table. Nonetheless some cases seemed to be unreferenced, as they were sometime visible in the data. The power regulation can sometimes be very slight, which means that it could be possible that some cases were not spotted during the data analysis.

9 Modelling efforts

Although extremely valuable the data from the two demonstration projects, the data themselves are not sufficient to document the operational model(s) that is intended to emerge from this project.

Therefore, we have started several different modelling activities, which *intentionally* to some extent are redundant. Thus, if different modelling efforts results in comparable results, the quality of the models will be tested outside the physical range where data are available.

The engineering models presently applied for calculating production losses due to wake effects from neighbouring wind turbines are based on local unit-by-unit momentum equations, disregarding a two-way interaction with the atmosphere, Frandsen et al. (2006). On the other hand, another group of models, which did not reach engineering maturity, predict the array efficiency of very large wind farms by viewing the wind turbines as roughness elements. A third option is to apply CFD[2] schemes. These models encompass the individual wind turbines and thus track and integrate the momentum and energy budget for the whole wind farm, but has hitherto not been applied for the two way interaction with the atmosphere. Another computational technique, *L*arge *E*ddy *S*imulation (LES), has a much finer spatial resolution and may therefore simulate the vortices shed from the blades and the subsequent breakdown of the vortices into chaotic eddies. The high resolution presently prohibits the application of LES for wind farms with hundreds wind turbines, but a special technique, where the simulated wake from a rotor is fed cyclically on to the same rotor, is presently being tested. While the method is not yet operational in the engineering sense, it may be used to emulate an infinite row of wind turbines, which is a key element of the first model presented below.

9.1 Analytical hybrid model

The analytical model in question is a computationally economic model-complex that links the small and large-scale features of the flow in wind farms. Thus, if successful it will be applicable for any size of wind farm. The model is being evaluated and adjusted and calibrated by means of measurements and the numerical techniques mentioned above. Further, the model is being numerically implemented, See Section 9.3.

As it is often needed for offshore wind farms, the analytical model[3] handles *a priori* a regular array-geometry with straight rows of wind turbines and equidistant spacing between units in each row and equidistant spacing between rows. Firstly, the base case with the flow direction being parallel to rows in a rectangular geometry is considered by defining three flow regimes. Secondly, when the flow is not in line with the main rows, solutions may be found for the patterns of wind turbine units emerging corresponding to each wind direction. The solutions are in principle the same as for the base case, but with different spacing in the along wind direction and different distance to the neighbouring rows.

---

2 Computational Fluid Dynamics – numerical solutions to the equations of motion of the fluid.

3 The model presented in Section 9.3 handles any geometry.

Returning to the base case and counting from the upwind end of the wind farm, the model encompasses 3 main regimes as illustrated in Figure 76.

In the first regime, the wind turbines are exposed to multiple-wake flow and an analytical link between the expansion of the multiple-wake and the asymptotic flow speed deficit are derived.

The second regime materializes when the (multiple) wakes from neighbouring rows merge and the wakes can only expand upward. This regime corresponds (but is not identical) to the flow after a simple roughness change of terrain.

The third regime is when the wind farm is "infinitely" large and flow is in balance with the boundary layer.

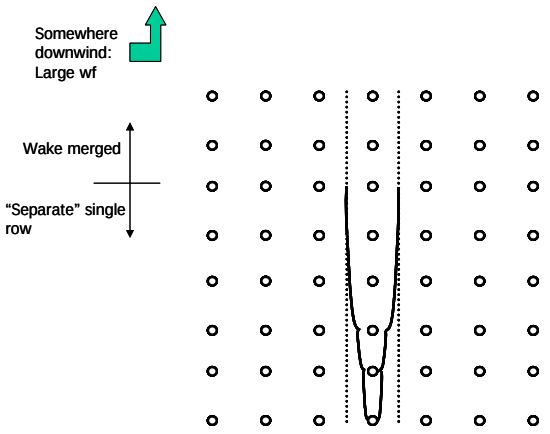

Figure 76. Illustration of the regimes of the proposed model. The wind comes from the "South", parallel to the direction of the rows.

Additional regimes need to be defined when the model is to be practically applied, i.e. the first row facing the wind is obviously not exposed to wake conditions, and most frequently the wake hits the ground before it merges with the wakes from the neighbouring rows. However, it is here chosen to disregard these in order to produce a clearer presentation. For the same reason and because it plays a lesser role than the mass momentum flux, the surface friction is disregarded in regimes 1 and 2, but not in regime 3. Should experimental evidence point to it, it is possible to include the surface blocking and stress in the model explicitly or implicitly by making the wake expansion and/or the growth of the internal boundary layer in regime 2 dependent on surface roughness.

The mathematical details are found in Frandsen et al (2006) and the effort to programme a more general version of the model is given in Section 9.3.

9.2 Extension of WA^{S}P

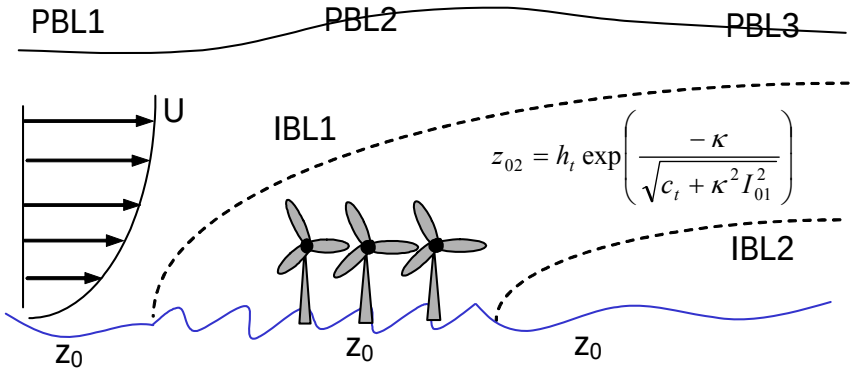

Figure 77. Illustration of the added roughness approach to wind farm modelling.

Given current understanding that wind farm models under-estimate wake losses in large offshore wind farms an alternative approach is to depict the wind farm as an area of higher roughness. This can be done either within the wind farm model using both wake modelling and the added roughness layer or within a simple 2-dimensional model. In the 2D model the roughness element causes an internal boundary layer to grow over the wind farm. The area of higher roughness causes the wind speed at hub-height to increase. After the wind farm when the roughness returns to an open sea value (either an abrupt change or with an exponential decay) the wind speed is allowed to recover. The impact on wind speed is dictated by the wind farm thrust coefficient and the spacing of the turbines in the wind farm.

As shown in Figure 78, the impact of the wind farm is estimated to be advected at least 10 km downstream. Results of comparison of this approach with standard wake modelling in WAsP indicates that using higher roughness areas allows longer for the atmosphere to recover from the impact of wind farms taking 6-8 km for hub-height wind speeds to recover to 98% of their initial value. This is in line with results from CFD modelling.

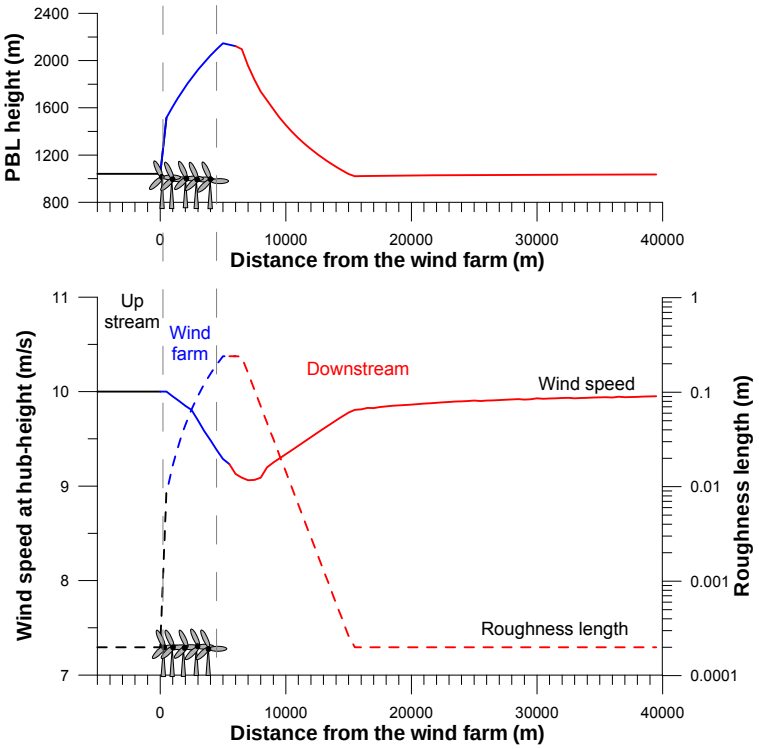

Figure 78. Results from the added roughness model

Model	Distance in km for wind recovery (to 98% of its initial value)
WAsP z0(block) 0.1 m	6
WAsP z0(block) 0.5 m	7
WAsP z0(block) 1.0 m	8
WAsP wake decay 0.075	2
WAsP wake decay 0.05	3
Added roughness: exponential z0 decay	14 (5%-7.5)
Added roughness: constant z0	14 (5%-5.5)

EMD CFD model: z0 0.1-0.5 m	8
EMD CFD model: z0 1 m	7

Discussion of the application of the Simple WAsP-like models

Above, the wind shadows behind larger wind farms are estimated, using versions of the roughness change models, applied in the WAsP program. We shall discuss the possibilities a little closer, comparing with the data, obtained in the observation program, described and discussed in Section 8, and in further details in the separate data report to be issued later.

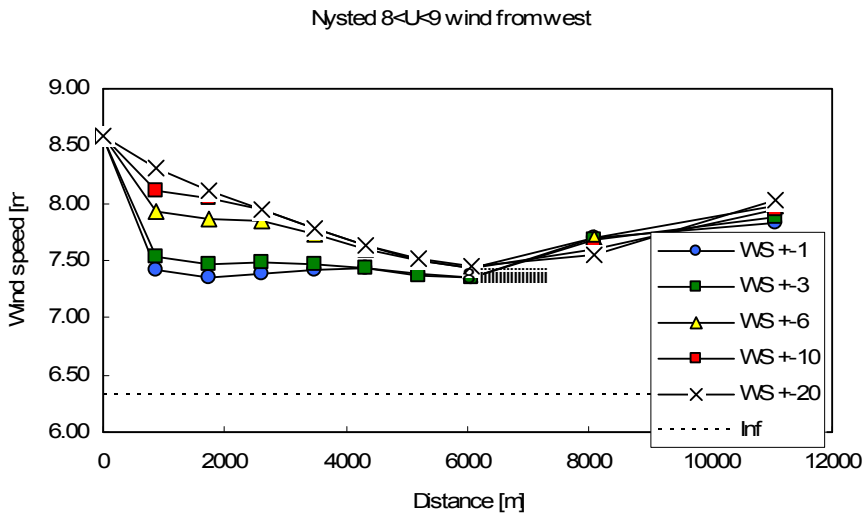

Figure 79. Variation of the mean speed through and behind the wind farm at Nysted, at hub height 70 meter. The different curves correspond to the number of wind angle sectors enters into the averaging.

Figure 79 illustrates that the wind speed behind the farm divided by the upstream wind are pretty robust, and can be taken as: 0.86, 0.88 and 0.93 at about 6000, 8000 and 11000 m behind the leading edge of the farm. In the following we shall see how close the different versions of the roughness change model can get to these figures

In roughness change models the wind farm is associated with a surface roughness as seen in Figure 77 and Figure 78 above.

In the roughness change models we associate the surfaces involved with surface roughness. Following the above figures, we assume two dimensional modelling, having to

estimate roughness values for the water surfaces before and behind the wind farm and for the wind farm itself. From standard formulations (reference) we take the basic water roughness as: z_{ow}= 0.0002 m.

The formula shown on Figure 77 expresses the wind farm equivalent surface roughness from the area averaged thrust coefficient, the hub-height and the background turbulence intensity. For the situations reflected in the figure above, we find the wind farm roughness to: z_{oWF} = 0.68 m.

The internal boundary layers in the roughness change model are assumed to grow as:

$$\frac{dh}{dx} = C\frac{u_*(h)}{U(h)},$$

where *h* is the height of the internal boundary layer growing from the roughness change point. u_* is the friction velocity and *U* is the mean speed. The surface friction within the new internal boundary layer is found by matching the up stream and the down stream wind speed at the height *h*. For the simplest case with two logarithmic profiles we find:

$$U_0(h_1) = \frac{u_{*0}}{\kappa}\ln(\frac{h_1}{z_{0w}}) = \frac{u_{*1}}{\kappa}\ln(\frac{h_1}{z_{0WF}}) = U_1(h_1),$$

where we have considered the growth of the internal boundary layer over the wind farm, when the up-stream over-water wind blows over the wind farm. It is seen that we can determine the down stream profile from the up-stream profile and the two roughness values.

The different roughness change models are characterized by different assumption about the profile formulation, the variation of u_* with height, different growth formulas for *h* and different estimates of the surface roughness. This does all sound quite arbitrary, but as we illustrate later the roughness changes models are actually quite robust. This is illustrated below using the simplest IBL modeling (based on surface layer and logarithmic profiles) for the wind behind the wind farm.

Using the notation from above, it is seen that the ratio between the wind speeds at hub height in front of the wind farm and behind it can be written for a given distance *X*.

$$\frac{U_2(h_{ub})}{U_0(h_{ub})} = \frac{\ln(\frac{h_1}{z_{0w}})}{\ln(\frac{h_1}{z_{0WF}})}\frac{\ln(\frac{h_2}{z_{0WF}})}{\ln(\frac{h_2}{z_{0w2}})}\frac{\ln(\frac{h_{ub}}{z_{0w2}})}{\ln(\frac{h_{ub}}{z_{0w}})}$$

Where we have basically used the matching of the two boundary layers twice rather than once, used before. The two heights, h1 and h2 refer to the two IBLs shown on Figure 77. The water roughness behind the wind farm can in general be different, as is indeed illustrated in the first part of this section 9.2. If the two water roughness values are just close, the last ratio in the equation is approximately one. The equation illustrates the robustness of the modeling, in that uncertainty on both the IBL heights and the roughness values tend to cancel.

Figure 80 shows the recovery of the wind behind the wind farm, according to the data above and from results from the basic surface layer model (SL) model with modified profiles and standard logarithmic wind profiles and with modified profiles, as described in (Sempreviva et al., 1990). We will not expect the model to provide useful results just behind the wind farm (first data point), since the height of the new internal boundary layer developing behind the wind farm is much lower than the hub height. At the second point at 8 km, the IBL height, in last IBL, is of the order of 450 m, and hence a roughness change model may work. At the last point at 11 km the roughness layer model should be best. The model is seen to shown somewhat faster return to upstream conditions than the data.

Figure 81 shows the behavior of the same SL model, where the roughness upstream roughness has been modified, following the WAsP methodology, where far upstream roughness values, here the wind farm roughness, converges exponentially towards a general background roughness, here the water roughness.

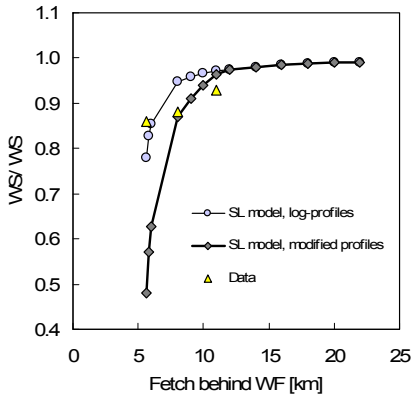

Figure *82* illustrates that this approach indicates and even faster recovery of the wind behind the wind farm that the basic SL model. This is an expected result since the WAsP approach accelerates the return towards conditions over a free water surface by this exponential change of the wind farm roughness value.

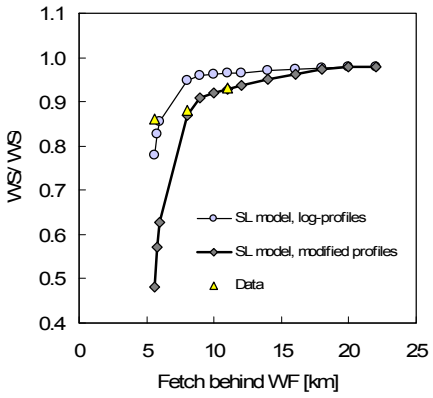

In

Figure *83*, the roughness change model includes the behaviour of the internal boundary layers above the surface layer, with associated modifications of both the wind profiles and the turbulence level that is responsible for the growths of the IBLs. The effect of this

modification is minor, and still the model predicts a faster recovery of the wind after the wind farm than does the model.

For this type of models it is important to characterize the turbulence that drives the growth of the IBLs involved in the model, since the turbulence structure of each IBL is different. It is normal to use the turbulence from the boundary layer with the strongest turbulence level as driver of the IBL growth In this case the strongest turbulence is associated with the largest roughness, that is the wind farm. However, after the wind farm this turbulence slowly decays leaving only the turbulence over the water surface to drive the continued growth of the IBL after the farm. In figure 4 this is modeled by having both IBLs grow with the wind farm turbulence until about 1 wind farm scale (5 km) downstream, where the final growth is taken over by the over-water –turbulence. This approach is seen to improve the prediction at the 11 km data point.

We therefore conclude a roughness change model may be modified to provide a reasonable match to the data, introducing physically sensible modification. Additional work on the full data set will be performed to further evaluate this conclusion.

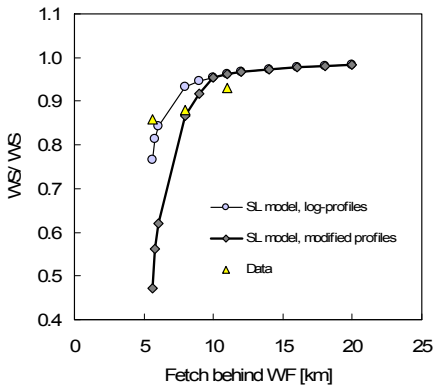

Figure 80 SL roughness change model.

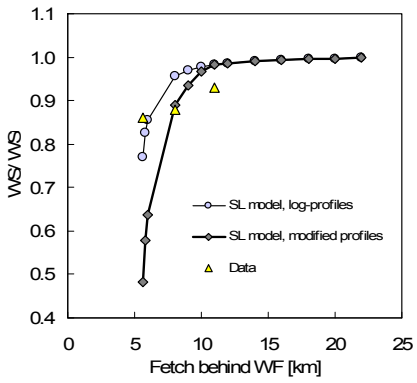

Figure 81 SL roughness change model with WAsP roughness modification.

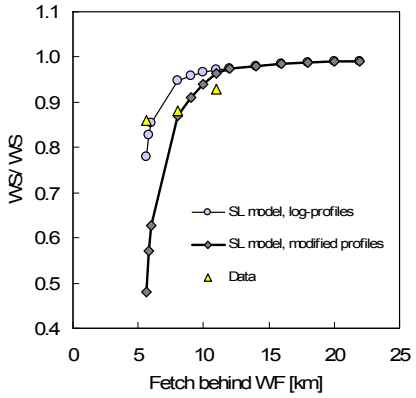

Figure 82 Roughness change model including effect of boundary layer height.

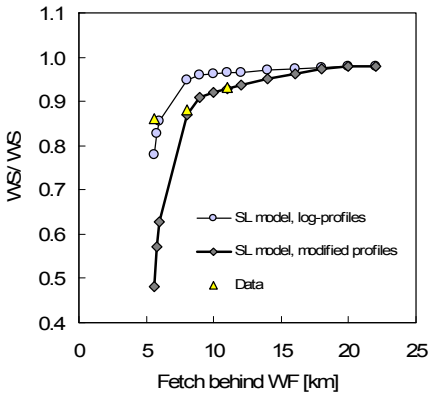

Figure 83 Roughness change model with boundary layer heights and mixed.IBL growth.

References

Gryning, S-E., Batchvarova. E., Brümmer, B., Jørgensen, H.E. and Larsen, S.E. , 2007: On the extension of the wind profile over homogeneous terrain byond the surface boundary layer. Boundary-Layer Meteorol. (article in press)

Larsen, S.E., 2007, Offshore Meteorology. Symposium: Decentralised energy systems-Integrated renewable energy technologies in tomorrow's energy supply, Oldenburg (DE), 15-16 Feb 2007

9.3 Revised PARK model

The analytical model presented in Section 9.1 may only be implemented for wind farms with simple geometry. However, the model presented here is a generalized version of the analytical model.

The work has been directed to the development of a “Mosaic Tiles” model, where “Mosaic Tiles” refers to the pattern of more or less overlapping wakes at a certain down wind vertical plane in a wind farm wind. No linear approximations are applied in this model. The near-range wind flow around a turbine rotor is described be classical theory as depicted in Figure 84.

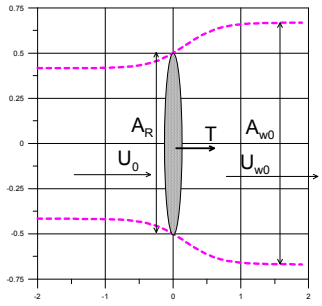

Figure 84. Near range flow around the rotor.

For each “Tile” (sub-area) in the “Mosaic”, characterized as being covered by a single or a number of overlapping wakes originating from upwind turbines, the wind speed deficit is calculated from the balance equations for wind volume and momentum flow. The principle is illustrated in Figure 85 and Figure 86.

The individual turbine wakes are assumed to expand according to a power-law with an exponent 1/k between 1/3 and 1/2, but modified with abrupt expansions due to the local stream-line expansion around enshrouded turbines. This is described in the following equations for the wake diameter D_W in dependence if downwind distance x:

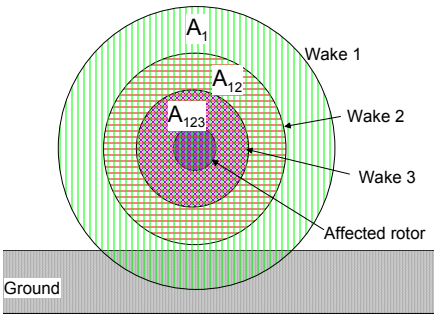

Figure 85 Tiles in wake for straight row of wind turbines in line with wind direction.

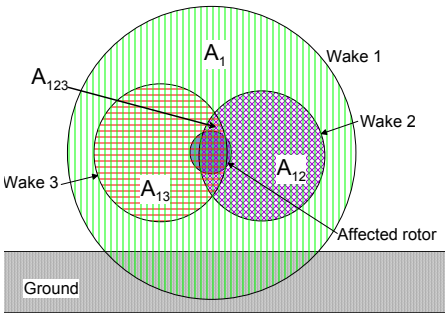

Figure 86 Tiles for “arbitrary” wind farm geometry and wind direction.

$$D_w(x) = D_R\left[\max\left(\beta^{k/2}, \alpha\frac{x}{D_R}\right)\right]^{1/k} \quad \Psi\ ,\ A_w(x_j, \Psi^{[j]}) - A_w(x_j, \Psi^{[j-1]}) = \Delta A_{T,j}$$

where β denotes the initial wake area relative to the rotor area and α is a dimensionless wake expansion parameter of the order of 1. Ψ is a parameter, which from an initial value of unity, steps up every time another downwind turbine “j” is passed, each step corresponding to the stream-line area-expansion ΔAT,j around the downwind turbine.

The model parameters are to be determined by comparative predictions with data from Danish off-shore wind farms.

The wake model with parameters 1/k = 1/3 and α=1.2 has been tested against data from the Horns Rev offshore Wind Farm in the North Sea West of Esbjerg, Figure 87.

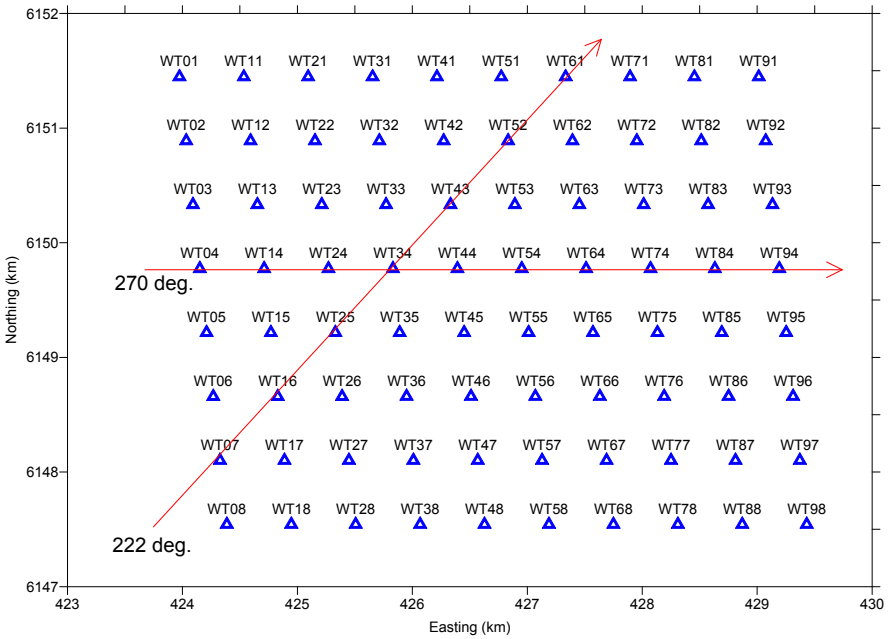

Figure 87. Horns Rev Wind Farm Layout. 80 Vestas 2MW turbines. Rotor diameter: 80 m, Hub height: 70m. Spacing: about 7 rotor diameters.

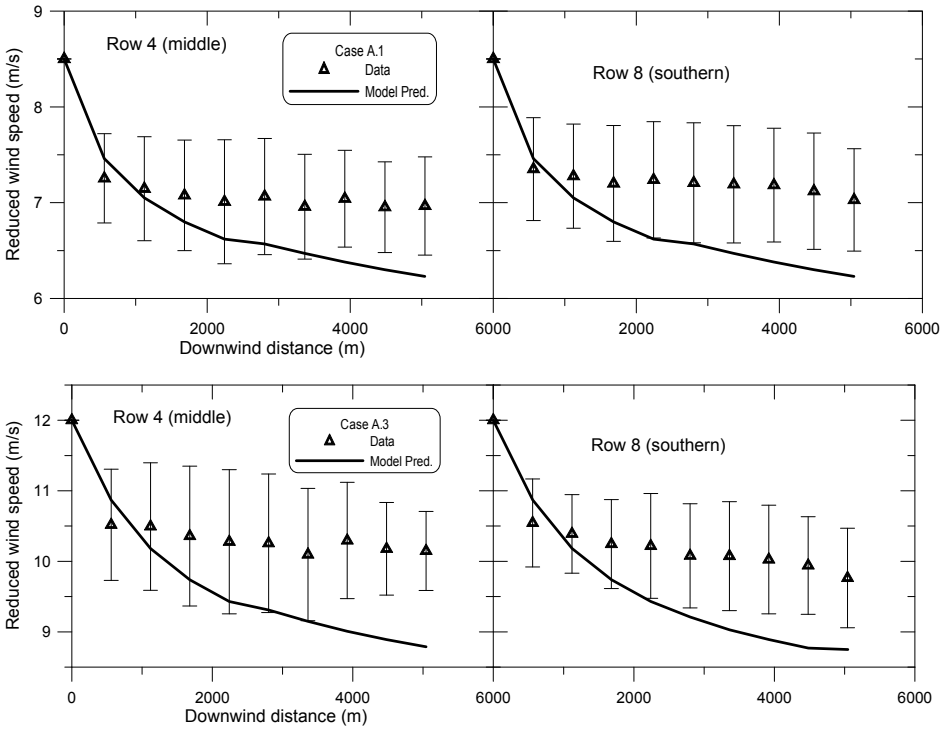

Figure 88. Model predictions at wind direction 270° +/-3° compared to data. Free wind

speed: 8.5 m/s +/- 0.5 m/s (top) and 12.0 m/s +/- 0.5 m/s (bottom).

The wind directions along the main rows and the diagonal rows are indicated by arrows. Wind data with these directions were used when comparing to model results as shown in Figure 88 and Figure 89.

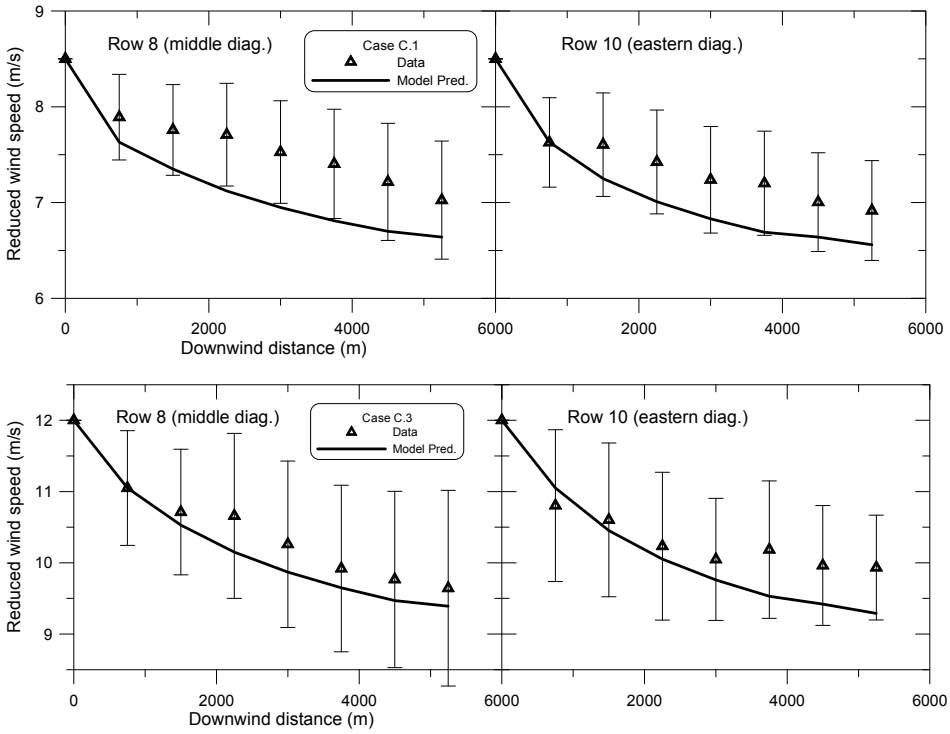

Figure 89. Model predictions at wind direction 222° +/-3° compared to data. Free wind speed: 8.5 m/s +/- 0.5 m/s (top) and 12.0 m/s +/- 0.5 m/s (bottom).

Clearly, whereas the present version of the mosaic-tile model is able to catch the level of the speed deficits correctly, it is not able to represent the experimental fact that – in the downwind direction - the wind speed drops markedly from the first to the second turbine but thereafter only drops insignificantly as you go further down wind the wind farm. Hence, the further development of the mosaic-tile wake model will be focused on adjustment of the model parameters (power-law exponent 1/k and the wake expansion coefficient α) based on comparisons with available data from Danish off-shore wind farms. This model adjustment will also allow for the parameters to not having fixed values but to depend on wind turbine operating characteristics (thrust and power) and on the wake overlapping.

9.4 Adopted Canopy model

In the following we have used the modelling concept introduce by Belcher et al 2003. The model concept is also very similar to that of Wasp and WaspEngineering. The models are all based on the linearization of the Navier-Stokes equations and only the perturbations of the flow (in this case the logarithmic profile) are modelled. In contrast to the roughness change models we have in this model introduced a volume drag force in both the x,y and z

directions. The model is here only derived as 2D system but can easily be extended to 3D. Figure 90 illustrates the modelling domain where we have a background flow, which is logarithmic, over a small roughness, the wind farm which acts as drag force on the flow up till the height h with a characteristic drag length scale L_c, and finally a domain where there is readjustment to the background flow. The closure to the turbulence modeling is illustrated in the figure. Here shown as a profile of the mixing length, which here is assumed to grow linearly with height, which again is in correspondence with the logarithmic background profile.

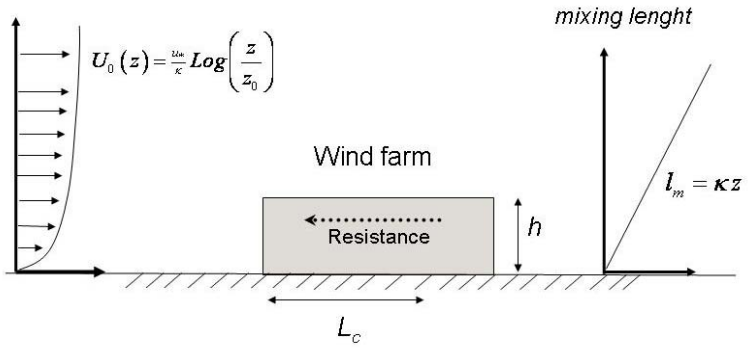

Figure 90 Illustration of the model setup with a incoming windprofile and a wind farm which acts with a force on the incoming flow the height h is considerably higher than the roughness and therefore the modeling of the flow through the wind farm has to be established to predict how the flow behind the wind farm behaves.

The model equations for the setup in Figure 18 then become:

$$U_j \frac{\partial U_i}{\partial x_j} + \frac{\partial P}{\partial x_i} = \frac{\partial \tau_{ij}}{\partial x_j} - f_i$$
$$\frac{\partial U_i}{\partial x_i} = 0 \qquad (1.1)$$

Here f_i is the drag force smoothed in time and space over the wind farm. U_i and P are the flow components also smoothed in time and space and τ_{ij} is the Reynolds stress tensor including the dispersive terms from the spatial smoothing.

The drag force F_i on a single object (i.e a wind turbine) can be modelled as:

$$F_i = \tfrac{1}{2} c_d A_t U_i |U| \qquad (1.2)$$

here c_d is the drag coefficient and A_f the area. We can now convert the force to a volume average over $h\,A_f$,and the volume force f_i then becomes:

$$\begin{aligned} f_i &= \tfrac{1}{2} c_d A_t U_i |U| / h A_f \\ &= U_i |U| / L_c \qquad (1.3) \\ L_c &= \frac{2h\,A_f}{c_d\ A_t} \end{aligned}$$

L_c is defined as the characteristic wind farm drag length scale of wind turbine park with the effective height h and the drag c_d corresponds to the thrust coefficient C_t. We can then express can L_c in terms of wind farm parameters as:

$$L_c = \frac{h\ s_r s_l\ 8}{\pi\ C_t} \qquad (1.4)$$

Here s_r and s_l are the distance between the columns and rows in the wind farm expressed in rotor diameters D.

We also need to model the shear stress tensor $\tau_{ij} = \langle u_i u_j \rangle$ which in terms of gradients can be modelled as:

$$\tau_{ij} = l_m^{\,2} \sqrt{\left(\frac{\partial U_p}{\partial x_q} + \frac{\partial U_q}{\partial x_p} \right)} \frac{\partial U_p}{\partial x_q} \left(\frac{\partial U_i}{\partial x_j} + \frac{\partial U_j}{\partial x_i} \right) \qquad (1.5)$$

here the mixing length l_m is proportional to $l_m = \kappa z$ (please note that parts of the shear stress is absorbed in the divergence of the pressure, hence therefore not shown in (1.5)). Belcher et al. (2003) have assumed that the terms $\tau_{11} = \tau_{22} = \tau_{33} = 0$, but we have chosen to include all terms of (1.5). According to Belcher et al. (2003) the wind farm is considered as a weak forest and the mixing length approach with a linearly increase is appropriate.

The model equations (1.1) have been linearized and in following we have reduced the equations to 2D. Details of the linearization can be found WaspEngineering references. The equations are now reduced to:

$$\begin{aligned} &U_0 \frac{\partial u}{\partial x} + w \frac{\partial U_0}{\partial z} + \frac{\partial p}{\partial x} = \frac{\partial \tau}{\partial z} - f \\ &U_0 \frac{\partial w}{\partial x} + \frac{\partial p}{\partial z} = \frac{\partial \tau}{\partial x} \qquad (1.6) \\ &\frac{\partial w}{\partial z} + \frac{\partial u}{\partial x} = 0 \end{aligned}$$

By eliminating the pressure *p* and using the continuity equation (i.e. the last equation in (1.6)) we obtain the following equation for the perturbations *w*:

$$U_o\left(\frac{\partial^2 w}{\partial z^2}+\frac{\partial^2 w}{\partial x^2}\right)-\frac{\partial^2 U_0}{\partial z^2}w=-\frac{\partial^2 \tau}{\partial z^2}+\frac{\partial^2 \tau}{\partial x^2}+\frac{\partial f}{\partial z} \qquad (1.7)$$

This equation can now be Fourier transformed in x and we obtain the following:

$$U_o\left(\frac{\partial^2 \tilde{w}}{\partial z^2}+k^2\tilde{w}\right)-\frac{\partial^2 U_0}{\partial z^2}\tilde{w}=-\frac{\partial^2 \tilde{\tau}}{\partial z^2}+k^2\tilde{\tau}+\frac{\partial \tilde{f}}{\partial z} \qquad (1.8)$$

This equation is an ordinary differential equation which is solved numerical for each wave number *k* and the solution is transformed back into real space. Based on the continuity equation we can hereafter calculate the *u* perturbations and add them to the background flow which in this case is a logarithmic wind profile.

In the following we have calculated the effect of the Horns rev wind farm on the background flow. L_c has been estimated to approximately 15600 m but with comparisons between the measurements at Horns rev an appropriate value of 0.8 L_c has been chosen. The roughness outside the wind farm is set to z_o=0.0002 m and the background u_*= 0.33 m/s. The effective height is set to h = 100 m. The height of boundary layer is set to 500 m to limit the calculation domain. The solution is calculated for 64 different wave numbers. Here is should be stated that there is an analytic solution to the wavenumber k=0 which corresponds to the average wind profile for the whole of the domain. The resolution is chosen to 560 m

The results of the calculation are shown in Figure 91 and Figure 92. The first figure show the perturbations as function of height and downwind distance with respect to the logarithmic background profile. The wind farm is shown as the grey area around 16 km downwind from the start of the calculation and it here seen how the flow is blocked through the park and then accelerating to the background profile after the wind farm

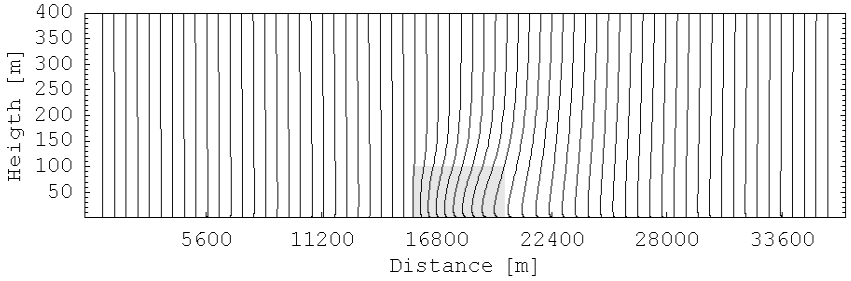

Figure 91 The wind profile relative to background profile at different downwind distances. The gray area shows the location of the volume force which is distributed equal over this volume.

In the last figure wind speed deficit at different heights are show normalized with the wind speed in front of the park. The solution is compared to the data from Horns rev and agrees very well. The solution has recirculating boundary conditions which also is seen in the solution.

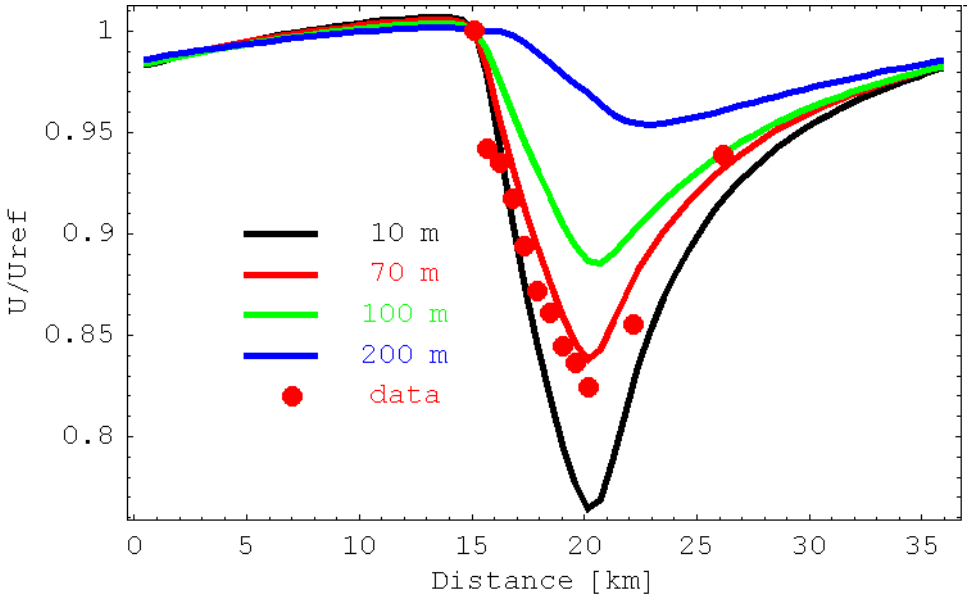

Figure 92. Normalized wind speed through the wind farm and behind the wind farm compared to measurements at Horns rev.

References

Belcher S.E., Jerram N., Hunt J.C.R (2003). Adjustment of a turbulent boundary layer to a canopy of roughness elements. JFM vol 488 pp 369-398.

9.5 MESO-SCALE model

In this section of work the mesoscale KAMM is used to model the flow at 50 m in the region around very large idealized offshore wind farms. The effect of the wind turbines on the flow is prescribed by a higher surface roughness than the surroundings. Different ways of distributing the same area of wind farm over a region are investigated; from using one large wind turbine group to using many smaller wind turbine groups. The results are presented by using mean wind speed maps of the wind farm region and transects of mean wind speed. The findings show the characteristics of the simulated wind reduction and recovery within and downwind of the wind turbine groups.

KAMM model. The Karlsruhe Atmospheric Mesoscale Model, known as KAMM, is a 3-dimensional, non-hydrostatic atmospheric mesoscale model (Adrian and Fiedler, 1991). It has it's origins in applications in regional flow and dispersion research.

The model can be used with its current set-up with a horizontal resolution down to about 2 km. The atmospheric flow is initialized using a forcing wind in geostrophic and hydrostatic balance. The forcing flow is prescribed by giving a vertical profile, using 4 different heights above sea level, of wind speed, direction and temperature. The forcing does not change in the horizontal direction.

Experimental configurations. For the mesoscale modelling a domain with a 2.5 km horizontal resolution is used. The domain size is 150 x 150 km in the horizontal and 5.5 km in the vertical. There are 25 model levels in the vertical and 61 x 61 cells in the horizontal directions. The entire domain has a surface elevation of 0 m; only surface roughness length, z_0, varies. The surface roughness length is set according to whether the mesoscale model grid cell represents open water or open water and turbines. The surface roughness length for open water grid cells is 0.0002 m and for open water and turbines is 0.5 m.

Mesoscale model experiments using different configurations of wind farms grid cells and open water grid cells are performed. The different wind farm configurations represent the same total number of wind farm grid cells, and therefore the same sea area exploited for wind energy. The difference in the configurations is the grouping of the wind farm grid cells. The grouping ranges from having one big wind turbine group to having very many small wind turbine groups. The different wind farm configurations are shown in the below table.

Exp ID	Number of wind farms	Size of wind turbine group [km]	Distance between wind turbine groups[km]	Size of whole wind farm [km]	Total wind farm area [km^2]
1	1	30 x 30	-	30 x 30	900
2	4	15 x 15	15	45 x 45	900
3	9	10 x 10	10	50 x 50	900
4	16	7.5 x 7.5	7.5	52.5 x 52.5	900
5	36	5 x 5	5	55 x 55	900
6	144	2.5 x 2.5	2.5	57.5 x 57.5	900

Table giving details of the different wind farm configurations used in the mesoscale modelling. All the configurations have the same total area of wind farm, only the wind farms groupings differ.

The mesoscale model is forced by a climatological average profile defined by geostrophic wind speed, direction and potential temperature, calculated using the NCEP/NCAR reanalysis dataset over the period 1965 to 1998 for the location 11.25^{o}E 53.75 ^{o}N at the heights 0 m, 1500 m, 3000 m and 5500 m above sea level.

For each of the 6 wind farm configurations the forcing profile is used with 3 different wind directions, 260^{o}, 270 ^{o} and 280 ^{o}. The models is run for 6 hours of simulation time and then the model winds for model levels at 20.3 m and 58.7 m are interpolated to give the wind

speed and direction at 50 m above sea level. The vector mean of the 50 m wind using the 3 direction simulations is calculated for each wind farm configuration.

Results. Figure 93 shows vector mean amplitudes and directions for the 6 wind farm configurations over the entire modelling domain. The wind direction is turned slightly anticlockwise relative to the forcing wind direction because of the surface friction acting on winds in the boundary layer producing the Ekman spiral. The effect of the higher roughness of the wind farm grid cells can be seen in the reduction in the wind speed downwind of the wind turbine groups. For the larger turbine groups, the reduction in the wind speed within the turbine group can also be seen. This effect gives a markedly lower wind speed for grid cells located along the downwind edge of the turbine group.

Figure 94 shows the mean wind speed for the 6 wind farm configurations along 61 transects of constant northing. Black and red lines show transects that do pass and transects that do not pass through the wind farm grid cells respectively.

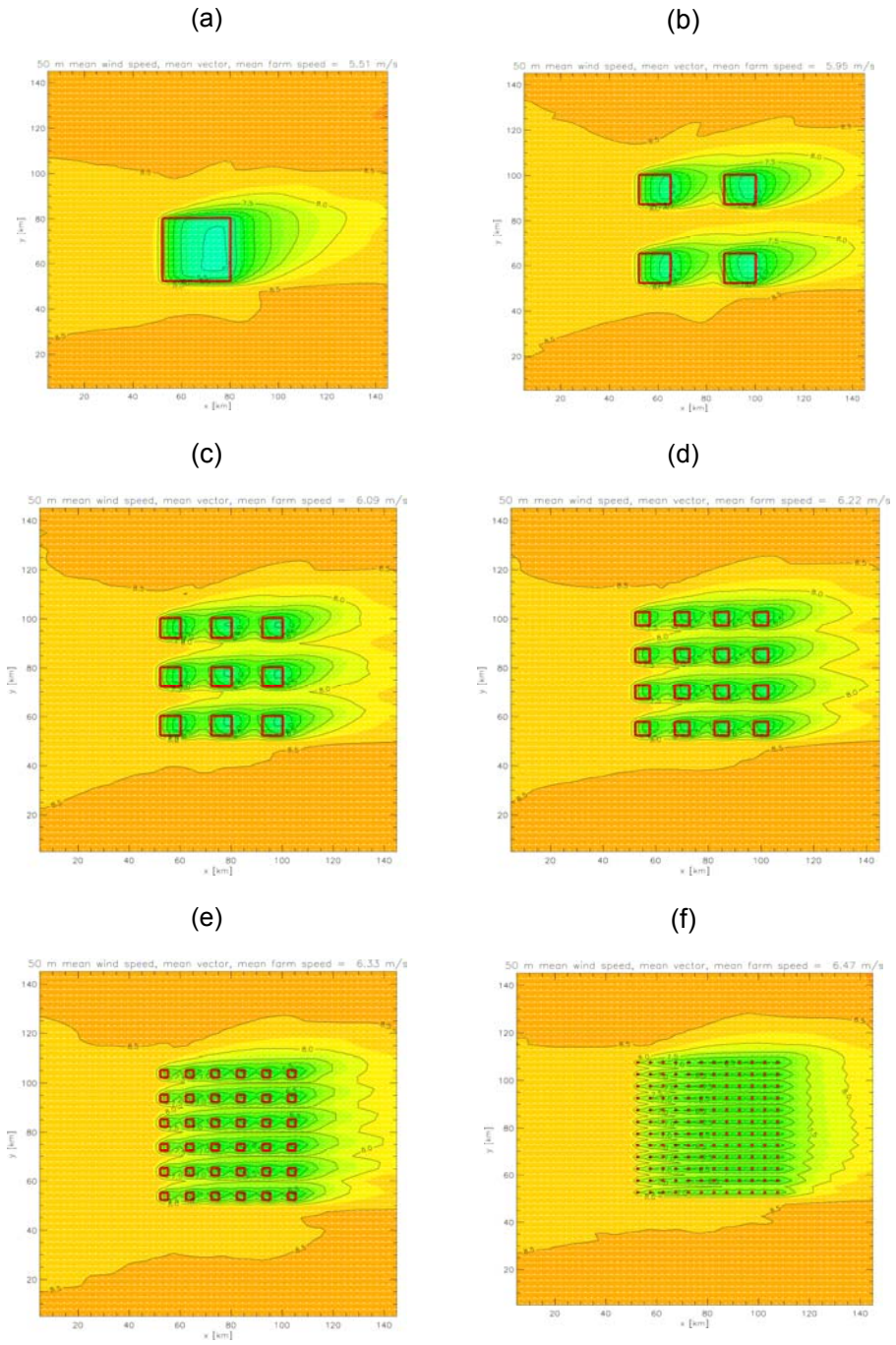

Figure 93. Plots showing mean wind speed (colours) and vector wind (arrows) calculated for 3 simulations in the westerly sector, for each of the 6 wind farm configurations listed in the above table: Exp ID 1, (a), 2, (b), 3 (c), 4, (d), 5, (e), 6, (f). The red squares show the extent of the wind turbine groups in each configuration.

For the transects that pass through the wind farm grid cells, a relatively abrupt reduction of the wind speed is seen as the flow enters the wind turbine group. The rate of reduction decreases with distance into the turbine group. The wind speed inside the largest wind turbine group approaches an asymptote, at which point the wind farm grid cell roughness has lead to an nearly complete adjusted to steady wind profile.

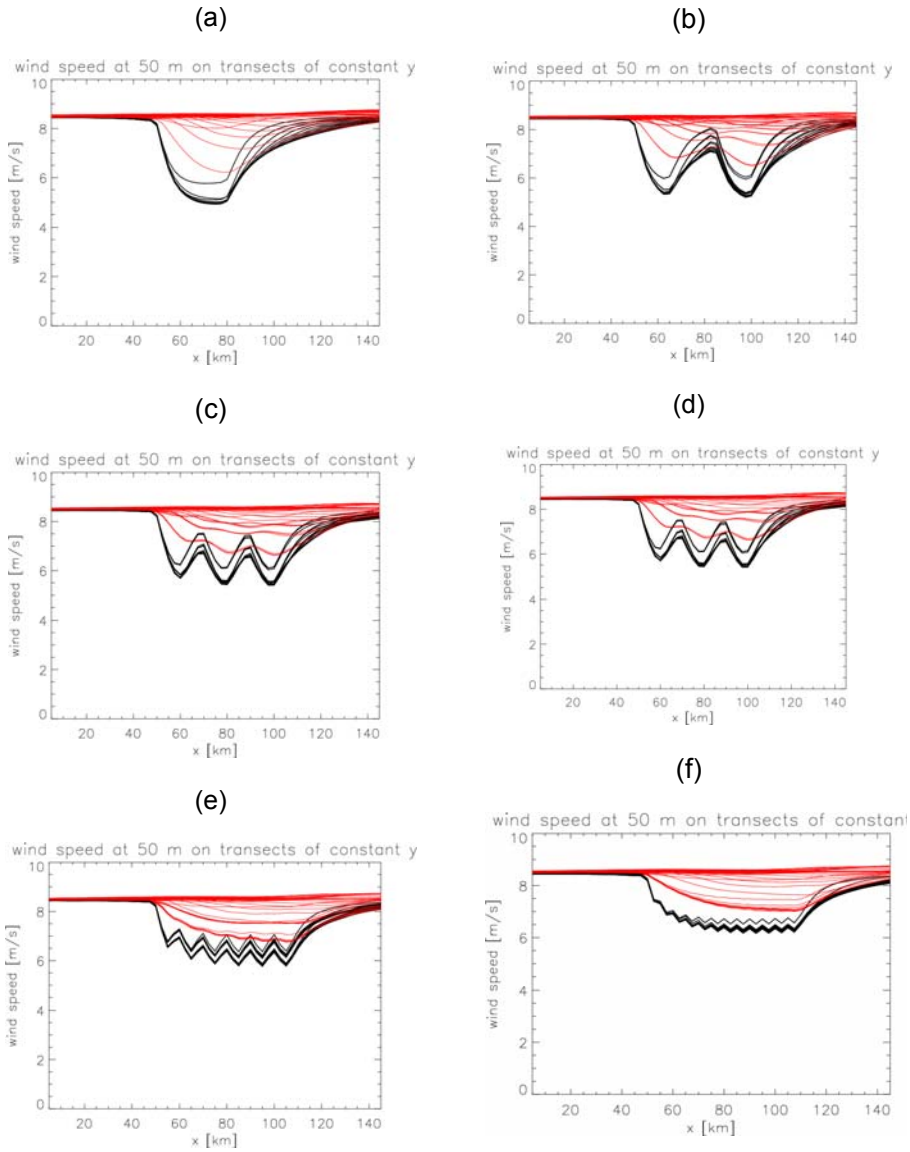

Figure 94. Plots showing transects along constant northing of the mean wind speed calculated for 3 simulations in the westerly sector, for each of the 6 wind farm configurations listed in the table: Exp ID 1, (a), 2, (b), 3 (c), 4, (d), 5, (e), 6, (f). Black and red lines show transects that do pass and transects that do not pass through the wind farm grid cells respectively.

Downwind of the wind farm cells the wind speeds increase steadily until the wind speeds observed upwind or far to the sides of the wind farm cells are approached. For the smaller wind turbine groups the recovery to the open water wind speeds is not reached, because the distance between turbine groups is too small. On the other hand the reduction of the wind speed is smaller for the smaller turbine groups.

Conclusions and discussion. This study has given mesoscale modelling results for a set of idealized wind farm configurations. The total wind farm area is fixed but the manner in which the wind turbines are grouped is varied.

The mean wind speed and mean vector wind is shown for 3 simulation for each wind farm configuration. The 3 simulation use different wind forcing directions (260^{o}, 270^{o} and 280^{o}) covering the westerly sector. The mean wind speed for wind farm grid cells is higher for smaller turbine groupings compared to larger turbine groupings. The approach to an asymptotic minimum wind speed within the largest turbine group takes approximately 20 km. The minimum wind speed within the turbine groups decreases in successive downstream turbine groups. For smaller turbine groups the successive downstream minimum wind speeds within the turbine groups also looks asymptotic. This suggests new effective roughness for clusters of small wind turbine groups.

The downstream wind speed recovery or wake decay looks similar in all configurations. Recovery to flow upwind of the turbine groups takes approximately 30 – 60 km. When the distance between turbine groups is small there is a reduced recovery. It is seen that the wake direction is similar to surface flow direction and this flow is turned slightly southerly, due to surface friction (Ekman spiral).

The mean wind speeds within the wind turbine groups give an indication of the production of the different farm configurations. Although the small groupings of turbines may give the best power production for a given number of turbines, the overall area used by the wind farm is larger. Therefore any further analysis to reach some kind of efficiency score of the different farm configurations needs a careful consideration of what quantity is to be maximized.

It would be of interest to investigate the assignment of different surface roughness to the wind farm grid cells, and to check the sensitivity of the results. Also of interest is to investigate if the decreased wind associated with the wind turbine groups is associated with a wind and wake turning. Investigation of alternative and improved ways to parameterize the effect of wind turbines on the flow will be required in order to apply more fully at higher resolution model results in this kind.

References

Adrian, G. and F. Fiedler, 1991: Simulation of unstationary wind and temperature fields over complex terrain and comparison with observations. Beitr. Phys. Atmosph. 64, 27-48.

Orlandski, I., 1976: A simple boundary condition for unbounded hyperbolic flows. J. Comp. Phys. 21, 251-269.

Klemp, J. B. and D. R. Durran, 1983: An upper boundary condition permitting internal gravity wave radiation in numerical models. Mon. Wea. Rev. 111, 430-444.

Blackadar, A. K., 1962: The vertical distribution of wind and turbulent exchange in a neutral atmosphere. J. Geophys. Res. 67, 3095-3102.

9.6 CFD modelling

Introduction. The method propose is an attempt to extend the data available from the offshore wind farm Horns Rev, using a Computational Fluid Dynamics (CFD) code. The outcome of this method is meant to give extra information to calibrate engineering models, which can then be used in a systematic way.

The basic idea of the method is to estimate the wind properties at the exit of a wind farm and to model the development of the wake downstream of the wind farm. The key element is how to specify the wind farm wake correctly at the computational inlet.

The data set available includes 3 meteorological masts surrounding the wind farm (one at a corner, and two aligned with a row of turbines, see Figure 73). The two aligned masts give an idea on how the wind is recovering from the influence of the wind farm, but with only two locations, no trends can be seen. The idea is to use these two met masts to “extrapolate“ a trend of the wind speed recovery after the wind park.

A steady CFD code is used to model the wind exiting the wind farm. The domain modeled is beginning at the location of the first met mast downstream the park and is encompassing a large area downstream the wind farm, including the second met mast. The turbulence model used is the k-ε model, which implies that the inputs needed at the inlet are the mean wind speed U_{mean}, turbulent kinetic energy k, and dissipation distribution ε, the free stream friction velocity u_*, and the roughness coefficient of the sea z_0. All these parameters are estimated from the met masts measurements whenever it is possible, or, otherwise, derived from physical considerations.

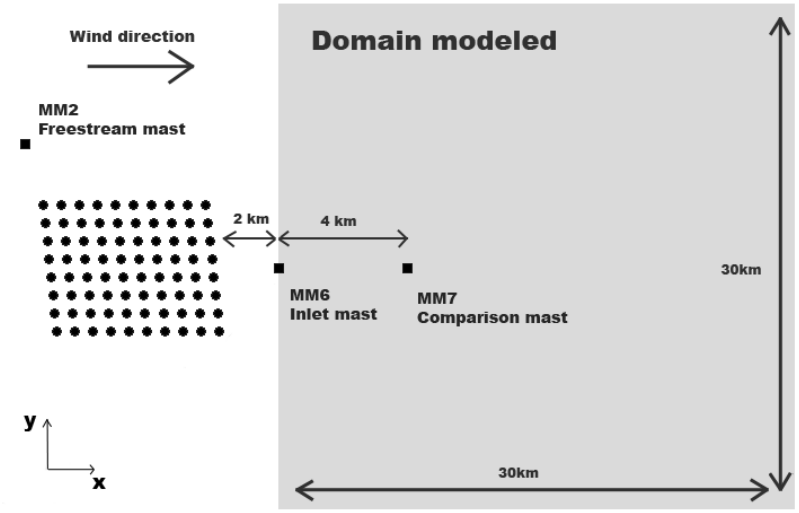

Figure 95. Model Setup.

The side boundary conditions are taken as symmetric, while the top boundary condition is taken as an inlet boundary, and the bottom as a wall boundary with a no-slip condition.

As previously mentioned, the inlet boundary is composed of two main regions, a free stream region, where the flow is assumed to be undisturbed by the wind farm, and a wake region, Figure 96.

The wake region is defined as a rectangle of 5km of width and 200m of height. In addition a linear transition region of 100m around the wake region is applied to smooth the resulting shear forces generating by the difference of wind speed from one region to another.

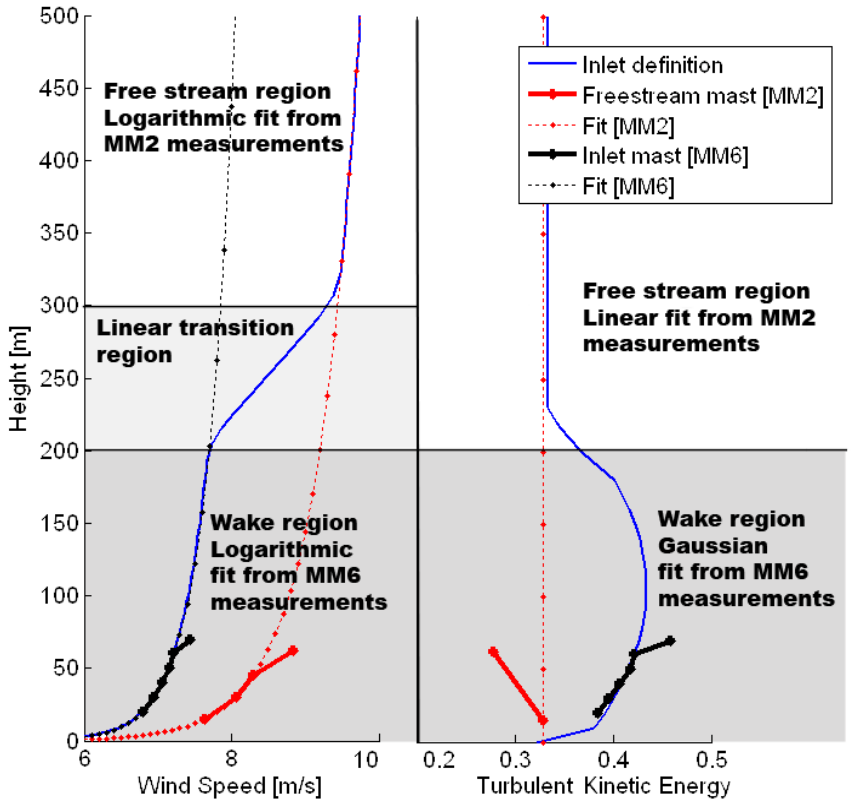

Figure 96. Inlet specification

Results. The vertical mean wind speed distribution 4km inside the domain seems in good agreement with measurements, Figure 97.

On the other hand the turbulence profile is largely different from the measurements, Figure 97. In addition the expected trend of the turbulence would be to decrease constantly instead of increasing as shown in Figure 98. This turbulence plot clearly shows the weakness of this model. As there is no physical model of the balance between mean wind speed profile and turbulence profile at the inlet, the arbitrary wind shear of the transition area yields a dramatic increase of the turbulent kinetic energy and dissipation until they reach a balance, and begin to decrease

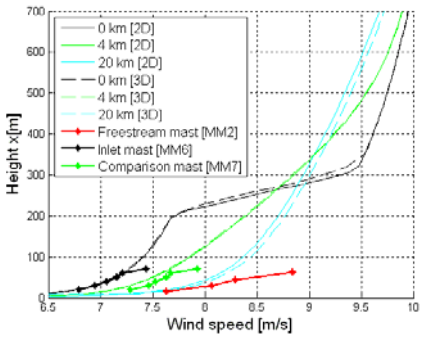

Figure 97. Mean wind vertical profile in the center plane of the domain

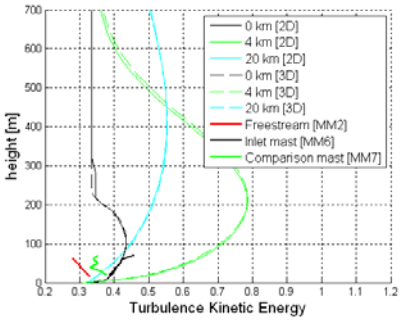

Figure 98. Turbulent kinetic energy vertical profile in the center plane of the domain

Shortcomings and limitations of the method. The rate of the wake recovery is directly dependent on the prescribed turbulent kinetic energy and dissipation at the inlet. While the first one can be partly estimated from the available measurements, the second is totally unknown and requires a more detailed description.

Similarly, the transition area, defined as linear, is also unphysical. This high velocity gradient generates a high shear directly responsible for the unrealistic increase of turbulent kinetic. In order to avoid this jump, this transition area also necessitates a better specification of the turbulence profile.

For these reasons, without a proper physical wake definition of a wind farm, or more detailed information on the flow leaving a wind farm, the method still needs further investigation to obtain reliable results.

Acknowledgements

The report is based on the final summary report of the project *Store mølleparkers skyggevirkning: malinger og dataanalyse*, financed by the Danish Public Service Obligation (PSO), project no. Energinet.dk 6505. The original report reference is:

Sten Frandsen, Rebecca Barthelmie, Ole Rathmann, Hans E. Jørgensen, Jake Badger, Kurt Hansen, Søren Ott, Pierre-Elouan Rethore, Søren E. Larsen, Leo E. Jensen 2007: Summary report: The shadow effect of large wind farms: measurements, data analysis and modelling. Risø-R-1615(EN).

The report can be downloaded from: http://www.risoe.dk/rispubl/reports/ris-r-1615.pdf

DEWEK 2006 PRESENTATION PAPER
Deutsche Windenergie Konferenz
Bremen, 22-23 November 2006

Title: **New Developments in Precision Wind Farm Modelling**

Session: 6 Wind Farm Effects
Authors: Wolfgang Schlez, Anja Neubert, Gillian Smith
Affiliation: Garrad Hassan and Partners Ltd
Contact: Wolfgang Schlez
Address: Garrad Hassan and Partners Ltd, Katharinenstr 18,, 26121 Oldenburg, Germany
Email: wolfgang.schlez@garradhassan.com
Tel: +49 (0)441 957 2387
Fax: +49 (0)441 957 2388

NEW DEVELOPMENTS IN PRECISION WIND FARM MODELLING

Wolfgang Schlez, Anja Neubert and Gillian Smith
Garrad Hassan and Partners Ltd

Contact: Wolfgang Schlez, Garrad Hassan and Partners Ltd,
Katharinenstr 18 , 26129 Oldenburg, Germany
wolfgang.schlez@garradhassan.com Tel: +49 (0) 441 957 2387 Fax: +49 (0)441 957 2388

Keywords: wind farm, wake model, close spacing, offshore, close spacing, eddy viscosity, WindFarmer

Summary

For over 20 years, Garrad Hassan and Partners Ltd have been offering cutting edge technology in wind energy consultancy services. The technologies used for wind farm analysis are also made available to the wider wind energy community in form of the GH WindFarmer software. Starting with the highly accurate and comprehensively validated eddy viscosity wake model, further improvements of the wind farm energy yield prediction model have recently been implemented and the models tested in challenging new project environments. The models, results and validations presented in this paper concentrate on cases of closely spaced turbines and large offshore wind farms where traditional models can predict the wind farm energy yield up to 20% higher than is achieved in practice depending on layout and wind conditions.

It has been found that traditional wake models do not model the wake accurately downstream of very closely packed lines of turbines. The newly implemented model is based on the eddy viscosity wake model but now additionally takes account of the merging of adjacent wakes which is expected to occur with tight spacing. This merging is postulated to lead to overall stronger wake effects but also reductions in horizontal velocity gradient and reductions in added turbulence intensity in the wake.

It has been shown in the past that offshore wake effects are well represented by the WindFarmer Eddy Viscosity model. Very large offshore wind farms however represent a challenge. Due to the spatial extent of such wind farms simple superposition of the wake and the wind profile is not anymore sufficient. The wind profile itself is modified by the wind turbines in a large wind farm. We have developed a model that considers this effect and allows more accurate energy prediction for large offshore arrays.

Introduction

In modern wind farms, the decrease in energy yield or increase in array losses arising from wake effects (Figure 1) ranges typically from 5 % to over 15 % depending on the wind farm layout. Knowledge of turbine wakes and their interaction is essential not only to predict the reductions in wind speed and corresponding yields but also helps to assess the additional loading on the turbines generated by the increased turbulence in the wakes.

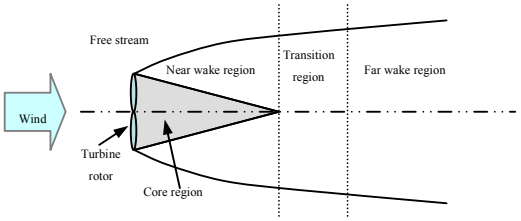

Figure 1 Wake structure

Dominant in industrial applications are models based on fundamental physical equations but including empirical assumptions to simplify the problem to an extent that it can be solved in an acceptable timeframe. These models are part of wind farm design software packages and have been proven to demonstrate good agreement with experimental and operational data in most situations [1-3]. An overview is given in [4].

Amongst over 40 GW of wind farm capacity analysed by Garrad Hassan over the past 21 years, a small number of the wind farms have stood out because of difficulties with modelling their annual energy yield. These wind farms have special features that make them unlike the majority of wind farms built worldwide. The observed wake losses for specific layouts and wind conditions can be up to 20% above those modelled with standard software tools.

One group of wind farms comprised multiple rows of very closely spaced turbines (Figure 2). Such wind farms are typically in locations with either uni- or bi-directional wind regimes. Inter-turbine distances from 1.1 to 2.5 times the rotor diameter (D) are typical. Along-wind inter-row distances are typically 6 to 9 D.

Another group of wind farms, few of which have been built so far, is that of very large offshore arrays. These wind farms consist from 20 up to several hundred turbines and have a depth of five or more turbines.

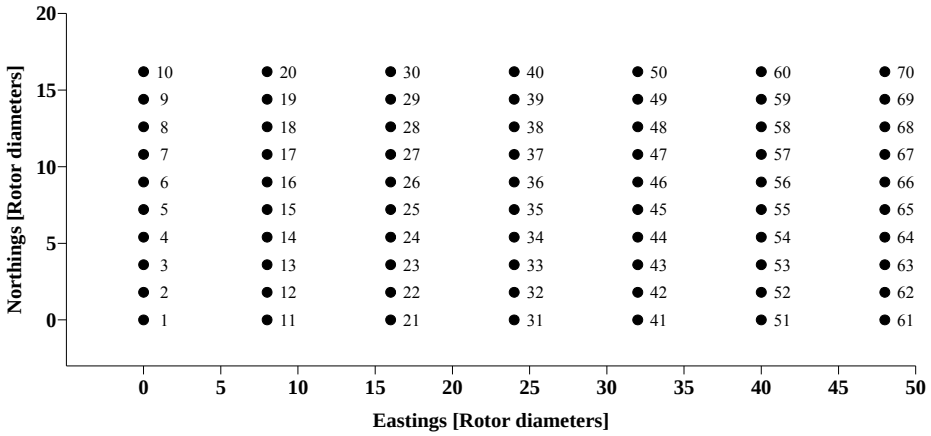

Figure 2 Example of a typical close spaced wind farm with spacing of approximately 1.8 D within the rows and 8 D from row to row.

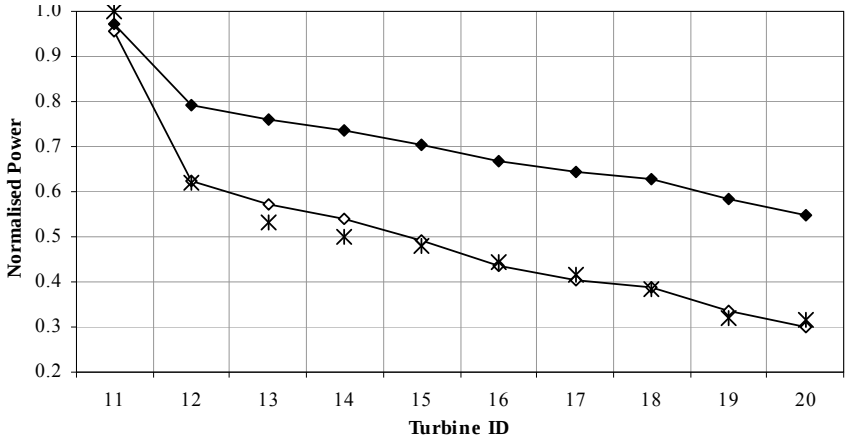

Figure 3 Row 2 (Turbines 11-20) of the example wind farm with close spacing.

Closely spaced wind farms

From practical experience, Garrad Hassan was aware of the problem with closely spaced wind farms and made significant downward adjustments of yields forecast. Whilst these pragmatic, experience-based adjustments satisfied the immediate need for accurate predictions, a better understanding and an improvement of analysis tools was required and this requirement stimulated the improvement of the model.

New wake model for closely spaced turbines

Published data and investigations concerning wakes with a distance of approximately 2 D or less behind a wind turbine rotor are extremely rare [1, 5-8]. Even fewer data are published from the wake of two or more adjacent turbines with an inter-turbine spacing of less than 2 D [9-11]. To improve general understanding and prediction accuracy for these particular cases, Garrad Hassan has undertaken an internal re-analysis of several closely spaced wind farms.

A new model [12,13] has been implemented to this effect with the following changes:

- For close spaced turbines the momentum deficit is allowed to add up cumulatively

- The added turbulence is reduced in the wake
- The Gaussian profile is replaced by a blunt profile taken from [14]

The last change is as necessary as it is radical because it results in an overall higher momentum deficit. In short this model predicts a change of the thrust characteristic of a turbine in a closely spaced wind farm compared with a single turbine of the same type.

The modified model has been able to reproduce the energy yield of several closely spaced wind farms to a high degree of accuracy.

Large offshore wind farms

Offshore wind farms benefit from generally lower turbulence intensity. This, however, causes wakes to be more pronounced and sustained longer. Existing commercial and research-type wake models have been validated in the Endow project [1] against data from offshore wind farms. The predictions from the eddy viscosity model [15] as implemented by Garrad Hassan have shown excellent agreement with the production data without the need for any manual adjustment to offshore conditions.

The Horns Rev wind farm (Figure 4) and data iare presented elsewhere in detail [16]. The good performance of the Eddy Viscosity Model was again visible for the first few rows of turbines of the Horns Rev offshore wind farm.

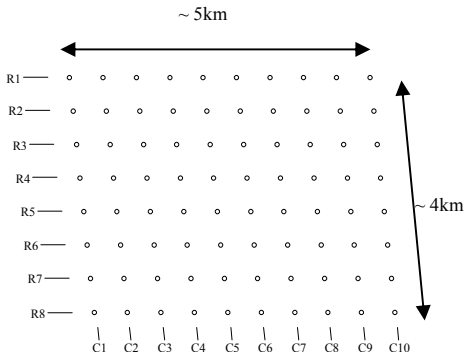

Figure 4 Large offshore wind farm (Horns Rev)

However further downwind, deeper into the wind farm, the modelling turned out to be increasingly less accurate. This type of effect is not observed in large onshore projects.

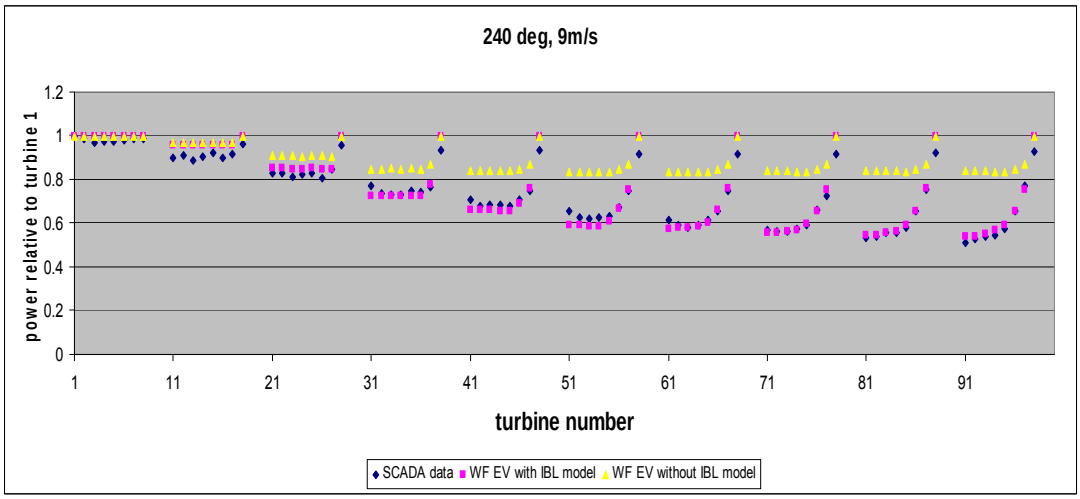

Figure 5 Energy Yield Horns Rev (240 deg,9 m/s) data compared with new and old model

New model for large offshore wind farms

As the effect seen in the data from Horns Rev and other offshore wind farms is not visible in onshore wind farms we need to identify what effects that are specific to offshore could be the cause for the discrepancy.

The most plausible explanation for this effect has indeed been under discussion since the dawn of the wind energy industry, e.g. [17]: The wind turbine does not only react passively to the wind regime but at the same time is part of it. Weather systems are not considered to be affected significantly at the scale of developments considered. However locally, by the presence of wind turbines, the boundary layer profile is modified.

A wind farm area can in this model be represented by an area of higher roughness. Due to the lower roughness offshore such an area of increased roughness has a pronounced effect, similar to a forest onshore. Onshore, on the other hand, such effect would be masked by the higher terrain roughness.

Based on this explanation we have developed a model that does not require the wind farm to have a particular shape. Instead of modelling an area of increased roughness we model the disturbance caused by each individual turbine. This allows us to consider the effect for a wider variation of wind farm layouts during the design phase and optimisation of a wind farm layout.

The model comprises simply of two components

- Calculation of internal boundary layer height
- Vertical offset of the boundary layer

On the basis of this model the ambient wind speed is corrected. The wake model itself stays unchanged. The model results are presented in Figure 5. The model reproduces well the results from Horns Rev for different wind speeds and directions.

Extreme caution is required with regards to the application of the offshore correction for large wind farms. The model has not yet been validated against multiple wind farms. As soon as data from such wind farms become available an update of the model is likely and therefore the current model results should be seen as preliminary.

Conclusions

The wake losses downstream from rows of very closely spaced turbines are much higher than predicted by conventional models. A modified, pragmatic approach to model the higher wake deficits has been presented and compared with operational data from a number of wind farms.

The prediction accuracy for wind farm cross-wind close-spacing and also for large offshore wind farms has been improved significantly.

The two new models are available to the wind energy community through their implementation within GH WindFarmer, Garrad Hassan's wind farm design software.

Acknowledgements

The authors are grateful for the access to the data from operational wind farms used in the work presented in this paper.

We would like to thank Elsam Engineering for making available the Horns Rev offshore wind farm data.

The work on large offshore wind farms is supported in part by the European Commission under contract #19945 (SES6) "UPWIND.

References

1. Barthelmie R et al. *Efficient development of offshore wind farms (ENDOW)*. Riso National Laboratory, Final report Riso-R-1407(EN), Roskilde, Denmark, 2003.
2. *GH WindFarmer Validation Manual*, Garrad Hassan and Partners, Bristol, UK; 2003

3. Raftery PG, Harman KD, Tindal AJ, Garrad AD Validation of energy and uncertainty predictions by comparison to actual production. *Procs Conf EWEC London;* 2004
4. Crespo A, Hernández J, Frandsen S. Survey of modelling methods for wind turbine wakes and wind farms, *Wind Energy* 1999; **2**:1-24
5. Taylor GJ *Wake Measurements on the Nibe Wind Turbines in Denmark*. National Power, ETSU WN 5020, United Kingdom, 1990.
6. Albers A, Beyer HG, Kramkowski T, Schild M, Schomburg A, Schlez W, Waldl HP, deWitt U. Results from a Joint Wake Interference Research Programme. *Conf. Procs, EWEC*, Travemünde Germany, 1993; 380-382
7. Helmis CG, Papadopoulos KH, Asimakopolos DN, Papageorgos PG, Solemes AT. An experimental study of the near-wake structure of a wind turbine operating over complex terrain. *Solar Energy* 54(6), 1995.
8. Seifert H. *Untersuchungen des Nachlaufs von Windenergieanlagen und dessen Auswirkung auf die Standsicherheit der benachbarten WEA in Parkaufstellung. Bericht* DEWI FO 0203-01, Wilhelmshaven, Germany, 2003.
9. Nierenburg R. *Wake Deficit Measurements on the Jess and Souza Ranches, Altamont Pass*. Altamont Energy Corp, Solar Energy Research Institute SERI/TP-257-3455, USA 1990
10. Smith D. *Wake Measurements behind Two Interacting Wind Turbines with Streamwise and Crossflow Separations*. National Power, Leatherhead, United Kingdom, 1990
11. Smith D. Multiple wake measurements and analysis *Conf. Procs. BWEA12* Norwich, 1990; 53-58
12. Liddell A, Schlez W, Neubert A, Peña A, Trujillo JJ. Advanced wake model for closely spaced turbines. *Conf Procs AWEA* Denver; 2005
13. Smith G, Schlez W, Liddell A, Neubert A and Pena A. Advanced wake model for very closely spaced turbines. *Conf Procs EWEC* Athens; 2006
14. Abramovich G. *The Theory of Turbulent Jets*. MIT Press Cambridge, Massachusetts, USA, 1963
15. Ainslie J. Calculating the flowfield in the wake of wind turbines. *Journal of Wind Engineering and Industrial Aerodynamics*, 1988; **27**: 213-224
16. Rathman, O., Barthelmie R and Frandsen, S. Turbine Wake Model for Wind Resource Software EWEC2006 Athens
17. Frandsen, S. On the Wind Speed Reduction in the Center of Large Clusters of Wind Turbines, J. Wind Eng. Ind. Aerodyn. 39, pp 251-256, 1992

Appendix 5: Deliverable 8.5 Uspcaling

Project funded by the European Commission under the 6th (EC) RTD Framework Programme (2002- 2006) within the framework of the specific research and technological development programme "Integrating and strengthening the European Research Area"

Project UpWind

Contract No.:
019945 (SES6)

"Integrated Wind Turbine Design"

Wp8: Flow
Deliverable D8.5
Wake reducing concepts

AUTHOR:	Gerard Schepers
AFFILIATION:	ECN
ADDRESS:	The Netherlands
EMAIL:	schepers@ecn.nl
FURTHER AUTHORS:	R.J. Barthelmie, E S. Politis
REVIEWER:	WP8 Project members
APPROVER:	

Document Information

DOCUMENT TYPE	Deliverable D8.4
DOCUMENT NAME:	WP8Flow8.1D1.doc
REVISION:	
REV.DATE:	
CLASSIFICATION:	
STATUS:	

Abstract

Abstract: A number of approaches to reducing power losses to wakes were investigated. These include those developed at ECN ‘Heat and Flux’ and ‘Controlling Wind’ that focus on operational strategies. An alternative is to upscaling turbines or using different sizes of turbine. All of the approaches have potential but the conclusions are based on calculations with large uncertainties.

Contents

STATUS, CONFIDENTIALITY AND ACCESSIBILITY										
Status				**Confidentiality**				**Accessibility**		
S0	Approved/Released			**R0**	General public			Private web site		
S1	Reviewed			**R1**	Restricted to project members			Public web site		
S2	Pending for review			**R2**	Restricted to European. Commission			Paper copy		
S3	Draft for comments	**x**		**R3**	Restricted to WP members + PL	**x**				
S4	Under preparation			**R4**	Restricted to Task members +WPL+PL					

PL: *Project leader* **WPL:** *Work package leader* **TL:** *Task leader*

1 Notations

a = axial induction factor
u = total velocity in the wake
U_∞ = free stream velocity
u_{def} = velocity deficit in the wake (U_∞- u)
u_m = (maximum) velocity deficit in wake centre
r = radial position in wake (wrt wake centre)
R_w = wake radius
A = rotor radius
D_{ax} = axial force on rotor
$C_{D.ax}$ = axial force coefficient
C_P = power coefficient
ϕ_y = yaw angle
χ_y = yaw angle
μ = radial position in wake relative to wake radius (r/R_w)
D = rotor diameter

2 Introduction

The majority of current wind turbines, both on-shore and off-shore, are located in wind farms, the size of which gets larger and larger. In these large wind farms, most turbines are located in the wake of one or more turbines by which the flow characteristics felt by these turbines differ considerably from the free stream flow conditions. The most important wake effect is generally considered to be the lower wind speed behind the turbine(s) since this decreases the energy production and as such the economical performance of a wind farm. The overall loss of a wind farm is very much dependant on the conditions and the lay-out of the farm but it can be in the order of 5-15%. Apart from the loss in energy production an additional wake effect is formed by increased velocity fluctuations (due to several causes) of a different character than free stream, which leads to higher fatigue loads. In the following we focus on power losses, changes in turbulence levels have not be considered.

With regard to minimisation of wake effects, two approaches can be distinguished

- A conventional approach in which the wind farm layout is optimized such that the wake effects are minimal. In this approach the turbine settings remain unaffected from their settings in free stream operation. All turbines in the farm are similar.
- An unconventional approach in which the wake effects are minimized using dedicated concepts.

In the first approach the turbine settings (e.g. pitch angle, rotor speed) are in principle optimized such that maximum energy output is balanced against minimal loads for an **individual** turbine. This generally implies that the turbines operate at maximum C_p although nowadays some turbines operate slightly below optimal C_P in order to reduce the thrust.

In this report the attention is mainly focused on the second approach. In the second approach the performance of the **entire wind farm** is optimised. It may then be beneficial to reduce wake effects by sacrificing some performance of the upstream turbines. Thereto the upstream turbine operates at sub-optimal conditions (sub-optimal in terms of individual wind turbine performance) where one can think of a non-optimal pitch angle/rotor speed, or a yaw misalignment. These sub-optimal settings will however lead to lower wake effects and hence an increased performance of the downstream turbines which can (over)compensate the loss in performance of the upstream turbines.

An intermediate approach lies in upscaling, since the rated power of a wind turbine increases with D^2 and the wake losses decrease linearly with D. Hence for given rated power and given area of a wind farm, upscaling of the turbines will allow a larger spacing between the turbines by which the wake losses will be lower.

Also non-conventional wind farms, e.g. wind farms which consist of turbines with unequal size may lead to an overall gain in energy production, since different sized wind turbines yield a different (and possibly a positive) wake impact. Furthermore the diameter can be used to design a ‘wake specific’ wind turbine (like it can be used to design a ‘site specific’ turbine, i.e. a turbine for a low wind speed climate will generally have a larger diameter).

The present report then summarizes research which has been carried out by the Upwind WP8 partners on the following wake reducing concepts:

- Heat and Flux. A wake reduction is achieved by setting the upstream turbines to a sub-optimal pitch angle.
- Controlling Wind: A wake reduction is achieved by yawing the upstream turbine.
- Upscaled turbines within a wind farm
- Turbines of unequal size within a wind farm.

Part of the research is carried out within Upwind but the research mainly builds on national projects. Results from these national projects are described in [1], [2], [4] and [9].

3 Heat and Flux

The work on the Heat and Flux (H+F) principle builds on previous work on a concept patented by ECN. In the Heat and Flux concept, the pitch angle of the upstream turbine(s) in a farm is set to a less optimal value. This obviously reduces the performance of the upstream turbine but it also reduces the axial force coefficient and the resulting momentum loss in the wake. The loss in performance on the upstream turbine may then be compensated by the reduced wake effects and as such the combined performance of both the upstream and downstream turbine can be increased. This is illustrated in figure 1. The figure shows the power coefficient and axial force coefficient as function of the axial induction factor, according to the well known relations:

$$C_{D.ax} = 4a(1 - a) \qquad [2.1]$$

$$C_P = 4a(1 - a)^2 \qquad [2.2]$$

Since the axial induction factor decreases with pitch angle, the figure can also be interpreted as the C_P and the $C_{D.ax}$ as function of minus pitch angle. The figure shows that the maximum value of C_P in normal operation is accompanied by a high value of $C_{D.ax}$ and hence considerable wake losses. In the Heat and Flux operation the pitch angle is decreased. This obviously leads to a lower C_P but the flat behaviour of C_P makes the decrease in C_P very limited. However the decrease in $C_{D.ax}$ is very large which may decrease wake losses considerably.

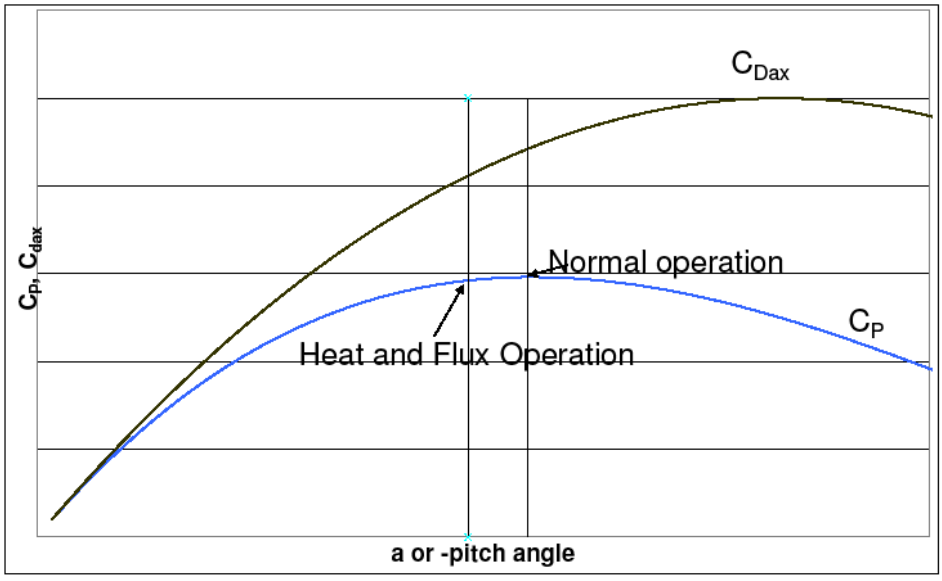

Figure 99: Power coefficient C_P and axial force coefficient C_{Dax} as function of axial induction factor from momentum theory

For the (very hypothetical) inviscid situation based on the conservation of momentum/energy, an increase of 4.1% of the combined power of 2 wind turbines in line is predicted where the axial induction of the 1st turbine should change to 1/5 instead of 1/3. Note that this assessment is purely based on the momentum theory under the assumption of full expansion. As such the outcome is not influenced by the distance between the turbines.

For the general case of a row of n turbines in line with the flow, it was derived that the optimum setting of the axial induction for the most upwind turbine equals $1/(2n+1)$.

In order to find a more firm confirmation of the potential for Heat and Flux, optimizations have been carried out with the program Fluxfarm. The Fluxfarm program is based on the WAKEFARM program [9], and it contains an optimisation module to find the optimal settings for Heat and Flux. The optimisations were performed on ECN's research farn EWTW, which is described in [10] and in section 2.1. The EWTW consists of 5 research turbines in a line set-up with a diameter and hub height of 80 m. The rated power of the turbines is 2.5 MW and the mutual distance between the turbines is 3.8D.

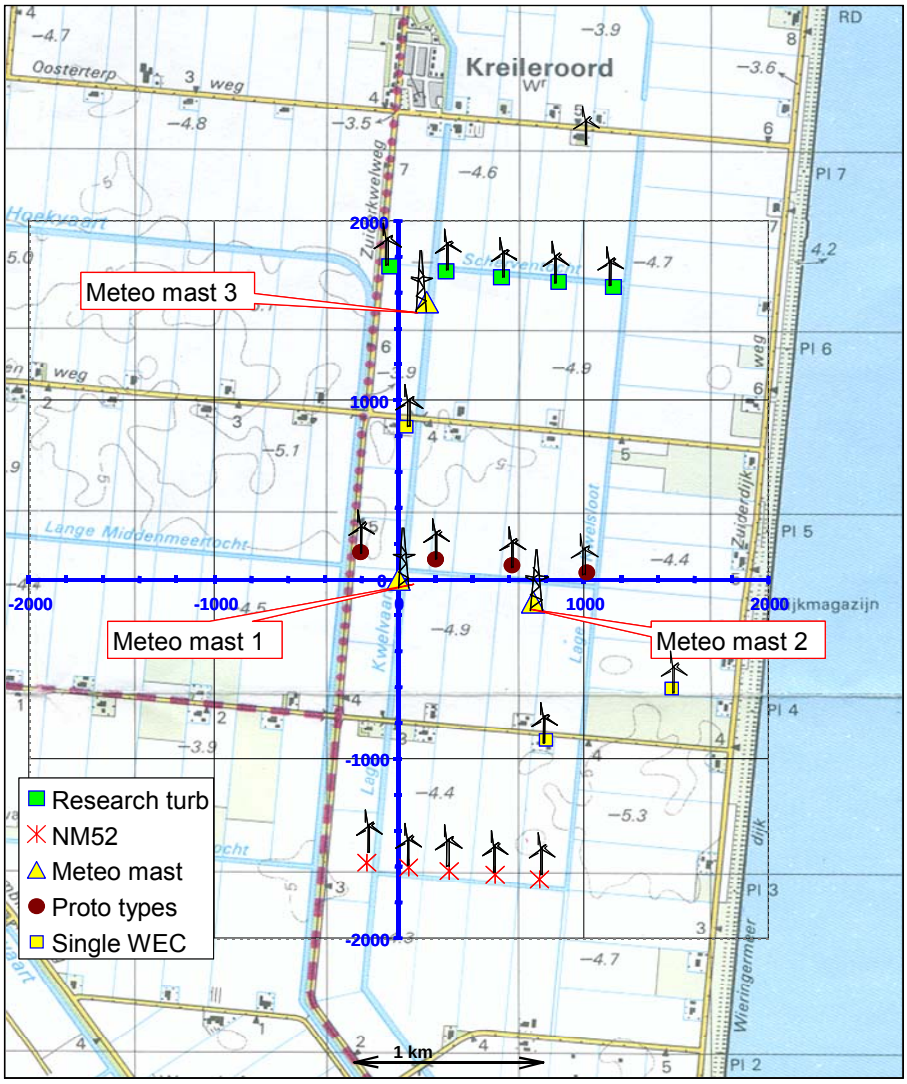

Figure 100: Lay-out of EWTW

Figure 3 presents the gain from Heat and Flux on the energy production of the EWTW. The results are given as function of wind speed and the misalignment between wind farm line and wind direction. Most important is that these results confirm a gain in energy production. Furthermore the figure shows a rapid decreasing gain with wind speed: The gain is in the order of 40% at the lower wind speeds and it reduces to zero at above rated conditions. Furthermore the gain decreases with the misalignment between wind direction and farm line but it is encouraging to see that even a 12 degrees misalignment in pitch angle still produces a gain. It must be noted that the large relative gain at low wind speeds is mainly a result of the fact that the H+F operation keeps the wake wind speeds just above the cut-in wind speed, where they fall below the cut-in wind speed at normal operation. The gain at low wind speeds however contributes little to the overall gain which is found from the summation over all wind speeds and wind directions.

Obviously the overall gain is very much dependant on the wind speed and wind direction distribution but it will generally be 0.5% or even less. At first sight, such gain may appear disappointing but most important is that the gain can be reached at very little additional cost. As a matter of fact, the only costs lie in the modification of the control algorithm, which should be made wind direction dependant and which should assure that the H+F settings only appear at wake conditions (in non-wake

conditions, the H+F settings lead to a loss in production). In view of the uncertain and fluctuating wind direction this obviously requires some safety margin in the wind direction. As already mentioned above, a 12 degrees misalignment still produces a gain in energy production.

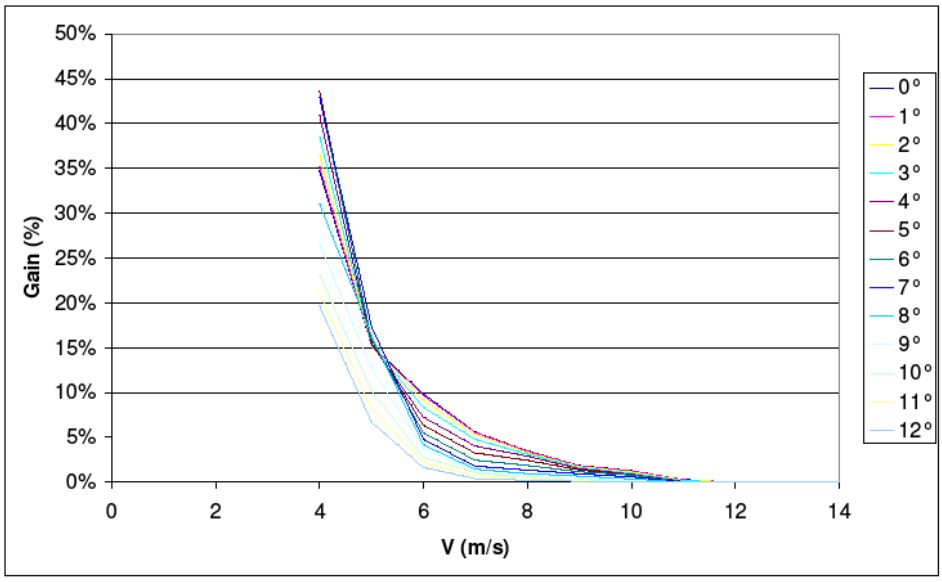

Figure 101: Gain in production of EWTW from Heat and Flux as function of wind speed and alignment

3.1 EWTW measurements on Heat and Flux

In order to validate the above mentioned Heat and Flux Concept several experiments have been performed on the ECN Wind Turbine Test Site (EWTW), the layout of which is given in Figure 2.

The EWTW consists of two rows of wind turbines, i.e. a Southern row with 'Prototype turbines' and a Northern row with 'Research Turbines'). The row with prototype turbines is reserved for commercial testing of wind turbines. These turbines are numbered from 1 to 4. For the present study, the 5 research turbines at the northern part are of relevance. The research turbines are numbered from 5 to 9 with turbine 5 the most Westerly wind turbine. The turbines are variable speed, pitch controlled, and they have a diameter and a hub height of 80 m. The rated power is 2.5MW. Near the research farm, there is a 108 m high meteorological mast (which is denoted as M(et)M(ast) 3).

The wind farm line is directed 95-275 degrees with respect to the North and the distance between the turbines is 3.8D. The operational parameters of the 5 turbines, the loads on turbine 6 and the meteorological data of the measurement mast were continuously measured during the field tests and stored in the measurement database.

In order to experimentally validate the Heat and Flux gain in the EWTW several problems were encountered:

- As mentioned above, the overall gain in the EWTW is expected to be in the order of 0.5%. Such low number is obviously very difficult to verify under atmospheric conditions. It should be realised however, that this overall gain is a summation over all wind directions, where the

verification only needs to consider the 'wake wind directions'. Under these conditions the higher gain from Figure 3 at a misalignment around 0 degrees is expected.

- The selection of relevant data was not straightforward. The data have been selected on basis of 10 minute averaged values. As mentioned above the wind farm is directed from Φ_w = 95 to 275 degrees. Data have only been selected at the westerly wind direction (i.e. at ~ 275 degrees), since this wind direction happens much more frequently than the easterly wind direction. Obviously some margin around this wind direction is needed in order to have sufficient data points, where on the other hand the margin may not be too large since the data should represent 'pure' wake conditions.
  Eventually wake conditions were selected to be at Φ_w = 275 +/- 10 degree where in addition a selection was made on the yaw angle of the upstream turbine (turbine 5): $\Phi_{yaw,turbine5}$ = 263.65 +/- 4 degrees. (Note that this angle differs from the wind farm line due to an off-set in the measured yaw angle).
- Initially a test matrix was specified for automatic turbine operation at a series of alternating blade pitch angles in order to measure the relatively small production increase with sufficient significance but such procedure required a control software modification which was only allowed by the manufacturer after very lengthy and costly quality control procedures. Therefore initial measurements were performed with the upstream turbine alternately under the Normal Operation (NO) for 12 hours, followed by 12 hours under the Noise Reduced Operation (NRO). The Noise Reduced Operation is a standard operational mode of the turbines and did not require any control changes. At the NRO, the turbine operates at an increased pitch angle and (above 7 m/s) a reduced rotor speed, which altogether leads to a significant decrease in axial induction factor and hence an 'exaggerated' Heat and Flux setting. After the measurements at the NRO were completed the manufacturer approved a procedure in which the pitch settings of the individual turbines were changed by means of its remote supervision system on request when ECN expected appropriate wind conditions. With this procedure measurements were conducted in the so-called "*22220*" mode. In this mode the pitch angles of the turbines 5 to 8 (ie the 4 upstream turbines) was set to 2 degrees where the pitch angle of turbine 9 is 0 degrees. This setting was calculated to be about optimal according to preliminary FluxFarm calculations [1]. Nevertheless they turned out to be unsuccessful in the sense that this setting led to a reduction in energy production (see section 2.1.2). Therefore a next campaign with "*20xxx*" control setting was performed. This implies a pitch angle of 2° for the first turbine (number 5) where the second turbine (number 6) operates at a pitch angle of 0°. The pitch angles of the remaining turbines remained unaffected. These pitch angles were beforehand calculated to be optimal for the combined power production of the turbines 5 and 6.
- The number of data points was limited. This is in particular true for the 20xxx campaign for which only 0.58 day of data points were collected (distributed over the entire wind speed range).

3.2 Noise Reduced Operation (NRO)

The results from the Noise Reduced Operation measurements are presented in Figures 4 and 5. They show the power binned versus wind speed. In Figure 4 the results for the upstream turbine (number 5) are given, whereas Figure 5 shows the summed power of the first two turbines (turbines 5 and 6) in the row. Figure 5 also indicates the standard deviation and it shows a comparison with calculations from ECN's WAKEFARM program. Figure 4 shows that the Noise Reduced Operation leads to a clear reduction in power of the upstream turbine. Nevertheless the summed power is almost similar (Figure 5).This then indicates that the losses from the NRO on the upstream turbine are fully compensated by the reduced wake effects which asserts the Heat-and-Flux hypothesis.

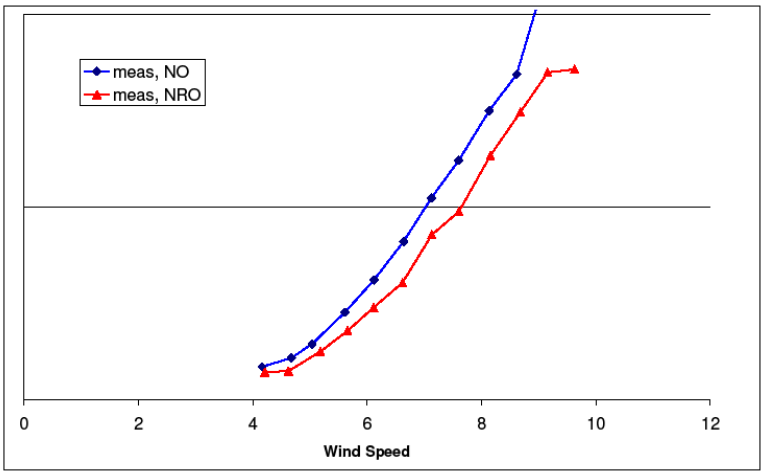

Figure 102: Power curve of upstream turbine (nr 5) at normal operation and Noise Reduced Operation

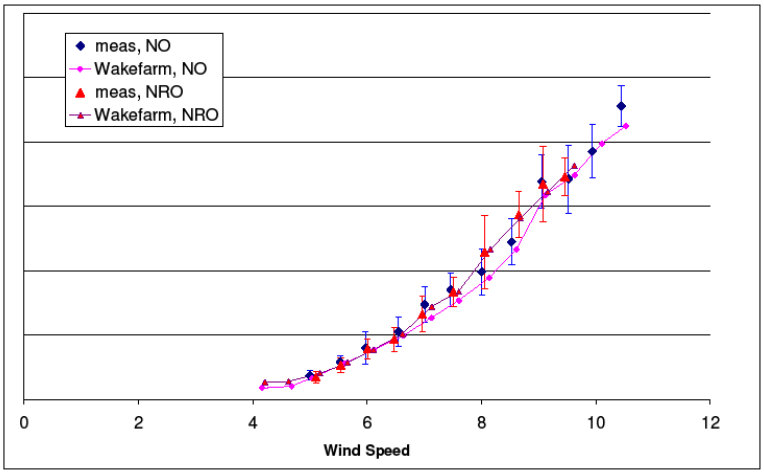

Figure 103: Power curve of downstream turbine (nr 6) where upstream turbine nr 5 is in normal operation or the noise reduced operation. A comparison is shown with WAKEFARM calculations

3.3 "22220" Operation

Figure 6 shows the power performance of the 5 turbines at the 22220 scenario, compared with the power performance at normal conditions (00000 scenario). A clear deterioration in power performance is visible when the turbines are in Heat and Flux operation. This holds for each individual turbine and ergo for the wind farm as a whole. Hence, although preliminary FluxFarm calculations indicated this configuration to be optimal, the measurements clearly show this to be wrong! Several explanations have been offered. One explanation lies in the poor multiple wake model which was applied in the preliminary FluxFarm calculations (later calculations with a more reliable multiple wake model indicated a loss for this configuration indeed). It must however also be realized that wake operation of all 5 turbines is based on the measurements taken at MM3 and the yaw angle of turbine 5, which are

both far remote from the most downstream turbines (figure 2). As such the Heat and Flux settings may have been applied with the downstream turbines in non-wake operation, which then leads to a loss in power of these turbines.

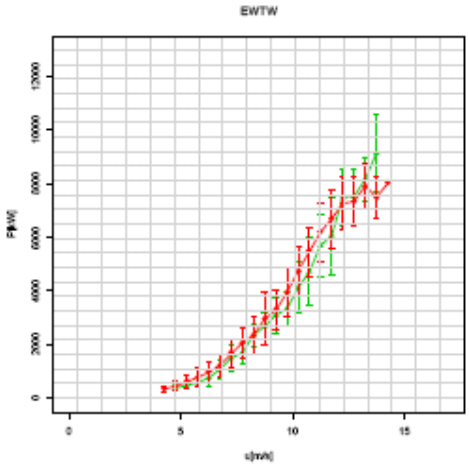

Figure 104: Total power performance of the EWTW farm for scenario 22220 (green triangles) compared with scenaro 00000 (red bullets)

3.4 20xxx" Operation

In the 20xxx operation, the attention has been focused on an assessment of the Heat & Flux operation of the first 2 turbines (turbine 5 and 6) in the farm: turbine 5 operates at a pitch angle of 2 degrees (Heat and Flux) and turbine 6 operates at the normal pitch angle of 0 degrees. As such it is only a single wake situation which needs to be considered without the complicating effect of multiple wakes. Additionally the wind direction measured at MM3 and the yaw angle of turbine 5 are believed to be good indicators for the operation of the first turbines.

Figure 7 shows a slight deterioration in power performance of turbine 5. This slight deterioration is expected since, as mentioned before, the power decreases only very slightly with pitch angle. As a matter of fact the deterioration is within the statistical uncertainty. At the same time an improvement of the performance of turbine 6 can be observed by which the combined power performance of turbine 5 and turbine 6 shows a systematic increase.

Note that scenario 20xxx also increases the overall wind farm production, i.e. the production of the turbines 5 to 9. More information on the results can be found in [1].

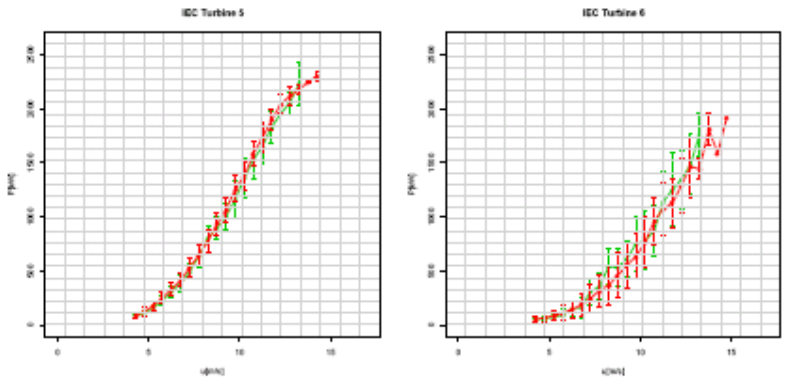

Figure 105: Power performance of turbine 5(left) and 6(right) for scenario 20000 (green triangles) and scenario 00000(red bullets)

3.5 Conclusions on Heat and Flux

An important conclusion from the Heat and Flux experiments is that an increased pitch angle of 2 degrees on the upstream turbine (number 5) hardly decreases the power of this upstream turbine where it does decrease the wake losses and increase the power of turbine 6 and so the summed power of the turbines 5 and 6. Nevertheless some remarks should be made:

- The amount of measurement data is limited.
- The distance between the turbines in the EWTW farm is only 3.8D where it is known that for larger distances between the turbines, the gain will be less.
- The determination of the optimal control settings beforehand is not straightforward since it should be realized that the dependency of **BOTH** power and wake losses to the pitch angle should be known very accurately since the loss in rotor power due to a sub-optimal pitch angle should be balanced with the increase in power of the downstream turbines due to reduced wake effects. Hence the optimal pitch angle can only be determined beforehand if very good **wake** and **rotor** models are available. Alternatively the optimal pitch angle could be determined by measurements.
- The current procedure where the wake effects are determined from the MM3 and turbine 5 measurements is not appropriate for multiple wake conditions. The variability of wind directions under these circumstances asks for mutually dependant control of the turbines, ie. the control of turbine x should depend on the wind direction and yaw angle of turbine (x-1) in order to avoid Heat and Flux Operation in non-wake conditions. The requirement of accurate wake models is even more difficult to fulfil for multiple wake situations.

4 Controlling Wind

The Controlling Wind concept is based on a deliberate yaw angle of the upstream turbine. This obviously produces a lower power and higher loads, but on the other hand, the yaw will deflect the wake behind the upstream turbine which may make it possible to control the wake such that the downstream turbine is not located in the wake of the upstream turbine anymore.

The successful implementation of a Controlling Wind strategy obviously requires a very good insight of the wake structure behind a yawed turbine. It should then be realized that yaw modeling on wind turbines is one of the most difficult areas in wind turbine aerodynamics, see eg [3] where it is explained that the flow around a yawed turbine is determined by the so-called advancing and retreating blade effect which interferes with a variation of the induced velocity over the rotor plane. Moreover the azimuthal variation of the angle of attack will often lead to dynamic stall effects which add to the complexity of the flow problem.

Most important for the Controlling Wind strategy is the determination of the so-called wake skew angle (χ), ie the angle between the wake flow and the nacelle direction. This wake skew angle is generally assumed to be constant and an often applied estimate for this angle assumes the in-plane velocity component unchanged from the in-plane free stream component ($V_w \sin \phi_y$) where the axial velocity changes from V_w to $V_w(1-a)$. This yields

$$\chi = \arctan (V_w \sin \phi_y / V_w \cos \phi_y (1-a)) \sim \phi_y (1 + a) \qquad [3.1]$$

(for small yaw angle and axial induction factor)

On basis of (a limited amount of) measurements from KTH [5], ECN derived a different formula of the following form

$$\chi = \Phi_w (1 + 2/3\, a) \qquad [3.2]$$

This formula has been implemented in Fluxfarm. which showed that Controlling Wind can yield a gain in the EWTW energy production of 1-1.5% (for the wind direction the wind farm line).
A slightly modified relation for the wake skew angle has been derived by TUDelft, [6]:

$$\chi = \Phi_w (1 + 0.3\, C_{Dax}) = \Phi_w (1 + 1.2a(1-a)) \qquad [3.3]$$

This formula has been derived on basis of free wake calculations, TUDelft wind tunnel measurements and Mexico [7] wind tunnel measurements.

It is noted that the formula from TUDelft and ECN compare rather well for design conditions (a=1/3), see Figure 8, which shows the wake deflection from both formula for different yaw angles in comparison with the relation from 3.1. The situation where the wake angle remains unaffected, i.e. where the wake angle remains equal to the yaw angle, is also shown (no skew).

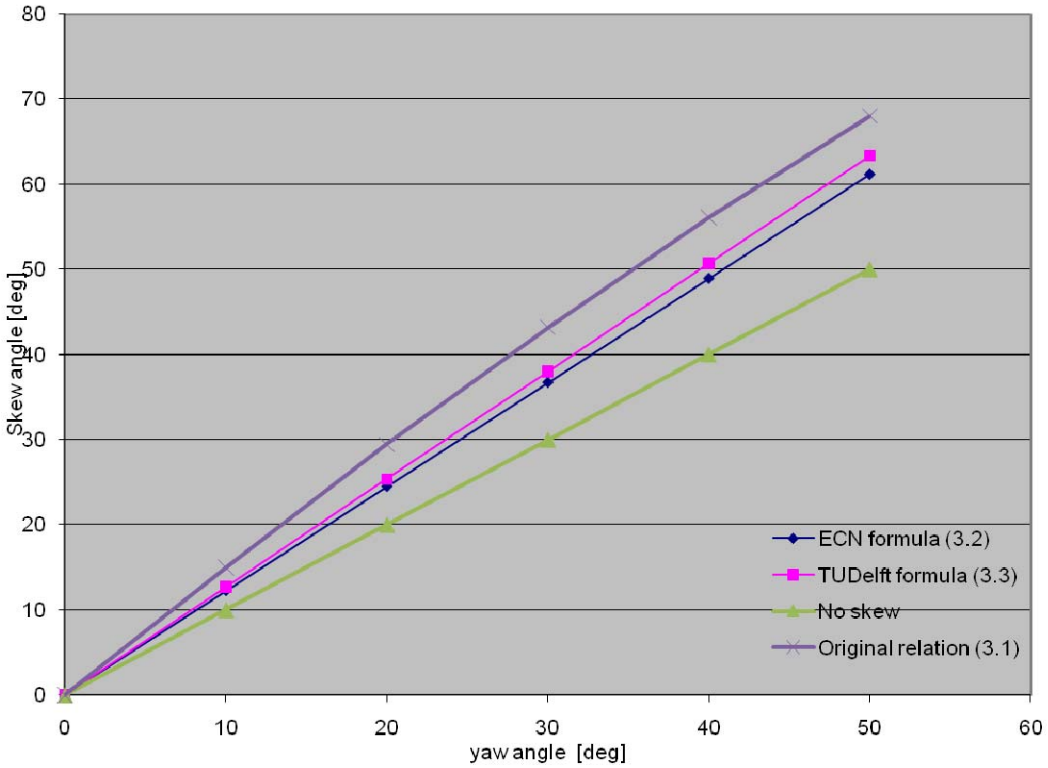

Figure 106: Wake skew angle as function of yaw angle according to the eqn's 3.1 to 3.3. The situation without skew (wake angle = yaw angle) is also shown

It is noted that all formula assume the wake skew angle to be constant throughout the entire wake. This is known to be a very rough approximation as shown in e.g. the EU project Mexico. In this project detailed aerodynamic measurements have been performed on a 4.5 meter diameter rotor placed in the German Dutch Wind Tunnel DNW. Amongst other things PIV measurements have been performed at yawed conditions. These PIV measurements were carried out in a horizontal plane in the form of axial traverses where furthermore the tip vortices have been tracked, see [7] for more details.

Figure 9 shows the resulting wake deflection from the tip vortex tracking experiments (red spots). The dashed line gives the tip vortex positions as derived from the axial traverses. The PIV measurements are done at an azimuth angle of 270 degrees but it is assumed that the measurements at negative yaw and an azimuth angle of 270 degrees correspond to positive yaw and an azimuth angle of 90 degrees. Furthermore the wake deflection from a so called cylindrical wake model with a constant wake skew angle according to relation 3.1 is shown.

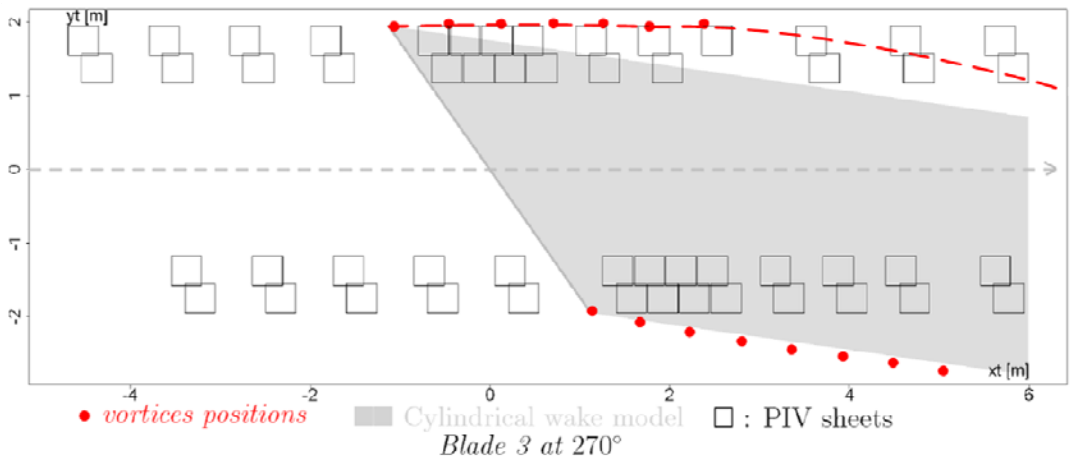

Figure 107: Mexico experiment: Tip vortex positions from vortex tracking experiments (red spots) and axial traverses (dashed line). The wake from a cylindrical vortex sheet method based on the skew angle from formula 3.1 is also shown

It can be seen that the skew angle does not only vary over the axial coordinate but also over the azimuth angle. The analysis from [4] shows this variation to be a result of the flow obstruction from the nacelle and of the variation in induction over the rotor plane. As a matter of fact the aim from [4] was to investigate the capabilities of CFD to reproduce the wake deflection as measured in the Mexico experiment. The main conclusion was that the results are predicted well in a qualitative sense but there is a large quantitative disagreement. Some improvements might be anticipated by refining the CFD model (The assessment from [4] was based on an actuator disc approach) but it is unlikely that CFD can provide the details of the wake deflection sufficiently accurate to form a basis for a successful control strategy. As such a good controlling wind strategy will most likely require tuning on basis of measurements.

For this purpose experiments are foreseen in the scaled farm of ECN. These experiments serve a twofold goal. They should demonstrate a potential for Controlling Wind but they should also provide the experience and guidelines for a successful implementation of a Controlling Wind strategy on other wind farms.

Another aspect which needs to be considered when applying a Controlling Wind strategy lies in the load increase which is expected from yawing the upstream turbines. Thereto it should be realized that the yawed load cases might for some turbines and components even be design driving[11]. However, these design driving load cases generally appear at relatively high wind speeds (rated or above rated wind speed) where Controlling Wind will mainly be applied at low wind speeds (wake losses donot play a role at above rated conditions).

4.1 Conclusion on Controlling Wind

Controlling Wind seems a promising technique to reduce the wake losses in a wind farm. It is however a far from simple technique. In order to determine the optimal Controlling Wind strategy beforehand, very accurate yaw aerodynamic models are required but unfortunately the modelling of a wind turbine under yawed conditions is extremely difficult. As such an optimal Controlling Wind strategy can only

be derived from measurements. A reliable yaw model is also needed to assess the increased loads on the upstream turbine since yawed load cases can be design driving. Possibly Controlling Wind should be applied at low wind speeds only.

5 Upscaling

5.1 Results obtained with WASp

Indiana University/Risoe DTU performed a study to investigate how the size of wind turbines and the scale of wind farms impacts the amount of energy that can be extracted from a given land area [12]. A number of options were considered for a 500 MW farm and simulations were conducted with WAsP for different turbine size and spacing as shown in Figure 10. The results are summarized in Table 1. This research indicates that increasing turbine size from 5 MW to 20 MW could increase energy capture from about 28.3 to at least 34.7 GWh km^{-2} where the wake losses can be decreased from 14.5% to 6.5%. A major assumption in this type of calculation is to understand whether wind turbine wake losses can be scaled linearly as they have been for small to medium wind farms disregarding any large wind farm impacts. If power output from large wind farms is also controlled by meteorological variables on a larger scale (e.g. [13],[14]) then this assumption will no longer be valid. Therefore, there is major uncertainty in this type of linear upscaling.

Table 1. Prediction of power output using WAsP

	Option 1	**Option 2 "Equal area"**	**Option 3 "Equal spacing"**
Turbine	5 MW	20 MW	20 MW
Hub height/rotor diameter (m)	90/126	153/252	153/252
Installed capacity (MW)	500	500	500
Area of installation (km^2)	8.8 × 8.8 = 77.4	8.8 × 8.8 = 77.4	8.8 × 7.1 = 62.1
Area capacity ($W\ m^{-2}$)	6.5	6.5	8.1
Turbine wake losses (%) (WAsP k=0.04, U=8.6 ms^{-1})	14.5	6.5	9.0
Annual production ($GWh\ a^{-1}$) (WAsP k=0.04, U=8.6 ms^{-1})	2197	2211	2152
Production density ($GWh\ km^{-2}$)	28.3	28.6	34.7

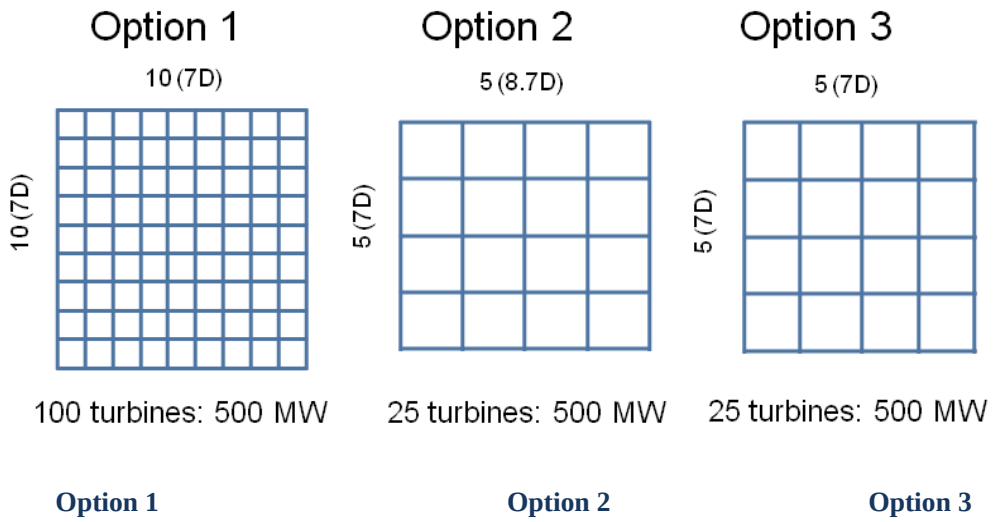

Figure 108: Layouts considered: Left 100 turbines with a rated power of 5MW, middle and right 25 turbines with a rated power of 20 MW

5.2 Results obtained with CRES–Farm

CRES also carried out a study to investigate how the size of wind turbines and the scale of wind farms affect the wake losses and the capacity factor. A number of options were considered for a 500 MW and a 1000 MW wind farm. Simulations were conducted with CRES–Farm tool for different turbine sizes (from 5 MW to 20 MW) using 7D x 7D spacing. CRES–Farm is an in-house tool that is used for the estimation of the annual energy production from wind farms that is based on the prediction of the effective wind roses at the machines' hub heights for a given wind farm layout. CRES–Farm employs the amended GCL wake model. The major assumption behind this simulation is that wind is not affected by meteorological variables on a larger scale. The wind turbine characteristics are included in Table 2. It is noted that in this preliminary estimation it is assumed that the difference in size does not affect the aerodynamic performance of the wind turbine (i.e. all wind turbine featured the same power coefficient and thrust coefficient distributions). The calculations have been performed for an annual wind speed of 10 m/s at a height of 90 m and a wind shear coefficient of 0.14

WT Rated power [MW]	5	10	15	20
WT Diameter [m]	126	178	218	252
Tip Speed [m/s]	80	80	80	80
Hub Height [m a. w. l.]	90	116	136	153
Table 2: Wind turbine characteristics as used by CRES				

The details of the different configurations are summarized in Table 3. It is noted that small differences in the overall capacity of the wind farm appear in the various configurations (since the overall power capacity would not precisely be realized with some wind turbines) that are reflected in small variations of the area used.

Wind turbine size [MW]	5	10	15	20
	500 MW wind farm			

Machines	10x10	7x7	6x6	5x5
Capacity [MW]	500	490	540	500
Area [km^2]	77.80	76.07	83.83	77.80
	1000 MW wind farm			
Machines	14x14	10x10	8x8	7x7
Capacity [MW]	980	1000	960	980
Area [km^2]	152.47	155.25	149.04	152.47

Table 3: Wind farm case details as used by CRES

The results are presented in Figure 1 and 2 in the form of the capacity factor and the wake losses as a function of the wind turbine rated power for the two wind farm sizes. This research indicates that increasing turbine size from 5 MW to 20 MW contributes to a direct decrease in the wake losses and therefore the capacity factor is increased. A contribution to the increase of the capacity factor should also be attributed to the increase in hub height that accompanies the increase in the rated power since a normal wind shear profile was assumed.

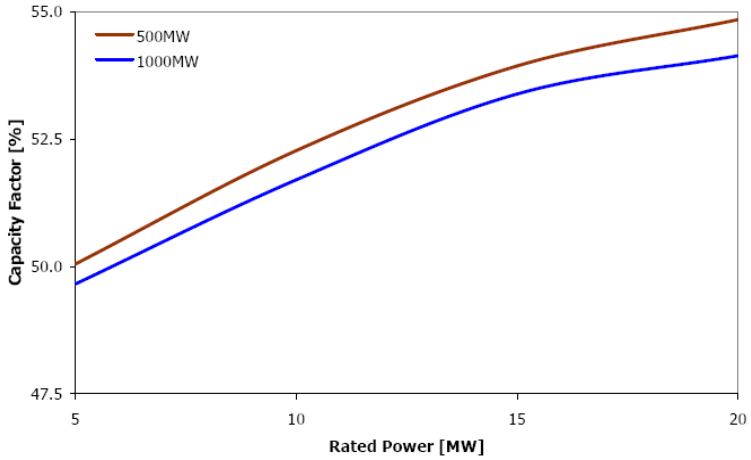

Figure 109: Wind farm capacity factor as a function of the wind turbine rated power for the wind farm cases as presented in table 3

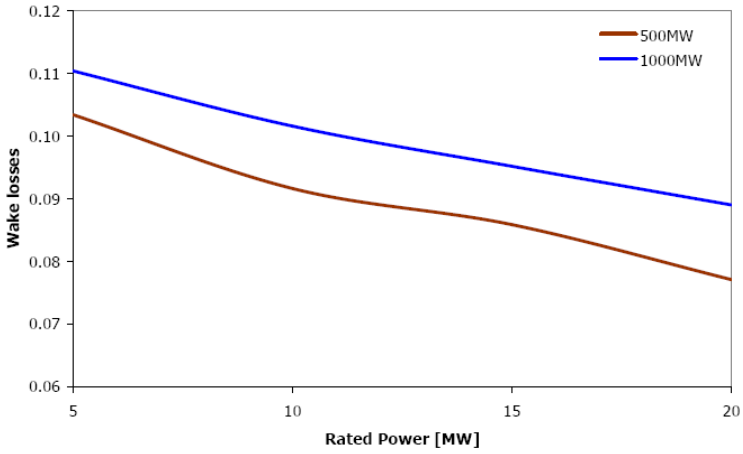

Figure 110: Wind farm energy loss due to wakes as a function of the wind turbine rated power for the wind farm cases as presented in table 3

5.3 Upscaling results obtained with Farmflow

In [2] a study is presented where the wake losses has been determined with the ECN code Farmflow. All scenarios which are investigated are based on the lay-out of the ECN Wind Turbine Test Site Wieringermeer, EWTW, see section 2.1.

The scenarios presented in this report all assume the basic lay-out unchanged from the original set-up i.e. a line set-up with 5 equi-spaced turbines. However some, or all, turbines have been upscaled to a diameter of either 90m or 100 meter compared to the original diameter of 80 meter. The length of the wind farm line was also made variable and ranged between 1220 m (the original length) to 2880 m.

It should be noted that it is not only the diameter which changed but also the power curve and the C_{Dax}-V curve. Until rated wind speed, the C_{Dax}-V curve is independant of turbine size but the rated power is also kept unchanged by which the wind speed reduces for an upscaled turbine. Since wake effects only play a role at above rated conditions, an upscaled turbine suffers less from wake effects. Hence, to some extent, an upscaled turbine can be seen as a wind turbine design suited for wake operation.

The results are presented in Figure 11. It can be seen that for given farm length, the wake losses for 5 equally sized turbines often decrease with increasing diameter despite the fact that the relative distance between the turbines is smaller for a larger diameter. This is most likely a result of the lower rated wind speed for the larger turbine as discussed above. The results also indicate that increasing the diameter of the downstream turbines in the farm (i.e. the turbines which are heavily exposed to wake effects) generally reduce the overall wake losses.

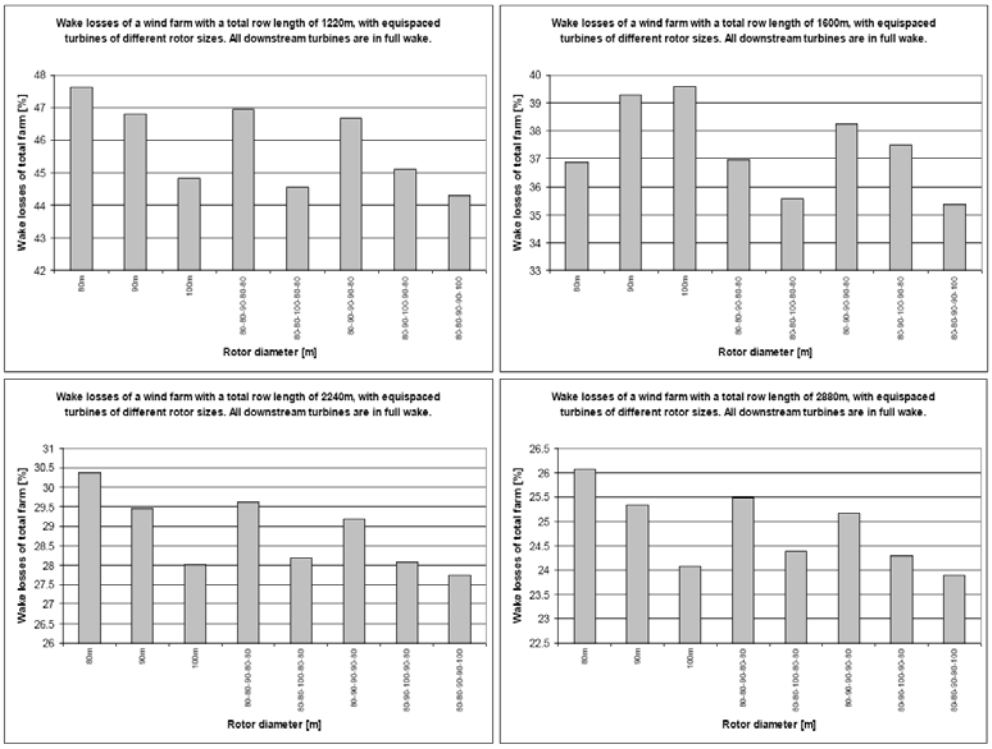

Figure 111: Wake losses for different EWTW lay-outs where all downstream turbines are in a full wake situation. Each graph represents a farm length (original farm length is 1220 m) . The diameters of the different turbines are presented along the horizontal axis (original diameter is 80 m). The three left bars assume all 5 turbine diameter to be the same (80m, 90m or 100m).

5.4 Conclusion on upscaling

On basis of calculations, it may be concluded that upscaling is a very promising option to reduce the relative wake losses. The wake losses in a farm with the same rated power but larger wind turbines are much less than the wake losses on a farm with small turbines. Also the use of 'wake specific designed turbines' i.e. differently scaled turbines within a wind farm has shown to have potential.

6 Aerodynamic scaling effects

The results as presented in the previous sections assume the aerodynamic wake effects to be scale independent. In this section the question will be addressed how valid this assumption is. First it is noted that several scaling dependencies could play a role but this study only considers scaling of 'single far wake' effects. Scaling effects are also expected to appear on the aerodynamic phenomena in the near wake but these scaling effects may be considered as secondary importance for the far wake (section 4.6). Moreover the mutual interaction of the wakes and the interference of the wake with the ground and upper atmosphere might be scale dependant phenomena. These phenomena are not considered in the present analysis.

The study investigates the scaling dependency on the velocity deficit in a single wake which is written in terms of:

$U_{def}(y,z) = U_{\infty}(z) - U_{wake}(y,z)$

In this expression it is assumed that the free stream velocity (U_{∞}) is subject to a vertical wind shear only, ie. it is a function of the vertical coordinate *z* but the velocity in the wake and so the wake deficit has also become a function of *y,* the horizontal coordinate. As explained below it will be assumed that the velocity defect iis axi-symmetric around the wake center ie. it can be written as function of r, the radial coordinate with respect to the wake center.

The modeling of the velocity deficit is then largely in line with the model from Schlichting [8] where the following assumptions are made:

- The wake deficit u_{def} is assumed to be axi-symmetric around the rotor (wake) centre, i.e. the wake deficit is written in terms of a radial coordinate r
- The stream wise pressure gradient *dp/dx* is neglected (this assumption is valid for say $x > 2D$)
- The boundary layer assumption is made (i.e. the length scale in streamwise (*x*) direction is assumed to be long compared to length scale in radial (*r*) direction)
- The rotor is modelled as an actuator disc with axial force coefficient $C_{D.ax}$
- The wake flow is fully turbulent, ie. turbulent friction is much larger than laminar friction
- The velocity deficit u_{def} is small compared to the free stream velocity.

With the above given assumptions and a simple mixing length eddy viscosity model, a self similar velocity profile is found in the form of:

$$u_{def}(r) = u_m f(r/R_w) = u_m f(\eta) \qquad [4.1]$$

with η the ratio between the radial position and the wake radius R_w,

$\eta = r/R_w$

Hence equation [4.1] gives an axi-symmetric velocity deficit as function of η where the velocity deficit is maximum (u_m) in the wake centre (η =0).

The self-similar solution f(η) is given in [8] and takes the following form:

$$f(\eta) = [1 - \eta^{1.5}]^2 \qquad [4.2]$$

Note that equation [4.2] can be shown to approach closely an exponential behaviour

$f(\eta) \sim exp(-\eta^2 / 0.27)$.

In order to express the velocity deficit u_m and the wake radius the momentum deficit over the wake is found by:

$D_{ax} = \int \rho u \, (U_\infty - u) \, 2\pi r dr$

Which gives, with the above mentioned assumption of small u_{def} and $\eta = r/R_w$
and equation 4.1:

$D_{ax} = \int R_w^2 \rho U_\infty u_m f(\eta) 2\pi \eta d\eta$

which gives:

$$u_m/U_\infty = \lambda C_{D.ax} A / R_w^2 \qquad [4.3]$$

in which λ is a constant $\lambda = \int 4\pi f(\eta) \, \eta d\eta)^{-1} \sim 0.6189$

Equation 4.3 shows the velocity deficit to scale with R_w^{-2}
The wake radius R_w is still unknown. It is modelled along the following lines:

- The rate of increase of R_w is proportional to transverse velocity v'
- v' follows from a simple eddy viscosity mixing length model:

  $$v' \sim l \, du/dr \qquad [4.4]$$

  in which the mixing length scales with the wake radius

  $$l = \alpha R_w \qquad [4.5]$$

  Where α is assumed to be constant and the average shear over the wake radius can be approximated as the maximum velocity deficit divided by the wake radius:

  $$du/dr \sim u_m/R_w \qquad [4.6]$$

- Hence $dR_w/dt \sim U_\infty \, dR_w/dx \sim \alpha \, u_m$ by which

  $dR_w/dx \sim \alpha u_m/U_\infty$

  Which gives with eqn 4.3:

  $R_w \sim (\alpha \, \lambda \, C_{D.ax} A x)^{1/3} + R_{w,0}$

  Or

$$R_w \sim (\alpha \lambda C_{D.ax} A)^{1/3} (x - x_0)^{1/3} \quad [4.7]$$

From which the 'relative' wake radius R_w/R is found as:

$$R_w/R = k(C_{D.ax})^{1/3} [(x - x_0)/R]^{1/3} \quad [4.8]$$

(with k a constant in which α is 'hidden')

With equation 4.8 the maximum velocity deficit can be found from equation 4.3:

$$u_m/U_\infty = \lambda_2 C_{D.ax}^{1/3} [R/(x-x_0)]^{2/3} \quad [4.9]$$

(With $\lambda_2 = \lambda \pi k^{-2}$)

Note that, in principle, the unknowns λ_2 and x_0 can (for given $C_{D.ax}$) be found from equation 4.9 with two velocity measurements at hub height at different x positions.

6.1 Scaling dependencies

Wake effects are often considered in terms of

- u_{def}/u_m as $f(r/R)$
- R_w/R as $f(x/R)$
- u_m/U_∞ as $f(x/R)$

In this form the equations 4.1, 4.8 and 4.9 show that all scale dependencies (i.e. all dependencies on rotor radius (or rotor diameter)) are eliminated (note that r/R_w in equation 4.1 can be written as $r/R \cdot R/R_w$).

This is however only true when x_0/R and λ_2 (i.e. α) are independent of the rotor radius which is not a-priori known.

It is noted that a similar conclusion can be drawn when assessing scaling effects from a turbulent Reynolds number written in the following form:

$$Re_{turb} = U_\infty x/\nu_{turb} = U_\infty x / (l^2 du/dr) = 1/[\alpha^2 k \lambda_2 C_{Dax}^{2/3}] x/R [(x-x_0)/R]^{1/3}$$

This again shows the turbulent Reynolds number at given x/R to be independent of rotor scale, apart from a possible scale dependency on x_0/R and α (or λ_2)

As such scaling (in)dependency can be determined if the values of x_0/R and λ_2 are calibrated for a number of experiments at different scales. As mentioned above this requires, theoretically speaking, only 2 measurement points per experiment (for given C_{Dax}). In practice however the scatter in the measurements, as well as the fact that the real velocity behaviour will not perfectly obey the above given modelling assumptions asks for a need of much more measurement data.

Finally it can be noted that the value of x_0 represents a boundary condition from the near wake. The near wake is obviously largely determined by the aerodynamic behaviour of the rotor in front of the wake which is known to be Reynolds number dependant. Nevertheless this dependency may be relatively weak at the high Reynolds numbers of nowadays turbines (> 5M) since scaling effects become weaker with increasing Reynolds number.

Furthermore, although some Reynolds number dependency on x_0 may be expected, the far wake will be rather insensitive on the precise value of x_0 (x_0 is often found to be in the order of 1.5-2D which is relatively small compared to the values of x in the far wake (5-10D)). As such the determination of the precise value of x_0 is expected to be of secondary importance.

6.2 Conclusion on scaling dependency of the 'far single wake'

The question of scaling (in)dependency of wake effects has been reduced to the determination of two parameters: λ_2 (basically α) and x_0 where most likely the overall influence of x_0 is limited in particular when rotor Reynolds numbers exceed values of say 3M. As such it is only the $\lambda_2(\alpha)$ which remains to be calibrated from wake experiments at different scales.

The calibration of α in boundary layer experiments [8], showed little scale influence which leads to the expectation that scaling dependency in wake aerodynamics might also be limited.

7 References

1. Machielse, L.A.H.; Barth, S.; Bot, E.T.G.; Hendriks, H.B.; Schepers, J.G.(2008) *Evaluation of "Heat and Flux" Farm Control. Final Report*, ECN-E--07-105.
2. C. Van Gestel.*Wake effects of off-shore wind farms, Sensitivity studies of row lay-outs*. ECN Wind Memo-10-063, 2010
3. Snel, H. and Schepers, J.G. (1994) *JOULE 1: Joint investigation of Dynamic Inflow Effects and Implementation of an Engineering Method*, Energy Research Center of the Netherlands, ECN-C-94-107, December 1994
4. A.K. Kuczaj. *Virtual Blade Model Simulations of the Mexico experiment*. NRG-21810/09.97106, NRG Petten, the Netherlands, November 2009.
5. Medici, D. *Wind Turbine Wakes under Different Running Conditions*. In proceedings of 16th Symposium on IEA Joint Action on Aerodynamics of Wind Turbines, NREL, Boulder, USA, May 2001, Editor Sven Erik Thor.
6. D. Micallef *MEXICO Data Analysis, Stage V - Investigation of the Limitations of Inverse Free Wake Vortex Codes on the Basis of the MEXICO Experiment*, TUDelft/University of Malta
7. J.G. Schepers, L. Pascal and H. Snel. *First results from Mexnext: Analysis of detailed aerodynamic measurements on a 4.5 m diameter rotor placed in the large German Dutch Wind Tunnel DNW*. Presented at the European Wind Energy Conference, EWEC, April 2010, Warsaw Poland.
8. H. Schlichting and K. Gersten. *Boundary Layer Theory*. 8th ed. Springer-Verlag 2004, ISBN 81-8128-121-7
9. J.G. Schepers and S.P van der Pijl *Improved modelling of wake aerodynamics and assessment of new farm control strategies*, Science of Making Torque in J. Phys.: Conf. Ser. 75 (2007) 012039
10. Schepers, J.G. *Analysis of 4.5 years EWTW wake measurements* ECN-E--09-057
11. J.G. Schepers, J.J. Heijdra, D. Foussekis, S Øye, R. Rawlinson Smith,; M. Belessis, K. Thomsen, T. Larsen, I. Kraan, I. B. Visser, I. Carlen, H. Ganander, H. L. Drost *'Verification of European Wind Turbine Design Codes, VEWTDC'* final report, ECN-C--01-055, Energy Research Center of the Netherlands, ECN, April 2002, http://www.ecn.nl/publicaties/default.aspx?nr=ECN-C--01-055
12. Barthelmie RJ, Frandsen ST, Pryor SC (2009) Energy dynamics of an infinitely large wind farm. *European Offshore Conference 2009,* Stockholm, 14-16 September 2009 (Poster).
13. Frandsen S, Barthelmie RJ, Jorgensen HE, Rathmann O, Badger J, Hansen K, Ott S, Rethore P, Larsen SE, Jensen L (2009) The making of a second-generation wind farm efficiency model-complex. *Wind Energy* 12:431-444
14. Frandsen ST, Barthelmie RJ, Rathmann O, Jørgensen HE, Badger J, Hansen K, Ott S, Rethore PE, Larsen SE, Jensen LE (2007) Summary report: The shadow effect of large wind farms: measurements, data analysis and modeling. *Report No. Risø-R*-1615(EN), Risø National Laboratory/DTU, Roskilde

Appendix 6: Deliverable 8.6 Lifetime Loads

Project funded by the European Commission under the 6th (EC) RTD Framework Programme (2002- 2006) within the framework of the specific research and technological development programme "Integrating and strengthening the European Research Area"

Project UpWind

Contract No.:
019945 (SES6)

"Integrated Wind Turbine Design"

Wp8: Flow
Deliverable D8.6 Lifetime Cost Modelling

AUTHOR:	Malcolm Heath
AFFILIATION:	Garrad Hassan and Partners Ltd
ADDRESS:	St. Vincent's Works, Silverthorne Lane, Bristol, BS2 0QD
TEL.:	+44 117 972 9900
EMAIL:	Malcolm.heath@gl-garradhassan.com
FURTHER AUTHORS:	
REVIEWER:	Graeme McCann
APPROVER:	Wolfgang Schlez

Document Information

DOCUMENT TYPE	Deliverable D8.6
DOCUMENT NAME:	Lifetime Cost Modelling
REVISION:	1
REV.DATE:	20 January 2011
CLASSIFICATION:	Published
STATUS:	Issue

Abstract: An illustrative cost model has been developed to demonstrate the use of lifetime costing in the design of wind farm layouts. This has been combined with a fatigue loads database to show the effect of turbine spacing on loading and hence its potential for use in lifetime cost calculation.

Contents

Status				Confidentiality				Accessibility	
S0	Approved/Released			**R0**	General public			Private web site	
S1	Reviewed			**R1**	Restricted to project members			Public web site	
S2	Pending for review			**R2**	Restricted to European. Commission			Paper copy	
S3	Draft for commends			**R3**	Restricted to WP members + PL	**x**			
S4	Under preparation	**x**		**R4**	Restricted to Task members +WPL+PL				

PL: *Project leader* **WPL:** *Work package leader* **TL:** *Task leader*

8 Introduction

The principle goal of the designer of a commercial wind farm will be to make that wind farm as profitable as possible. This is not as straightforward as simply establishing the layout of turbines which generates the highest energy yield. The energy yield represents the income generated by the farm, but to understand its profitability it is also necessary to understand the costs involved in its construction and operation.

Many costs are easy to model – the procurement price of a turbine is a known quantity, for example. Others are much harder to establish. For example, the maintenance cost of a wind farm will depend on many factors, such as the wind conditions, operational strategy, turbine design and build quality and so on.

As part of UPWIND Work Package 8, GL Garrad Hassan have developed a cost model to illustrate how a financial analysis of a wind farm layout should be performed. This cost model considers the lifetime economics of the farm, including both the capital investment and operational costs.

It is aimed at helping the wind farm designer establish the optimum turbine layout. For this reason it can safely be restricted to analysing only those costs which will vary with the layout. The procurement costs of the turbines, for example, have been ignored since for a fixed number of turbines they will not change, regardless of where on the site the turbines are installed.

A central part of this cost model has been to analyse the costs incurred as a result of turbulence induced fatigue loading on the turbines. This is arguably the most complex part of the analysis, since it involves calculation of wake induced turbulence, fatigue loading and consequent repair and maintenance costs.

9 Fatigue loads database

Fatigue damage to wind turbines caused by wake-affected turbulence is a significant factor in the design of wind farm layouts. It affects the cost of energy both directly in terms of maintenance costs, and indirectly by determining the IEC class of turbine which is used on the site.

Currently, industry practice is to assess the extent of fatigue by calculating a *design equivalent turbulence*, in accordance with IEC 614100-1, Annex D [1]. This is based around the 'Frandsen method', and is commonly implemented in wind farm design software such as *WindFarmer*. Calculated equivalent turbulence levels are compared against the envelope of acceptable levels in the IEC classifications, to give a pass/fail determination of whether conditions at a potential turbine location are acceptable.

This conventional approach is limited in the detail which it can determine, and researchers have been investigating potential improvements. One possibility is to quantify the wind conditions which a turbine is expected to experience, and use this as the input to an aero-elastic model such as *Bladed*. This would yield highly detailed results, allowing analysis of the loading on any component in the turbine, but would be very time consuming, requiring several hours of work. It would not be feasible to follow this approach when considering a choice of many possible layouts of a multi-turbine wind farm.

GL Garrad Hassan developed an intermediate approach. The fatigue loads on a turbine under a very wide range of possible wind conditions are pre-calculated using *Bladed*. The results are stored in a *fatigue loads database*. The fatigue loads for a particular wind condition can then be quickly recalled by reading from the database. The process of creating the database is relatively slow, but only needs to be performed once for a given turbine model. The speed of reading from the database makes this initial investment worthwhile.

A research version of *WindFarmer* was written which contains an interface to the loads database. When configured with a turbine layout and ambient wind conditions, *WindFarmer* calculates the incident wind speeds and turbulence intensities, including wake effects. These are used to interrogate the fatigue loads database, which returns the margin between the design and calculated loads for a selection of critical components. It also returns a simple 'pass/fail' flag, which indicates when loads exceed their design limit.

An example of the output available from the loads database is shown in 1 below. Results for six turbines in a single wind farm are given. Data represents the margin between the calculated fatigue load and the design load, as a percentage. A negative value indicates that the calculated load exceeds the design load.

Turbine ID	Load Test	Blade root Mx (%)	Blade root My (%)	Rev at level (%)	Tower top Fx (%)	Yaw bearing Mz (%)	Stationary Hub My (%)
1	pass	3.2	2.1	5.1	8.7	8.1	8.1
2	fail	1.0	-4.9	3.8	-0.3	-0.8	0.2
3	pass	3.0	5.4	2.9	9.9	9.0	8.7
4	pass	4.3	7.1	4.6	14.4	13.4	12.8
5	fail	2.9	-0.6	6.8	6.4	6.0	6.8
6	pass	4.3	5.0	7.7	12.6	12.3	12.4

Table 1 . Example output from fatigue loads database

10 Cost Model

A cost model is required to establish the economics of a wind farm.

A wide variety of different costs is incurred during the lifetime of a wind farm. They can be broken down into capital costs such as turbine purchase and installation; and operational costs such as repairs and maintenance.

It should be remembered that ultimately the design must also have a low enough environmental impact to gain planning permission. It is difficult to apply a quantitative analysis to environmental impact, and so no attempt has been made here. The assumption is made that only layouts which meet environmental constraints will be subject to a financial analysis.

An alternative to profit as a measure of the quality of a wind farm design is the Cost of Energy. This measure was described by the IEA [2], and is also sometimes referred to 'levelised production costs':

$$CoE = \frac{\sum \left[(I_t + M_t + F_t)(1+r)^{-t} \right]}{\sum \left[E_t (1+r)^{-t} \right]}$$

Where: CoE = Lifetime levelised Cost of Energy
I_t = Investment expenditures (capital costs) in the year t
M_t = Operations and maintenance (O&M) expenditures in the year t
F_t = Fuel expenditures in the year t
E_t = Electricity generation in the year t
r = Discount rate

The Cost of Energy is calculated over the economic lifetime of the project, typically 20 years. Since wind power is a renewable energy source, the fuel costs can be considered to be zero, and ignored.

For a wind farm with a given number of turbines of a given model, the aim of the designer will be to establish the turbine layout with the lowest Cost of Energy.

Costs, whether they are capital or O&M, can usefully be divided into those which are fixed regardless of the turbine locations, and those which will vary. Fixed costs would include items such as the capital cost of the turbines, and routine maintenance. Variable costs would include items such as the infrastructure connecting turbines, and damage caused by excessive fatigue. The fixed costs will not influence the optimiser's choice of turbine locations, and so can safely be ignored. Only the variable costs will be considered in this report.

A cost model has been developed which demonstrates the principles of calculating the Cost of Energy. A great deal more research is required to refine this model to the point where it produces reliable and generally applicable results, but it serves to illustrate how such a model might be used to aid the wind farm designer.

The model considers a sample set of the most significant variable costs. These are:

- Civil and electrical infrastructure (capital cost)
- Fatigue induced maintenance (O & M cost)

These are combined year by year with the energy yield, on a discounted basis, to give a lifetime Cost of Energy. The flow of data through the cost model is shown in Figure 1 below.

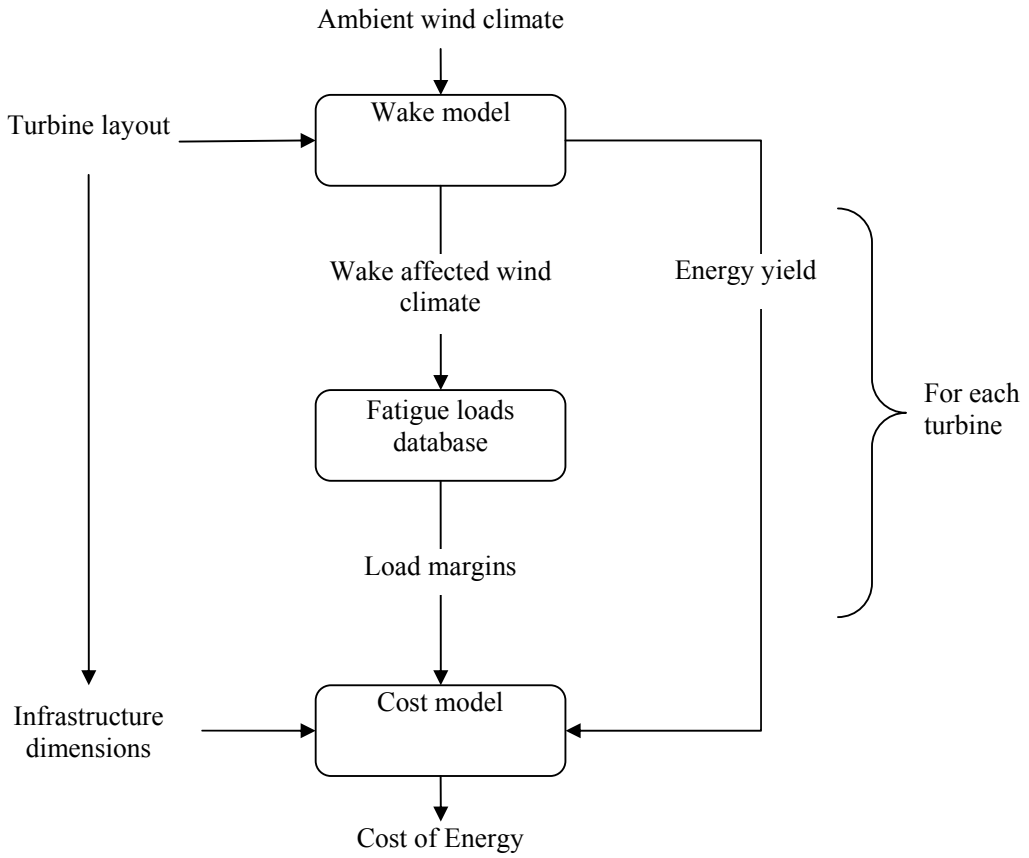

Figure 1112. Cost model structure

10.1 Civil and electrical infrastructure

Any wind farm will require a network of electrical cabling to be installed between the turbines and the point of common connection with the electrical grid. Onshore wind farms can also be expected to require access tracks to be built to turbines.

The cost of this infrastructure is a significant part of the capital cost of a wind farm, and can vary considerably with the layout of the turbines. Attempting to calculate it automatically from an arbitrary layout of turbines is challenging, as the model is required to determine what route the tracks and cables would follow. This is a variation of the classic 'travelling salesman' problem which, while solvable, is computationally intensive.

Constraining the layout to a regular, 'symmetrical', grid makes this problem considerably easier. Tracks and cables can be assumed to run in straight lines along rows, and calculation of their length becomes trivial. The cost can then be calculated by simply multiplying the length by a cost per meter factor. This constraint is assumed for this illustrative cost model.

10.2 Fatigue induced maintenance

Turbulence in the wind induces fatigue in the components of a turbine, and high levels of fatigue can be expected to cause components to fail. Repair of failed components is a cost which contributes to the overall Cost of Energy.

The fatigue loads database described in section 9 can be used to quantify the margin between the design loads and site specific loads for critical components in a turbine. Where a site specific load exceeds the design load, that particular site can be considered unacceptable for a turbine.

Where the site specific load is less than the design load, the site is acceptable, and is suitable for financial modelling. A probabilistic approach is taken, analysing every critical component of every turbine in the wind farm. The size of the margin between the loads can be considered to determine the probability of failure of that particular component. The probability of failure in any given year multiplied by the cost of repair gives the annual maintenance cost for each component.

Further research is required to establish precisely what probability distribution should be used for this modelling. The conclusions are unlikely to be straightforward, and can be expected to differ for each component. For this illustrative cost model, a log-normal distribution has been assumed, but it should be emphasised that this is for illustrative purposes only. The load margin is used to scale the mean component lifetime, such that a positive margin results in an increased mean lifetime.

Figure 2 shows how this model predicts an increasing probability of component failure with the age of the turbine.

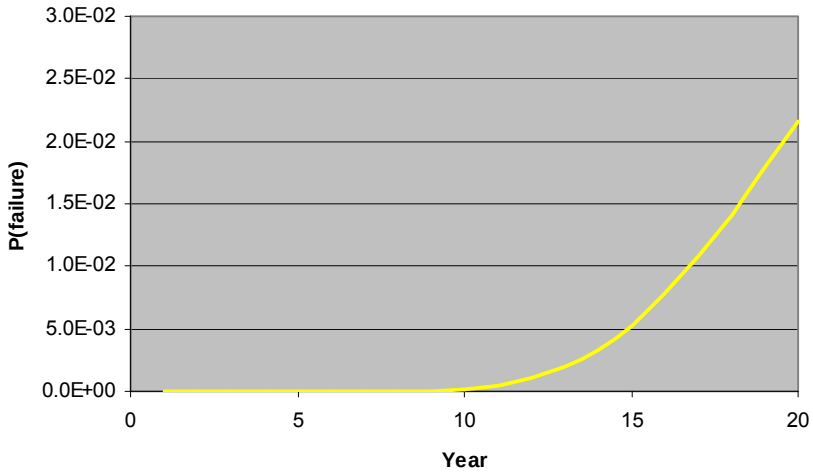

Figure 2. Increasing probability of failure with age

11 Example Optimisations

To demonstrate the use of Cost of Energy in establishing the optimum layout of turbines, two example optimisations have been performed:

- In a uniform, unidirectional wind climate
- On a hill top, with higher wind speeds at the top of the hill

The simplest possible wind farm has been modelled: two turbines of the same type. In this case, a generic 2MW, 80m diameter turbine has been studied.

The separation between the turbines has been varied. *WindFarmer* software has been used to calculate the wake effects, with resultant loss of wind speed and increase in turbulence at the downwind turbine, and consequent energy yields from the turbines.

The wind conditions modelled by *WindFarmer* were used to index the fatigue loads database, which output the margins on six key loads. This data was input to the cost model, which calculated probability of failures and cost of repair. These are the only operational costs considered by this cost model.

The cost model also calculated the capital cost of civil and electrical infrastructure, by applying a simple cost per meter figure to the separation distance between the two turbines. These are the only capital costs considered by this cost model.

Throughout the following discussion, only costs which vary with turbine layout are considered. A great many other costs are, of course, incurred but these would not affect the choice of turbine layout, and so are not considered here.

Key assumptions made in this implementation of the cost model are detailed in Appendix 1. It should be remembered that these assumptions, and the results drawn from them, are purely for illustration and should not be considered authoritative.

11.1 Uniform wind climate

In this example, a simplistic wind regime has been assumed:

- Mean hub height wind speed: 8m/s
- Uniform ambient wind conditions across the site
- Unidirectional wind flow directly between the two turbines

The two turbines were modelled such that one was directly downwind of the other, as shown in Figure 3. In this situation, the wind incident on the upwind turbine will be unaffected by the separation distance of the two turbines.

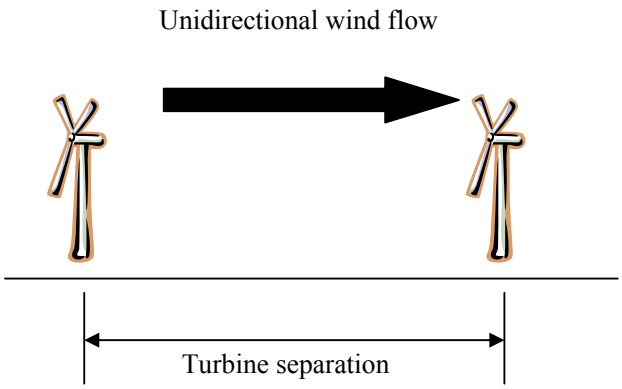

Figure 4. Uniform wind climate site

The *WindFarmer* model showed that, as can be expected, the mean wind speed incident on the downwind turbine increases as the turbines are moved further apart. This is because it is directly in the wake of the upwind turbine – increasing the separation decreases the wake, and so increases the mean wind speed. This increased wind speed generated a corresponding increase in energy yield, as shown in Figure 5.

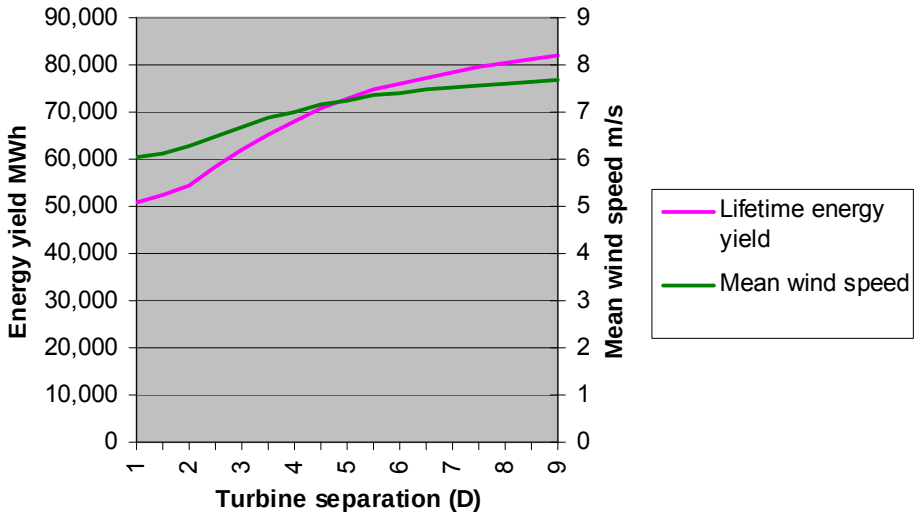

Figure 5. Variation in wind speed and energy yield

Energy yield goes on increasing with increased separation, but in practice the rate of increase has more or less flattened out once a separation of 10D has been reached.

Increasing turbine separation also causes a reduction in turbulence intensity. This was quantified here by reading the load margins from the fatigue loads database. The cost model converted this into a total lifetime cost for repairs and maintenance. This is shown in Figure , together with an example load margin – that for the blade root M_y.

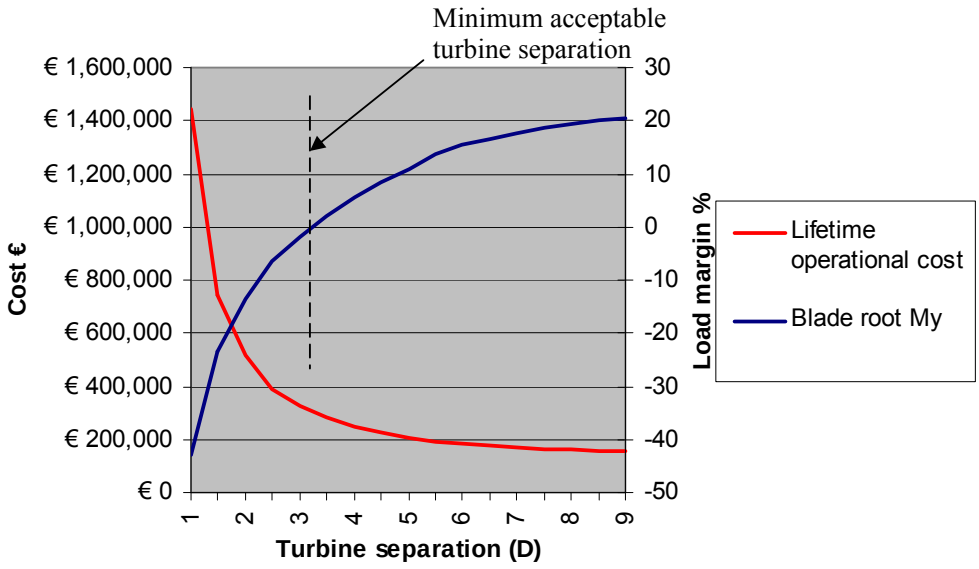

Figure 6. Variation in loading and operational cost

It can be seen that at small separation distances the margin for the loading on the blade is below zero. This indicates that the fatigue loads will exceed the design limits, and in practice it would be unacceptable to place turbines with such a small separation. In this case, the minimum separation is around 3.5D.

As with energy yield, operational costs continue to improve as turbines are spaced further apart. However, capital costs, here determined by the infrastructure connecting the two turbines, increase as turbine spacing increases. When these are added to the operational costs to give the lifetime total costs, there is a separation distance at which the total costs are at a minimum. This can be seen in Figure 113. In this case, the minimum cost occurs at a separation distance of approximately 6D.

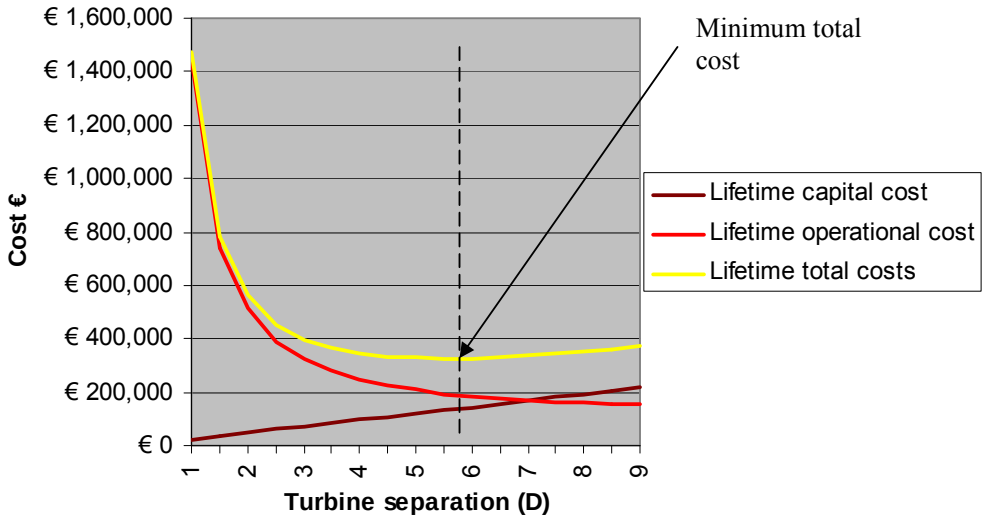

Figure 113. Variation of costs with separation distance

The separation with the minimum total cost will not represent the optimum separation distance. This is found at the minimum Cost of Energy. Figure 114 shows the result of combining the total cost with the lifetime energy yield, to give the Cost of Energy.

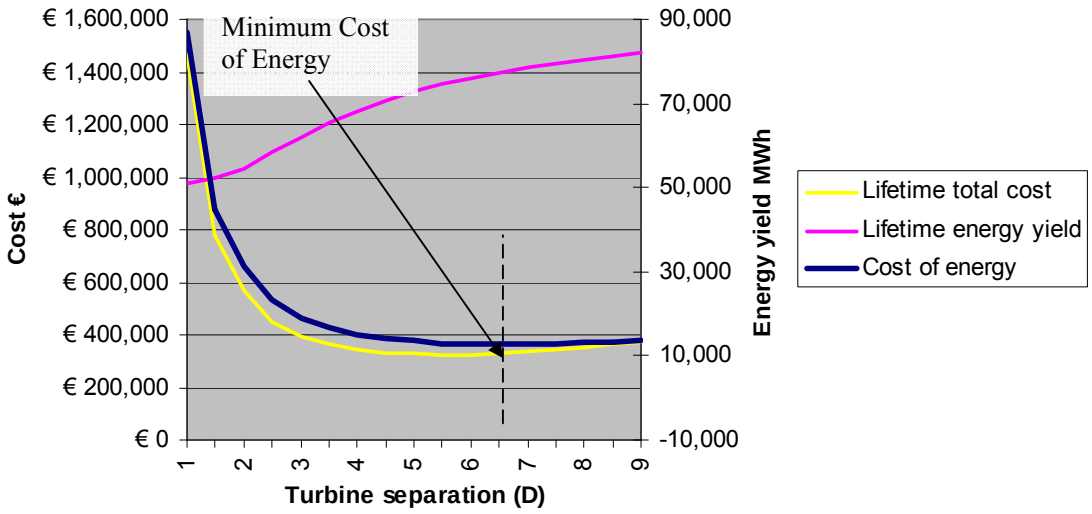

Figure 114. Variation of Cost of Energy with separation distance

It can be seen that the minimum Cost of Energy, and hence the optimum turbine separation distance, in this simple case occurs at around 6.5D.

11.2 Hilltop wind regime

In this example, two turbines were placed in a more realistic situation, as shown in Figure . Notably:

- Wind speed was highest at the top of the hill
- Wind rose was varied, but one turbine was downwind of the other in the prevailing wind direction

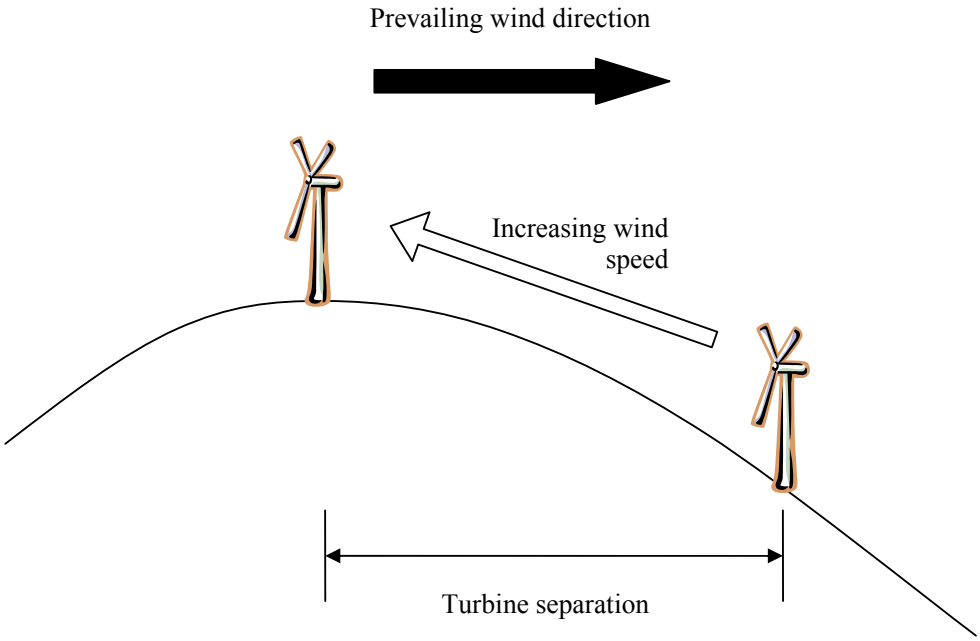

Figure 9. Hilltop site

For these tests, the upwind turbine remained in a fixed location at the top of the hill, and the downwind turbine was moved further away. This moved it down the hill, into decreasing wind speeds, as can be seen inFigure 10. Wrinkles in the curves are caused by irregular terrain. This effect worked contrarily to the decrease in wake loss with increasing distance, and resulted in a maximum incident wind speed and energy yield at a separation of around 5D. This is the separation which can be expected to result from the use of a conventional layout optimiser. Note that the maximum at 2D has been ignored here because loads exceed the design limit.

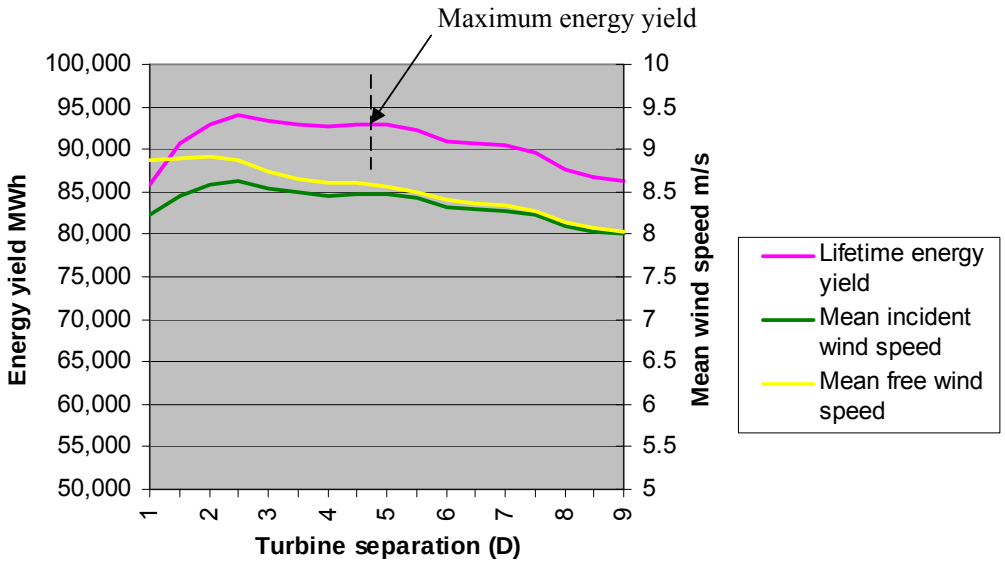

Figure 10. Variation in wind speed and energy yield

The energy yield was combined with the lifetime capital and operational costs to determine the Cost of Energy curve. As Figure shows, this reaches a minimum at a turbine spacing of around 4.5D – this will be the optimum spacing in this example.

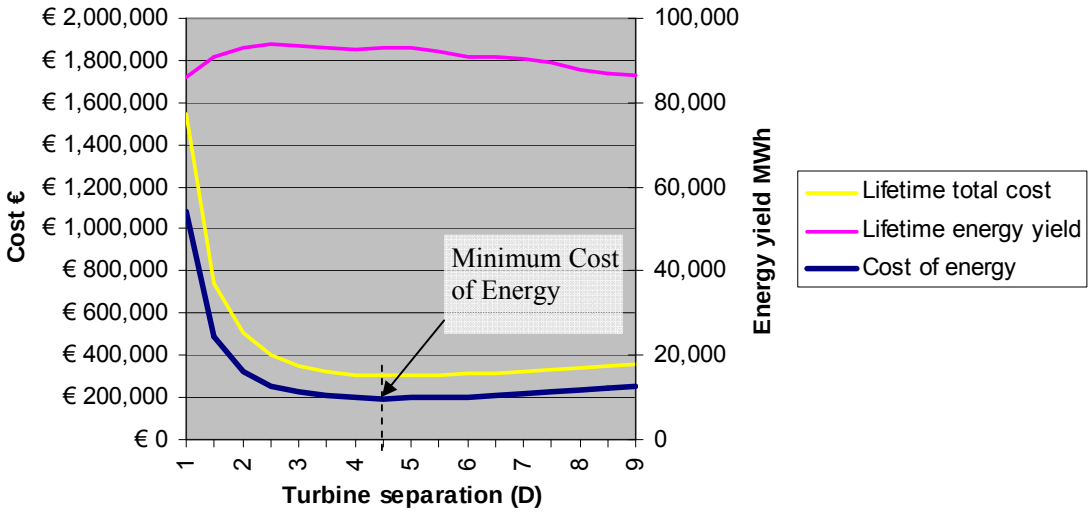

Figure 11. Variation in Cost of Energy

12 Conclusion

This work has shown an approach for establishing an optimum turbine layout based on economic performance. This represents an improvement on conventional optimisers which target maximum energy yield.

Costs which vary with turbine layout, both capital and infrastructure, have been included in the cost model. Development of the fatigue loads database has created a technique for rapidly establishing the site specific loading on critical components, at speeds which are fast enough to be usable in an optimisation routine.

Preliminary testing has shown that the use of Cost of Energy as the target for layout optimisation gives different results from the use of energy yield. This will be valuable to wind farm developers, for whom economic performance is ultimately of prime importance.

Considerable further work is required to refine the cost model. Its structure is currently purely illustrative. The process of establishing the relationship between maintenance costs and fatigue loading in particular is currently little understood, and needs to be further investigated.

13 REFERENCES

1. International Electrotechnical Committee, *IEC 61400-1: Wind Turbines Part 1: Design Requirements*, 2005

2. IEA, OECD, NEA, *Projected Costs of Energy*, 2005 Update.

Appendix A: Key assumptions of the cost model

The assumptions made here are purely to illustrate the functioning of the cost model. Values used are illustrative only, and should not be considered to be authoritative.

Financial assumptions

- Project lifetime: 20 years
- Discount rate: 5%

Cost assumptions

- Infrastructure cost: €300/m
- Tower replacement cost: €2,400,000
- Blade replacement cost: €700,000
- Hub replacement cost: €700,000
- Gearbox replacement cost: €500,000
- Yaw system replacement cost: €80,000

Appendix 7: Guideline to wind farm wake analysis

Guideline to wind farm wake analysis

Kurt S. Hansen,
Department of Mechanical Engineering, DTU

Abstract

A guideline on performing wake analysis on wind farms has been formulated as part of UPWIND-WP1A2. This guideline is derived from preparing dataset and analysing data from several large offshore wind farms. The results of these wake analysis have been used to validate flow models in UPWIND-WP8.

Contents

14 Introduction

SCADA data has shown to be of great value for flow model validation, but the quality of SCADA data is not always sufficiently high and a comprehensive validation is required before use. This paper is summarises the experience obtained with organizing and analysing measurements from 4-5 large wind farms as part of UPWIND-WP8. The paper has been organized as a guideline on how to establish a proper dataset for extracting wake properties; which can document the flow behaviour inside a wind farm during different flow conditions. A previous paper [1] has presented a general guideline for data validation, but this paper will focus on input to the UPWIND WP8 model validation.

The guideline identifies 6 important tasks; which should be addressed before the wake flow cases can be formulated and extracted from the dataset. The data analysis is often performed by a person who have not been involved in the data acquisition process and who might not have a detailed technical knowledge on how to structure huge dataset. The data qualification process requires technical skills concerning validating meteorological data and wind turbines operational behaviour. The technical part of data organization will not be addressed in this document, but the subtask will be illustrated with examples from the data analysis performed in UPWIND-WP8. The flow cases are focusing on presenting either the speed or the power deficit behind a single or a group of wind turbines in relation to the free undisturbed wind speed or wind turbine power. The dataset used in UPWIND-WP8 have been organized in a MySQL® database; which enabled the use of SQL. The data queries have been organized and performed with Matlab®.

15 Purpose

The validation of wind farm flow models developed and implemented in EU-UPWIND WP8 has been based on measurements from a number of wind farms. The wind farm measurements are often limited to SCADA data, recorded as part of the standard wind farm monitoring system. Unfortunately the documentation of calibration and maintenance of the sensors included in the SCADA system is not available; which influences the quality of the recorded signals and a validation is required before use.

State-of-the-art models ranging from large CFD models to engineering models like WAsP® and WindFarmer® have been included as part of UPWIND-WP8 in the validation and it became necessary to formulate flow cases, which could be implemented to different kind of models. The aim was to perform wake analysis that could enable a complete model validation, taking into account combinations of flow direction, wind speed and atmospheric stability.

15.1 Signals

A flow case query requires access to a number of signals and a considerable number of [10 minute] statistical values from either a dedicated measurement system or from the wind turbine *Supervisory Control And Data Acquisition* [SCADA] system. The signals should as a minimum include:

- Individual wind turbine power;
- Individual wind turbine yaw position and yaw misalignment;
- Wind speed and wind direction at hub height on a free undisturbed mast (optimal).

All statistical values should be screened to:

- Identify records with turbines of line;
- Identify records with reduced power settings;
- Identify wind farm offline situations;
- Identify site specific deviations e.g. turbine size, hub height, regulation type and terrain.

15.2 Definitions

Some basic definitions have been adapted during the flow validation procedure. When analysing flows inside wind farms, the input refers to wind speed or [wind turbine] power and the output is expressed as the ratio between output and input values or as a deficit. The following definitions have been used:

Speed ratio: $\eta_s = U_{free} / U_{wake}$

Power ratio: $\eta_p = Power_{free} / Power_{wake}$

Speed deficit: $\eta_{sd} = 1-U_{free} / U_{wake}$

Power deficit: $\eta_{pd} = 1-Power_{free} / Power_{wake}$

Turbine spacing, unit= [Rotor] diameter

The deficit is presented according to the [ambient] flow conditions as function of distance between the [wake] object wind turbine and the wake generating turbine as function of flow direction. The power deficit distribution is illustrated in 2 different presentations below:

Figure 115; illustrates the power deficit distribution - as function of the normalized inflow direction where each circle represents the mean power deficit for a five degree flow sector between two turbines. The distribution is fitted with a Gaussian expression and reveals a mean wake expansion of 28°. The deficit distribution represents all atmospheric conditions in the wind speed interval 7 – 9 m/s for 7D spacing in the Horns Rev wind farm.

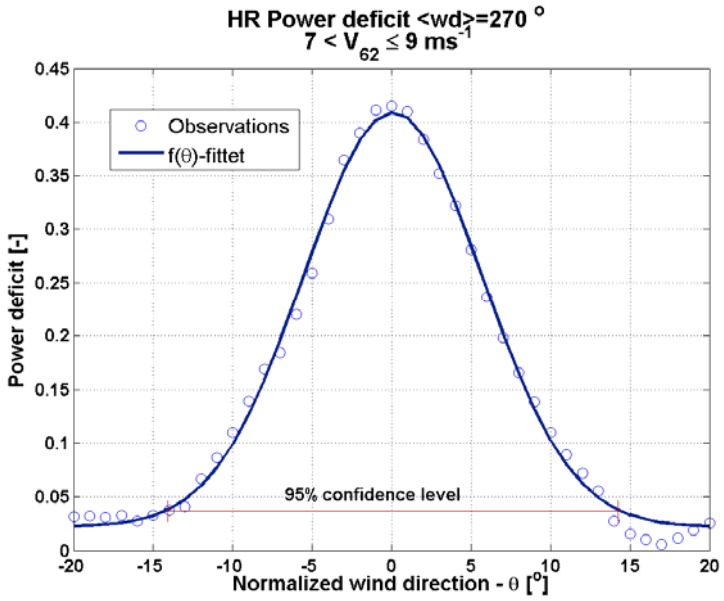

Figure 115: Example of power deficit as function of normalized wind direction between two turbines with 7D spacing.

Figure 116; shows the mean power deficit downstream, along rows of turbines with 7D spacing for 8 m/s wind speed and a 5 degree flow sector. The figure illustrates how the main part of deficit 30-40% occurs between the 1th and the 2th turbine. Adding some additional turbines to the row, only increases the power deficit with 10% - with reference to the first turbine. The power deficit level and shape highly depends on the wind speed, flow direction and the atmospheric stability.

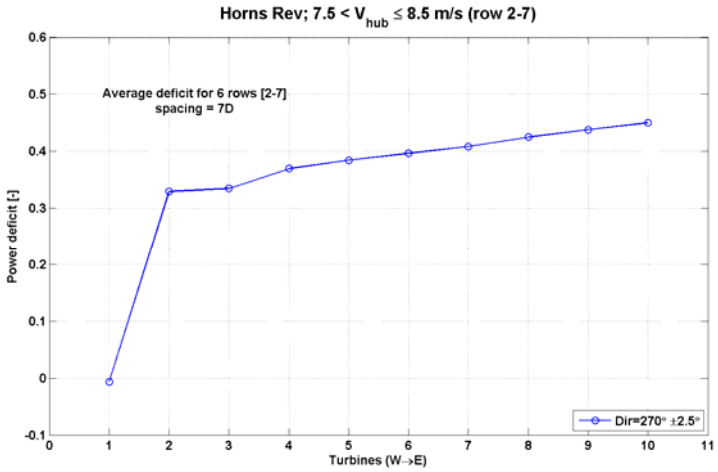

Figure 116: Averaged deficit along 6 rows of turbines with reference to wt07 for a 5 degree flow sector.

16 Data preparation

Before a wake analysis can be performed it is necessary to establish a high quality dataset to give confidence to the results. The recommended number of reliable observations is at least 30-60 minutes of good measurements for each flow case, which can be difficult to obtain after the data filtering. This requires a large number of "raw" observations corresponding to at least 1- 2 years of wind farm operation.

The necessary subtasks for qualifying a dataset to wake analysis are:

1. Data organization and synchronization;
2. Data qualification;
3. Wind farm layout;
4. Calculation of derived parameters;
5. Identification of descriptors and flow cases;
6. Define data filter criteria;

It is important to address all the tasks listed above; otherwise the data query will suffer from large scatter or a lack of observations.

16.1 Signals, organization and synchronization

The required data for wake flow analysis should include both primary signals like individual power values, wind speed and wind direction at hub height. Furthermore a lot of secondary signals e.g. individual values for yaw position, nacelle wind speed, pitch angle and rotor speed. The secondary values are important for validating the quality of the primary signal quality and also for validating the operational behaviour of the wind turbine. The signal statistics should include mean, standard deviation, minimum and maximum values both for primary and secondary signals.

Table 9: Required SCADA signals, used to qualify the wake flow properties in a wind farm

Number	Signal	Importance
1	Electric Power from all wind turbines	High

2	Wind speed from undisturbed mast(s) 4	High
3	Wind direction at hub height	High
4	Yaw position from all individual turbines5	High
5	Nacelle wind speed from all wind turbines	Medium
6	Rotor speed from all turbines6	Medium
7	Pitch angle from all turbines	Medium
8	Temperatures	Medium

The data organization should be appropriate to avoid additional scaling or calibration during queries. Furthermore it should be possible to perform queries with a number of constraints.

The data transfers include many GB of data, stored in huge compressed [ASCII] files and a data conversion to a robust format is required. Such format can be a database or a software dedicated format. A database solution enables the use of efficient tools based on ***STRUCTURED QUERY LANGUAGE*** [SQL].

The wind farm statistics are available from different sources as the *Supervisory Control And Data Acquisition* /SCADA] system or stand-alone [meteorological] logger systems. It is extremely important to facilitate a robust synchronization of the different sources of measurements, because system clocks can be unstable for stand-alone systems. The quality of the synchronization should be within 1 minute; which has to be checked throughout the whole measuring period.

16.2 Wind farm layout

The exact knowledge of the wind farm layout is essential, both during the data qualification and for the wake analysis. The wind turbine coordinates are available as geographical coordinates, but often it is more appropriate to use the rotor diameter as plotting unit demonstrated in Figure 117. This figure presents the layout of an [offshore] wind farm with 80 turbines and the position of three masts. It is important to identify free inflow sectors both for the masts observations and for wind turbines. Figure 118 identifies the three principal flow directions corresponding to 7D, 9.4D and 10.4 D spacing at the NW corner of the wind farm. This information is essential when validating the signal quality.

The wind turbine coordinates are used to identify the wake generating turbines, according to the inflow sector.

4 This will require several masts, but in case such signal is not available, it is necessary to use the power values to determine the inflow conditions.

5 This signal is equal to nacelle position, and can be a substitute to the wind direction signal.

6 The rotor speed is important for validating the operational behavior of dual or variable speed turbines.

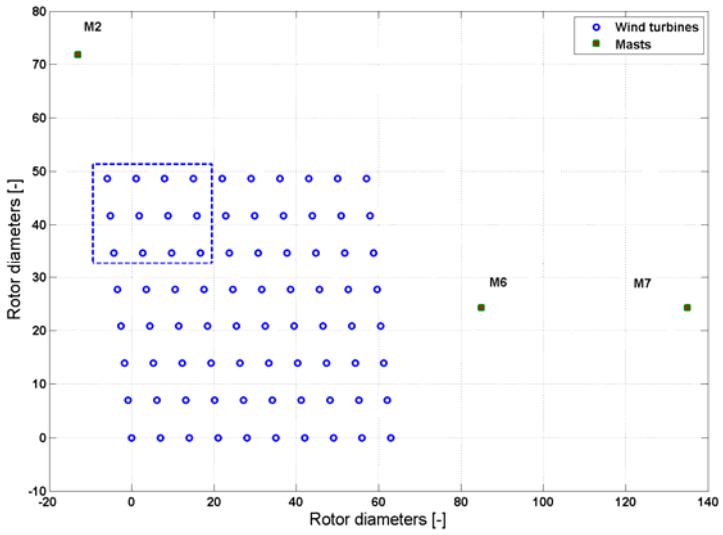

Figure 117: Layout of the Horns rev wind farm, unit=rotor diameter (=80m).

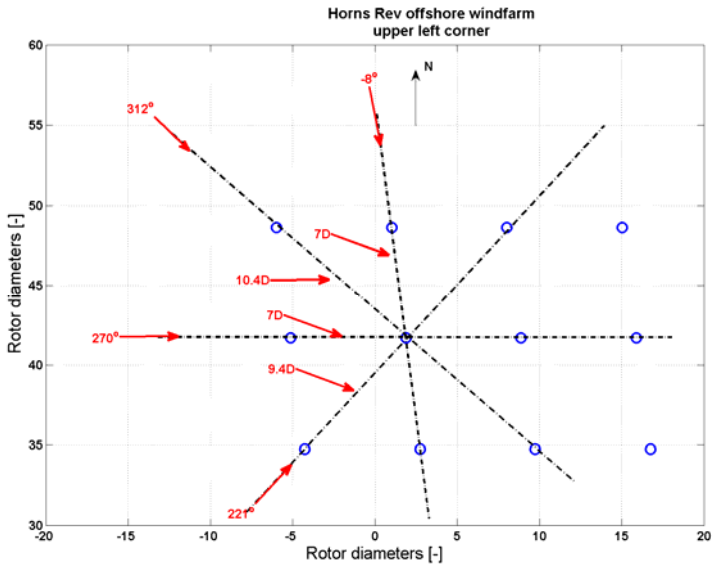

Figure 118: Main flow directions and principal spacing distances at Horns Rev wind farm.

Wind farms located in complex terrain are often installed in irregular shapes optimized to the landscape or dominants flow sectors. It can be difficult to determine a unique inflow reference due to the complexity of the terrain and the lack of undisturbed masts. This is shown in Figure 119, where the masts are located inside the wind farm or behind the wind farms compared to the dominant flow direction.

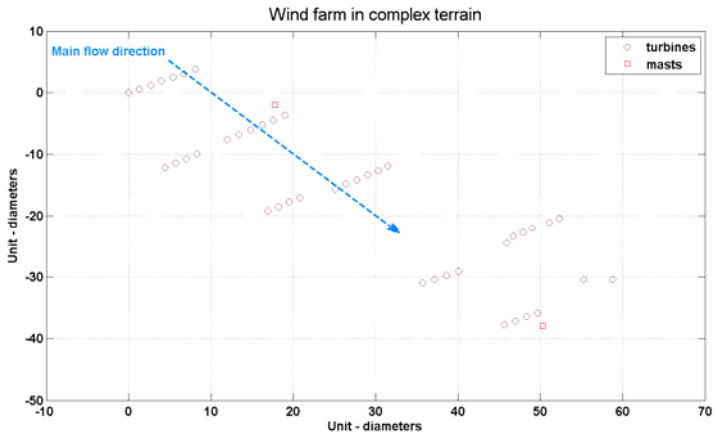

Figure 119: Example of a wind farm installed in a complex terrain with a dominant flow direction.

16.3 Data qualification

Before use, all data need to be quality checked while the data has been moved to another media using a transfer protocol. Furthermore data is not necessarily checked during the operational phase due to lack of time or skilled personnel. It is important to identify and exclude erroneous observations instead of using modified observations and exclusion might be implemented using a quality number as defined in [2]. Below is a list of potential error sources related to the signals in Table 9, which need to be verified.

Power signals can:

- include outliers, which can influence the analysis;
- include periods where the turbine is in transition mode like start, stop or emergency stop sequence;
- be limited due to power de-regulation.

The main part of deviating power observations can be identified through scatter plot of the power as function of nacelle wind speed. It can even be necessary to establish a correlation between the official power curve and the mean power curve based on the nacelle wind speed as shown in Figure 120.

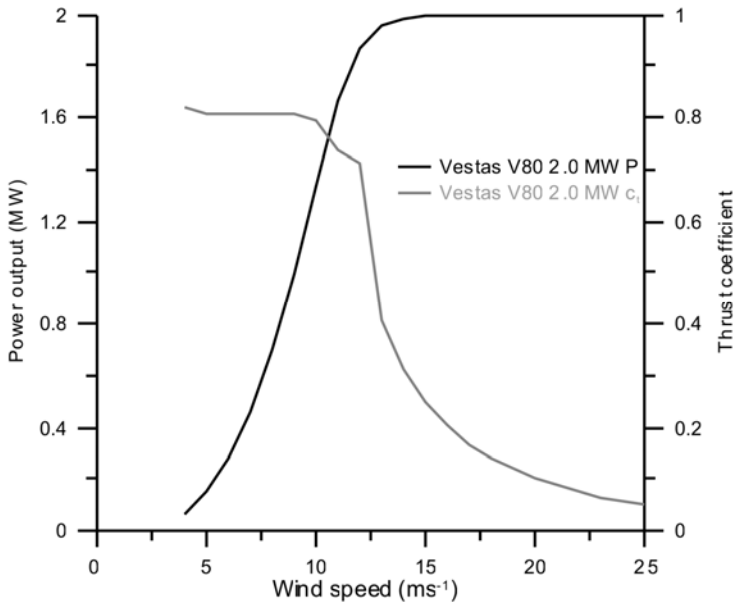

Figure 120: Official power and thrust coefficient curve for VESTAS V80.

A scatter plot of the power value as function of the nacelle wind speed can be used to identify outliers if there is a lack of undisturbed wind speed observations, especially for wind turbines located in a wind farm. A qualifying scatter plot is shown in Figure 121 including a disqualification line and circle. The level of the disqualification line depend a.o. on the wind turbine control and the local turbulence intensity variation.

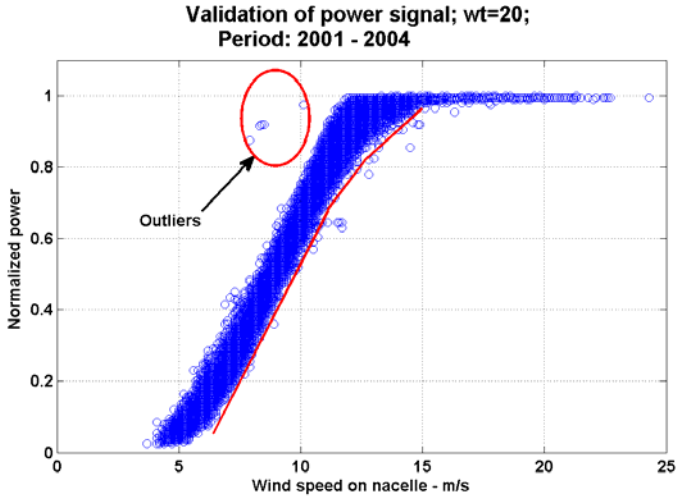

Figure 121: Example of qualification of power values, all observations below the red line and inside the red circle are marked as outliers and disqualified.

If the power values contain a high degree of scatter it is necessary to include an "acceptance" band for each wind speed interval with reference to the standard deviation of the power.

Wind speed at hub height

- could be checked for correlation with other heights;
- Could be checked for occurrence of stationarity, spikes and drop-outs through scatter plots.

The signal correlation is a robust method to identify data outliers and scatter plots of turbulence can be used but to identify signal stationarity. Unfortunately it is impossible to verify the instrument calibration due to lack of documentation.

Wind direction at hub height

- could be checked for correlation with other heights;
- Could be checked for occurrence of stationarity through scatter plots.

Yaw position of wind turbine

The wind turbine yaw position offset is often not correct or calibrated and it is necessary to perform a data analysis to determine this offset. A correlation against the wind speed direction is sufficient for a free wind sector; otherwise the signal could be verified in sectors with an expected power deficit along a line of turbines, as shown in Figure 122. It is sufficient to validate the yaw position for 3 – 4 reference turbines; which can represent the flows from different direction into the wind farm, if the number of masts is limited. The yaw position offset can change during the measuring period and this also need to be verified.

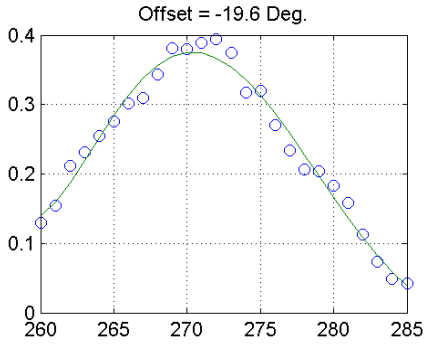

Figure 122: Determination of yaw position offset from Horns rev, wt02.

Each observation in Figure 122 is determined with a moving average technique using a window of 5 degrees. The moving window technique reduces the deficit scatter and is a robust technique to extract information from small datasets.

16.4 Derived parameters

The wind farm dataset does not always include the sufficient signals for wake analysis. This section identifies important signals, which should be included as constraints in the wake analysis.

Free wind direction

The wind direction signal is extremely important, while the flow deficit highly depends on the flow direction (Figure 122) and the spacing between the wind turbines. With a lack of direction measurements it is necessary to establish an artificial wind direction based yaw positions from 2-4 wind turbines to cover the whole wind rose. NOTE: The artificial signal is only valid for grid connected wind turbines, while the wind turbine yaw position could misbehave when the turbine is idling or stopped.

Monin-Obukhov length, L.

The M-O length can be derived either from sonic measurements or from a combination of the temperature and the wind speed gradient. To determine a robust M-O lengths in onshore and complex terrain sites, it is important to select proper observation heights and it is recommended to consult the literature on this topic.

Atmospheric stability classification

The offshore stability classification can be based on the Monin-Obukhov length L, as listed in Table 10

Table 10: Definition of stability classes based on length, L (m).

Class	Obukhov length [m]	Atmosperic stability class
cL=-3	-100 ≤ L ≤ -50	Very unstable (vu)
cL=-2	-200 ≤ L ≤ -100	Unstable (u)
cL=-1	-500 ≤ L ≤ -200	Near unstable (nu)
cL=0	|L|>500	Neutral (n)
cL=1	200 ≤ L ≤ 500	Near stable (ns)
cL=2	50 ≤ L ≤ 200	Stable (s)
cL=3	10 ≤ L ≤ 50	Very stable (vs)

The stability classification for Horns Rev has been based on the Bulk-Ri number with success - as demonstrated in [3,4]. The speed measurements from 15 m amsl (recorded below tip-bottom height) seem to be applicable in combination with the temperature difference between air and water. The robustness of this classification has been documented in [4] and an example from Horns Rev has been demonstrated in Figure 123.

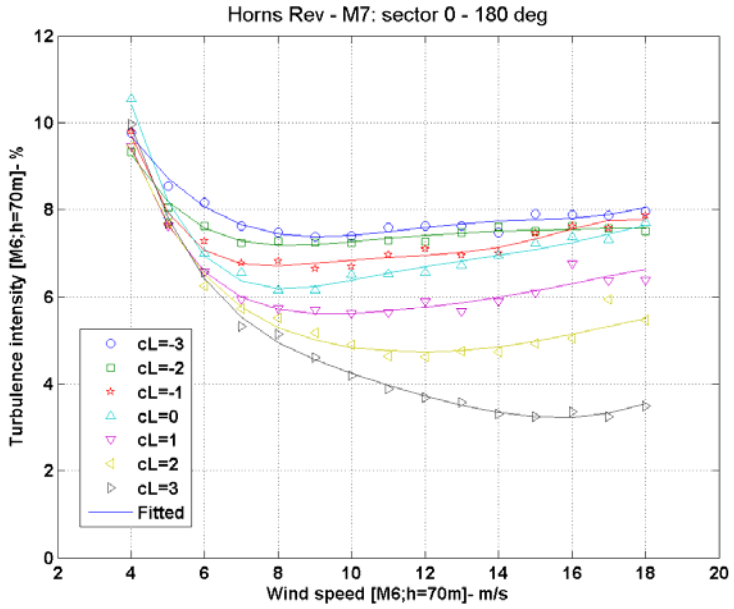

Figure 123: Example of averaged turbulence intensity for different stability classifications, measured at Horns Rev offshore wind farm, Denmark.

16.5 Identifications of descriptors and flow cases

The two most important descriptors for analysing the flow inside a wind farm is 1) the undisturbed wind speed and 2) wind direction at hub height measured outside the wind farm. Unfortunately such observations are not always available and another option is to use recordings from a upwind turbine, e.g. power values and yaw position as indicated in Figure 125.

The power range is selected according to the official power curve, Figure 120, for a given wind speed interval, but this method requires a signal validation as described in section 4.3 before the analysis can be performed.

The inflow sector is limited with reference to the [upwind] free wind turbine yaw position as illustrated in Figure 126. Using the wind turbine yaw position increases the directional uncertainty, while the wind turbine yaw misalignment averaging procedure is not documented, but a |yaw misalignment| > 0 can be expected7. Many observations are required to reduce the scatter in the measurements compared to wind vane signals.

Other descriptors can be the ambient turbulence intensity and/or the stability classification as listed in the section 4.4.

7 Caused by a hysteresis, in the yaw misalignment.

The flow case is defined together with the users who are validating flow models; which is could either be the code developers or the end-users who need the flow model performance.

The flow cases are defined in steps; ranging from simple [flow] cases to very complicate [flow] cases and a list with increasing complexity is given in Figure 124:

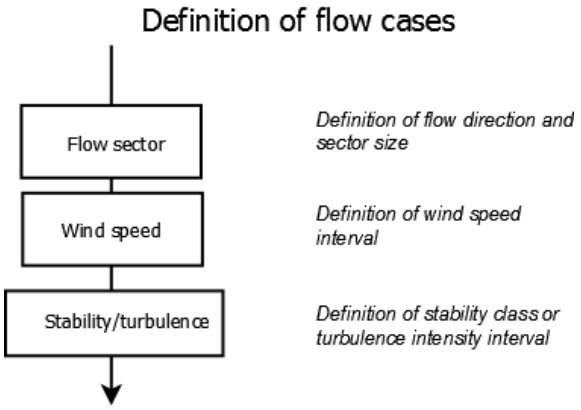

Figure 124: Definition of flow cases with increasing complexity.

i) Flow within a limited sector, along a line of wind turbine;
ii) Flow within a limited sector, along a line of wind turbines and a limited wind speed interval;
iii) Flow within a limited sector, along a line of wind turbines, a limited wind speed interval and a stability class.

The simple flow case i) is applicable for a limited number of observations and depends only on the selected sector size. Increasing complexity requires much more observations and flow cases from class iii) can only be fulfilled with a limited number of combinations of wind speed, flow sectors and stability classes.

The number of flow cases derived from class iii) could include 18 flow sectors x 12 wind speeds interval x 7 stability classes – in total 1512 flow cases8. Such amount of cases requires a proper verification and planning before the queries can be performed. The size of the flow sector should be applicable for the flow model verification and may vary between 5 and 30 degrees.

8 Many flow cases can be eliminated due to symmetry, depending on the wind farm layout and inflow complexity.

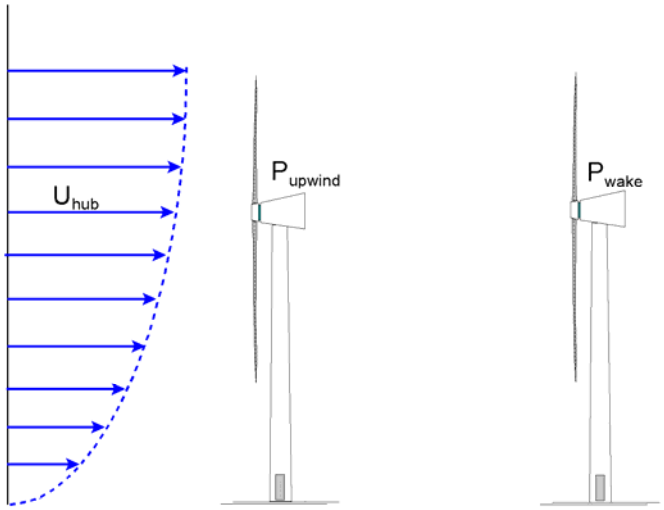

Figure 125: Wind farm inflow conditions

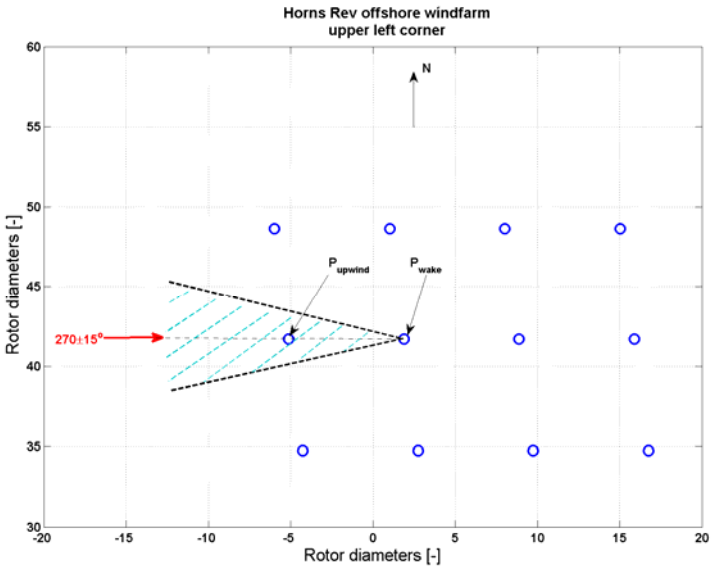

Figure 126: Definition of 30 degrees flow sector along a row of turbines.

I

16.6 Data filtering

The purpose of using data filtering is to identify the exact flow conditions in the wind farm. The simple flow case includes only two turbines, a free turbine and a turbine operating in the wake of the free turbine Figure 125. Increasing inflow complexity results in more than 2 turbines, and it necessary to include the operational conditions of all upstream turbines; which can influence the operational behaviour of the turbine operating in the wake. The filtering process consists of a number of subtasks with reference to Figure 125 and Figure 126 and according to the list of conditions below:

i) The free [upwind] wind turbine is grid connected 100% during each 10 minute period;
ii) The object [wake] wind turbine is grid connected 100% during each 10 minute period;
iii) All wake generating wind turbines should be grid connected 100% during each 10 minute period;
iv) Flow stationarity through the whole wind farm is required.

Rule iii) requires a detailed mapping of the wind farm with reference to the actual flow sector. It is required that all wind turbines inside the flow sector are grid connected as shown in Figure 126. This criterion could involve 5-10 turbines depending on the inflow sector, but turbines at a distance larger than 40-50 diameters can be neglected.

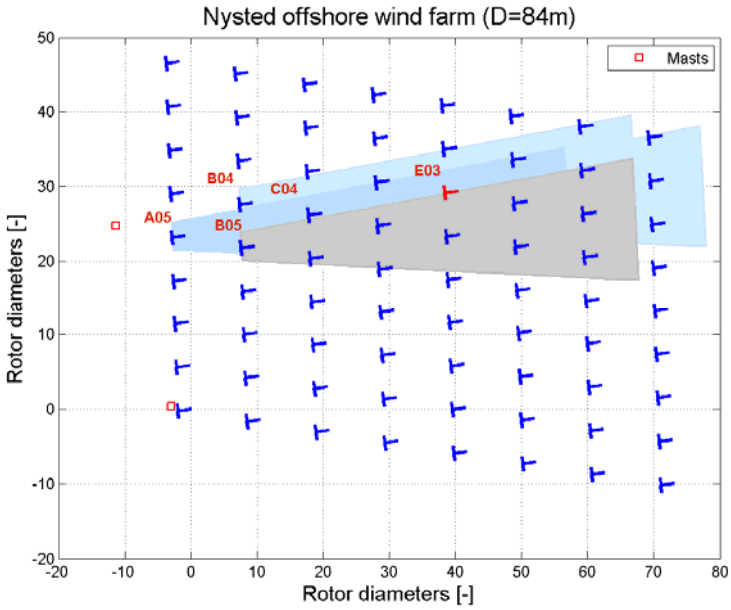

Figure 127: Wake generating wind turbines located upwind to the turbine E03 for a westerly inflow sector of 263±2.5°.

Figure 127 illustrates an inflow sector equal to 263±2.5° for turbine E03. The the wake generating turbines; which have to be taken into account are A05, B04, B05 & C04 when using an offshore wake expansion coefficient 0.05.

Rule iv) on flow stability throughout the wind farm has been included to identify and exclude situations where the wind farm is partly covered by a weather front9. The size of a wind farm determines whether it is necessary to implement these criteria.

17 Data query and wake analysis

The complexity of data query depends on the amount of available turbines ranging from 1) small wind farms with 10 - 40 turbines distributed in irregular patterns (complex terrain and complex inflow conditions) and low availability; to 2) large wind farms consisting of 30 – 100 wind turbines and requires more than 1 complete year of operation distributed in regular patterns (offshore and regular inflow conditions). Both types of wind farms or a combination can be analysed; but wind farms situated in a complex terrain is a big challenge due to the complex inflow conditions and even varying hub heights caused by the topography. Such analysis requires more than 1 year of observations to establish a robust estimate of the power deficit distributions.

The wake analysis can be formulated according to the complexity of the flow conditions and the purpose:

9 Flow stability can be obtained by only selecting the second of two consecutive records.

i) Deficit for pairs of turbines as function of wind direction;
ii) Deficit for pairs of turbines with different spacing;
iii) Maximum deficit as function of turbulence intensity and spacing;
iv) Deficit along rows of turbines;
v) Deficit for partly covered turbines as function of flow direction;
vi) Deficit variations at different atmospheric conditions;
vii) Park efficiency.

These analyses require a well-organized and quality controlled dataset according to the guidelines given in the previous section.

i) Deficit for a pair of turbines.

This basic query requires a pair of [identical] turbines with spacing between 2-10D. The purpose of this analysis is to determine the deficit distribution a function of wind direction - as illustrated in Figure 115. Refined analysis can reveal the dependence due to wind speed level, rotor speed, pitch angle or turbulence intensity, because the angular deficit distribution depends on the actual operational turbine condition.

ii) Deficit for a pair of turbines with different spacing.

The deficit distribution for some distinct spacing can be derived from a group of turbines located in a wind farm. With turbines arranged in an ordinary grid; this enables at a number of spacing to be validated when taking into account the diagonals directions. Figure 118 defines three distinct spacing 7D, 9.4D and 10.4D for the Horns Rev wind farm.

iii) Maximum deficit as function of turbulence intensity and spacing.

The maximum deficit is determined for a narrow flow sector as function of turbulence intensity and spacing as shown in Figure 128. The flow sector size depends on the number of available observations, but increasing the flow sector decreases the maximum deficit value. Figure 128 illustrates a clear correlation between deficit, turbulence intensity and spacing. This query can furthermore be applied for more than two turbines and will then result in a multiple wake deficits estimate.

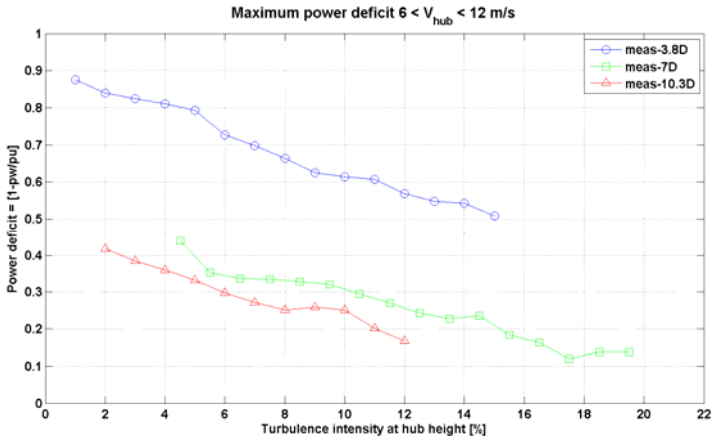

Figure 128: Maximum power deficit for three different spacing - as function of turbulence intensity.

iv) Deficit along row of wind turbines.

The state-of-art wake analysis has been focusing on the power deficits along row of turbines. The query sequence consists of a "guided walk" from wt01 to wt98 with reference to the "upwind turbine" including the filtering constraints as defined in the previous section .

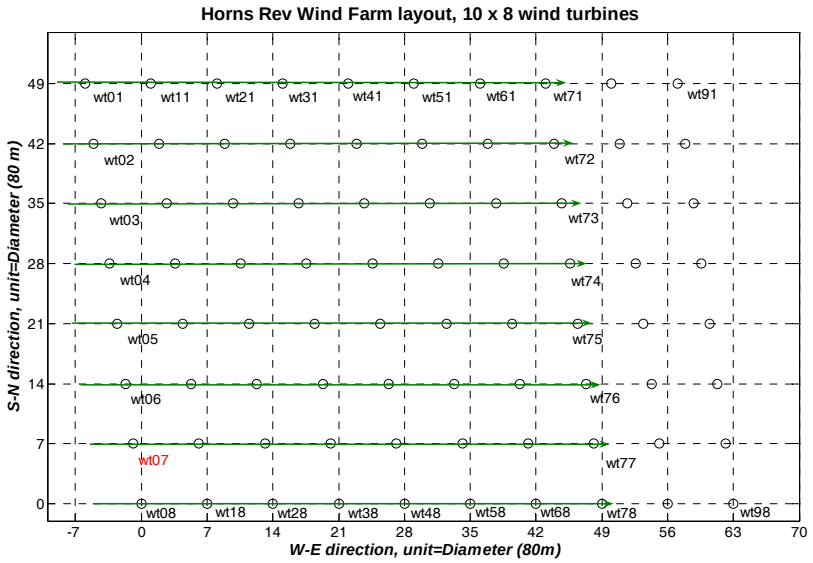

Figure 129: Horns Rev offshore wind farm, with an indication of 270^o flow direction along the rows of wind turbines. The reference turbine for this flow analysis is wt07.

A flow case from the Horns Rev wind farm, Figure 129 estimates the deficit for a narrow flow sector along the lines of turbines in a small sector (270 ±2.5°). The power deficit is presented in tables (Table 11) with reference to wt07. Each number in the table represents approximately 6 hours of measurements after data filtering. Reducing the data filtering criterion will result in more observations and increased scatter, where the scatter is defined as the standard deviation of the power deficit values. The flow direction is perpendicular to the first column (Col 1) of turbines and the findings indicate a small lateral power gradient for this flow case; which represents 3-4 km distance. A lateral power gradient is often observed in large offshore wind farms and depends on local inflow conditions like fetch distance. The power deficit is visualized in Figure 130 and indicates a scatter between the rows, partly due to the lateral gradient. The deficit for row 1 and 8 has been excluded in the averaged deficit due to partly free inflow.

Table 11: Mean power deficit at Horn Rev for flow direction = 270±2.5° and V_{hub}=8±0.5m/s

Flow case 8: Power deficit [filters: wake & stationarity]										
	Col 1	Col 2	Col 3	Col 4	Col 5	Col 6	Col 7	Col 8	Col 9	Col 10
row 1	1.02	0.74	0.73	0.71	0.72	0.68	0.65	0.63	0.61	0.59
row 2	1.01	0.72	0.71	0.69	0.65	0.65	0.63	0.58	0.57	0.57
row 3	1.02	0.69	0.69	0.64	0.63	0.61	0.61	0.58	0.57	0.56
row 4	1.02	0.69	0.67	0.65	0.63	0.61	0.57	0.59	0.58	0.57
row 5	0.99	0.67	0.67	0.62	0.62	0.60	0.60	0.59	0.59	0.55
row 6	1.01	0.64	0.64	0.60	0.60	0.59	0.58	0.58	0.55	0.54
row 7	1.00	0.63	0.62	0.58	0.56	0.55	0.55	0.53	0.52	0.51
row 8	0.99	0.64	0.63	0.61	0.60	0.58	0.60	0.61	0.63	0.62

The park efficiency is calculated with reference to wt07 to 66%. The inflow condition for this number is an inflow sector: 270±2.5° and a wind speed, V_{hub} = 8±0.5 m/s and the number has been calculated as the average of all individual wind turbine deficit numbers from in Table 11.

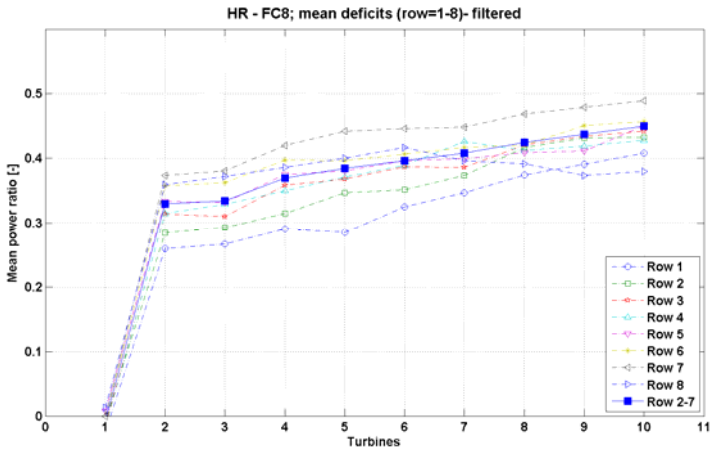

Figure 130: Horns Rev Flow Case 8, power deficit along wind turbine rows.

v) Deficit of turbines operating partly in wakes.

When the flow direction deviates from the line of turbines the turbines are operating partly in wake and a query process identical to case *iv)* can be used. The results are organized in tables' analogue to the example given in Table 11. Figure 131 defines the inflow sector with turbines, operating partly in wake, divided in 5 degree sectors. The averaged power deficit curves are shown for in Figure 132 for 7 different sectors ranging from sector 255, 265, .., 285° and the curves clearly illustrates how the power deficit depends of the wake coverage.

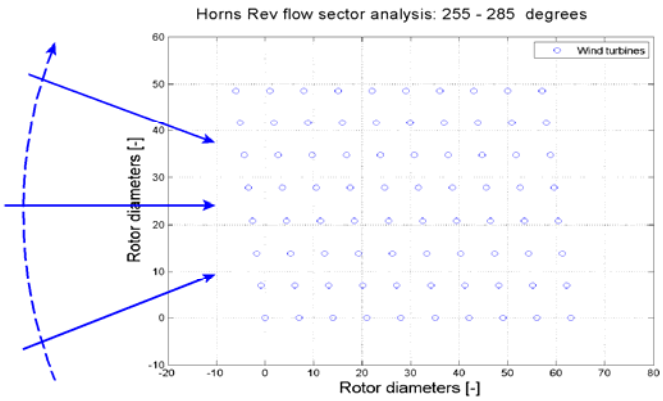

Figure 131: Example of wind farm flow sector analysis for Horns Rev wind farm.

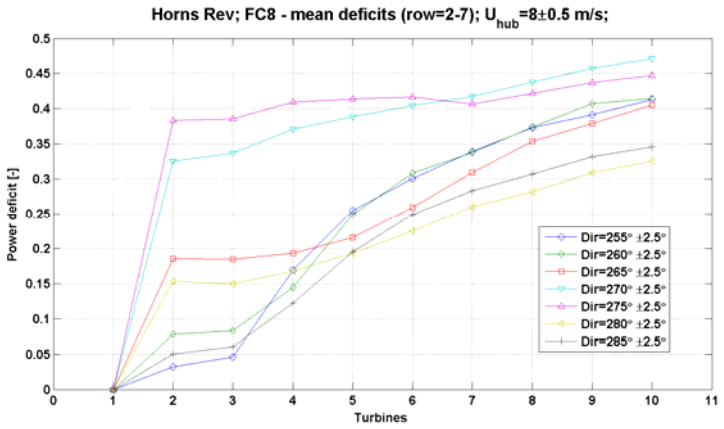

Figure 132: Mean deficit for turbines operating partly in wake.

When the flow direction deviates from the turbine row direction a speed-up effect is visible on the outer row, because this row is partly facing the wind. This is illustrated in Figure 133 for an inflow deviation of 15°, compared to the direction of the row, and the power deficit is reduced considerably.

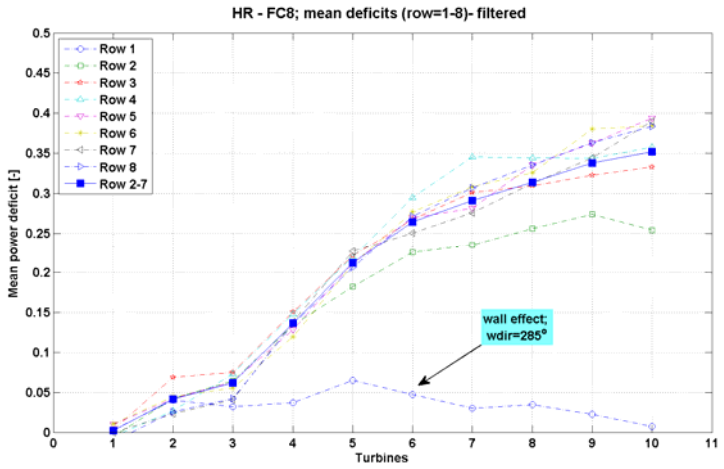

Figure 133: Power deficit at Horns Rev wind farm for V_{hub}=8 m/s, WDIR=285±2.5°.

vi) Deficit sensitivity due to stability.

Adding an additional constraint in terms of stability in the data query, reduces the number of available observations but reveals an important correlation between the deficit and the stability classification. To obtain a recent amount of data for this query, both the wind speed interval and flow sector has been increased considerably. The previous 1 m/s wind speed interval combined with 5 degree flow sectors requires a huge amount of data when including the stability constraint. Large wind speed intervals results in averaged wind turbine operational conditions; which are difficult to interpret and evaluate afterwards. The power deficits distributed according to the classification are shown in Figure 134 and indicates a distinct correlation to the atmospheric stability.

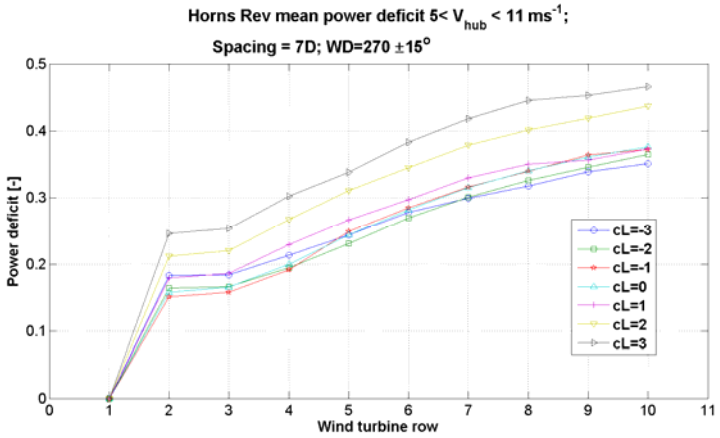

Figure 134: Power deficit along rows of wind turbines for different atmospheric stability conditions.

vii) Wind farm efficiency.

The efficiency of the wind farm deviates from an isolated wind turbine due to the wake deficit as determined above. The determination of the wind farm efficiency requires access to a free, undisturbed reference wind speed for all flow directions; which can be difficult - at least for offshore wind farms. If there is a lack of free, undisturbed inflow signals, one or two validated [corner] turbines can be used as reference in the problematic flow sectors. This method has been used with limited success to validate park model with the Dutch Egmond aan Zee wind farm park production. The layout of the wind farm is visualized in Figure 135 and illustrates the lack of free wind and instead two corner turbines have been included as reference.

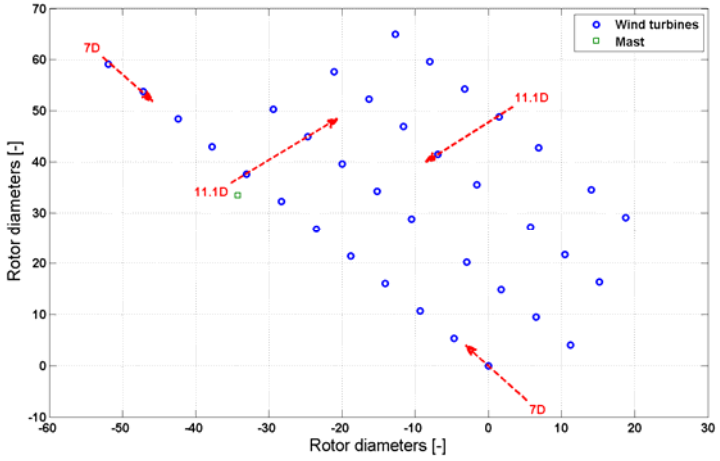

Figure 135: Layout of the Egmond aan Zee(NoordZee) wind farm including an indication of 7D and 11.1D spacing directions.

The query has been performed for U_{hub}=8 m/s using the mast as reference for the SW sector and two turbines for the remaining sectors. The wind speed interval is transferred to a power interval when using the wind turbines as reference. The analysis has been divided into 5 degree flow sectors where the normalized, averaged park power is shown in Figure 136 with an indication of problematic sectors where park production decreases.

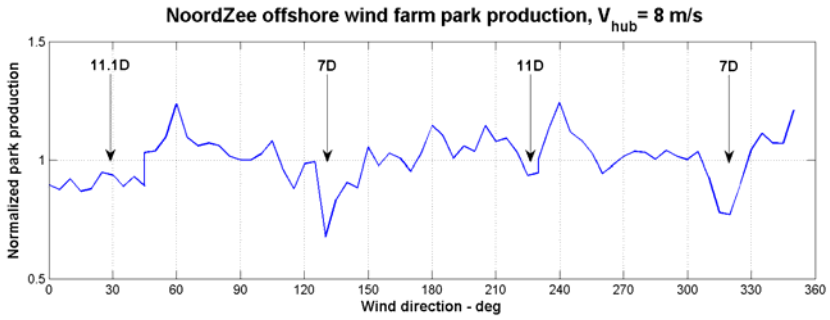

Figure 136: Example of a normalized, directional park power production from the Egmond ann Zee offshore wind farm.

The process of determining the park production as function of wind direction and wind speed is the final step for a complete park model verification.

18 Conclusion

As part of the UPWIND WP8 code validation, a number of procedures to facilitate wind farm wake analysis have been formulated to improve and verify the data quality. A number of steps for data filtering have been formulated, which enabled a robust determination of the power deficit as function of direction, wind speed, spacing and atmospheric stability. Many power deficit results inside wind farms have been identified and used in the flow model validation during the UPWIND-WP8 flow model verification.

Large offshore wind farms with a simple geometrical layout seems to be straight forward to analyse with a fair amount of high quality data (1-2 years). Wind farms with irregular layout can be more difficult to analyse, due to a lack of a robust references (mast or turbines). Wind farms located in complex terrain is difficult to analyse due to both lateral gradients and complex inflow. The most important lesson learned is that the quality of the wake analysis correlates very much on quality and the amount of data.

19 Acknowledgement

Horns Rev offshore wind farm: We would like to acknowledge VESTAS A/S, Vattenfall AB and DONG Energy A/S for data from the Horns Rev wind farm.
Nysted offshore wind farm: We would like to acknowledge Siemens Wind Power, DONG Energy A/S and E.On Sweden for data from the Nysted wind farm.
NoordZee/Egmond Aan Zee offshore wind farm: We would like to acknowledge VESTAS A/S and NoordZeeWind B.V. for data from the NoordZee wind farm.

20 References

[1] Réthoré et al. “Systematic Wind Farm Measurement Data Filtering Tool for Wake Model Calibration”, Presented at the European Offshore Wind Conference(EOW2009), Stockholm 2009

[2] Database of Wind Characteristics; http://www.windata.com/

[3] Larsen, G.C. et.al. ” The dependence of wake losses on atmospheric stability characteristics. To be submitted in 2011.

[4] Hansen,K.S.;Barthelmie,R.;Jensen,L.E.;Sommer,A. ” The impact of turbulence intensity and atmospheric stability on power deficits due to wind turbine wakes at Horns Rev wind farm”, submitted to Wind Energy, Wiley in 2010.

REFERENCES

Ainslie, J.F.: 1988, 'Calculating the flow field in the wake of wind turbines', Journal of Wind Engineering and Industrial Aerodynamics 27, 213-224.

Barthelmie, R.J., Folkerts, L., Ormel, F., Sanderhoff, P., Eecen, P., Stobbe, O. and Nielsen, N.M.: 2003a, 'Offshore wind turbine wakes measured by SODAR', Journal of Atmospheric and Oceanic Technology 30, 466-477.

Barthelmie, R.J., Folkerts, L., Rados, K., Larsen, G.C., Pryor, S.C., Frandsen, S., Lange, B. and Schepers, G.: 2006, 'Comparison of wake model simulations with offshore wind turbine wake profiles measured by sodar', Journal of Atmospheric and Oceanic Technology 23(7), 888-901.

Barthelmie, R.J., Frandsen, S.T., Nielsen, M.N., Pryor, S.C., Rethore, P.-E. and Jørgensen, H.E.: 2007, 'Modelling and measurements of power losses and turbulence intensity in wind turbine wakes at Middelgrunden offshore wind farm', Wind Energy (in review).

Barthelmie, R.J. and Jensen, L.E.: 2010, 'Evaluation of power losses due to wind turbine wakes at the Nysted offshore wind farm', Wind Energy DOI: 10.1002/we.408.

Barthelmie, R.J., Larsen, G.C., Pryor, S.C., Jørgensen, H.E., Bergström, H., Magnusson, M., Schlez, W., Rados, K., Lange, B., Vølund, P., Neckelmann, S., Mogensen, S., Schepers, G., Hegberg, T. and Folkerts, L.: 2003b, 'Efficient development of offshore windfarms (ENDOW): Final report to the European Commission.' Risø National Laboratory, Roskilde, Denmark, p. 30 pp.

Bowen, A.J. and Mortensen, N.G.: 1996, 'Exploring the limits of WASP: the wind analysis and application programme.' in European Union Wind Energy Conference, H.S. Stephens and Associates, Bedford, UK, Goteborg.

Crespo, A., Hernandez, J. and Frandsen, S.: 1999, 'Survey and modelling methods for wind turbine wakes and wind farms', Wind Energy 2, 1-24.

Frandsen, S.: 2005, 'Turbulence and turbulence-generated fatigue loading in wind turbine clusters', Risoe National Laboratory, Roskilde, p. 128

Frandsen, S., Barthelmie, R., Pryor, S., Rathmann, O., Larsen, S., Højstrup, J. and Thøgersen, M.: 2006, 'Analytical modelling of wind speed deficit in large offshore wind farms', Wind Energy 9, 39-53.

Frandsen, S. and Thøgersen, M.L.: 1999, 'Integrated fatigue loading for wind turbines in wind farms by combining ambient turbulence and wakes', Wind Engineering 23, 327-339.

Hansen, K.H., Barthelmie, R.J., Jensen, L.E. and Sommer, A.: 2010, 'The impact of turbulence intensity and atmospheric stability on power deficits due to wind turbine wakes at Horns Rev wind farm', Wind Energy Submitted 8 September 2010. WE-10-0149.

Jensen, L.: 2004, 'Wake measurements from the Horns Rev wind farm', in European Wind Energy Conference, EWEA (on CD), p. 9 pp.

Katic, I., Højstrup, J. and Jensen, N.O.: 1986, 'A simple model for cluster efficiency', in European Wind Energy Association, Rome, pp. 407-409.

Magnusson, M., Rados, K.G. and Voutsinas, S.G.: 1996, 'A study of the flow down stream of a wind turbine using measurements and simulations', Wind Engineering 20, 389-403.

Magnusson, M. and Smedman, A.S.: 1999, 'Air flow behind wind turbines', Journal of Wind Engineering and Industrial Aerodynamics 80, 169-189.

Mechali, M., Jensen, L., Barthelmie, R., Frandsen, S. and Rethore, P.E.: 2006, 'Wake effects at Horns Rev and their influence on energy production', in European Wind Energy Conference and Exhibition, Athens, Greece, p. 10.

Mortensen, N.G., Heathfield, D., Landberg, L., Rathmann, O., Troen, I. and Petersen, E.: 2000, 'Getting started with WASP 7.0', Risø National Laboratory, Roskilde, p. 60.

Mortensen, N.G., Heathfield, D.N., Myllerup, L., Landberg, L. and Rathmann, O.: 2005, 'Wind Atlas Analysis and Application Program: WAsP 8 Help Facility', Risø National Laboratory, Roskilde, Denmark. 335 topics. ISBN 87-550-3457-8.

Quarton, D. and Ainslie, J.: 1990, 'Turbulence in wind turbine wakes', Wind Engineering 14, 15-23.

Rados, K., Larsen, G., Barthelmie, R., Schelz, W., Lange, B., Schepers, G., Hegberg, T. and Magnusson, M.: 2002, 'Comparison of wake models with data for offshore windfarms', Wind Engineering 25, 271-280.

Rathmann, O., Frandsen, S.T. and Barthelmie, R.J.: 2007, 'Wake modelling for intermediate and large wind farms', in European Wind Energy Conference and Exhibition, Milan.

Schepers, G., Barthelmie, R.J. and Politis, E.S.: 2010, 'Wake reducing concepts. Upwind WP8 Deliverable 8.5', ECN, Petten, p. 30.

Schepers, J.G.: 2003, 'ENDOW: Validation and improvement of ECN's wake model', ECN, Petten, The Netherlands, p. 113.

Schlez, W., Umaña, A.E., Barthelmie, R., Larsen, S., Rados, K., Lange, B., Schepers, G. and Hegberg, T.: 2002, 'ENDOW: Improvement of wake models within offshore windfarms', Wind Engineering 25, 281-287.

Thomsen, K. and Sørensen, P.: 1999, 'Fatigue loads for wind turbines operating in wakes', Journal of Wind Engineering and Industrial Aerodynamics 80.

Risø DTU is the National Laboratory for Sustainable Energy. Our research focuses on development of energy technologies and systems with minimal effect on climate, and contributes to innovation, education and policy. Risø DTU has large experimental facilities and interdisciplinary research environments, and includes the national centre for nuclear technologies.

Risø DTU
National Laboratory for Sustainable Energy
Technical University of Denmark

Frederiksborgvej 399
PO Box 49
DK-4000 Roskilde
Denmark
Phone +45 4677 4677
Fax +45 4677 5688

www.risoe.dtu.dk